UNIVERSITY OF BIRMINGHAM

THE USE OF POSITRON EMISSION PARTICLE TRACKING (PEPT) TO DETERMINE THE GRINDING MECHANISMS WITHIN A VERTICALLY STIRRED MEDIA MILL

by

THOMAS RICHARD SKUSE

A thesis submitted to the University of Birmingham
for the degree of
DOCTOR OF PHILOSOPHY

Department of Chemical Engineering
School of Engineering
University of Birmingham
September 2015

For my family

Abstract

A Positron Emission Particle Tracking (PEPT) based technique was developed and used to study laboratory grinding of calcium carbonate in a vertically stirred media mill. The PEPT data along with particle fracture data obtained by micromanipulation were used to understand the grinding mechanisms.

The PEPT methodology allowed measurements of grinding media occupancy, velocity, force, stress and media–media collisions at different positions within the mill. The stresses exerted by the media were compared with calcium carbonate strength measurements made using the micromanipulator to determine the percentage of the grinding media with sufficient stress to overcome the strength of the calcium carbonate particle. The collision frequency and total number of collisions were estimated using a modified Arrhenius equation approach by measuring the mean relative velocity of the grinding media (estimated to be the standard deviation of velocity measurements made in a block volume) and the number of media particles in a unit volume.

This approach was used to characterise the behaviour of a benchmark grinding experiment performed under standard conditions and to understand the effect different operating conditions had on the number of collisions and stress exerted at these collisions. A number of suggestions for improved mill performance are given.

Acknowledgements

I would like to thank everyone who helped and supported me throughout my PhD. In particular I am very grateful to my supervisors Neil Rowson for his guidance, support, and stories, Andy Ingram for all his help and Richard Tamblyn for his insights into comminution and providing equipment for experiments.

In addition I would like to thank Tom Leadbeater for his help with PEPT, Joseph Gargiuli for providing the PEPT tracers, James Bowen for his training using the interferometer and other Science City equipment, Phil Robins for his help scripting, Zhibing Zhang and Sen Liu for training me on the micromanipulator and Nigel Rowe for teaching me to operate the laboratory stirred media mill.

I would like to thank Imerys and the ESPRC for giving me this opportunity and financial backing.

I would also like to thank Neil's research group and everyone I've met in Birmingham for their friendship. I would especially like to thank Sarah for always being there.

Finally, I would like to thank my Mum, Dad, Ben, Will, Joe, Kate, Jack and Anna for all they have done for me.

TABLE OF CONTENTS

LIST OF FIGURES

LIST OF TABLES

NOMENCLATURE

A	Area (m^2)
a	Minimum distance between two media particles when a feed particle can still be stressed (m)
a'	Relative distance between a and x ()
a_c	Critical crack length (m)
acc	Resultant acceleration (ms^{-2})
a_i	Cubic spline coefficient ()
a_l	Crack length (m)
a_x	Acceleration in x (ms^{-2})
a_y	Acceleration in y (ms^{-2})
a_z	Acceleration in z (ms^{-2})
b_i	Cubic spline coefficient ()
C	Compliance (mN^{-1})
c	Average velocity of a particle (ms^{-1})
$\bar{c}$	Relative speed of particles (ms^{-1})
c_i	Cubic spline coefficient ()
c_v	Solids volume concentration (m^3m^{-3})

D	Displacement (m)
d	Particle diameter (m)
d_a	Diameter of sphere with equal (m^2)
d_{act}	Diameter of the active volume in which feed particles can be stresses (m)
d_{GM}	Average diameter of a grinding media particle (m)
d_i	Cubic spline coefficient ()
d_s	Diameter of sphere with equal surface area (m^2)
d_v	Diameter of sphere with equal volume (m^3)
E	Young's Modulus (Nm^{-2})
E_a	Activation energy (J)
E_c	Particle fracture energy (J)
Ei_n	Grinding energy input (kWh/tonne)
E_m	Specific energy required to achieve a specific product quality (Jkg^{-1})
e^-	Electron
F	Force (Nm^{-2})
F_c	Particle fracture force (N)
f	Proportion of remaining LORs having removed outliers ()

f_{opt}	Optimal proportion of LORs removed to give minimal error ()
h	Cylindrical coordinates position in h (m)
K	Reaction rate (s^{-1})
LOR	Line of Response
l	Distance from pot wall (m)
l_0	Position of pot wall ()
M	Gradient of the voltage-time plot (Vs^{-1})
m	Mass (kg)
$\dot{m}_p$	Production rate (kgs^{-1})
$m_{p,Ch}$	Solids mass of the charge (kg)
N	Number of particles in a volume ()
N_{block}	Number of grinding media particles in a block volume ()
N_C	Number of stress events/ Media-media collisions ()
N_{GM}	Number of grinding media particles in the mill ()
N_{LOR}	Number of LORs used for a location ()
N_{opt}	Optimal value of N to give minimal error ()
N_p	Number of feed particles ()
N_{rev}	Number of revolutions of the stirrer (s^{-1})

n	Neutron
occ_{block}	Occupancy of a specific block volume ()
P_{GC}	Power consumed within the grinding chamber (W)
P_s	Probability a stress event results in fracture ()
p	Proton
R	Universal gas constant (J)
s	Sensitivity (NV^{-1})
S	Surface energy (J)
S_a	Average roughness of a surface (m)
SE	Stress energy (J)
SE_{GM}	Stress energy of the grinding media (J)
SI	Stress intensity (Jm^{-3} or Nm^{-2})
$S_{i(x)}$	Cubic spline
SN	Frequency with which feed particles are stressed ()
S_q	Root mean square roughness (m)
$Strength_{mean}$	Mean strength of a calcium carbonate particle (Nm^{-2})
$Stress_{mean}$	Mean stress exerted by a grinding media at a collision (Nm^{-2})
T	Temperature (K)

T_C	Coincident rate (s^{-1})
T_{end}	Grind time (s)
t	Time (s)
t_{ch}	Dispersion time (s)
U	Total strain released (J)
U^*	Strain energy (J)
u	Speed (ms^{-1})
V	Volume (m^3)
V_{GC}	Volume of the grinding chamber (m^3)
v_{GM}	Velocity of a grinding media particle (ms^{-1})
V_{PD}	Voltage (V)
V_m	Average volume of a grinding media particle (m^3)
v_{max}	Tip speed of the impeller (ms^{-1})
V_{tot}	Volume of block (m^3)
v	Velocity/ speed (ms^{-1})
v_t	Tip speed velocity of the impeller(ms^{-1})
v_x	Velocity in x (ms^{-1})
v_y	Velocity in y (ms^{-1})

v_z	Velocity in z (ms^{-1})
W	Spatial resolution of the camera (m^3)
x	Maximum distance between two media particles when a feed particle can still be stressed (m)
y	Average distance between two particles in suspension (m)
Z	Collision rate (s^{-1})
$Z_{kWh/tonne}$	The grinding media collisions per kWh/tonne
Z_{tot}	The total number of grinding media collisions
$Z(x,y)$	Function representing the height of the surface dimension x and y ()
β	Crack width (m)
β^+	Positron
Υ	Specific surface energy (Jm^{-2})
Υ_p	Photon pair
Δ	Precision (m^3)
Δ_c	Deformation at the onset of fracture (m)
Δ_x	Deformation (m)
ε	Strain ()
ε_{GM}	Porosity of the grinding media at rest ()

θ	Cylindrical coordinates position in θ (°)
ν	Neutrino
ρ	Cylindrical coordinates position in ρ (m)
ρ_{GM}	Density of the grinding media (kgm^{-3})
σ	Stress (Nm^{-2})
σ_x	Collision cross-section (m^2)
σ_c	Particle compressive strength (Nm^{-2})
σ_f	Fracture stress (Nm^{-2})
Φ	Filling ratio ()

1 INTRODUCTION

1.1 PROJECT BACKGROUND

After the initial ore extraction, both metaliferous ores and industrial mineral feedstocks are often subjected to grinding processes, either to improve liberation and beneficiation or to improve the functionality. However, grinding processes, especially ultrafine grinding processes, are energy inefficient with a majority of the input energy being dissipated as heat and noise. It is estimated that grinding processes are only between 3 and 26 % efficient and accounts for 0.5% of the world's total energy consumption (Tromans, 2008).

Grinding machines are designed to reduce mineral or metal ore product size by imparting sufficient stress to the feed material to cause breakage (Kwade, 1999_A). The fine grinding of metal ores and minerals (sub 20 microns) is frequently carried out using stirred media mills instead of tumbling and other rotating mills. This is because the impact motion from an impeller results in greater stress intensities being imparted on the charge. These operations are usually performed wet to reduce agglomeration effects (Mingzhao, et al., 2004)

1.2 STIRRED MEDIA MILLS

Stirred media mills are essentially a stirred vessel containing both grinding media and mineral slurry phases. The impeller is usually mounted vertically to reduce installation costs and utilises either rotating disc or pins to fluidise the mill charge (Lofthouse & Johns, 1999). As the impeller rotates, grinding media in the vicinity is accelerated and takes up kinetic energy. This high velocity media then collides with lower velocity media away from the impeller and loses energy which can be used for comminution (Kwade, 1999_A).

Vertically stirred media mills have been under development for many years. Designs have evolved from simple pin mills to recent sophisticated tower designs (Jankovic, 2003). Energy efficient operation of such mills remains a key objective especially as energy requirements increase as product particle size distribution decreases (Klimpel, 1997).

1.3 CALCIUM CARBONATE

Calcium carbonate ($CaCO_3$) is a highly abundant natural material which comprises more than 4% of the Earth's crust (Tegethoff, et al., 2001) and is a highly important industrial mineral with a number of applications in the aggregates and additives/ fillers industries (Kogel, et al., 2006). It is estimated that 15-20 Mt of calcium carbonate per year is finely ground to improve functionality (Kogel, et al., 2006).

Ground Calcium Carbonate (GCC) is a key material for Imerys accounting for €550 M sales a year (Imerys, 2014). Although calcium carbonate occurs as chalk, limestone and marble deposits (Tegethoff, et al., 2001), many industrial processes, including some of those at Imerys, utilise marble feedstocks. The marble is mined and processed to achieve a d90 of as fine as 2μm for use predominantly in the paper, plastic and paint industries (Fortier, et al., 2004).

1.4 AIMS AND OBJECTIVES

Particulate materials in a vertically stirred media mill are fractured as grinding media collide and apply sufficient stress to break trapped feed particles. Therefore the comminution process is determined by two factors, the frequency with which the feed particles are stressed (number of stress events) and the magnitude of the stress exerted at each stress event (Kwade, 1999_B). For a comminution process to be efficient there must be a high number of breakage events with sufficient stress to break the feed particles. Currently, it is unclear where in the mill these criteria are met. However, it is assumed that the optimal conditions occur in the vicinity of the impeller (Kwade, 1999_A).

The aim of the work presented here is to determine the regions within a vertically stirred media mill where breakage can occur. This is to be achieved by: (i) measuring the stress required to fracture calcium carbonate particles at a breakage event and (ii) determining the regions within the mill where such stresses suitable to cause comminution occur.

1.5 MEASURING THE STRESS REQUIRED TO FRACTURE CALCIUM CARBONATE PARTICLES

The fundamental properties of the fracture processes such as force required to fracture a particle can most effectively be understood using controlled fracture experiments on single particles (Salman, et al., 2007). However, such characterisation becomes increasingly difficult when dealing with sizes in the micro and nano size ranges. Here these difficulties were overcome by performing the measurements using a micromanipulator based technique.

1.6 DETERMINING THE REGIONS WITHIN A VERTICALLY STIRRED MILL SUITABLE TO CAUSE COMMINUTION

As grinding media collide kinetic energy is dissipated to surrounding grinding media and the feed material, leading to the assumption that breakage occurs in regions of high acceleration. Positron Emission Particle Tracking (PEPT) is a non-invasive technique for studying the flow in a particulate system by tracking the motion of a radioactively labelled tracer particle. In previous papers, PEPT has been used to measure flow patterns in vertically stirred mills to understand a number of performance indicators and to validate computational models (Conway-Baker, et al., 1999; Conway-Baker, et al., 2002). Here PEPT is utilised to measure the force acting on the irradiated grinding media particle to determine where in the mill the force acting on the tracer is greater than the force required to fracture the calcium carbonate feed material.

1.7 THESIS OUTLINE

This thesis comprises seven chapters. Chapter 1 is an introduction. Chapter 2 outlines the theoretical background of the work. In Chapter 3, the materials and methods are described, along with a description of the PEPT data handling. In Chapter 4 the results of laboratory scale grinding experiments are discussed and the effect of varying a range of operating parameters are reported. In Chapter 5 a micromanipulation technique was used to determine the fracture properties of calcium carbonate particles in the size range of 5-30 μm. There are two parts to Chapter 6. In the first part a detailed PEPT analysis of a standard laboratory grind is described. In the second part the PEPT analysis is used to understand the effects of changing the mill operating parameters. In Chapter 7 the conclusions of the work are summarised and suggestions for further work are given.

2 LITERATURE REVIEW

2.1 FRACTURE MECHANICS IN COMMINUTION

Comminution is defined as the process by which particulate materials are reduced from a coarse feed size to a smaller final size for downstream processing or end use by imparting sufficient stress to cause cracks to propagate through the feed particles which split into smaller fragments (Wang & Forssberg, 2007; Kwade & Bernotat, 2002). Particle breakage within comminution equipment is dependent on: (i) the material properties of the feed material, (ii) the stressing conditions exerted and (iii) the environment encountered (Tavares, 2007).

2.1.1 Material properties

The material properties relevant to particle breakage are fracture strength and deformation behaviour (Tavares, 2007). Fracture strength is defined as the energy or stress required to fracture a feed particle (Tavares, 2007; Kwade, 1999_A) and material deformation is defined as either elastic or inelastic (Askeland, et al., 2006).

2.1.1.1 Deformation Behaviour

Deformation behaviour is dictated by defects within a material's crystalline structure (Callister, 2001). These defects are defined as lattice irregularities which deviate by one or more atomic diameter from the idealised atomic or ionic arrangement (Askeland, et al., 2006). Several imperfection types exist including: (i) point, (ii) line (dislocations) and (iii) surface defects. However, dislocations are responsible for different deformation behaviours (Askeland, et al., 2006; Callister, 2001).

A dislocation is a defect around which at least one of the atoms in the lattice is misaligned. Figure 2.1-1 shows a visualisation of the atoms and bonds around a dislocation. If a shear stress is applied, acting in parallel to the dislocation, the bonds between the atoms adjacent to the dislocation can be broken and new bonds formed with the atoms at the edge location. Therefore the dislocation has shifted from its original position to the exterior of the crystal resulting in a permanent rearrangement in the crystalline structure.

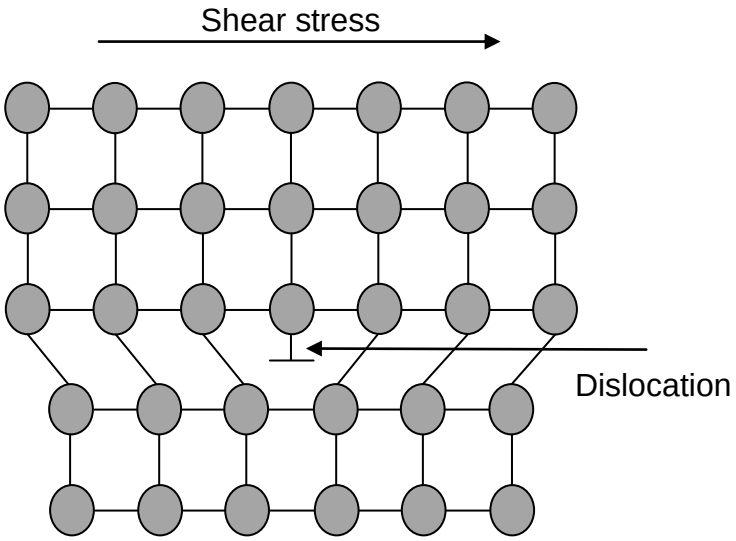

Figure 2.1-1 Visualisation of a dislocation within a crystalline material (Askeand, et al., 2006)

Elastic deformation is a time independent temporary change in shape that occurs when a stress is applied to a material. After the stress is removed, the material returns to its original shape. The change in shape results from the stretching of the interatomic bonds, and no dislocation movement occurs (Askeland, et al., 2006).

Plastic deformation however, is an irreversible change in shape that remains after the stress is applied. Plastic deformation results from the applied stress causing dislocation movement rearranging the crystalline structure of the material (Askeland, et al., 2006).

Ceramic materials tend to only exhibit elastic behaviour even though dislocations are present within the material. However, the strength of the ionic bonds are sufficiently large that other failure criteria are met before dislocations can move. Therefore ceramic materials can be assumed to undergo elastic deformation up to the point of failure.

2.1.1.2 Fracture strength

Fracture occurs when the maximum nominal stress at a point within the material exceeds the strength of the atomic bonds between the material's atoms. This however only holds true for systems with uniform stress fields such as perfect crystals. Materials with irregular stress fields containing stress concentrations (which result from shape effects, surface flaws and cracks within the material) tend to fail at stresses lower than the strength envelope of the material (Sun & Jin, 2012).

Figure 2.1-2 (a) shows a visualisation of the stress experienced when a material with a crack (length a_l) is loaded by a stress (σ) (Gope, 2012). It can be seen that the material bordering the crack is unloaded whilst the remaining material continues to be stressed. This results in a stress concentration at the crack tip where the stress of the unloaded region is exerted. Early attempts to predict fracture strength could not account for sharp cracks because stresses would approach infinity at the crack tip. Therefore the material would be predicted to have near zero strength. To overcome

this, Griffith developed an energy-balance method which uses the strain energy (U^*) per unit volume (V) as shown in Equation 2.1-1 (Griffith, 1921) to predict fracture strength of a material

$$U^* = \frac{1}{V}\int F dx = \int \sigma d\varepsilon \qquad \textbf{Equation 2.1-1}$$

where F is the force applied and ε is the strain.

If the material is elastic (Young's modulus (E) equals the stress divided by the strain) then the strain per unit volume is shown in Equation 2.1-2.

$$U^* = \frac{\sigma^2}{2E} \qquad \textbf{Equation 2.1-2}$$

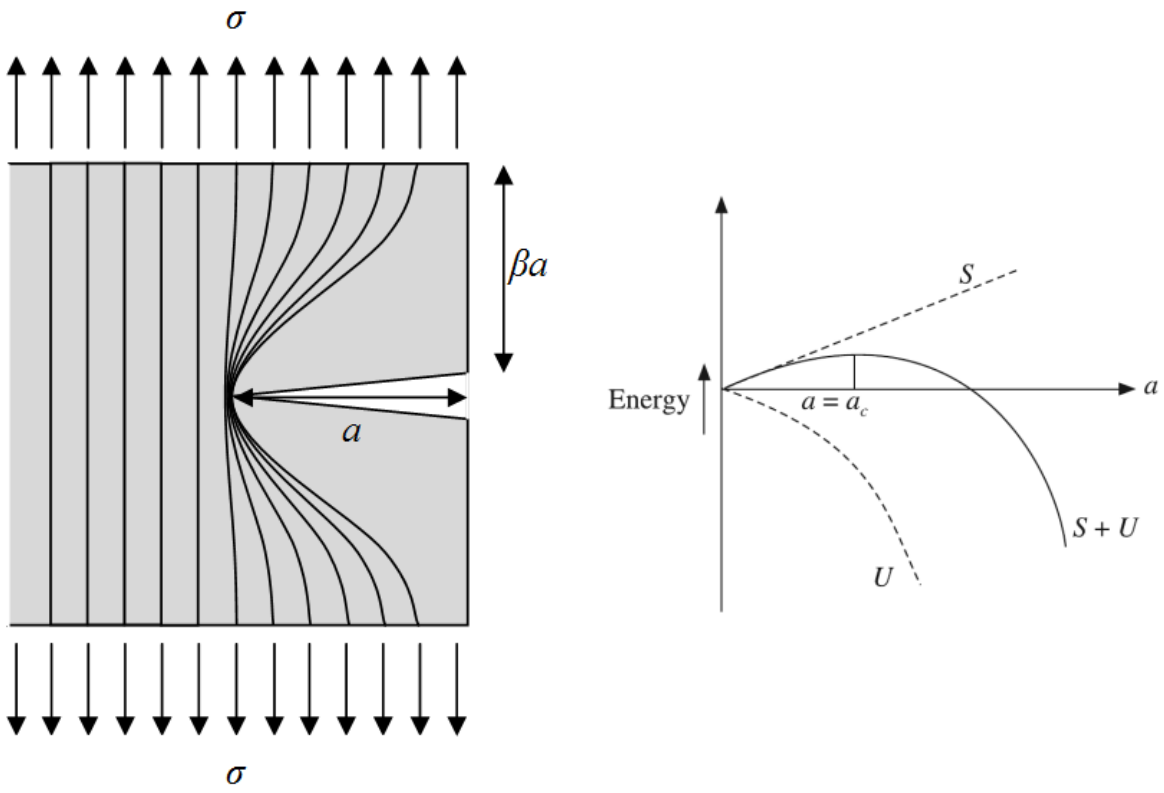

(a) (b)

Figure 2.1-2 (a) Unloaded region around a crack (b) Energy fracture balance (Gope, 2012)

The unloaded region can be represented as two triangular regions either side of the crack with length a_l and height βa_l. Therefore the total strain energy released (U) at the crack tip equals the strain energy per unit volume multiplied by the volume of the unloaded region. If the strain energy at the crack tip exceeds the energy required to break the internal bonds within the material (surface energy (S)) the crack will grow and new surfaces will be created. Equation 2.1-3 and Equation 2.1-4 show the strain energy released at a crack tip and surface energy required to create new surfaces when $\beta = \pi$

$$U^* = \frac{-\sigma^2}{2E}\pi {a_l}^2 \qquad \textbf{Equation 2.1-3}$$

$$S = 2\gamma a_l \qquad \textbf{Equation 2.1-4}$$

where γ is the specific surface energy (Jm^{-2}).

Figure 2.1-2 (b) shows the stress energy and energy released as a function of crack size. The total energy associated with the crack is the sum of the energy absorbed to create new surfaces minus the strain energy liberated. At small crack sizes the surface energy is greater than the energy released at the crack tip and additional stress is required to fracture the material. However at a critical crack length (a_c) the energy released at a crack tip becomes greater than the stress energy and crack growth is spontaneous and catastrophic. Critical crack growth occurs when $S = U$. Therefore fracture stress (σ_f) is proportional to the square root of the surface energy and Young's modulus of the material and inversely proportional to the length of the crack as shown in Equation 2.1-5.

$$\sigma_f = \sqrt{\frac{2E\gamma}{\pi a_l}}$$ **Equation 2.1-5**

As the size of a particle decreases it can be assumed that cracks are distributed randomly throughout a particle, and therefore the number of cracks present within a particle decreases as the particle size decreases (Yashima & Kanda, 1987). In comminution processes (especially when grinding ultra-fine particles) it can also be assumed that the size of the cracks decreases as particle size decreases as previous upstream processing would result in fracture at any larger cracks present. Therefore because Equation 2.1-5 shows that the stress required to fracture a particle (and therefore the strength of the particle) is dependent on the largest crack within its volume, the fracture strength of a particle is dependent on particle size.

Particle strength data are frequently represented using the specific energy required to fracture a particle (Sikong, et al., 1990; Yashima & Kanda, 1987). Figure 2.1-3 shows the relationship between the energy required to fracture a particle (E_c) and specific energy (E_c/m (where m is the mass of the particle)) for borosilicate glass spheres ranging in size from 10 to 0.01 cm diameter (Yashima & Kanda, 1987). It can be seen that as particle size decreases the energy required to fracture a particle decreases, but the specific energy increases.

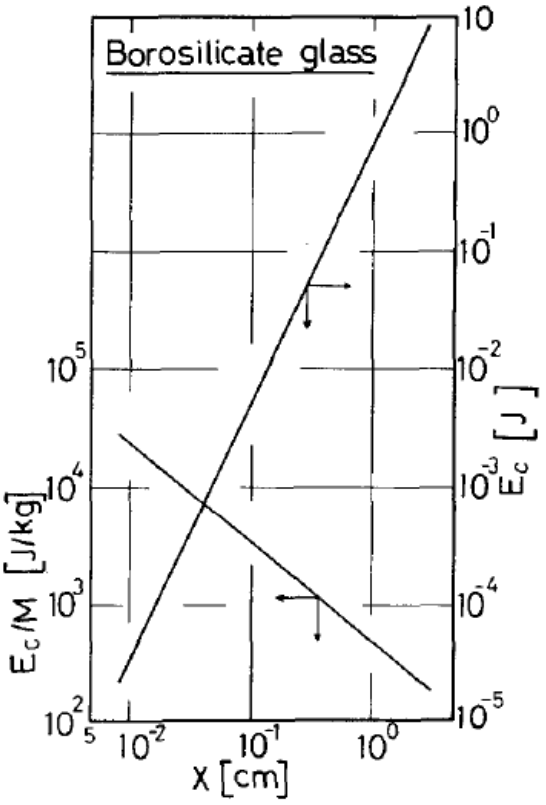

Figure 2.1-3 Relationship between size X and specific fracture energy E_c/M or fracture energy E_c for borosilicate glass (Yashima & Kanda, 1987)

Particles of the same material within a comminution process exhibit variations in size, shape and cracks (King, 2001). Therefore it is very difficult to know the exact stress required to fracture a particle. Figure 2.1-4 shows cumulative distributions of the specific fracture energies required to fracture two quartz samples of differing size (3.35-4.00 mm and the second 0.5-0.7 mm) (Bourgeois, 1993). It can be seen that the specific fracture energy varies within each sample. The specific fracture energy for the 3.35-4.00 mm quartz varies between 0.01 and 0.25 Jg^{-1} and the 0.5-0.7 mm quartz varies between 0.1 and 1.2 Jg^{-1}.

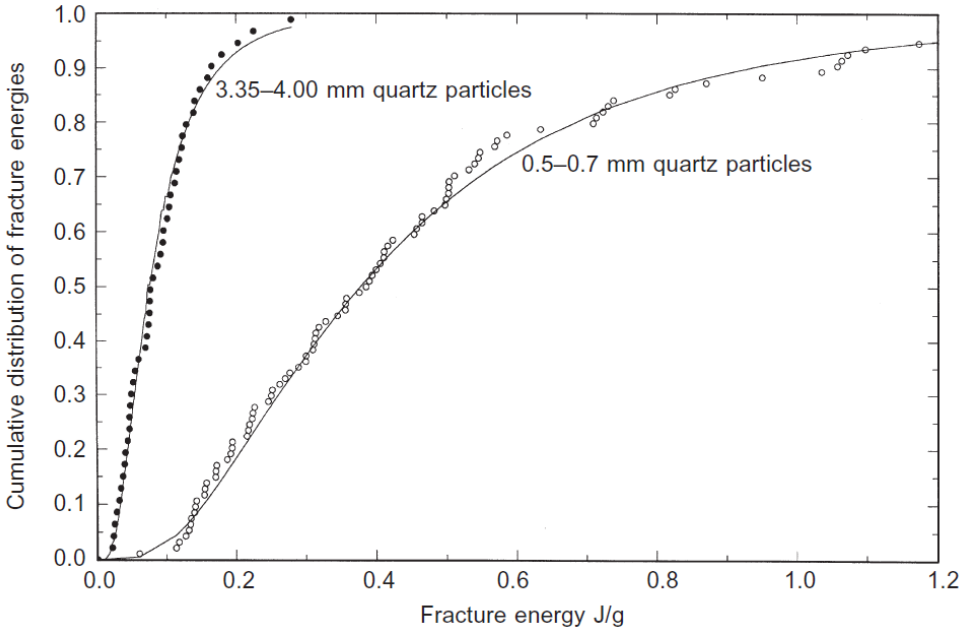

Figure 2.1-4 Measured distribution of particle fracture energies for two sizes of quartz particles (Bourgeois, 1993)

A cumulative distribution of the specific fracture energies can also be used to determine the probability of fracture when a feed particle experiences a given specific fracture energy (King, 2001). The sample size used in Figure 2.1-4 to determine the cumulative distribution of specific fracture energies was considered representative of the entire population. Therefore if a population of 0.5-0.7 mm quartz particle experience 0.2 Jg^{-1} of specific energy then approximately 15 % of the particles will be fractured. However if a population of 3.35-4.00 mm particles experience 0.2 Jg^{-1} then approximately 85 % of the population will be fractured. Thus the probability of fracturing decreases from 85 % to 15 % as quartz particle size decreases from 3.35-4.00 mm to 0.5-0.7 mm particles.

At a certain particle size the yield strength will become greater than the fracture strength and thus reach the brittle-plastic region (Kendall, 1978; Sikong, et al., 1990). At this point particles become ductile and are flattened when compressed instead of fractured. It is estimated that the fracture limit for calcium carbonate is around 1 μm (Kendall, 1978) although plastic yielding as opposed to brittle behaviour has been observed at 2-3 μm in other studies (Sikong, et al., 1990).

2.1.2 Stressing conditions

The stressing conditions dictate how stresses are imparted by the comminution equipment to the feed particles. Particle breakage is considered to occur via one or more of four methods: (i) impact, (ii) compression, (iii) attrition and (iv) abrasion (Prasher, 1987). However, two of the methods are said to be more common in comminution processes: (i) the major mode, impact, where a particle is subjected to the rapid application of compressive stress resulting in the parent particle shattering, producing a broad spectrum of progeny particles and (ii) the minor mode, attrition, where the stress at a breakage event is not sufficient to fracture the parent particle, the particle remains largely the same size, but becomes more rounded as daughter particles are chipped off. Industrial comminution processes typically utilise impact stressing conditions and as a result particle shattering is the most common breakage method (Tavares, 2007; King, 2001).

The rate at which stresses are imparted to a material can affect the strain field within a particle. As a particle is impacted a wave of elastic strain energy propagates through the solid and is distributed throughout the particle. The conditions of the stress field can change due to internal reflections of the wave if the impact time is shorter than time to propagate through the particle (Tavares, 2007). However this is unlikely, as for this to occur in a particle the impact speed must be in excess of 100 ms^{-1} assuming elastic deformation behaviour (Schonert, 1991). Inelastic behaviour is more dependent on strain rate. Therefore throughout the work presented here it is assumed that as long as the particles examined exhibit elastic behaviour, the strength of the material is independent of stressing rate.

2.2 STIRRED MEDIA MILLS

Comminution equipment selection is dependent on the material properties and desired particle size of the feed material to be ground (Sikong, et al., 1990). Particle size is generally classified as coarse, intermediate, fine and ultrafine (Wang & Forssberg, 2007). However, as shown in Figure 2.2-1 energy requirements increase as feed particle size decreases (Wang & Forssberg, 2007).

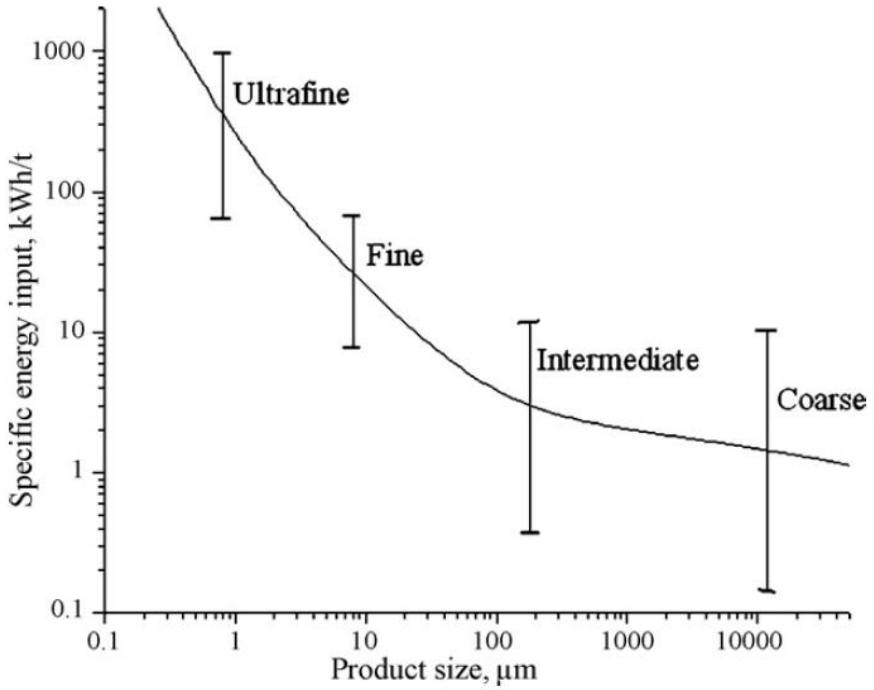

Figure 2.2-1 Required energy for size reduction in comminution (Wang & Forssberg, 2007)

Due to their high unit output and high-energy efficiency when compared to other techniques, stirred media mills are frequently utilised to achieve ultra-fine particle sizes (Tamblyn, 2009). A stirred media mill consists of a stationary grinding chamber and a high speed impeller made up of discs or pins. The charge added to the chamber is typically made up of grinding media and mineral slurry (mineral, water and possibly other additives) which, as the impeller rotates, are fluidised (He, et al., 2006).

The vertically stirred mill used throughout this work was first developed by English China Clays in the 1960s to grind minerals such as calcium carbonate at high solids fractions (75 % by weight) to ultrafine particle sizes at laboratory scale (Lofthouse & Johns, 1999). Vertically stirred mills can be operated in a batch or continuous manner. At full scale, grinders are usually run continuously with a number of grinders in a cascade. However at laboratory scale, for ease of operation, a batch process is usually utilised.

2.3 FACTORS WHICH AFFECT COMMINUTION EFFICIENCY

A comminution process is considered most efficient if the required product quality is achieved in the shortest production time and lowest operational cost (Kwade, 2006). The main parameters which affect production rate $\dot{m}_p$ are given below in Equation 2.3-1

$$\dot{m}_p = \frac{m_{p,Ch}}{t_{Ch}} = \frac{P_{GC}}{E_m} \qquad \textbf{Equation 2.3-1 (Kwade, 2006)}$$

where $m_{p,Ch}$ is the solids mass of the charge, t_{Ch} is the dispersion time of the charge, P_{GC} is the power consumed inside the grinding chamber and E_m is the specific energy required for a specific product quality.

Maximum production rate and therefore efficiency is achieved if the power draw consumed is at a maximum and the specific energy required to achieve a desired product size is reduced to a minimum. In order to improve production rate efficiency it is important to understand what parameters have the greatest effect on production rate.

A number of mill parameters affect grinding performance (Jankovic, 2003). Although many of these only have a minor effect on performance, the most important have been extensively studied (Jankovic, 2003; He, et al., 2006). These include: (i) mill design (ii) impeller speed (iii) grinding media composition and (iv) slurry composition.

2.4 BREAKAGE MECHANISM

For a grinding process to be efficient two criteria must be fulfilled (Kwade, 1999_B): (i) the number of times a feed particle is stressed must be high enough for comminution to occur at an appreciable rate and (ii) the stress exerted at a breakage event must be sufficient to break the feed particles. Therefore for a breakage mechanism to be efficient, individual breakage events must occur frequently. Although it is still unclear where in the mill breakage occurs (Kwade, 1999_A) it is proposed that as the impeller rotates the grinding media and mineral are fluidised resulting in regions of high velocity around the impeller and low velocity elsewhere in the mill. Because the resultant shear forces are too low to fracture a crystalline material (Kwade, 1999_A) it can be assumed that breakage can only occur when grinding media particles with high velocity collide with grinding media particles with lower velocity with enough stress to fracture the particle. From this it can be inferred that the comminution process is determined by: (i) the stress of a collision between media particles being sufficient to fracture the feed material and (ii) how often each feed particle is stressed.

2.4.1 Stress at a collision

The stress required to fracture particles at a collision is dependent on the number of particles stressed at a collision. Work determining the number of particles trapped in a collision was introduced by Kwade in 1999 (Kwade, 1999_A). The following section outlines his work. Figure 2.4-1 shows two grinding media colliding and stressing a feed particle. The volume highlighted indicates the region where particles must be to be trapped during a collision, and corresponds to the volume in which a particle size (x) is captured between grinding media with a diameter d_{GM}. This only occurs if the particles are not carried with the displaced fluid, and if the mineral phase is fully dispersed.

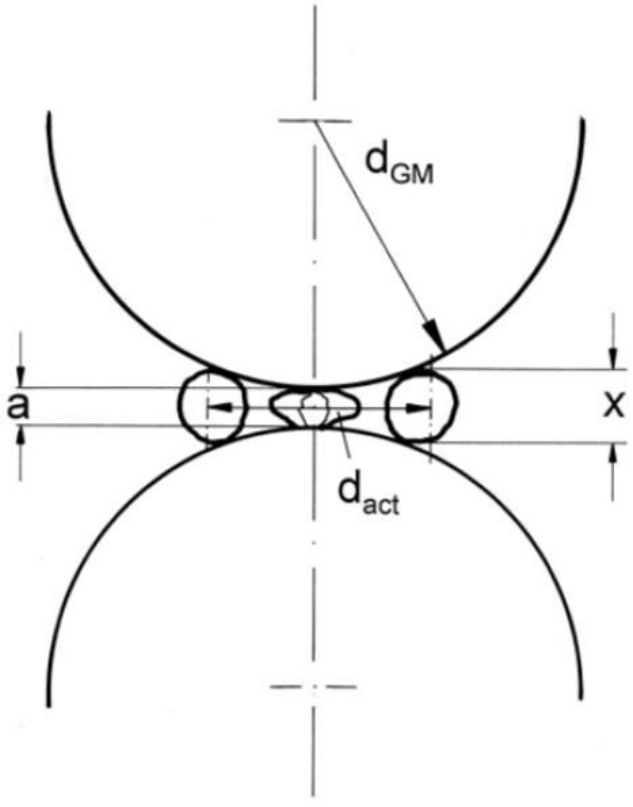

Figure 2.4-1 Active volume where particles can be stressed between grinding media (Kwade 1999_A)

Depending on the number of particles present in the active volume, three cases exist:

1. Only one particle is captured, which is stressed with the entire force or energy of the collision.
2. More than one particle is stressed, and all particles are stressed independently of each other. Here the particle which has the smallest distance between the media is initially stressed with the maximum force or energy of the collision, and then other particles are stressed with considerably reduced effect.
3. A particle bed is captured and stressed. If this occurs then the stress of the collision is divided and dependent on the number of particles in the active volume.

The number of particles captured in the active volume can be evaluated by calculating the ratio between the diameter of the active volume (d_{act}) and the average distance between two particles in suspension (y). As shown in Equation 2.4-1.

$$\frac{d_{act}}{y} = \sqrt[3]{\frac{6c_v}{\pi}} \sqrt{2(1-a')\frac{d_{GM}}{x} + 1 - a'^2} \; ; \quad a' = \frac{a}{x}$$

Equation 2.4-1 (Kwade, 1999_A)

where c_v is the solids concentration by volume of the suspension and *a* and *x* are the minimum and maximum distance between of grinding media respectiely when the feed particle is stressed. The diameter of the active volume is shown in Figure 2.4-1 as the maximum distance between the media centreline where a particle could still be trapped.

The ratios of d_{act}/y obtained for different relative distances ***a'*** at a solids volume concentration of 0.2 is plotted against the ratio between media and particle size (d_{GM}/x) in Figure 2.4-2.

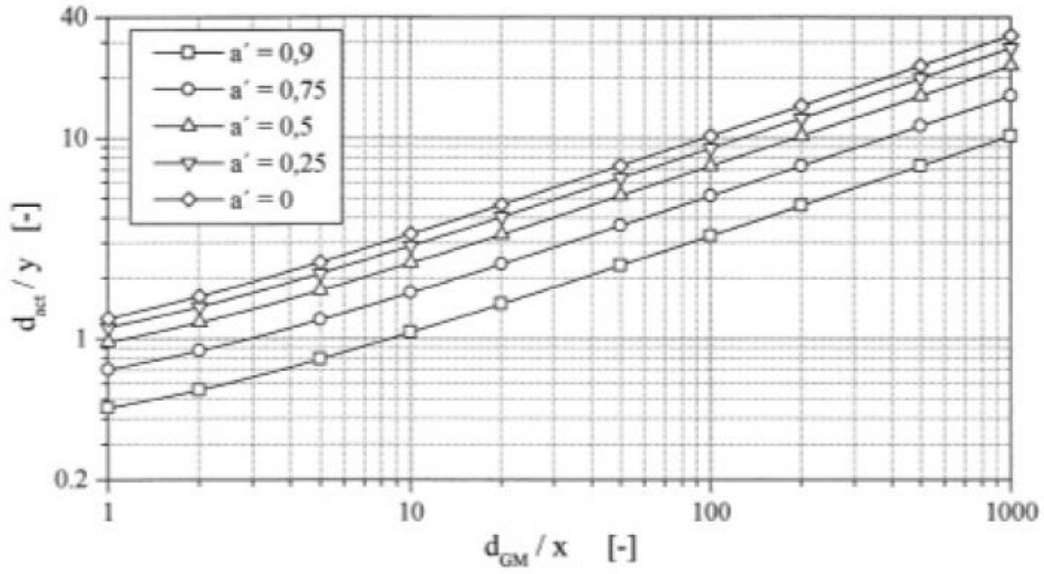

Figure 2.4-2 Ratio d_{act}/y as function of ratio d_{GM}/x for different a' (Kwade, 1999_A)

Figure 2.4-2 also shows that media size has a critical effect on grinding efficiency. Assuming it is desirable to stress only one particle at a breakage event according to Kwade the diameter ratio d_{GM}/x must be selected such that d_{act}/y is less than 4. If ***a'*** equals 0.5, a diameter ratio d_{GM}/x of 30 is required to stress only one particle at a collision. Therefore to grind a 50 µm feed particle the media selected must be smaller than 1500 µm.

Although Kwade states that the ratio of d_{act}/y of four or more is required to capture more than one particle, the ratio of d_{act}/y required to capture more than one particle increases as particle size decreases. However, the investigation showed that at 1 µm the suspension viscosity increases and that the freedom of motion of the particles decreases which would potentially allow more than one particle to be stressed. It is suggested though that to stress a bed of particles would require particle sizes less than 1 µm.

Kwade's work is carried out at solid concentrations of 20 % by volume. Industrial grinding processes are usually performed at solids volume concentrations as high as 54 % by volume to improve plant efficiency and improve overall throughput. It is unclear from the work presented how many particles would be stressed at a collision. Throughout the course of this work it is assumed that only one particle is stressed at a collision.

2.4.2 Stress number and stress intensity models

Tamblyn outlined the different approaches for modelling stirred media mills (Tamblyn, 2009) and suggests that the most established are the stress number and stress intensity models, based on the work presented in the previous section developed by Kwade (Kwade, 1999-A; Kwade 1999_B).

As discussed, breakage can occur as feed particles are trapped and sufficiently stressed between grinding media particles. Therefore the frequency with which feed particles are stressed (stress number (*SN*)) in a batch is dependent on the number of collisions between the grinding media particles (stress events (N_C)), the probability that a particle caught is sufficiently stressed to cause fracture (P_s) and the number of feed particles (N_p) as shown in Equation 2.4-2.

$$SN = \frac{N_c P_s}{N_p} \qquad \textbf{Equation 2.4-2}$$

The number of collisions between grinding media particles are assumed to be proportional to the number of impeller rotations (N_{rev}), the grind time (t) and the number of grinding media particles within the mill (N_{GM}) as shown in Equation 2.4-3. The filling ratio of the mill (ϕ) and porosity ($\boldsymbol{\varepsilon}_{GM}$) of the bulk grinding media within the pot chamber (V_{GC}) gives an estimation of the volume the media occupies. Therefore packing fraction is also important to the number of media collisions.

$$N_c \propto N_{rev} t N_{GM} \propto N_{rev} t \frac{V_{GC}\phi_{GM}(1-\varepsilon_{GM})}{\frac{\pi}{6} d_{GM}^3} \qquad \textbf{Equation 2.4-3}$$

where d_{GM} is the diameter of a grinding media particle.

As the mill contents are fluidised, air is entrapped within the charge so it is not possible to determine the volume in which the media are present. Therefore it is currently not possible to measure the porosity of the charge during mixing. An improvement to the stress number model could be made by measuring the volume in which the grinding media are located. An attempt to improve the measurement of media-media collisions using collision frequency of perfect gases is found in Section 3.2.5.

The stress intensity (*SI*) model states that the stress intensity of a collision is proportional to the stress energy (*SE*) imparted to a feed particle as a faster moving media particle collides with a slower particle as shown in Equation 2.4-4

$$SI \propto SE \propto d_{GM}^{3} \rho_{GM} v_t^2 \qquad \textbf{Equation 2.4-4}$$

where d_{GM} is the diameter of the grinding media, ρ_{GM} is the density of the grinding media and v_t is the tip speed velocity of the impeller.

The model assumes that (directly quoted from (Stender, et al., 2004)):

1. Only single particles are stressed intensively between two grinding media and therefore the stressed particle volume does not depend on the size of the grinding beads.
2. The tangential velocity of the grinding beads is proportional to the tip speed of the disks (impellers).
3. The mill size and geometry stay constant.
4. The displacement of the suspension between two approaching grinding media causes no essential decrease of the media velocities and, thus, of the kinetic energy of the two grinding media.
5. The elasticity of the feed material is much smaller than that of the grinding beads and therefore the kinetic energy of the beads is nearly completely transferred to the feed particles and not partly consumed by the deformation of the beads.

In real world comminution processes feed particles are not stressed equally by the average stress energy at each stress event. Therefore stress energy can only be fully described by a distribution (Kwade, 2006). Figure 2.4-3 shows the frequency distribution of stress energies within a mill. It can be seen that the frequency of high energy collisions is low compared to the frequency of low energy collisions. This is because high stress collisions only occur in small regions around the impeller (Stender, et al., 2004). It is currently not possible to measure such distributions so the model relies on the average stress energy (Kwade, 1999_B; Kwade, 2006).

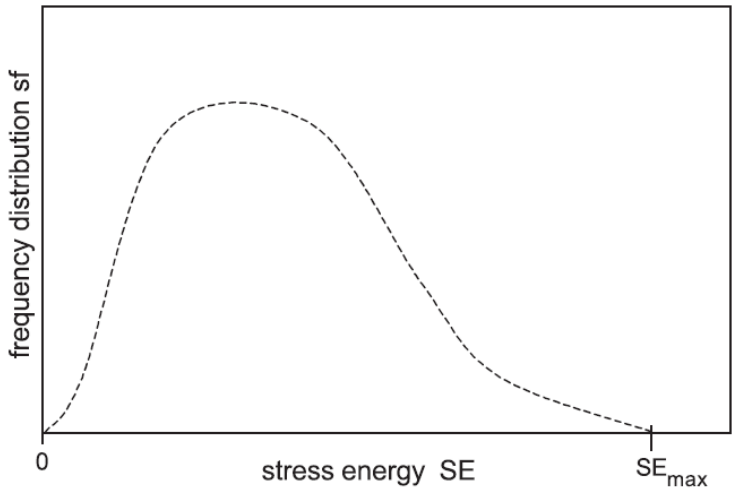

Figure 2.4-3 Qualitative frequency distribution of the stress energy in a stirred media mill (Stender, et al., 2004)

2.5 MEASUREMENT TECHNIQUES TO DETERMINE PARTICLE COMPRESSIVE STRENGTH

The fundamental properties of fracture processes can be most effectively understood using controlled experiments on single particles (Tavares & King, 1998). Numerous techniques exist which can be utilised to measure the compressive strength of a particulate material depending on the stressing conditions and particle size (King, 2001; Tavares, 2007; Sikong, et al., 1990; Yap, et al., 2006). These techniques are classified depending on their contact points: (i) single impact, (ii) double impact or (iii) slow compression (Tavares, 2007).

Within a vertically stirred mill it is assumed that breakage occurs when a slow moving grinding media is impacted by a faster moving particle, therefore double impact conditions are assumed. Double impact tests are carried out using drop weight, pendulum and impact load cells (Tavares & King, 1998; Tavares, 2007). However, characterisation becomes increasingly difficult when stressing ultrafine particles.

Micromanipulation techniques have been developed to measure a number of fracture properties of numerous micron sized materials including microcapsules, pharmaceuticals, minerals and coals (Zhang & Stenson, 2009; Yap, et al., 2006; Kendall, 1978; Sikong, et al., 1990). A micromanipulator is a device consisting of a force transducer and a load cell which physically interacts with single particles under a microscope. As a single particle is compressed between two parallel surfaces the force acting on the particle is recorded. This allows measurements of the particle fracture energy (E_c) and particle fracture strength or stress (particle compressive strength (σ_c)) required to fracture a particle as shown in Equation 2.5-1 and Equation 2.5-2 respectively

$$\frac{E_c}{m} = \int_0^{\Delta_c} \frac{F_c}{m}\, d\Delta_l$$ **Equation 2.5-1**

$$\sigma_c = \frac{4F_c}{\pi d^2}$$ **Equation 2.5-2**

where Δ_l is the deformation, F_c and Δ_c are the force and deformation at the onset of fracture respectively, m is the mass of the particle and d is the particle diameter.

2.6 POSITRON EMISSION PARTICLE TRACKING (PEPT)

Positron Emission Particle Tracking (PEPT) allows the non-invasive study of flow parameters in particulate systems by tracking the motion of a radioactively labelled particle. This technique has been utilised to better understand a number of industrial processes including the flow patterns of grinding media within a vertically stirred mill (Conway-Baker, et al., 1999; Conway-Baker, et al., 2002).

PEPT was developed in the 1990s at the University of Birmingham from the medical imaging technique Positron Emission Tomography (PET) (Parker, et al., 1993). PET maps the concentration and distribution of a radioactive species to produce a 3D image and PEPT tracks a single radioactive particle as it moves through a system in three dimensions. When using PET, data must be collected over a large time period (minutes to hours) to generate statistically accurate images and thus PET is rarely used for industrial dynamic systems. However, because an irradiated particle acts as a point source, the time required to acquire sufficient information to produce a statistically meaningful measurement is greatly reduced and therefore PEPT can be used to study dynamic systems. However, to construct an accurate flow field diagram data must be acquired for long enough to ensure that the tracer travels everywhere in the system multiple times (Leadbeater, et al., 2012).

The PEPT tracer added to the system is created by irradiating a particle taken from the bulk material in the system under study and irradiating it with a ^{3}He ion beam from the University of Birmingham MC40 cyclotron to create radio isotopes which undergo beta plus decay (Conway-Baker, et al., 1999; Conway-Baker, et al., 2002). The irradiated tracer produced decays and a proton (p) is converted to a neutron (n), a positron (β^+) and a neutrino (v). This is shortly followed by the released positron annihilating with a surrounding electron (e^-) to produce a back to back 510 keV photon pair ($2\gamma_p$) as shown in Equation 2.6-1 and Equation 2.6-2.

$$p = n + \beta^+ + v \qquad \textbf{Equation 2.6-1}$$

$$\beta^+ + e^- \rightarrow 2\gamma_p \qquad \textbf{Equation 2.6-2}$$

For the studies carried out on stirred media mills some of the oxygen within a single grinding media particle are converted to the beta plus radionuclide ^{18}F which has a half life of two hours (Fan, et al., 2006).

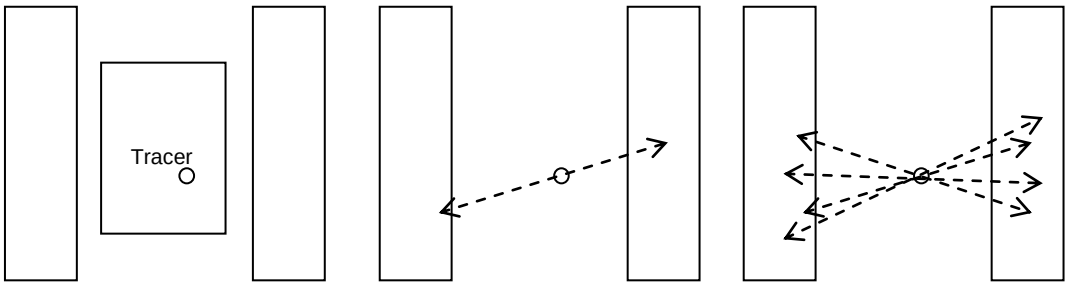

Figure 2.6-1 (a) System placed between positron camera heads (b) Tracer decaying producing photon pair detected by camera (c) Multiple true photon pairs used to triangulate tracer position

The tracer is added to the system and placed within the detectors of a specially adapted gamma camera as shown in Figure 2.6-1 (a). As the tracer decays the detectors, which consist of two sodium iodide scintillator crystals (Leadbeater, et al., 2012; Bakalis & Fryer, 2004) detect the photon pair in coincidence. If both detectors register a photon within a 12 ns timing window the camera calculates a Line of Response (LOR) along which the annihilation must have occurred as shown in Figure 2.6-1 (b). This allows the tracer particle position to be triangulated by using a location algorithm developed at the University of Birmingham to determine the position of the tracer in x,y,z at time t when a predetermined number of photon pairs overlap as shown in Figure 2.6-1 (c). The algorithm includes an automatic correction for random coincidence detections. Randoms are defined as a coincident detection of two photons which do not originate from the same point of annihilation or a scattered photon, both of which result in an LOR which does not represent a true annihilation event.

The location algorithm is an iterative process which aims to determine a common origin of annihilation events for multiple detections (Parker, et al., 1993; Leadbeater, et al., 2012). However a number of the photons detected are random coincidences resulting in a LOR which does not pass through the tracer location. The aim of the algorithm is to discard such events to give an accurate tracer location. Starting with a set number of LORs (N_{LOR}) the position of the tracer is calculated as the position where the sum of the perpendicular distances between LORs is at a minimum (minimum distance point). This point is taken as an initial estimate of the particle location, and the majority of LORs will pass close to or through this location. Those which are furthest from this point are deemed corrupt and removed from the set.

This process repeats until a predefined proportion of the set remain (*f*). Once this is achieved the final position of the tracer is given as the minimum distance point of the remaining LORs (Leadbeater, et al., 2012).

The values *f* and N_{LOR} are variables that must be optimised for a given system to optimise accuracy. The precision (Δ) of a location is given below in Equation 2.6-3 (Leadbeater, et al., 2012)

$$\Delta = \frac{w}{\sqrt{f N_{LOR}}}$$ **Equation 2.6-3**

where *w* is the spatial resolution of the camera. Spatial resolution is defined as the minimum separation distance between two point sources to distinguish them. It is measured as the full width half max (FWHM) of the point source intensity distribution. The spatial resolution of the PEPT camera is 5 mm (Parker, et al., 2008).

Optimal values of *f* and N_{LOR} can be determined using a stationary particle within the system to be investigated.

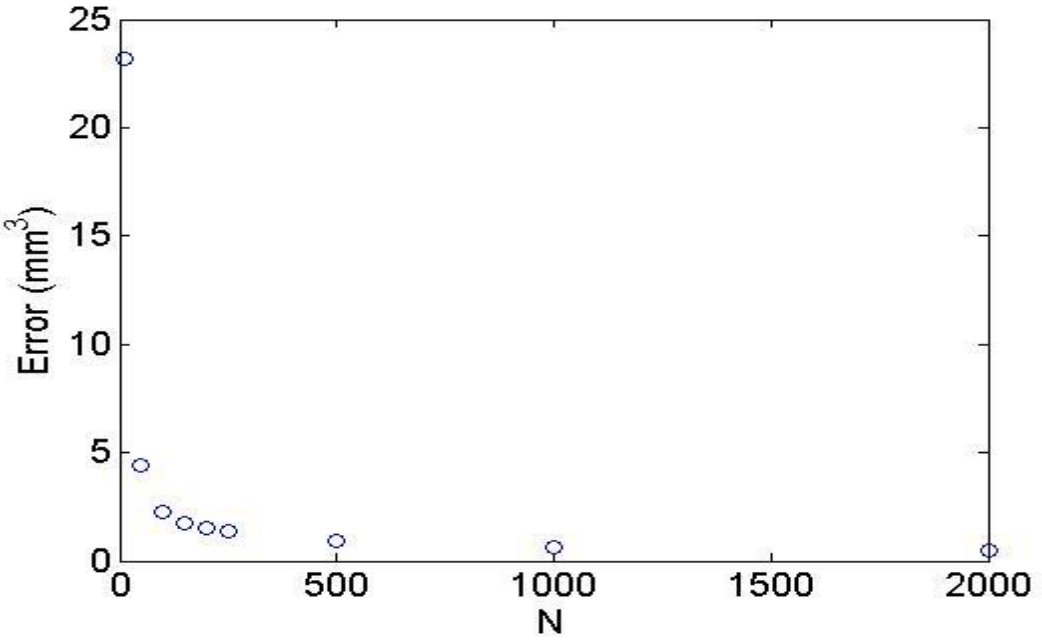

Figure 2.6-2 Location precision of a PEPT tracer by varying the number of LORs used to determine a particle's location

Figure 2.6-2 shows how the precision of a stationary zirconium silicate media particle varies with N_{LOR}. It can be seen that precision becomes arbitrarily small as N_{LOR} is increased as higher amounts of data results in a more accurate location. However this is not true for moving tracers. As the tracer moves, the LORs detected will not converge at a single point but instead be spread throughout the mill. Therefore a smaller value of N_{LOR} must be selected based on tracer velocity. No method currently exists for optimising N_{LOR} as a function of tracer velocity; however, two strategies were outlined (Leadbeater, et al., 2012). They suggest choosing a value of N_{LOR} such that (i) the distance moved by the tracer is similar to the precision of the location or (ii) the distance moved equals the spatial resolution of the camera. They also suggest that the latter approach is more appropriate for PEPT use.

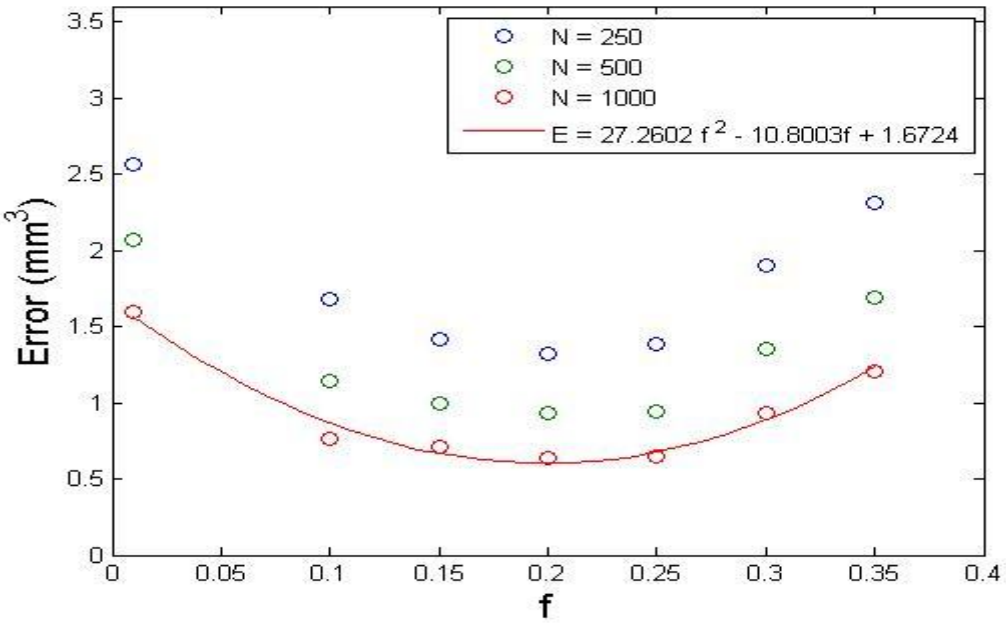

Figure 2.6-3 Location precision of a PEPT tracer particle varying (a) the number of LORs (*N*) and (b) the proportion of LORs (*f*)

Figure 2.6-3 shows how precision varies with *f*. Initially as only a small fraction of the LORs are removed the precision improves. However, if *f* is increased beyond an optimal amount only a small statistical data set remains resulting in Poisson noise dominating measurement precision (Leadbeater, et al., 2012). The optimal vale of f (f_{opt}) for each system is calculated by fitting second order polynomial fit to the data as shown in Figure 2.6-3 and calculating the minima. It can be seen that for this system a value of 0.2 results in optimal precision.

3 MATERIALS AND METHODS

3.1 MATERIALS

3.1.1 Calcium carbonate

Calcium carbonate is a polymorphous variform compound which occurs in three different crystal structures: vaterile, aragonite and calcite. Although all three can exist together calcite is by far the most common and crystallises in a rhombohedral system with a crystal lattice shown in Figure 3.1-1 (Tegethoff, et al., 2001).

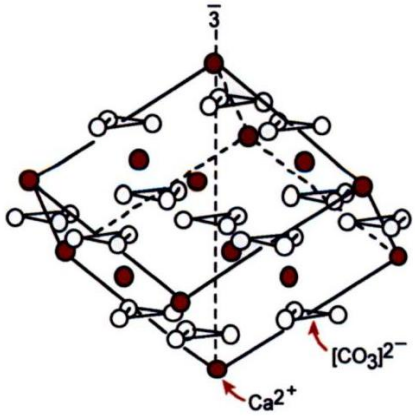

Figure 3.1-1 Elementary crystal lattice of calcite (Tegethoff, et al., 2001)

Calcite is one of the most common minerals within the Earth's crust and is extracted from limestone, chalk and dolomite for use within industry. Limestone is metamorphosed to marble at pressures over 1000 bar and temperatures from 200 to 500 C in two different ways, by re-crystallisation or chemical reactions between the individual components (Tegethoff, et al., 2001). Marble extracted from the Imerys deposit in Marmara, Turkey was used throughout the course of this work. The

material supplied by Imerys had been jaw crushed and dry milled into a coarse powder (d90 of 55 μm). In a production environment this coarse powder is slurried in water with dispersant prior to the start of the wet grinding process through a cascade of vertical stirred media mills.

3.1.2 Grinding media

The physical properties of the grinding media used drastically alters mill performance. It is known that the stress which can be exerted on the feed material is dependent on the size, density and surface properties of the grinding media used (Jankovic, 2003). Table 3.1-1, Table 3.1-2 and Table 3.1-3 outline the grinding media used throughout this work.

Table 3.1-1 Media density

Brand name	Supplier	Principle composition	Specific gravity	Media size (mm)
Carbolite	Carbo, USA	Mullite	2.7	1.4-2.4
Kings	Kings Ceramics, China	Zirconium silicate	3.9	1.48-1.68
Kings HD	Kings Ceramics, China	Zirconium silicate	4.2	12.-1.6
Sigmund-Lindner	Sigmund-Lindner, Germany	Zirconia	6.0	1.0-1.6

Table 3.1-2 Media size

Brand name	Supplier	Principle composition	Specific gravity	Media size (mm)
Kings	Kings Ceramics, China	Zirconium silicate	3.9	0.6-1.0 1.48-1.68 1.60-2.00 2.0-2.4

Table 3.1-3 Surface roughness

Brand name	Supplier	Principle composition	Specific gravity	Media size (mm)
80/20	Imerys (non commercial sample)	Zirconia / alumina	5.5	3
Sigmund-Linder	Sigmund-Lindner, Germany	Zirconia	5.5	3

3.1.3 Dispersant

Process and handling of high weight fraction calcium carbonate slurries requires the addition of a dispersant to give low slurry viscosity and to prevent aggregation allowing pumping, screening, subsequent transportation and facilitating end use applications (He, et al., 2006).

Sodium polyacrylate dispersants typically have a weight average molecular mass of approximately 5000. They are polyanions and work by an electrosteric mechanism in which the dispersant is adsorbed at the calcium carbonate surface, thereby (a) imparting a negative charge to the particles and (b) also giving a steric stabilisation effect (Rogan, et al., 1994_A; Rogan, et al., 1994_B).

The dispersant used throughout this work was a proprietary sodium polyacrylate supplied by Imerys as a 40 weight percent aqueous solution. To fully disperse d90 of 2 µm calcium carbonate a 0.8% weight concentration (dry dispersant on dry mineral) was required.

3.2 METHODS

3.2.1 Size measurement

Particles are distinct three dimensional objects that, unless they are perfect spheres, cannot be fully represented by a single dimension such as radius or diameter (Merkus, 2009). Therefore to allow comparison, it is often convenient to define a particle's size using an equivalent sphere diameter based on another particle property such as volume (*V*) surface area (*SA*) or projected area (*A*). The equations used to calculate equivalent particle diameters are given below in Equation 3.2-1 Equation 3.2-2 and Equation 3.2-3 (Holdich, 2002).

Diameter of sphere with equal volume d_v

$$d_v = \left(\frac{6V}{\pi}\right)^{\frac{1}{3}} \qquad \textbf{Equation 3.2-1}$$

Diameter of sphere with equal surface area d_S

$$d_s = \left(\frac{A}{4\pi}\right)^{\frac{1}{2}} \qquad \textbf{Equation 3.2-2}$$

Diameter of projected area d_A

$$d_A = 2\sqrt{\frac{A}{\pi}} \qquad \textbf{Equation 3.2-3}$$

It is important to note that different measurement techniques use different equivalent sphere models and therefore will not necessarily give the same result for the particle diameter.

3.2.1.1 Laser diffraction

The size of a particle can be measured by passing a laser beam through a particulate sample dispersed in a solvent (usually water). Large particles result in a small angle of scatter and small particles scatter light at large angles (Wills & Finch, 2015) as illustrated below in Figure 3.2-1. The angle of the scattered light is analysed to calculate the size of the particles responsible for creating the scattering pattern, using the Mie theory of light scattering. The particle size is reported as a volume equivalent sphere diameter (d_v) (Malvern Instruments, 2012).

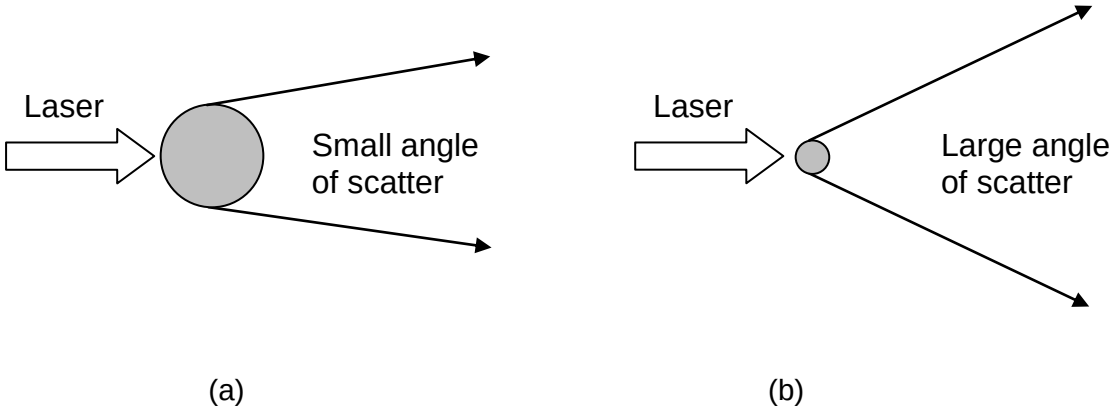

Figure 3.2-1 Light scattered by (a) large particles (b) small particles

Throughout the course of this work the particle size of ground calcium carbonate was measured with a Mastersizer 2000 (Malvern Instruments, UK) at the University of Birmingham. The added sample is passed through a measurement cell as shown in Figure 3.2-2. Here particles are illuminated by a laser and the resultant scattering detected by a series of detectors over a wide range of angles.

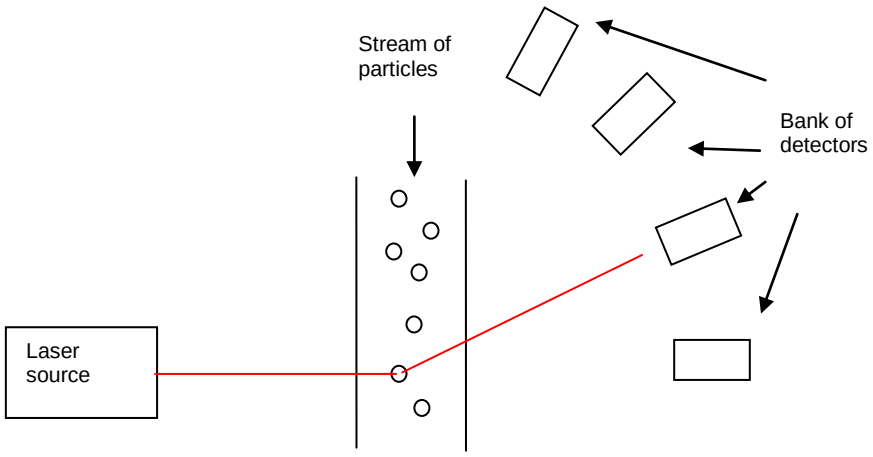

Figure 3.2-2 Light scattered by stream of particles through measurement cell

Sample dispersion is critical to ensure correct measurement. If the sample concentration is too high multiple scattering occurs, whereby light is scattered by more than one particle resulting in incorrect detection. If the concentration is too low the scattered light is indistinguishable from background noise. It is also vital that the sample is stable. If the impeller speed of the dispersing unit is too low or too high the particles may sediment or break down and give inaccurate size measurements.

Mie theory requires knowledge of the refractive index and adsorption of both the particles and the suspending liquid. These values are listed below in Table 3.2-1.

Table 3.2-1 Optical properties of calcium carbonate and dispersant

Material	Refractive index	Adsorption
Calcium carbonate	1.596	0.01
Water	1.330	N/A

3.2.1.2 Operating procedure

The test calcium carbonate suspension from the grinder (2-3 drops) was placed in a sample pot and tap water (20 mL) was added and mixed thoroughly by manual inversion (Sample A) and stored for subsequent size analysis.

The Malvern apparatus was flushed with distilled room temperature water twice prior to each test. For each test, water (500 mL) was re-circulated through the device until the background response was stable. Once stable, the background noise was recorded and Sample A was added drop wise to a target obscuration between 1.5 and 2.0. At this point particle size measurements were recorded three times and an average particle size distribution computed.

3.2.2 Grinding apparatus

The comminution of calcium carbonate was performed using a laboratory scale Imerys laboratory grinder consisting of a vertically mounted impeller made of a pair of pins and a 2L cylindrical pot as shown in Figure 3.2-3. (a) and (b)

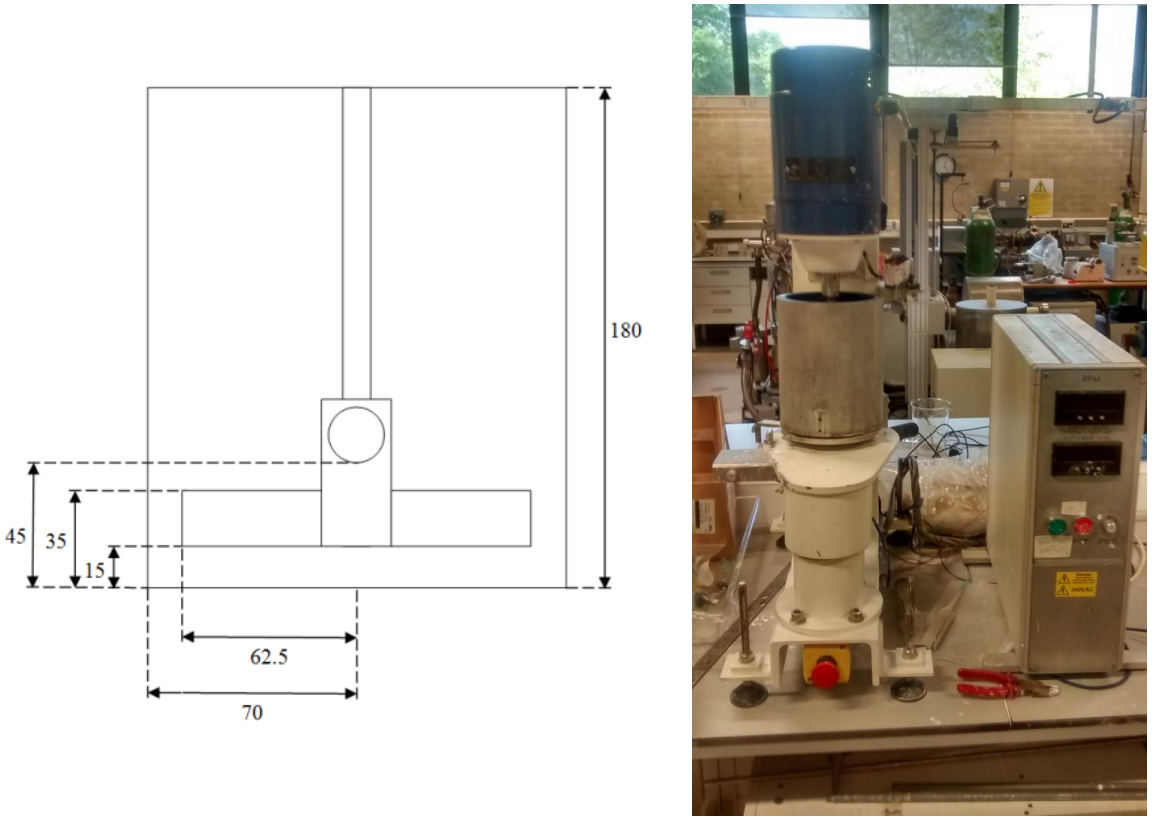

(a) (b)

Figure 3.2-3 (a) Grinder configuration (dimensions given in mm) (b) Photograph of grinder

The pot is lined with polyurethane to withstand the high temperatures and abrasion without affecting product quality. The pot is mounted on a freely rotating plate which has a metal arm resting on a load cell. This enables torque, and therefore energy input into the system, to be measured.

The mill is designed to grind a 1.1 L charge with impeller speeds up to 1500 rpm. The charge consists of grinding media, calcium carbonate, water and dispersent. The reference conditions are given below in Table 3.2-2.

Table 3.2-2 Basic grinding conditions

Parameter	Amount
Total volume	1.1 L
Media volume concentration	0.52 %
Solids concentration slurry	75 %
Dispersant concentration (active sodium polyacrylate concentration on dry mineral)	0.8 %

3.2.2.1 Operating procedure

In a typical operating procedure calcium carbonate (750 g) and grinding media (1500 g) were dry mixed in a plastic bag and added to the grinding chamber. Water (250 g) was then added to the grinding chamber and the impeller speed increased from 0 to 400 rpm. Then the dispersant solution (13.0 g of 46 % weight solution) was added over 30 seconds. The impeller speed was increased to the desired rpm and the load cell engaged and the grind allowed to proceed. As each successive 50 kWh energy input was reached, water was added to allow for evaporative losses and the grinder was stopped and sampled (3-4 drops were taken from the grinder and mixed with water (20 mL) (Sample A in Section 3.2.1.2). This was continued until the energy input reached 400 kWh at which point the grinder was stopped.

3.2.3 Surface roughness

Surface roughness is a measure of the vertical deviation on a normalised surface. Roughness plays an important role in determining how a material will interact with its surroundings. Rough surfaces often wear quicker due to surface irregularities acting as stress raisers (Askeland, et al., 2006). Media with different surface properties could result in different flow patterns or different numbers of feed particles being trapped between media.

There are a number of parameters used to measure the roughness of a surface, but the most common are S_a (average roughness of a surface) and S_q (root mean square roughness). These parameters are calculated using Equation 3.2-4 and Equation 3.2-5 (Whitehouse, 2002)

$$S_a = \iint_a |Z(x,y)| dxdy \qquad \textbf{Equation 3.2-4}$$

$$S_q = \sqrt{\iint_a \left(Z(x,y)\right)^2 dxdy} \qquad \textbf{Equation 3.2-5}$$

where *Z(x,y)* is a function representing the height of the surface at positions *x* and *y* and the integral, *a*, represents the area measured.

Roughness can be measured using an interferometer which uses a laser to measure the relative difference between the test surface and a reference surface as shown below in Figure 3.2-4. Throughout the course of this work a MicroXAM-100 interferometer (KLA Tencor, USA) was used to calculate the surface roughness of different grinding media surfaces.

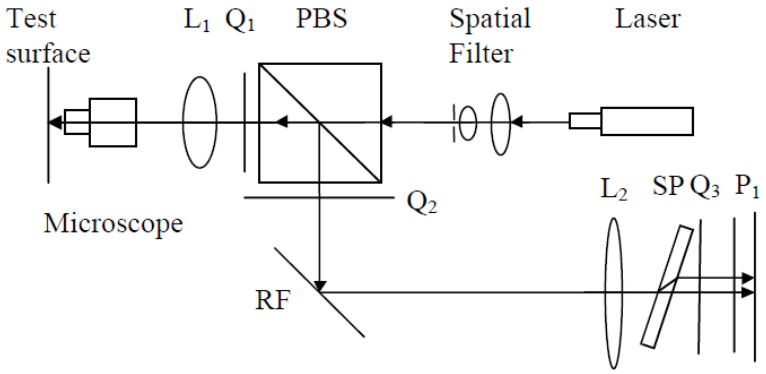

Figure 3.2-4 Diagram representing the configuration of an optical interferometer used to measure surface roughness

3.2.3.1 Operating procedure

Grinding media particles (30) were glued to a glass slide and placed under the interferometer microscope. A grinding media particle was positioned such that the laser was in focus directly above a single media particle. Once aligned, the measurement was started and the glass slide moved vertically through the focal point. As the media passed through the focal point variations in height were measured producing a 3D image of the grinding media surface. Roughness measurements were determined by mathematically removing the radius of curvature from the surface, and measuring the variations in height of the resulting flat surface which was fitted to Equation 3.2-4 and Equation 3.2-5 to measure *Sa* and *Sq* respectively. This procedure was repeated for each grinding media particle and the average roughness values determined.

3.2.4 Micromanipulation

Due to the small particle size of the calcium carbonate particles investigated, a micromanipulation technique is required to evaluate their fracture behaviour. A micromanipulator is a device consisting of a force transducer and a load cell which physically interacts with single particles under a microscope. The technique has been used to determine the fracture properties of a number of materials including precipitated calcium carbonate under compression (Yap, et al., 2006).

The micromanipulator used was built in-house at the University of Birmingham. Figure 3.2-5 (a) shows a schematic of the equipment used and Figure 3.2-5 (b) shows how the force transducer and probe interact with a glass slide containing dispersed particles. The probe was made from extruded borosilicate glass which was filed down to achieve a flat end with the desired cross-section. The force transducer is mounted to a 3-dimentional axis micromanipulator which is programmed to travel at a predetermined speed and vertical displacement. The following section summarises how fracture force and deformation are measured using a micromanipulator as outlined by Yap (Yap, 2006).

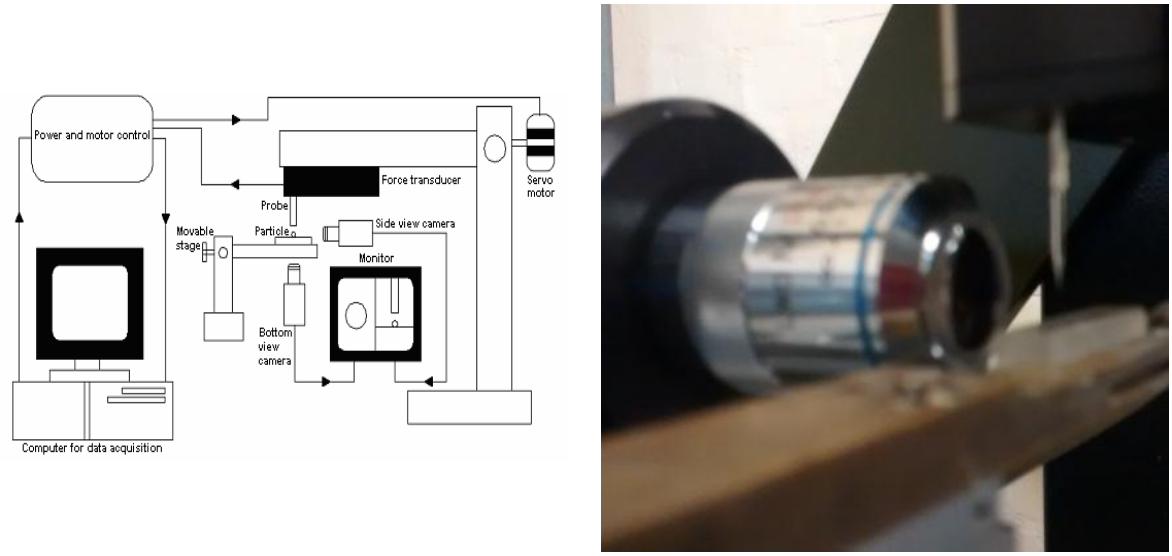

(a) (b)

Figure 3.2-5 (a) Micromanipulator schematic (Yap, et al., 2006) (b) Image of micromanipulator (microscope, glass slide and glass probe)

A force transducer works by measuring the force from the degree of bending of an internal cantilever beam. As higher forces are applied the beam bends further and induces a greater electrical voltage. Therefore, the raw data obtained are voltages (V_{PD}) as a function of time (t). The following equation is used to convert voltage to force (F)

$$F = V_{PD}\, s \qquad \textbf{Equation 3.2-6}$$

where the sensitivity (s) of the transducer is 0.5 mNV^{-1}

When loaded the movement of this cantilever is in the opposite direction to the movement of the micromanipulator. This additional movement must be corrected to determine the actual displacement of the force transducer. This additional movement, known as compliance (C), is derived from the linear gradient of the voltage-time plot (M) when tested against the glass slide using the following equation

$$C = \frac{v}{MS}$$ **Equation 3.2-7**

where *v* is the speed with which the force transducer is being loaded.

The displacement (D) of the particle is given from Equation 3.2-8.

$$D = ut - C\,F$$ **Equation 3.2-8**

3.2.4.1 Operating procedure

Calcium carbonate particles (0.1 g) were suspended in distilled water (20 g). The sample was inverted 20 times then two drops applied using a pipette onto a glass slide and left to dry. Once dried the slide was positioned within the micromanipulator. The slide was then raised until visible on the screen taking precaution not to allow the slide to come in contact with the glass probe. Once aligned, the slide was moved in the x and y axes until a calcium carbonate particle was in focus directly underneath the glass probe. The size of the calcium carbonate particle was then determined using a calibration scale on the computer screen and the test completed by stressing the calcium carbonate particle until fracture. This process was repeated between 30 to 50 times per sample.

3.2.5 Determination of media-media collision measurement using collision theory

3.2.5.1 Theory

The efficiency of a stirred media mill is dependent on the number of collisions between media particles and the proportion of these collisions with sufficient stress to fracture the trapped feed material. In this sense the sequence of events that take place in a stirred media mill are not unlike a chemical reaction in which reactant molecules are converted into products.

For a chemical reaction to occur, molecules must approach closely enough to disrupt their existing bonds and permit the creation of new ones. This encounter is called a collision and is considered the initial step of a reaction. These steps are usually very simple and only involve one, two or three chemical species which are classified below in Table 3.2-3.

Table 3.2-3 Comparison of initial steps in chemical equations

Unimolecular	$A \rightarrow Products$
Bimolecular	$A + B \rightarrow Products$
Termolecular	$A + B + C \rightarrow Products$

Within a stirred mill a breakage event occurs when a feed particle is trapped and stressed between grinding media. When modelling this system a breakage event can be considered unimolecular. This is because the feed material is considered evenly dispersed and at a high enough concentration that calcium carbonate particles are always present when media collide. Therefore breakage is dependent upon how frequently media collisions occur.

For a chemical reaction to occur, a collision must have sufficient energy to stretch and weaken the reactants' interatomic bonds to such an extent that the distortion of the electron cloud can then lead to the formation of new bonds between the reactants. This critical energy is known as the activation energy of the reaction and the more collisions that occur with energy higher than the activation energy, the faster the reaction rate. The same can be said for breakage events in a stirred media mill. In order for breakage to occur, grinding media must collide with sufficient stress to overcome the compressive strength of the trapped calcium carbonate particle.

According to kinetic molecular theory, a population of molecules at a given temperature can be described by the Maxwell-Boltzman distribution as shown in Figure 3.2-6.

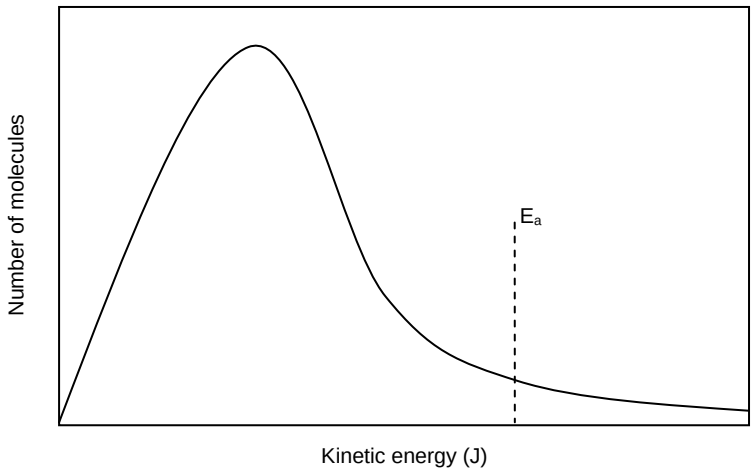

Figure 3.2-6 Maxwell-Boltzman distribution of a population of molecules (Atkins & De Paula, 2010)

A Maxwell-Boltzman distribution gives the distribution of kinetic energies within a population. From Figure 3.2-6 it can be seen that the proportion of molecules/ grinding media with a kinetic energy greater than the activation energy (E_a) can undergo a reaction/ breakage. This knowledge leads to the Arrhenius law as shown in Equation 3.2-9

$$K = Ze^{\frac{-E_a}{RT}} \qquad \textbf{Equation 3.2-9}$$

where K is the reaction rate, Z is the collision rate, E_a is the activation energy or the energy required to fracture a particle, R is the universal gas constant (8.314 $Jmol^{-1}K^{-1}$) and T is the temperature of the population in Kelvin. RT together gives the average kinetic energy of the population. For simplicity, steric effects have been ignored.

By knowing the: (i) distribution of stresses exerted by grinding media at a collision, (ii) the average compressive strength which calcium carbonate particles can withstand and (iii) the media-media collision rate, a relationship similar to the Arrhenius equation can be developed to determine the breakage rate of calcium carbonate particles in the mill.

3.2.5.2 Collision frequency

A collision is said to occur if the centre of two equal sized particles come within one diameters distance of each other (Atkins & De Paula, 2010). Collision frequency is calculated by freezing the position of all but one of the particles within the system and observing the position of the single unfrozen particle as it travels through the system. As the particle having diameter (*d)*, travels for a time (*Δt*) it sweeps out a collision cross-section (σ_x) with a volume shown in Equation 3.2-10

$$\sigma_x = \pi d^2$$

Equation 3.2-10 (Atkins & De Paula, 2010)

As the particle travels a distance ***cΔt***, where c is the average velocity of the particle, the particle collides with the particles with centres inside the volume (*V*). This results in the collision frequency (*Z*) shown in Equation 3.2-11

$$Z = \sigma_x c \frac{N}{V}$$

Equation 3.2-11 (Atkins & De Paula, 2010)

where *N* is the number of particles with centres inside the volume.

This however only takes into account one particle. To calculate the number of collisions between all particles in a unit volume the collision frequency must be multiplied by *1/2N/V* and c must be changed to $\bar{c}$ the relative speed of the colliding particles as shown in Equation 3.2-12 (Atkins & De Paula, 2010).

$$Z = \frac{1}{2}\sigma_x \bar{c} \left(\frac{N}{V}\right)^2$$

Equation 3.2-12 (Atkins & De Paula, 2010)

This equation shows that the collision frequency of a volume is dependent on the number and relative speed of the particles within the volume. This equation for

collisions was derived from existing equations using the kinetic theory of gases. Such theory is based on assumptions listed below:

1. The gas is a swarm of particles which move in a random motion
2. The particles have negligible size meaning that they are much smaller than the distances between them
3. The particles undergo elastic collisions

Previous studies have estimated the number of media -media collisions (N_c) by assuming that the number of collisions is proportional to the number of revolutions the grinding media completes within the mill (which is assumed to be proportional to the revolutions of the stirrer (N_{rev})), the grinding time (t) and the number of grinding media particles within the mill (N_{GM}) as described in Equation 3.2-13 (Kwade, 1999_B)

$$N_c \propto N_{rev} t N_{GM} \propto \frac{N_{rev} t (V_{GC}\, \phi_{GM}(1-\varepsilon_{GM}))}{\frac{\pi}{6} d_{GM}^3} \qquad \textbf{Equation 3.2-13}$$

where V_{GC} is the grinding chamber volume, ϕ_{GM} is the filling ratio of the grinding media, ε_{GM} is the porosity of the grinding media at rest and d_{GM} is the diameter of the grinding media.

3.2.5.3 Media-media collision rate and grinding rate equations

This approach does not take into account the velocity of the grinding media relative to other grinding media, or the number of particles in a unit volume within the mill during the grind. Therefore, the collision rate and proportion of the collisions suitable to fracture calcium carbonate particles will be determined using Equation 3.2-14 through 18 which calculate the collision rate per unit time per volume (*Z*), the total number of collisions (Z_{tot}), the collisions per kWh/tonne ($Z_{kWh/tonne}$) and the breakage rate per kWh/tonne (*K*)

$$Z = \frac{1}{2}\pi d^2 \bar{c} \left(\frac{N}{V}\right)^2 \qquad \textbf{Equation 3.2-14}$$

$$Z_{tot} = \frac{1}{2}\pi d^2 \bar{c} \frac{N^2}{V} t_{end} \qquad \textbf{Equation 3.2-15}$$

$$Z_{kWh/tonne} = \frac{Z_{tot}}{E_{in}} \qquad \textbf{Equation 3.2-16}$$

$$K = Z_{kWh/tonne} e^{-\frac{Strength_{mean}}{Stress_{mean}}} \qquad \textbf{Equation 3.2-17}$$

where *d* is the average diameter of the grinding media, $\bar{c}$ is the mean relative velocity of the grinding media, *N* is the number of grinding media in a unit volume *V*, t_{end} is the total grind time in seconds, E_{in} is the grinding input energy in kWh/tonne, $strength_{mean}$ is the average compressive strength of calcium carbonate at that size range and $stress_{mean}$ is the mean stress exerted by the grinding media at a collision.

3.2.6 Positron Emission Particle Tracking (PEPT)

PEPT is a non-invasive technique for studying flow patterns in particulate systems by tracking the position of a radioactively labelled tracer particle. This work utilised grinding media particles that were irradiated with a ^{3}He ion beam at the University of Birmingham MC40 cyclotron. This beam converts a fraction of ^{16}O present to the radionuclide ^{18}F which undergoes beta plus decay resulting in the emission of a back-to-back photon pair.

The tracer is added to the grinder and placed between the camera heads of a specifically modified ADAC forte gamma camera (Philips, USA) as shown in Figure 3.2-7. As the tracer decays, the camera heads (sodium iodine scintilator crystals) detect the emitted photon pair. If both detectors register a photon within a 12 ns time period the camera calculates a line of response (LOR) along which the annihilation must have occurred (ignoring scattering and attenuation). This allows the position of the tracer to be triangulated as the position where the photon pairs overlap.

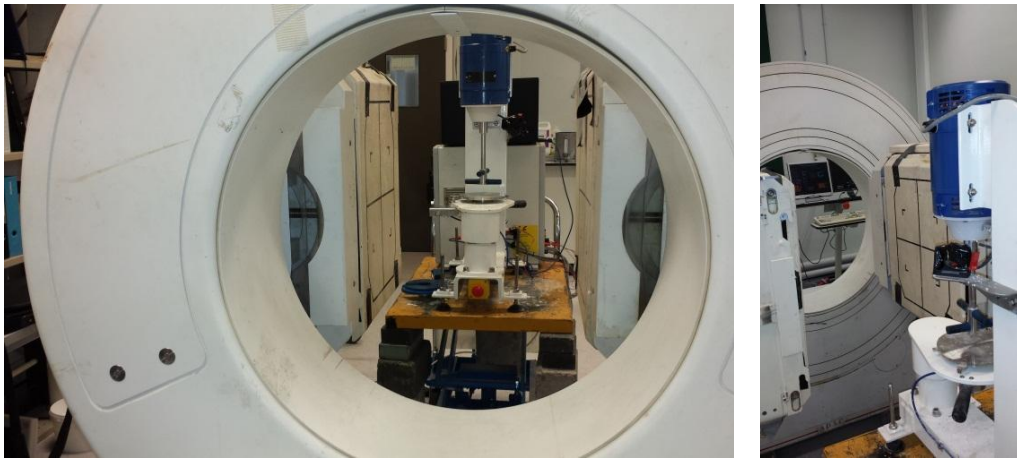

(a) (b)

Figure 3.2-7 (a) and (b) Laboratory grinder positioned next to the ADAC positron camera

3.2.6.1 Operating procedure

Grinding media particles (6-10) were randomly sampled to be directly irradiated. The process of directly irradiating a particle is summarised by Fan (Fan, et al., 2006). The grinding media particles were held within an aluminium target and bombarded by a 33 MeV ^{3}He beam. Once irradiated the activity of the grinding media particles was measured using a Geiger counter and the most active grinding media particle weighed and sized using a four decimal place balance and callipers.

The grinder was positioned on a trolley next to the ADAC camera. Each grinding experiment was prepared as described in Section 3.2.2.1. The irradiated particle was added to the grinder, the grinder wheeled between the camera heads and brought up to the operational stirrer speed. At this point the grinder and ADAC recording software were begun. After 50 Wh the ADAC software was stopped and the grinder switched off. When working with a new grinding media type, static measurements of the tracer were taken to determine optimum f and N values. After the experiment was concluded the tracer was recovered for subsequent experiments.

The initial PEPT camera output through the run was collected. These data comprise a list of excited detector pairs as a function of time. The PEPT location algorithm (see below) was then used to triangulate the grinding media position (x, y and z) as a function of time.

The following mill operational parameters were investigated:

(i) Mill motor energy input

(ii) Grinding media specific gravity

(iii) Grinding media particle size

(iv) Grinding media surface roughness

(v) Mill impeller speed

(vi) Calcium carbonate solids volume concentration

3.2.6.2 Location algorithm

The PEPT algorithm developed at the University of Birmingham is an iterative triangulation technique which removes scattered and attenuated LORs until a pre-defined fraction of the initial results remain (Leadbeater, et al., 2012). Figure 3.2-8 (a) (b) and (c) show how varying the proportion of LORs removed (f) affects location precision (Δ) for the mullite (s.g. 2.7), zirconium silicate (s.g. 3.9) and high density zirconium silicate (s.g. 4.2) used throughout the course of this work. Optimal precision occurs when the error associated with the static particle is at a minimum (f_{opt}), and calculated by fitting a second order polynomial to the N=100 dataset (trendline added to Figures 3.2-8 (a), (b) and (c)). F_{opt} values for each media type are shown in Table 3.2-4.

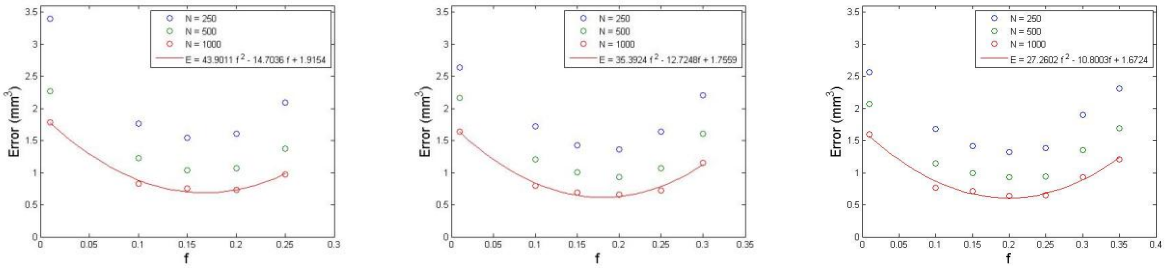

(a) (b) (c)

Figure 3.2-8 Location precision of (a) carbolite (s.g. 2.7) (b) zirconium silicate (s.g. 3.9) (c) high density zirconium silicate (s.g. 4.2) tracer particles varying the proportion of LORs (*f*)

Table 3.2-4 Optimum *f* for media used throughout the course of this work

Media	Carbolite (s.g.2.7)	Zirconium silicate (s.g.3.9)	High density zirconium silicate (4.2)
f_{opt}	0.165	0.180	0.189

When a tracer particle is stationary the precision of a location can be made arbitrarily small by increasing the number of LORs used to triangulate its position (*N*) as shown in Figure 3.2-9. However when the tracer is moving the LORs for each event are spread along the particle's trajectory. An exact argument for optimising N_{LOR} as a function of speed has not been found. However it is proposed that optimum values of N_{lor} (N_{opt}) should be selected such that the distance moved between locations approximately equals the spatial resolution of the scanner (*W*) as shown in Equation 3.2-18 (Leadbeater, et al., 2012).

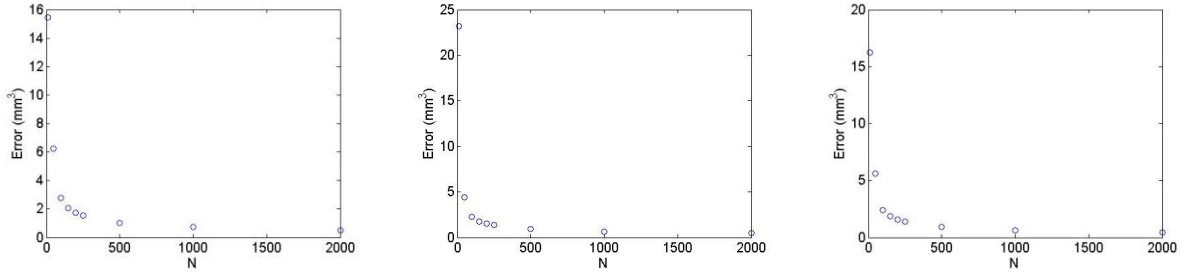

(a) (b) (c)

Figure 3.2-9 Location precision of (a) carbolite (s.g. 2.7) (b) zirconium silicate (s.g. 3.9) (c) high density zirconium silicate (s.g. 4.2) tracer particles varying the number of LORs (*N*)

$$\Delta \approx \left\{\frac{Wv}{fT_C}\right\}^{\frac{1}{2}}$$

Equation 3.2-18 (Leadbeater, et al., 2012)

where v is the speed of the tracer and T_C is the coincident rate. Therefore N_{opt} depends on the average velocity of the tracer and the rate of photon pairs detected.

3.2.6.3 Post processing data

3.2.6.3.1 Introduction

There are two different ways of measuring fluid flow within a three dimensional fluid system: (i) by tracking an individual particle as it moves through a system (Lagrangian) or (ii) observing the fluid at fixed locations (Eulerian). The PEPT technique utilises a Lagrangian approach. By irradiating a grinding media particle and measuring its position and time, the path of the grinding media particle through the mill can be determined by fitting a cubic spline to the coordinate data in x, y and z.

A cubic spline is a piecewise polynomial which passes through each data point creating a separate cubic polynomial for each interval with its own coefficients (*a*, *b*, *c* and *d*) as shown in Equation 3.2-19.

$$S_i(x) = a_i x^3 + b_i x^2 + c_i x + d_i \quad \text{for } x \in [x_i, x_{i+1}] \qquad \textbf{Equation 3.2-19}$$

The remainder of this section outlines the methodology used to measure the desired flow parameters: (i) occupancy, (ii) velocity, (iii) force, (iv) stress exerted and (v) media-media collisions and flow diagrams from cubic splines using an example set of PEPT data (total volume (1.1 L), MVC (52 %), impeller speed (1000 rpm), calcium carbonate solids by weight (75 % by weight), 1.2-2.0 mm carbolite grinding media of specific gravity 2.7).

Figure 3.2-10 (a) shows the path of a grinding media particle in x, y and z over a 1.85 second time interval and the cubic splines fit to each dataset calculated using Equation 3.2-20, Equation 3.2-21 and Equation 3.2-22.

$$x = a_x t^3 + b_x t^2 + c_x t + d_x \qquad \textbf{Equation 3.2-20}$$

$$y = a_y t^3 + b_y t^2 + c_y t + d_y \qquad \textbf{Equation 3.2-21}$$

$$z = a_z t^3 + b_z t^2 + c_z t + d_z \qquad \textbf{Equation 3.2-22}$$

It can be seen that the tracer exhibits two generalised forms of motion within a vertically stirred mill as discussed by Conway-Baker et al. (Conway-Baker, et al., 2002): (i) wall mode, where the grinding media particle moves slowly around the top of the pot above the impeller and (ii) impeller mode where the grinding media particle moves quickly in the vicinity of the impeller blades until returning to the region above the impeller.

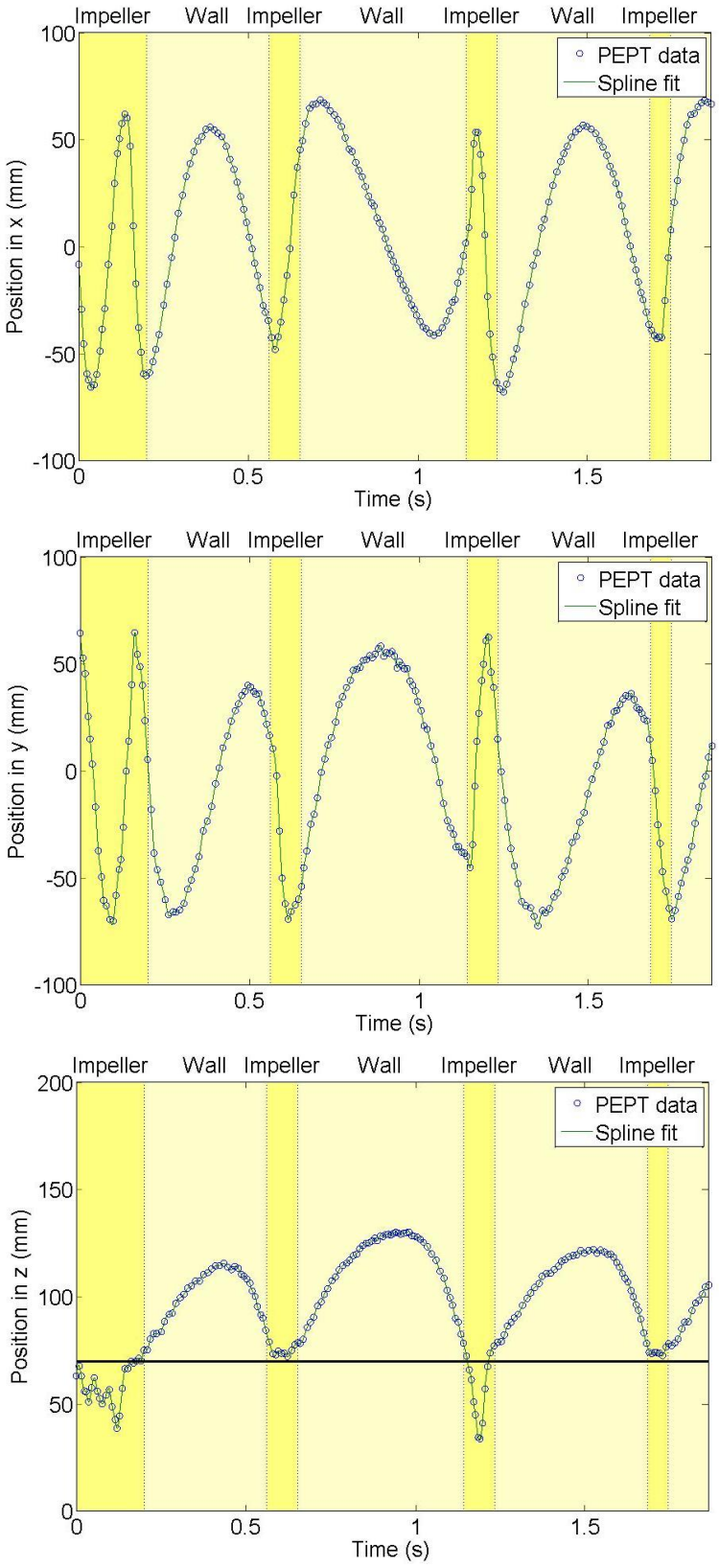
Impeller
Wall
Impeller
Wall
Impeller
Wall
Impeller
PEPT data
Spline fit
Position in x (mm)
Position in y (mm)
Position in z (mm)
Time (s)

(a)

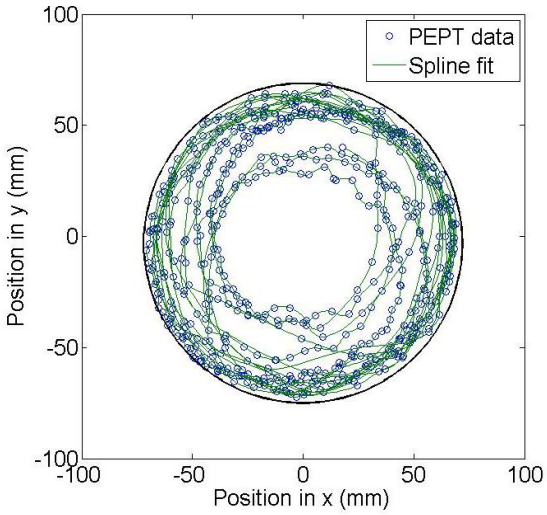

(b)

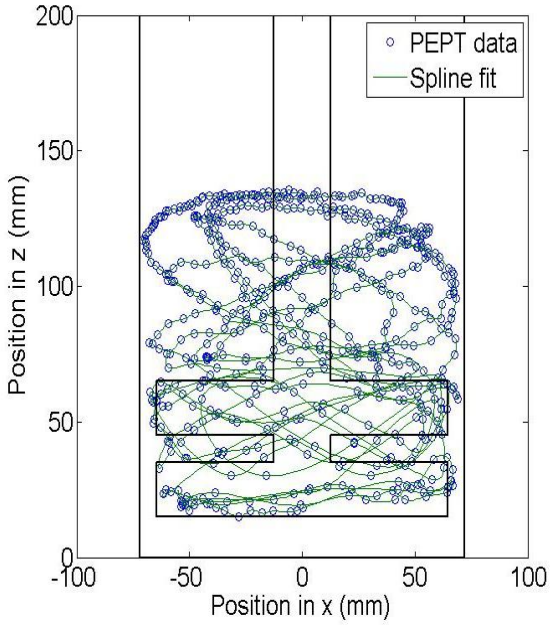

(c)

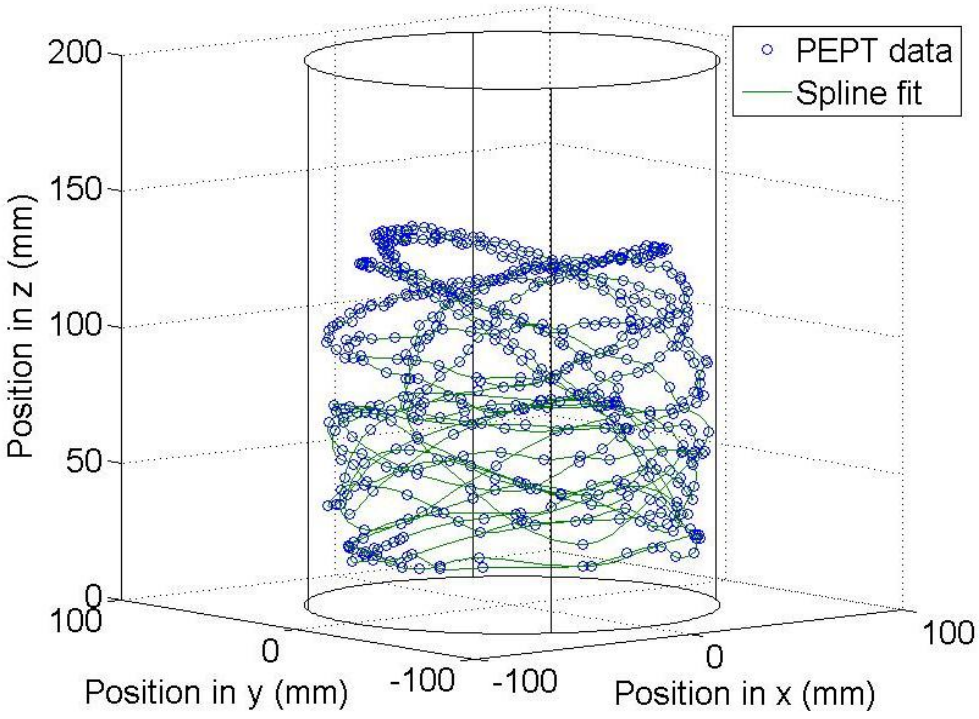

(d)

Figure 3.2-10 (a) Position of a grinding media tracer in x, y and z against time and spline fit over a 1.85 second time period (b) Position and spline fit of grinding media tracer along x and y axes over a 5.4 second time period (c) Position and spline fit of grinding media tracer in x and z axes over a 5.4 second time period (d) Position and spline fit of the grinding media tracer in x, y and z over a 5.4 second time period.

Figure 3.2-10 (b) (c) and (d) shows how the position of the grinding media tracer and the spline fit to the data points varies in x and y, x and z and x, y and z respectively over a 5.4 second time period. It can be seen that the tracer travels in a circular motion in x and y and that locations are less frequent as the tracer is lower in the mill than at the top. This suggests that the media travels faster in the region around the impeller.

3.2.6.3.2 Tracer velocity

Fitting polynomials allows the raw data set to be interpolated and other flow parameters such as particle velocity acceleration and force to be calculated. Figure 3.2-11 shows the velocity of the tracer particle along the x, y and z axes calculated by differentiating the splines fit to the data as shown in Equation 3.2-23 Equation 3.2-24 and Equation 3.2-25.

$$v_x = 3a_x t^2 + 2b_x t + c_x \qquad \textbf{Equation 3.2-23}$$

$$v_y = 3a_y t^2 + 2b_y t + c_y \qquad \textbf{Equation 3.2-24}$$

$$v_z = 3a_z t^2 + 2b_z t + c_z \qquad \textbf{Equation 3.2-25}$$

It can be seen that the velocity of the tracer is much higher in the impeller regions.

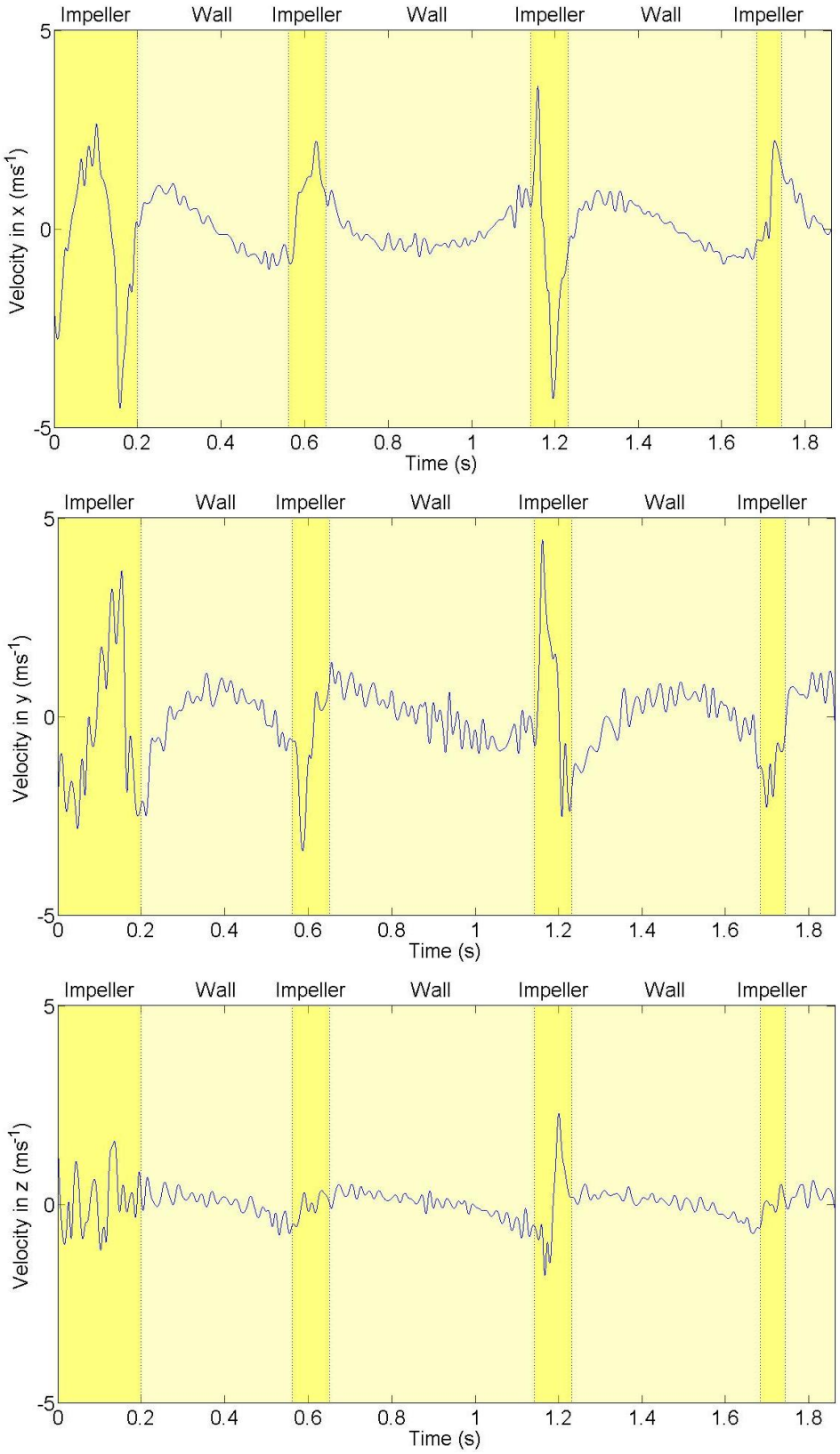

Figure 3.2-11 Velocity of the grinding media tracer in x, y and z against time over a 1.85 second time period

The resultant velocity of the tracer is determined by summating the velocity components in x, y and z as shown in Figure 3.2-12 using Equation 3.2-26. Again it can be seen that the resultant velocity of the tracer is higher in the impeller regions.

$$v = \sqrt{{v_x}^2 + {v_y}^2 + {v_z}^2}$$ **Equation 3.2-26**

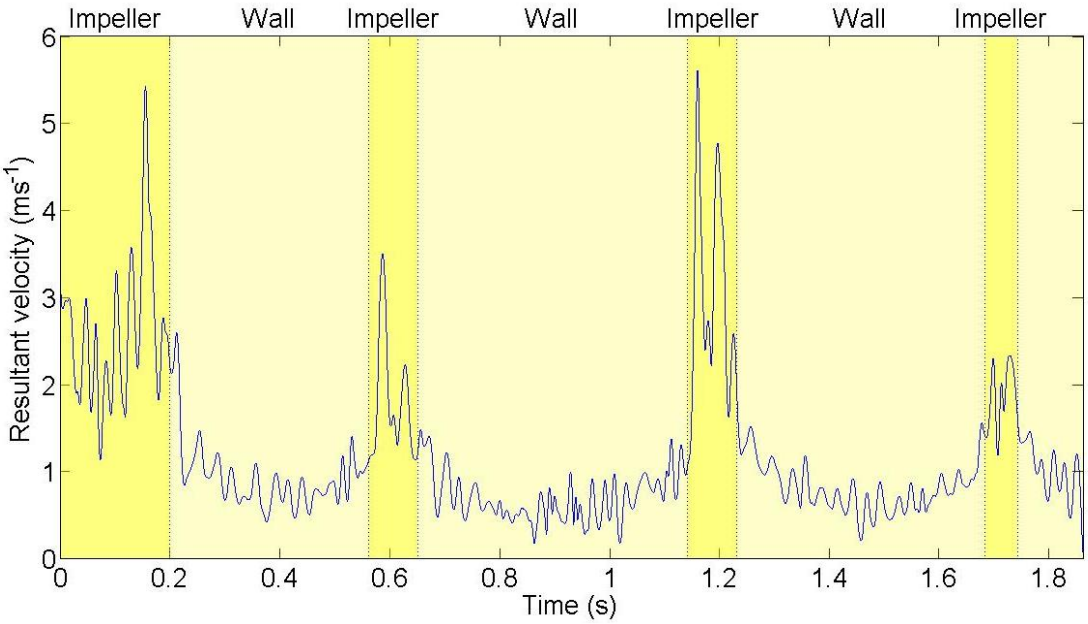

Figure 3.2-12 Resultant velocity of the grinding media tracer over a 1.85 second time period

3.2.6.3.3 Tracer acceleration

The second differential of the splines fit to the raw data in x, y and z gives the acceleration of the tracer as shown in Equation 3.2-27, Equation 3.2-28 and Equation 3.2-29. The acceleration of the tracer particle for a 1.85 second time period is shown in Figure 3.2-13. Again the tracer accelerates rapidly around the impeller.

$$acc_x = 6a_x t + 2b_x \qquad \textbf{Equation 3.2-27}$$

$$acc_y = 6a_y t + 2b_y \qquad \textbf{Equation 3.2-28}$$

$$\mathrm{acc}_z = 6a_z t + 2b_z \qquad \textbf{Equation 3.2-29}$$

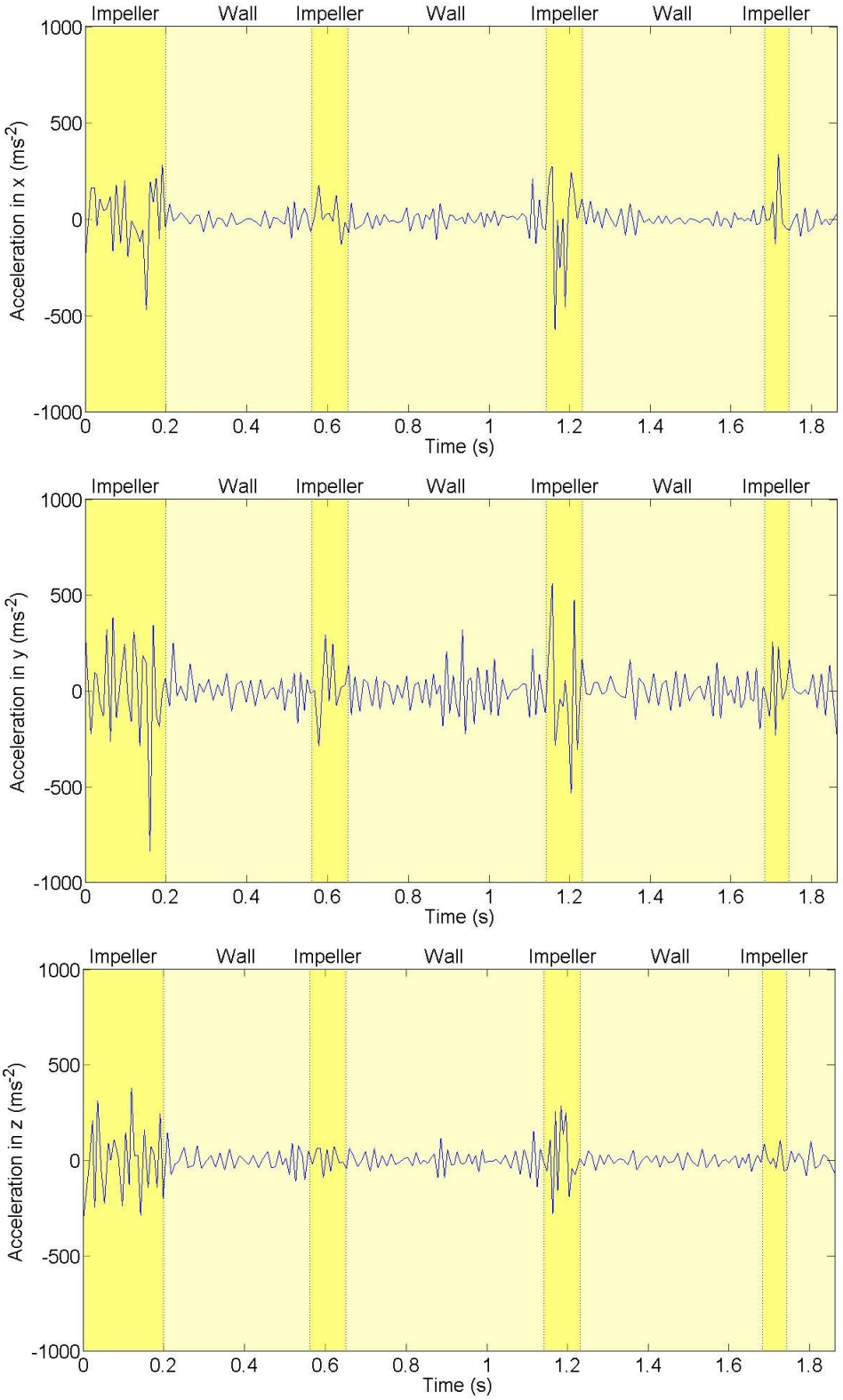

Figure 3.2-13 Acceleration of the grinding media tracer in x, y and z against time over a 1.85 second time period

The resultant acceleration is calculated by summating the acceleration in x, y and z as shown in Equation 3.2-30. Figure 3.2-14 shows how the acceleration of the tracer particle varies over a 1.85 second time period. Again the resultant acceleration is higher in the impeller region.

$$acc = \sqrt{{acc_x}^2 + {acc_y}^2 + {acc_z}^2}$$ **Equation 3.2-30**

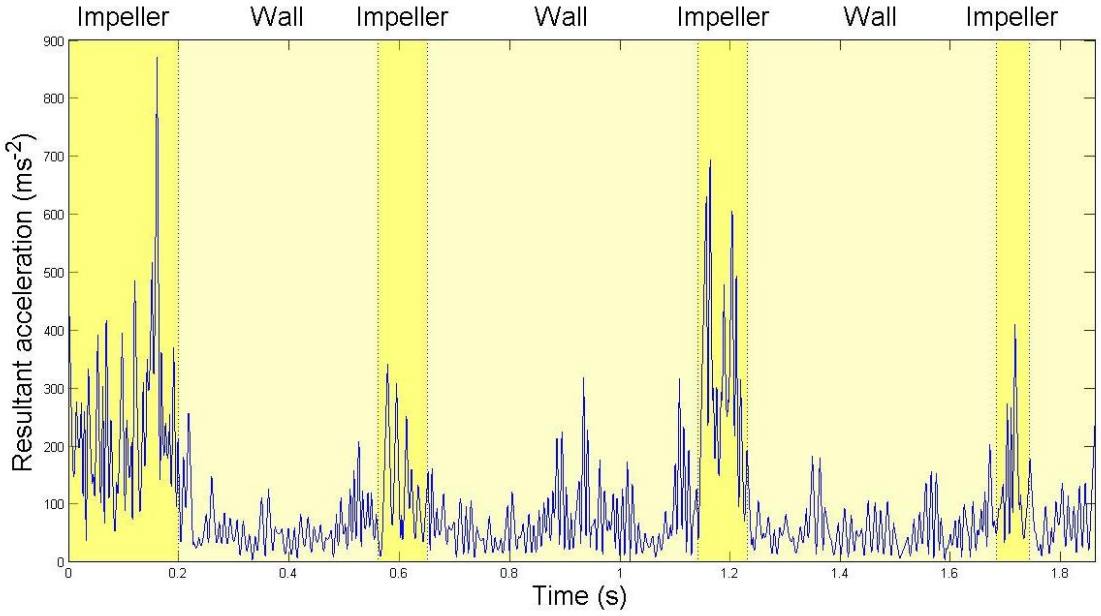

Figure 3.2-14 Resultant acceleration of the grinding media tracer over a 1.85 second time period

3.2.6.3.4 Tracer force and stress

Kwade et al state that vertically stirred mill efficiency is defined by: (i) how often each feed particle is stressed and (ii) how high the stress intensity is at each collision (Kwade, 1999_B). This assumes that only one feed particle is stressed in the active volume between media particles and that when stressed the feed particle fails elastically. A feed particle is fractured when the stress acting on the particle is greater than it can withstand. The stress (stress intensity) can be measured either as the energy transferred from the grinding media to the feed particle at a collision (Jm^{-3}) or the force acting on the cross-section of the grinding media particle (Nm^{-2}).

The force acting on a feed particle at a collision is equal to that experienced by the grinding media particle. This can be calculated from the resultant acceleration of the tracer using Equation 3.2-31 where *m* is the mass of the tracer.

$$F = m \cdot acc \qquad \textbf{Equation 3.2-31}$$

Figure 3.2-15 shows how the force acting on the tracer varies over a 1.85 second time period. It can be seen that when the tracer is not in the impeller zone the force acting is lower than when it is.

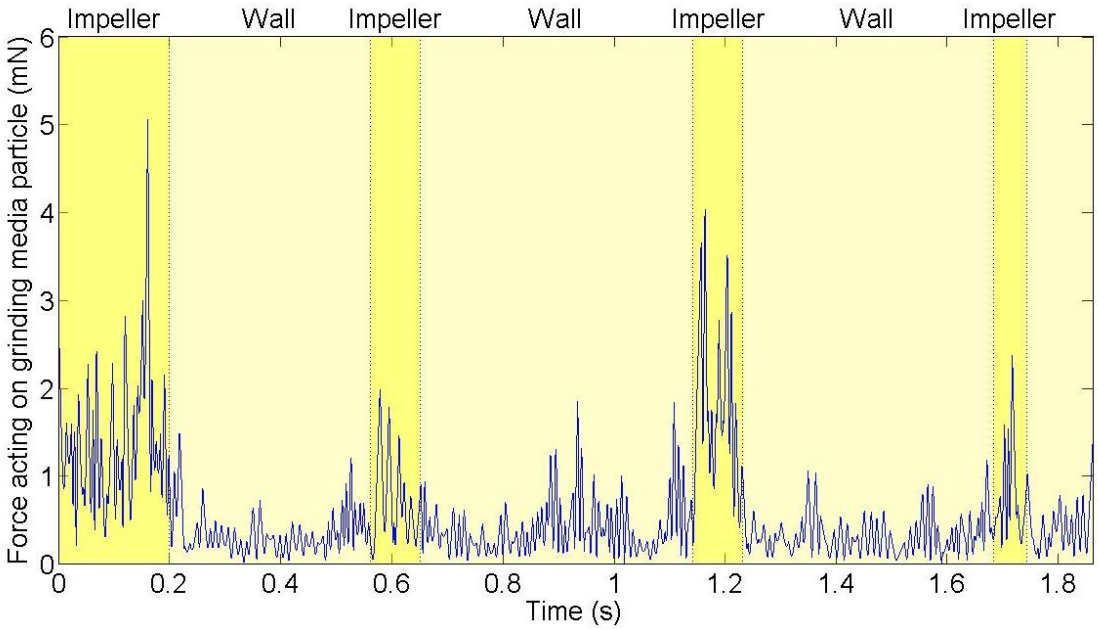

Figure 3.2-15 Resultant force acting on the grinding media tracer over a 1.85 second time period

Therefore throughout the course of this work the stress exerted by the grinding media is calculated as the force acting on the grinding media divided by the cross-sectional area of the feed material. This allows comparisons to be made between the stress exerted by the grinding media within a vertically stirred mill and the strength of the feed material calculated using micromanipulation.

Each PEPT experiment was run for 50 Wh, approximately 20 minutes. If the tracer particle travels everywhere in the mill over the duration of the run then the tracer can be considered representative of the entire particulate body (Leadbeater, et al., 2012). Figure 3.2-16 shows the distributions of forces that the tracer particle exerts throughout the course of a grind.

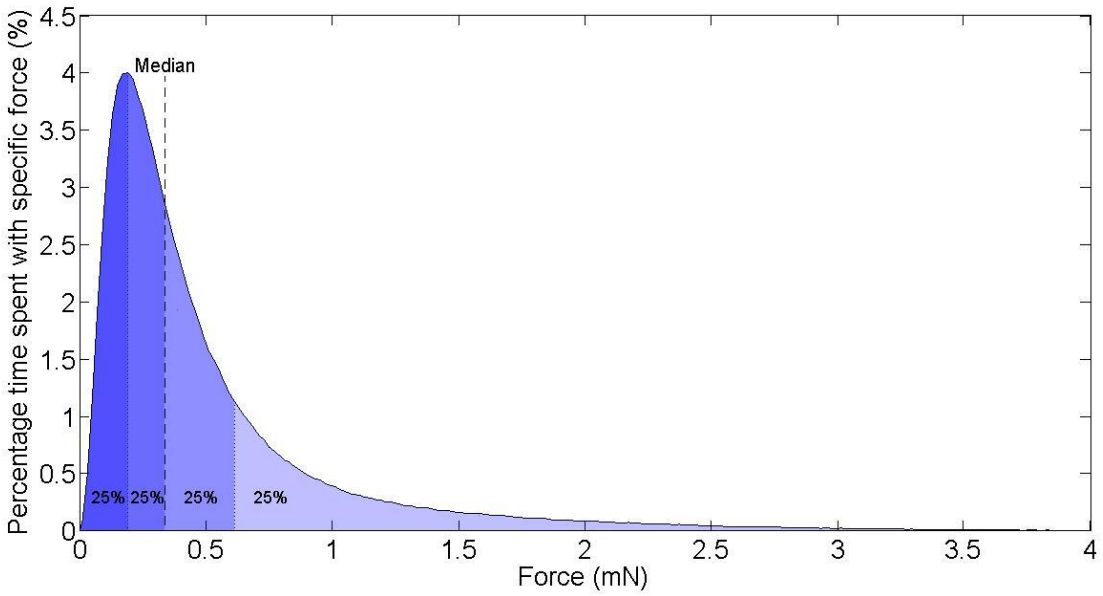

Figure 3.2-16 Grinding media force distribution plot

Because the tracer is considered representative of the entire particulate body it can be assumed that the percentage of the total time the tracer spends with a specific force equates to the percentage of the grinding media with that force within the mill. Figure 3.2-16 therefore also shows the force distribution plot the grinding media exert within the mill. It can be seen that the median force exerted by the grinding media is 0.34 mN and that the distribution is positively skewed. Table 3.2-5 shows the cumulative force distribution of grinding media within the mill. For this example it can be seen that 75 % of all the media within the mill exert less than 0.61 mN of force on their surroundings.

Table 3.2-5 Cumulative force distribution

Cumulative distribution (%)	Force (mN)
25	0.19
50	0.34
75	0.61
100	3.94

3.2.6.3.5 Contour plots

Contour plots allow easy visualisation of flow fields and comparisons between different regions of the mill. Fluid flow within the vertically stirred mill used throughout this project exhibits radial symmetry. Therefore a single radial slice can be used to represent the average flow parameters across the cross-section of the mill. Figure 3.2-17 (a) shows a visualisation of the radial slice through the cross-section of the mill and (b) the grid over which flow parameters are visualised.

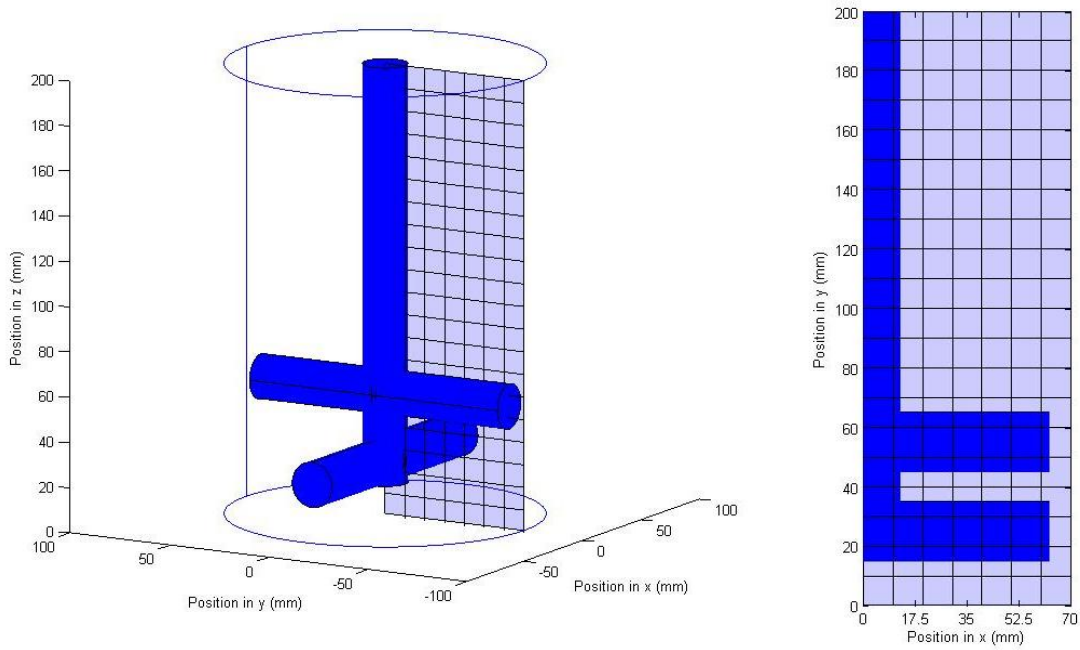

(a) (b)

Figure 3.2-17 (a) Visualisation of the radial slice used to visualise flow parameters within the mill pot (b) Grid representing the cross-section of the mill with imposed impeller.

Mean values are obtained by averaging flow parameters of the tracer as it passes through the predefined grid shown in Figure 3.2-17 (b) and neglecting their angular component. Figure 3.2-18 shows a visualisation of the path of the tracer through a 3D unit cell of the predefined grid. As the tracer passes through the cell, the time the tracer enters and leaves each cell is measured and a midpoint time determined. The time of the midpoint is then used in the Equations 3.2-23-31 to determine the magnitude of each flow parameter for that pass. All the individual passes are added up to obtain an average value within the block volume.

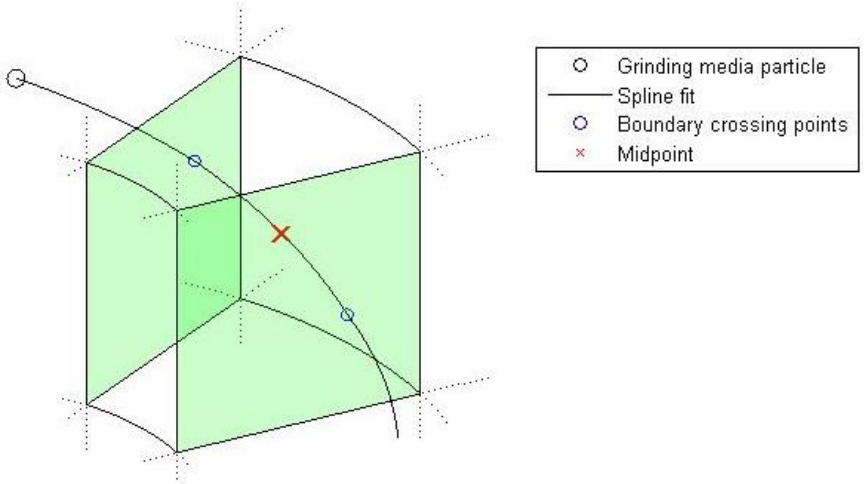

Figure 3.2-18 Visualisation of the path a grinding media takes through a block volume. Entry and exit points are shown in blue and the midpoint of the cell where flow parameters are calculated is shown as a red cross

Raw PEPT data are given in Cartesian coordinates (x, y and z). However, in order to generate the desired radial slice shown in Figure 3.2-17, the raw data must be converted into cylindrical coordinates (Θ ρ h) and divided into block volumes. Fitting cubic splines (Equation 3.2-32, Equation 3.2-33 and Equation 3.2-34) to cylindrical data points allow for interpolation with a predefined block volume as shown in Figure 3.2-19.

$$\theta = a_\theta t^3 + b_\theta t^2 + c_\theta t + d_\theta \qquad \textbf{Equation 3.2-32}$$

$$\rho = a_\rho t^3 + b_\rho t^2 + c_\rho t + d_\rho \qquad \textbf{Equation 3.2-33}$$

$$h = a_h t^3 + b_h t^2 + c_h t + d \qquad \textbf{Equation 3.2-34}$$

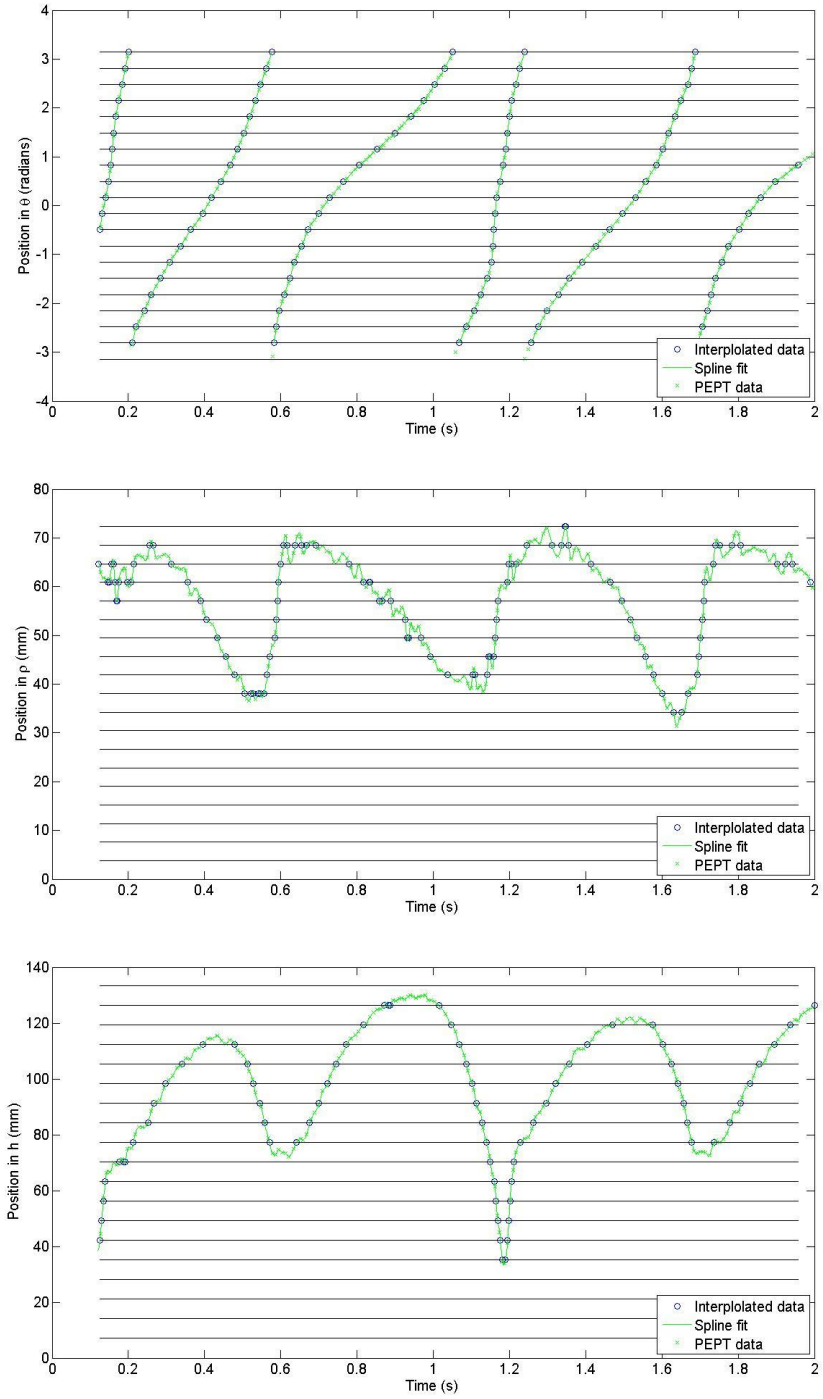

Figure 3.2-19 Cubic splines fitted to cylindrical raw PEPT data points and interpolated data points at block boundaries over a 1.85 second time period.

Figure 3.2-20 shows how a spline fit to 1.85 seconds of PEPT data varies across a cylindrical grid in (a) Θ and ρ and (b) the cross-section of the mill ρ and h. Flow parameters are calculated at the mid-point of the tracer's path through each block volume to determine average parameters. Again, if left for a sufficient length of time the tracer is said to travel everywhere within the mill and is representative of the fluid flow throughout the mill.

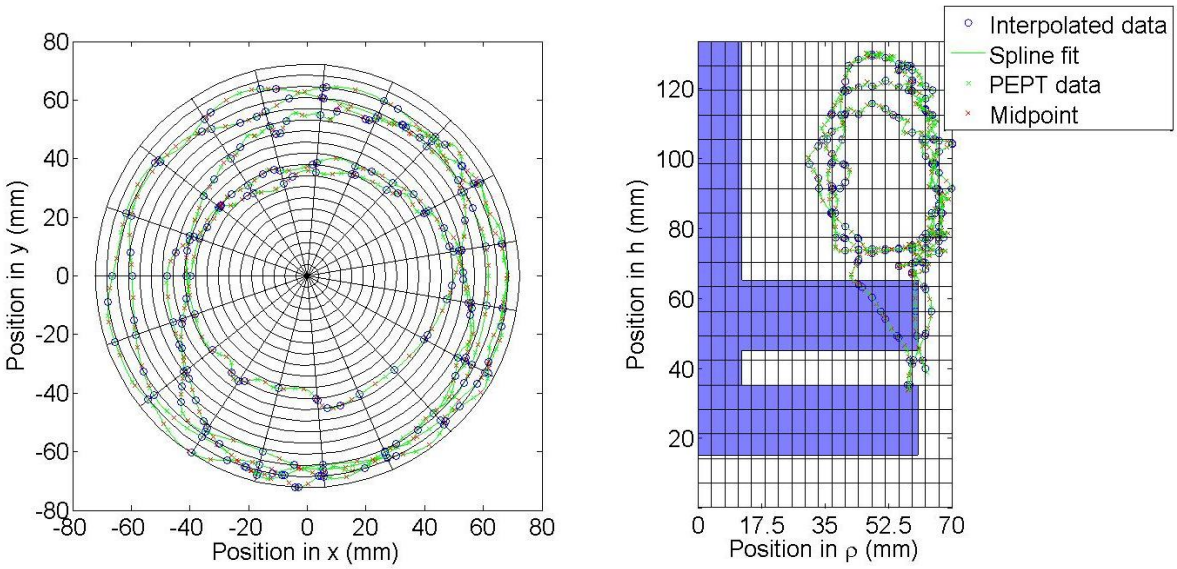

Figure 3.2-20 Boundary crossing points in (a) Θ and ρ and (b) ρ and h

3.2.6.3.6 Collisions

The number of media-media collisions was calculated using the method outlined in Section 3.2.5. The number of particles in a block volume N_{block} was calculated by dividing the volume of media in a block volume by the average volume of a grinding media particle V_m. The volume of grinding media in a block volume was assumed to be proportional to the time the tracer spends in a block volume and therefore the

percentage time the media spends in a block volume is proportional to the percentage volume of the media

$$N_{block} = \frac{V_{tot} * \frac{occ_{block}}{100}}{V_m} \qquad \textbf{Equation 3.2-35}$$

where V_{tot} is the total volume of grinding media and occ_{block} is the occupancy of a specific block volume. The method used to measure mean relative velocity is outlined in Section 6.2.2

3.2.6.3.7 Parameters visualised

Using this technique a number of flow parameters can be visualised:

1. Occupancy – the fraction of time spent in each block volume. This also gives a measure of the number of media particles within each block volume
2. Velocity – the average velocity of the grinding media within each block volume
3. Force – the average force of the grinding media within a block volume
4. Stress exerted – the average stress exerted by the grinding media within each block volume
5. Collisions – the number of collisions which occur within a block volume calculated using collision frequency. Details of such are described in Section 3.2.5

Figure 3.2-21 shows examples of each of the contour plots which can be created from PEPT.

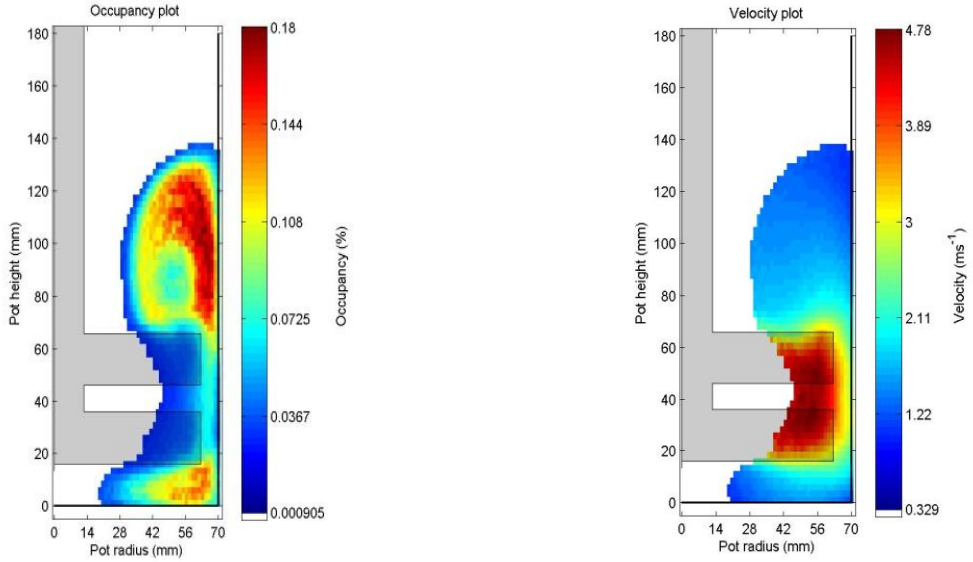

Figure 3.2-21 (a) Occupancy (b) Velocity (c) Force (d) Collisions across mill cross-section

4 LABORATORY GRINDING OF CALCIUM CARBONATE: RESULTS AND DISCUSSION

4.1 INTRODUCTION

Following on from the literature review in section 2.3, the mill operational parameters listed below were investigated:

(i) Mill motor energy input

(ii) Grinding media specific gravity

(iii) Grinding media particle size

(iv) Grinding media surface roughness

(v) Mill impeller speed

(vi) Calcium carbonate solids volume concentration

The objective was to understand the effect of these parameters on the operational performance of the laboratory grinding mill in terms of calcium carbonate particle size distribution of the suspensions produced at set points of a grind. The initial objective was to better understand the most significant factors that could allow a more energy efficient grinding process to be implemented for Imerys's calcium carbonate operations worldwide.

4.2 THE EFFECT OF ENERGY INPUT ON CALCIUM CARBONATE PARTICLE SIZE DISTRIBUTION

The data generated from a laboratory grinding test are shown in Figure 4.2-1 (a) which displays the calcium carbonate particle size (expressed as d90, as is industrial practice) as it varied as a function of mill energy input throughout the course of a grind performed under the following conditions in the laboratory mill described in Section 3.2.2; total charge volume including grinding media (1.1 L), MVC (52 %), impeller speed (1200 rpm), calcium carbonate solids by weight (75 % by weight), using 1.2-2.0 mm zirconium silicate grinding media of specific gravity 4.2.

A typical laboratory grind was run until a cumulative energy input of 530 kWh/tonne had been expended (based on standard mill protocols developed by Imerys over many years). Repeats were completed and found to be less that 5 % and therefore omitted for clarity. It can be seen the d90 dropped from greater than 8 μm to less than 2 μm over this energy range. Milled calcium carbonate products are normally sold over this particle size range for various paper, polymer and paint applications.

Figure 4.2-1 (b) shows how the grinding rate varied as a function of energy input.

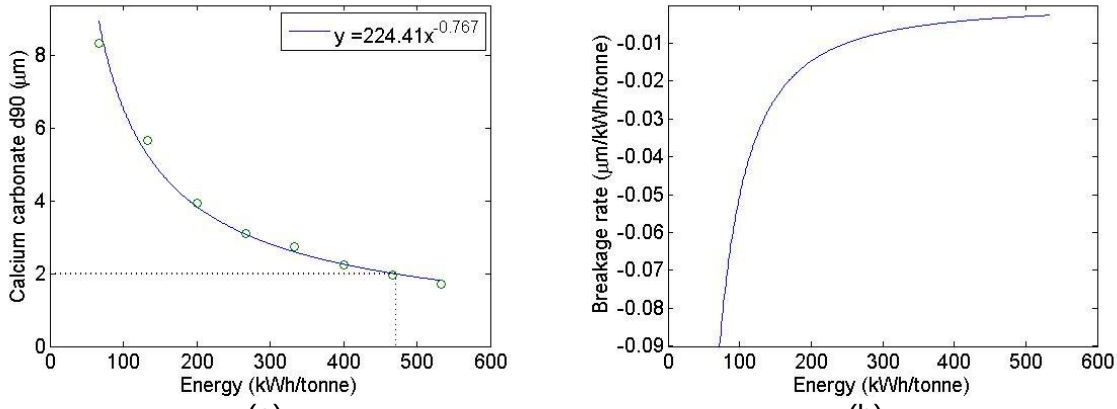

(a) (b)

Figure 4.2-1 (a) Plot showing calcium carbonate particle size (d90) against input energy (b) Plot showing change in grinding rate against input energy

The data in Figure 4.2-1 show that calcium carbonate particle size decreased as mill energy input increased. A typical industrial calcium carbonate has a d90 of 2 μm particle size; in this test this was achieved at an energy input of 471 kWh/tonne. Initially the particle size decreased rapidly as energy input increased. However at finer particle sizes (< 5 μm) more energy was required to achieve further size reduction and the breakage rate slowed. It can be seen that after 300 kWh/tonne the breakage rate was very low and therefore very few successful collisions occurred.

As the particle size of the feed decreased the energy required to fracture a feed particle decreased (Lichter & Davey, 2006; Yashima & Kanda, 1987). However, the number of particles per unit mass increased. The calculation displayed in Table 4.2-1 shows approximately how particle size affects the number of particles per gram of calcium carbonate. Assuming that fracture can only occur at a breakage event, statistically 1000 more collisions are required per unit mass to fracture 2 μm calcium carbonate particles than 30 μm particles.

Table 4.2-1 Calculated number of particles per gram of calcium carbonate as a function of particle size

Particle size (μm)	Number of particles per gram
30	1.4×10^4
10	3.7×10^5
5	3.0×10^6
2	4.6×10^7

4.3 THE EFFECT OF GRINDING MEDIA SPECIFIC GRAVITY ON MILL PERFORMANCE

Figure 4.3-1 shows how the particle size of calcium carbonate varied as a function of energy input throughout the course of a series of grinds performed with approximately equal sized, but differing specific gravity grinding media shown in Table 4.3-1. Other grinding conditions were as in Section 4.2: total charge including grinding media (1.1 L), MVC (52 %), impeller speed (1200 rpm) and calcium carbonate solids (75 % by weight). Figure 4.3-2 shows how the energy required to achieve a d90 of 2 μm varied with the specific gravity of the grinding media (these are typical grinding media used by Imerys for various mineral processing applications).

Table 4.3-1 Comparison of grinding media used (see Table 3.1-1 for further grinding media details)

Grinding media	Specific gravity
Mullite	2.7
Zirconium silicate	3.9
High density zirconium silicate	4.2
Zirconia	6.0

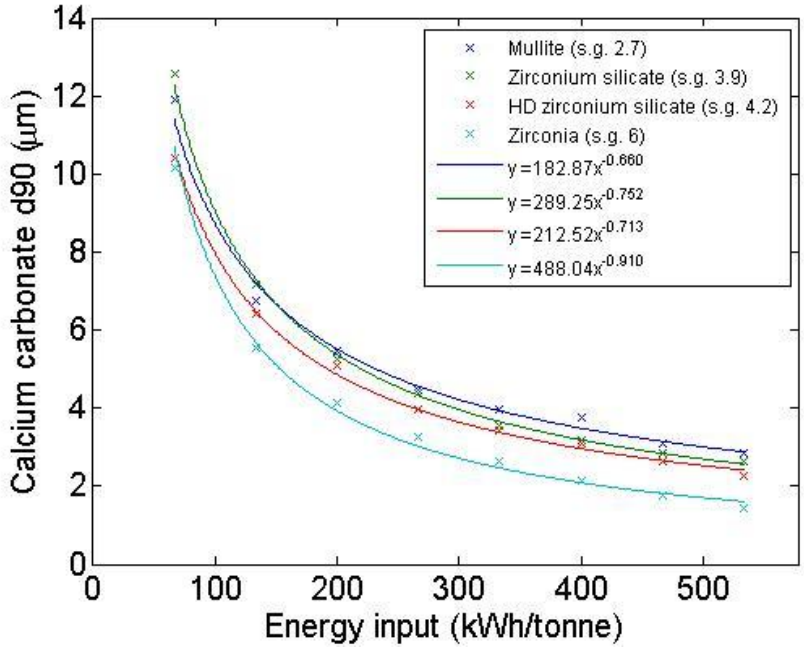

Figure 4.3-1 Plot showing calcium carbonate d90 against input energy with different specific gravity grinding media

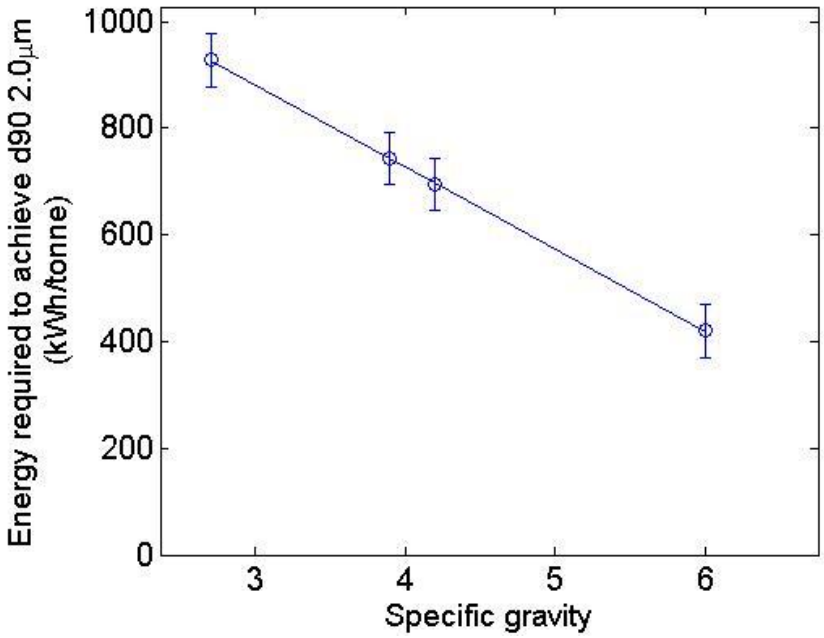

Figure 4.3-2 Plot showing the energy required to achieve d90 of 2 μm with changing specific gravity

The data in Figure 4.3-1 and Figure 4.3-2 show that increasing the specific gravity of the grinding media resulted in reduced energy requirements to meet a specific grinding objective (in this case a d90 of 2 μm). Figure 4.3-2 shows a linear relationship between specific gravity and the energy required to achieve a d90 of 2 μm. This relationship suggested that doubling the specific gravity resulted in 309 kWh/tonne saving in energy, and that the use of zirconia grinding media instead of mullite resulted in 45 % energy savings. In an industrial situation the higher price of high specific gravity grinding media and its wear rate would have to be considered against the energy savings. Zirconia is the highest specific gravity non-wearing, non-discolouring grinding media that is commercially available.

Because the same volume of approximately equal sized grinding media was used for each experiment it can be assumed that the grinding media specific gravity had little effect on the number of media-media collisions within the mill. Therefore the improved performance occurred as result of the increased stress energy (*SE*) resulting from the increased specific energy (ρ_{GM}) as described in Equation 4.3-1 (Kwade, 1999_B)

$$SE \propto SE_{GM} = d_{GM}^3 v_t^2 \rho_{GM} \qquad \textbf{Equation 4.3-1}$$

where SE_{GM} is the stress energy of the grinding media, d_{GM} is the diameter of the grinding media and v_t is the tip speed of the impeller.

4.4 THE EFFECT OF GRINDING MEDIA SIZE ON MILL PERFORMANCE

Figure 4.4-1 (a) and (b) shows how the calcium carbonate particle size varied as a function of mill energy input throughout the course of a series of grinds performed with different size zirconium silicate grinding media having specific gravity of 3.9 as shown in Table 4.4-1 (other conditions as in Section 4.2: total charge including grinding media (1.1 L), MVC (52 %), impeller speed (1200 rpm), and calcium carbonate solids (75 % by weight)). Figure 4.4-2 shows how the energy required to achieve a d90 of 2 μm varied with grinding media size.

Table 4.4-1 Comparison of zirconium silicate grinding media used (see Table 3.1-1 for further grinding media details

Grinding media size range (mm)
0.60-1.00
1.48-1.60
1.60-2.00
2.00-2.40

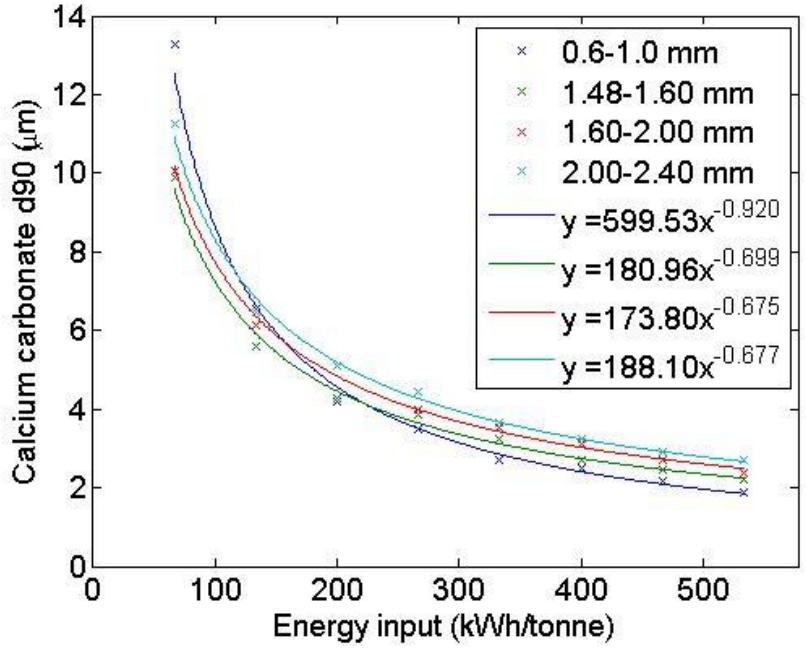

Figure 4.4-1 Plots showing the energy required to achieve d90 of 2 μm with changing grinding media size

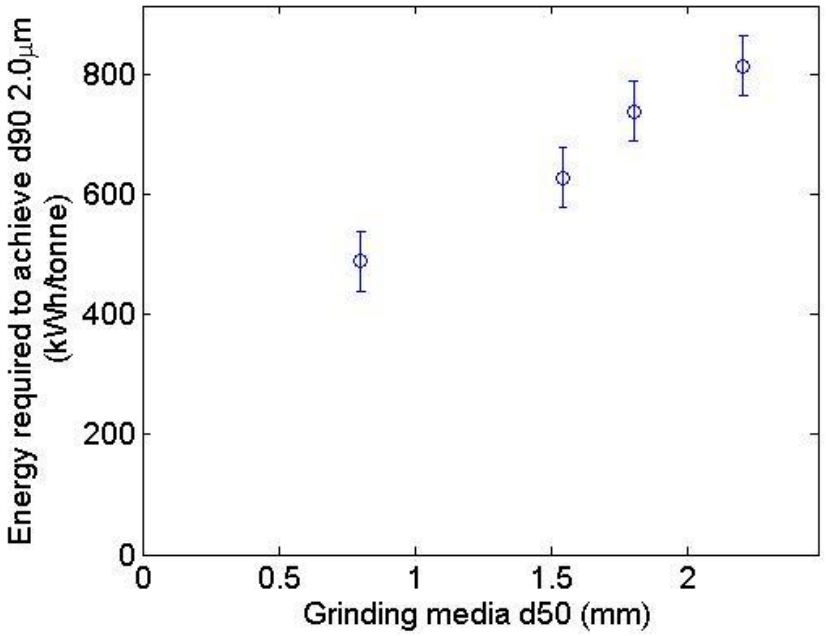

Figure 4.4-2 Plot showing the energy required to achieve d90 of 2 μm with changing grinding media size

The above data indicate that using smaller grinding media reduced the energy required to achieve the target d90. In the experiment presented here the energy saving achieved by reducing the grinding media size from 2.0-2.4 mm to 0.6-1.0 mm was approximately 325 kWh/tonne.

Reducing grinding media size reduced the stress energy of a collision and increased the number of media-media collisions per unit volume. The improved performance observed with finer grinding media likely occurs because the effect of increasing the number of collisions per unit volume of grinding media outweighed the effect of reduced stress intensity. Therefore, reducing the size of the grinding media increased the number of stress events within the mill (SN_f).

Further examination of Figure 4.4-1 indicates that although the lowest grinding energy input to reach a d90 of 2 μm was achieved with the finest grinding media investigated (0.60-1.00 mm), this grinding media was the least efficient during the coarse stage of the grind. This is suggestive that in an industrial process further energy efficiency could be achieved by using coarse grinding media during the early, coarse, stages of a grinding process and then switching to finer grinding media as the calcium carbonate particle size is reduced.

4.5 THE EFFECT OF GRINDING MEDIA SURFACE ROUGHNESS ON MILL PERFORMANCE

Grinding media are made by a variety of processes. The details of these processes are usually confidential. In this study the performance of experimental rough grinding media, supplied by Imerys, was compared with that of a conventional smooth surfaced zirconia-based grinding media having equivalent particle size distribution and specific gravity (both with 3 mm diameter and a specific gravity of 5.5). Other grinding conditions were as in Section 4.2.

Figure 4.5-1 shows surface profiles of the rough and smooth grinding media used measured using an interferometer as outlined in Section 3.2.3. Variations in height are represented as colour changes where black represents the minimum height and white the maximum. It can be seen that the smooth zirconia-based grinding media (a) had a more consistent colour varying very little in height compared to the rough experimental grinding media (b).

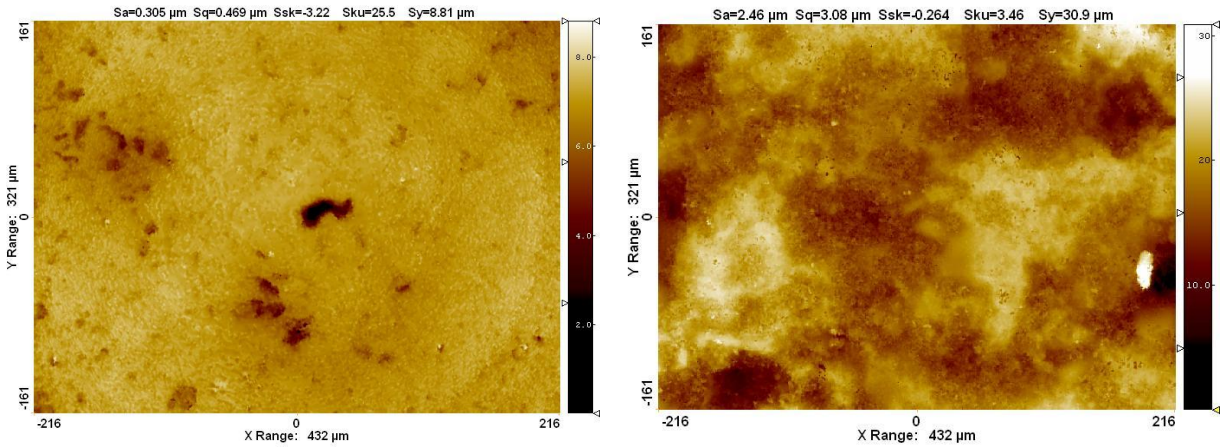

(a) (b)

Figure 4.5-1 Topographical surface of an area of a (a) spherical zirconia grinding media and (b) rough grinding media

Table 4.5-1 shows the surface roughness parameters S_a and S_q for the rough and smooth grinding media types calculated from the interferometer data.

Table 4.5-1 Surface roughness of rough and smooth grinding media

Grinding media	S_a (μm)	S_q (μm)
Smooth	0.6	0.8
Rough	5.7	7.6

Figure 4.5-2 shows how the calcium carbonate particle size varied as a function of energy input throughout the course of grinds performed with the grinding media shown in Table 4.5-1. Other grinding conditions were as in Section 4.2: total charge including grinding media (1.1 L), MVC (52 %) and calcium carbonate solids (75 % by weight) except impeller speed was reduced to 650 rpm and the total input energy was reduced to 200 kWh to prevent damage to the impeller from the large grinding media.

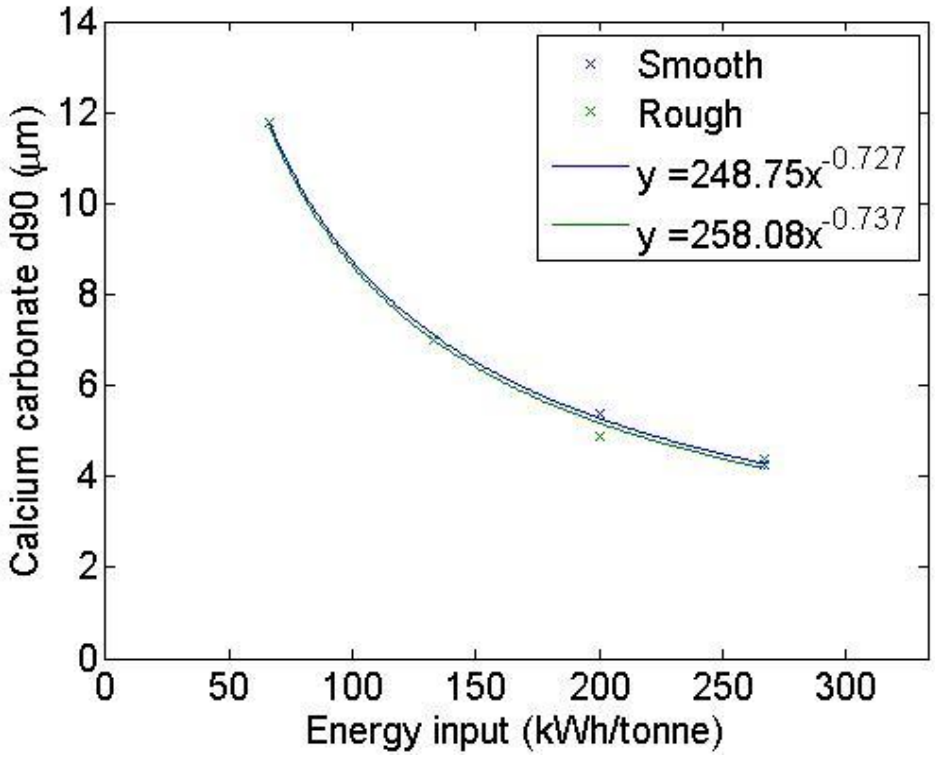

Figure 4.5-2 Plot showing the energy required to achieve d90 of 2 μm with changing grinding media surface roughness

Figure 4.5-2 suggests that surface roughness had no effect on grinding performance for calcium carbonate. However, from Figure 4.5-3, it can be seen that the power draw was considerably higher with the rough grinding media. This would result in better plant efficiency as the grind time was reduced by 20 %. The reasons for this behaviour are unclear, and will be revisited in parallel with the PEPT data reported in Section 6.3.3 In an industrial situation grinding media that do not get polished during continuous operation would be required.

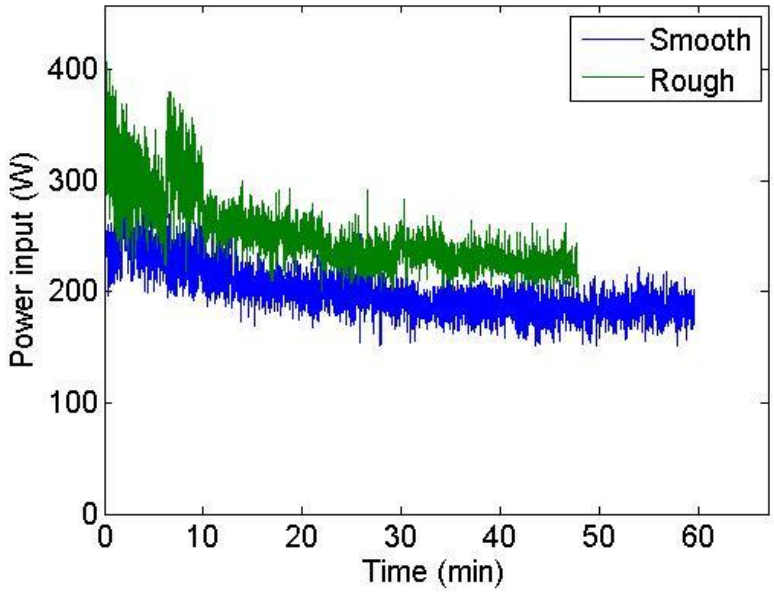

Figure 4.5-3 Plot comparing energy input for rough and smooth grinding media

4.6 THE EFFECT OF MILL IMPELLER SPEED ON PERFORMANCE

Figure 4.6-1 shows how calcium carbonate particle size varied as a function of energy input throughout the course of a series of grinds performed at different impeller speeds as shown in Table 4.6-1. Other grinding conditions were as in Section 4.2: total charge including grinding media (1.1 L), MVC (52 %), calcium carbonate solids (75 % by weight) and grinding media (zirconium silicate, 1.2-2 mm, specific gravity 4.2). Figure 4.6-2 shows how the energy required to achieve a d90 of 2 μm varied with the impeller speed. The impeller speed range investigated was from 600 to 1400 rpm. This impeller speed range is the operational speed range of the mill. At impeller speeds less than 600 rpm the grinder charge was not fluidised. At speeds greater than 1400 rpm shearing occurred in the mill with the impeller and part of the charge moving independently from the rest of the charge and the grinding chamber.

Table 4.6-1 Comparison of impeller speeds investigated

Impeller speed (rpm)	Impeller tip speed (ms^{-1})
600	4.0
700	4.6
800	5.3
1000	6.6
1200	7.9
1400	9.2

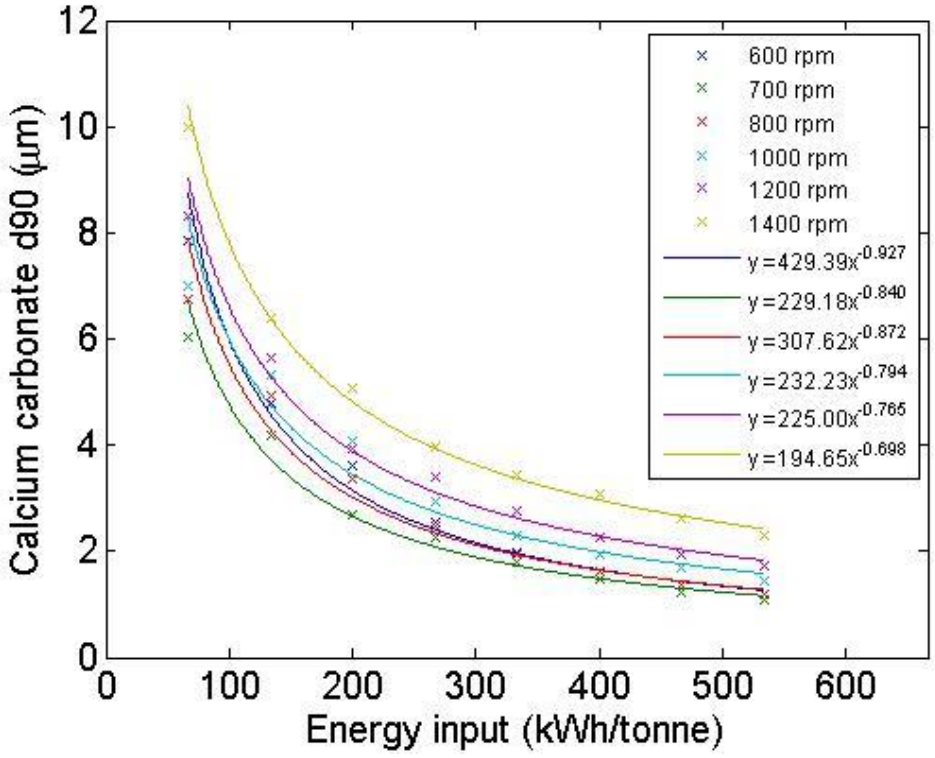

Figure 4.6-1 Plot showing calcium carbonate d90 against input energy with changing impeller speed

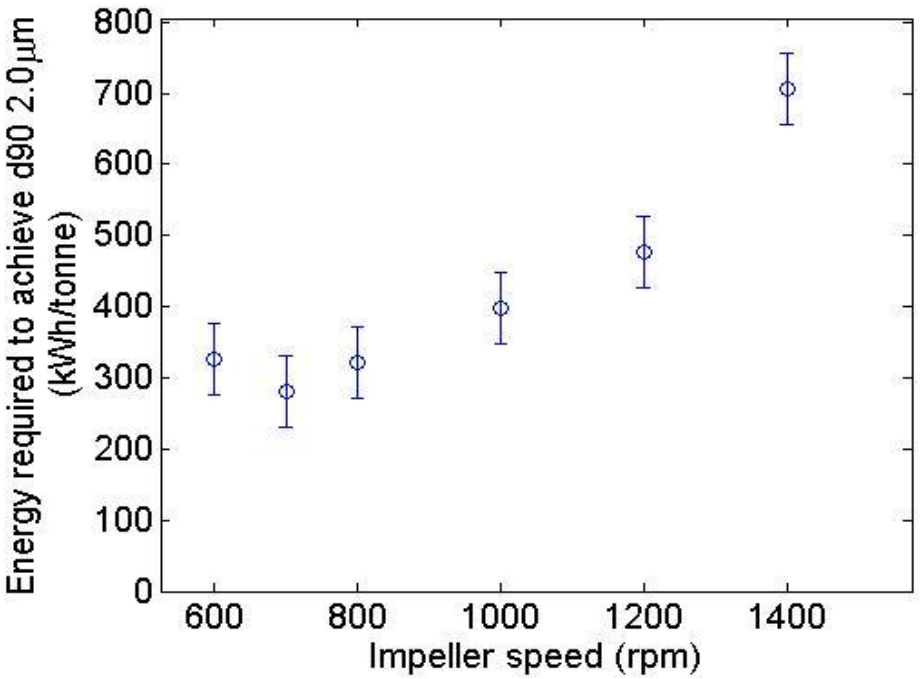

Figure 4.6-2 Plot showing the energy required to achieve d90 of 2 μm with impeller speed

The above data indicate that the optimum impeller speed in terms of energy input to achieve a target d90 was 700 rpm (impeller tip speed 4.2 ms^{-1}). This is likely because at impeller speeds lower than 700 rpm the stress energy supplied by the impeller to the grinding media was less than optimum to achieve calcium carbonate particle breakage at the size range required for this application. At impeller speeds greater than 700 rpm the stress energy supplied was in excess of the optimum required for particle breakage and therefore some energy was wasted. The highest efficiency was achieved at 700 rpm where it is likely that the stress energy was optimum. This observation will be explored further in Section 6.3.4.

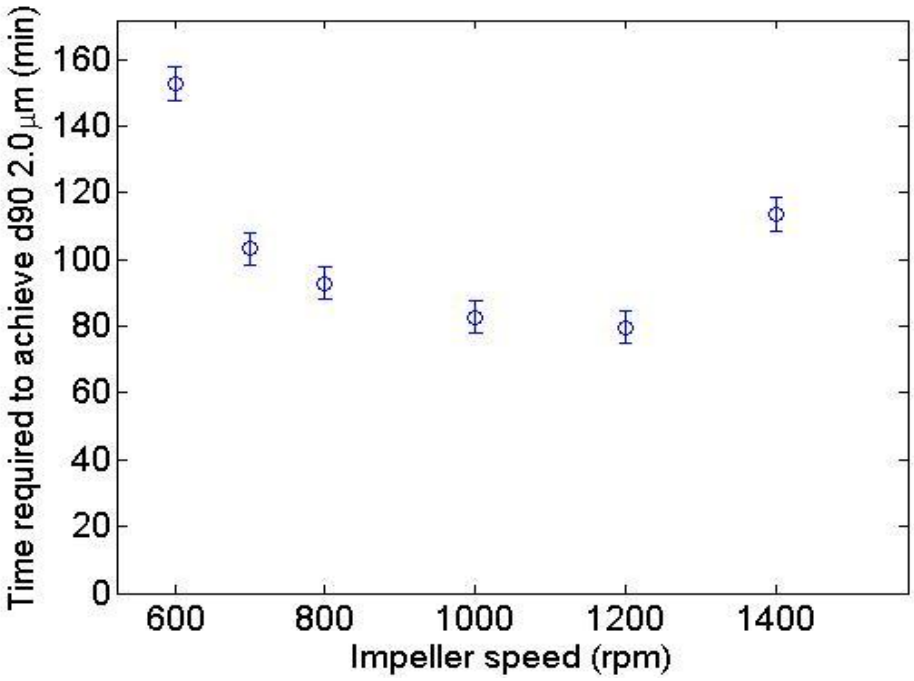

Figure 4.6-3 Plot showing the time required to achieve d90 of 2 μm with impeller speed

Figure 4.6-3 shows the time taken to achieve a target d90 of 2 μm as a function of impeller speed. It can be seen that the minimum time to reach the required particle size distribution (and hence maximum throughput) occurred at 1200 rpm despite this not being the impeller speed which corresponded to optimum energy efficiency. In an industrial environment the impeller speed chosen would be a trade off between energy efficiency and throughput (capital efficiency). An industrial plant would likely operate in a continuous manner and ideally utilise fixed speed gearboxes for optimal capital and maintenance performance. It would also be necessary to consider additional factors such as the role of the impeller in facilitating discharge through and cleaning of the grinder door screens. Nonetheless, the optimum impeller speeds for optimum energy efficiency and optimum throughput efficiency are important considerations in calcium carbonate plant design.

4.7 THE EFFECT OF SOLIDS VOLUME CONCENTRATION ON MILL PERFORMANCE

Figure 4.7-1 shows how calcium carbonate particle size varied as a function of energy input throughout the course of a series of grinds performed at different solids volume concentrations as shown in Table 4.7-1 (other conditions were as in Section 4.2: (total charge including grinding media (1.1 L), MVC (52 %), impeller speed (1200 rpm), and grinding media (zirconium silicate, 1.2-2 mm, specific gravity 4.2)).

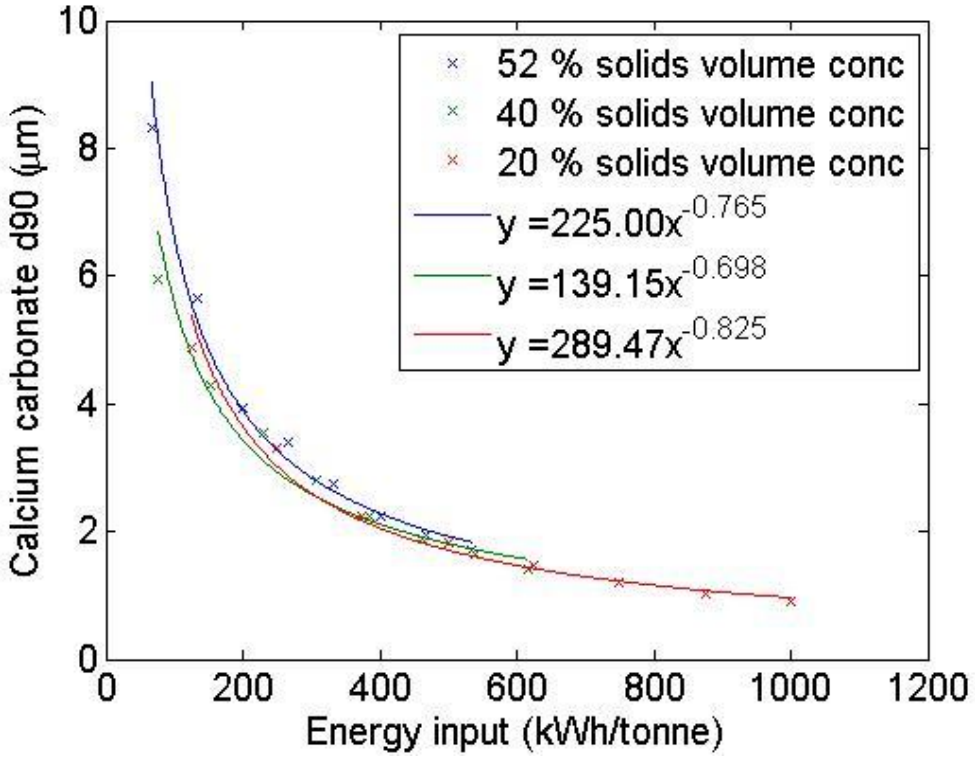

Figure 4.7-1 Plot showing calcium carbonate d90 against input energy with solids volume concentration

Table 4.7-1 Comparison of solids volume concentration investigated

Solids volume concentration (volume/volume %)	Solids (weight/weight %)
52	75
40	65
20	40

Figure 4.7-2 shows how the energy required to achieve a d90 of 2 μm varied with the solids volume concentration.

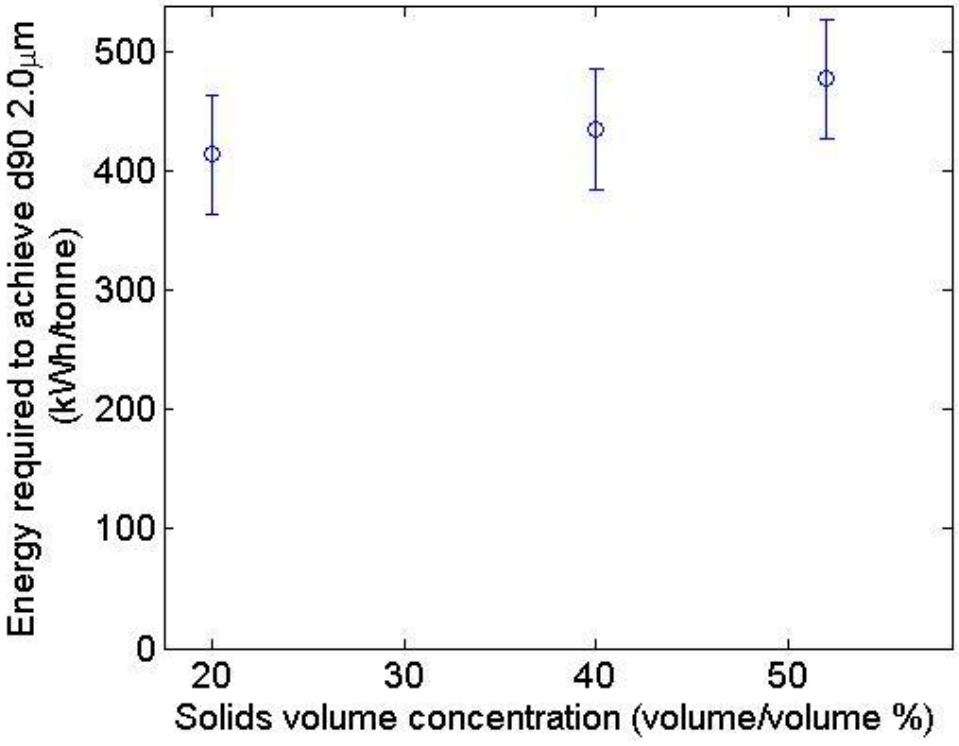

Figure 4.7-2 Plots showing the energy required to achieve d90 of 2 μm with solids volume concentration

These data indicate that the highest energy efficiency occurred at the lowest volume solids concentration and reducing the solids volume concentration from 52 % to 20 % resulted in a 63 kWh/tonne energy saving. Assuming one particle in the active volume, the reduction in energy efficiency is a result of the reduced number of calcium carbonate particles present in the mill.

4.8 DISCUSSION

The observations on the effect of changing grinding parameters described in this chapter are summarised in Table 4.8-1 below.

Table 4.8-1 Summary of effect of grinding parameters on grinding performance

Parameter	Effect	Possible mechanism
Grinding media specific gravity	Increasing specific gravity increased energy efficiency	Increased stress energy at a collision
Grinding media size	Reducing grinding media size increased energy efficiency	Increased number of collisions
Grinding media surface roughness	No impact on energy efficiency but decreased grind time	
Impeller speed	Optimum speed for best energy efficiency was 700 rpm	Optimum stress energy
Solids volume concentration	Low solids volume concentration improved energy efficiency	Reduced number of calcium carbonate particles to fracture

These data indicate that calcium carbonate comminution can generally be explained using the concepts of stress intensity and stress number described by Kwade and outlined in Section 2.4. Varying different mill parameters affected mill performance by altering: (i) the stress energy of a collision and (ii) the number of collisions.

Taken together the data indicate that optimum energy efficiency could be obtained by using:

(i) High specific gravity grinding media

(ii) Fine particle size grinding media

(iii) High MVC

(iv) Low solids volume concentration

(v) Optimal impeller speed

In an industrial environment the conditions chosen would most likely be a compromise between energy efficiency and other considerations such as:

(i) Throughput (and hence capital efficiency)

(ii) Cost of grinding media versus improved energy efficiency

(iii) Additional process steps required (for example grinding at low volume solids concentrations may necessitate subsequent process steps such as dewatering)

(iv) Specific application requirements (for example paper coating formulations must be produced at high solids to facilitate high solids coating)

5 DETERMINING THE FRACTURE PROPERTIES OF CALCIUM CARBONATE: RESULTS AND DISCUSSION

5.1 INTRODUCTION

Particle breakage events in comminution processes are poorly understood complex processes dependent on the material characteristics, stress conditions and environment of the stress events (Tavares, 2007).

Fracture occurs within a vertically stirred mill when grinding media particles are accelerated by the impeller and collide with slower moving grinding media further away from the impeller (Kwade, 1999_A). During a collision any feed particles trapped between the media are stressed. If the stressing conditions are larger than a feed particle can withstand then it will fracture and smaller daughter particles will be created.

Initial attempts were made using bulk compression tests (Adams model), however due to the brittle nature of the samples used the results were inconclusive. Experiments conducted on single particles have been used to better understand a number of the fundamental aspects of fracture processes Sikong, et al., 1990; Tavares, 2007; Zhang & Stenson, 2009; Yashima & Kanda, 1987). The material characteristics relevant to particle breakage are: (i) the fracture strength and (ii) the deformation behaviour of the feed material (Tavares, 2007). Fracture strength can be defined in terms of energy (particle fracture energy (E_c)) or stress (particle compressive strength (σ_c)) required to cause fracture as shown in Equation 5.1-1 and Equation 5.1-2 respectively

$$E_c = \int_0^{\Delta_c} F_c d\Delta$$ **Equation 5.1-1**

$$\sigma_c = \frac{4F_c}{\pi d^2}$$ **Equation 5.1-2**

where F_c the force applied at the onset of fracture, Δ_x is the deformation, Δ_c is the deformation at the onset of fracture and d is the particle diameter.

Material deformation behaviour can be classified as elastic or inelastic and depends on the conditions of the stress event. Stress conditions are classified as (Tavares, 2007):

(i) Type of stressing (compressive or shear)

(ii) Number of loading points

(iii) Stressing intensity

(iv) Stressing rate

Single particle fracture tests are designed to emulate the stress conditions experienced within a comminution process. As discussed, fracture occurs within a vertically stirred mill when a feed particle is stressed as a fast moving grinding media particle collides with a slower grinding media. To match these conditions a particle must be loaded such that it is stressed between two hard surfaces at a rate equivalent to the difference in the speed of the two grinding media particles. However, because of the size of the feed material investigated it is only possible to determine fracture parameters using a micromanipulator with a stressing rate of 0.5 μms^{-1}, considerably slower than 1 ms^{-1}, the relative velocity of the grinding media calculated in Section 6.2. This requires the assumption that the strength of the feed material is independent of stressing rate.

As particle size decreases the number of flaws present in a particle also decreases. This results in plastic behaviour as particles are deformed a considerable amount before fracture at a critical size. Studies show that this behaviour begins to occur at particle sizes around 2-3 μm (Sikong, et al., 1990) and that at 1 μm calcium carbonate particles theoretically exhibit entirely plastic behaviour (Kendall, 1978). Therefore, to ensure only elastic behaviour occurs calcium carbonate particles ranging from 35 to 5 μm were investigated in this work.

Throughout the course of this work the particle fracture force and particle compressive strength of calcium carbonate powder samples prepared from Turkish marble sourced from Marmara Island were measured using the micromanipulation technique outlined in Section 3.2.4.

Three samples were investigated: (i) a 45 μm to 30 μm sample, (ii) a < 30 μm sample and (iii) a commercial sample tradename G10 with a d90 of 10 μm supplied by Imerys. The 45 μm to 30 μm sample and the < 30 μm sample were prepared by dry screening the coarse calcium carbonate powder used as the feed for the grinding experiments reported in Chapter 4.

5.2 PARTICLE FRACTURE FORCE

Figure 5.2-1 (a) to (c) shows three calcium carbonate particles ranging from 10 μm to 30 μm prior to compression. For each experiment, a force displacement curve was generated as shown in Figure 5.2-2.

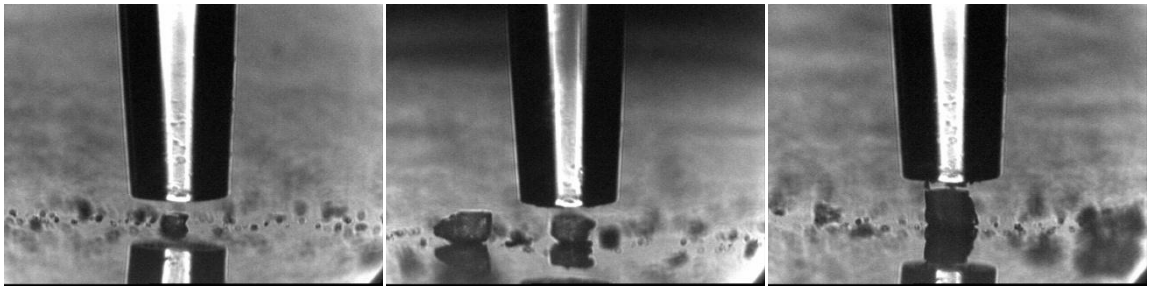

(a) (b) (c)

Figure 5.2-1 Micromanipulator prior to compression of (a) 10 μm (b) 20 μm and (c) 30 μm calcium carbonate particles

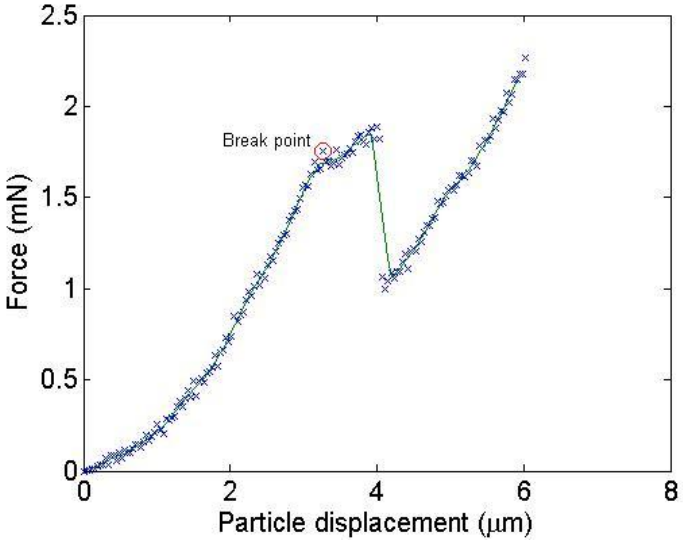

Figure 5.2-2 Typical force displacement plot of calcium carbonate particle

Figure 5.2-2 shows a typical relationship between force and displacement of a calcium carbonate particle. As force was applied the particle was displaced until a critical point when breakage occurred and the force experienced was temporarily

reduced. Figure 5.2-3 shows the distribution of different fracture forces as a function of particle size for the three samples. Figure 5.2-4 (a) is a composite of the data for all three samples and Figure 5.2-4 (b) presents these data on a log-log plot with a trendline showing the average compressive strength of a particle at a given size. There is a large degree of scatter due to irregularities in particle shape and surface flaws.

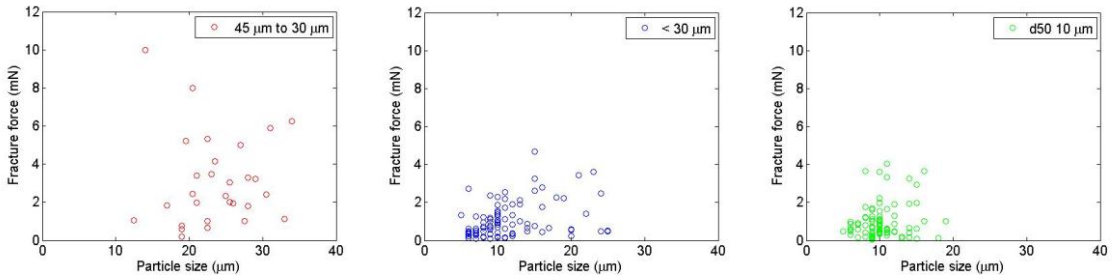

(a) (b) (c)

Figure 5.2-3 Particle fracture force of (a) 45 to 40 μm (b) < 30 μm and (c) commercial product G10 calcium carbonate particles as a function of particle size

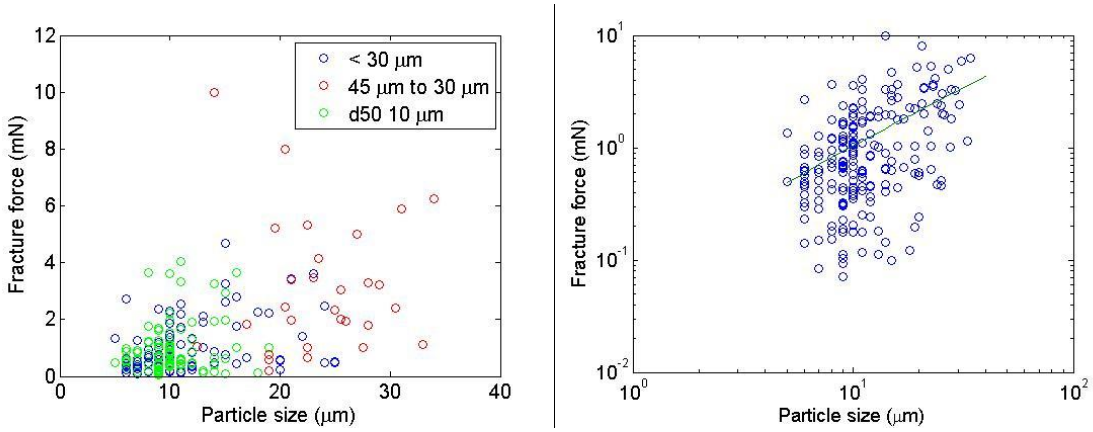

(a) (b)

Figure 5.2-4 (a) Fracture forces from samples (i) (ii) and (iii) against particle size (b) Fracture forces from samples (i) (ii) and (iii) against particle size presented on log-log axes

Figure 5.2-3 and Figure 5.2-4 show how particle fracture force varied with particle size. From Figure 5.2-3 (b) and (c) it can be seen that the force required to fracture 5 to 10 μm particles was largely between 0.1 and 2 mN of force.

Figure 5.2-4 (a) and (b) show all three samples plotted on the same graph. It can be seen that as particle size decreased particle fracture force also decreased. The results however show large variations in fracture force. This was due to microscopic flaws within the calcium carbonate particles and the orientation of the particle relative to the impacting force applied.

Because of the large distribution of cracks within each particle, irregularities in particle shape and orientation of each particle at a stress event, it is never possible to determine exactly if a particle will fracture when it experiences an applied force. Therefore cumulative distributions are used to determine the probability that a particle will fracture when a force is applied to it. Figure 5.2-5 shows the breakage probability of calcium carbonate particles divided into three size ranges; 5 to 10 μm, 10 to 15 μm, and >15 μm.

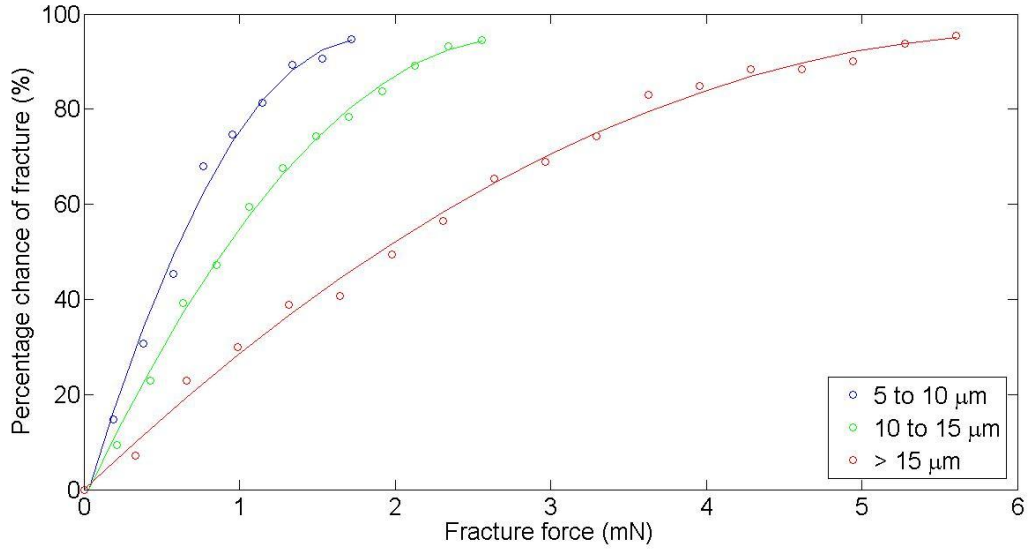

Figure 5.2-5 Breakage probability of calcium carbonate particles

Again it can be seen that finer particles required less force to induce fracture. The median force required to fracture each size fraction was determined from this plot as shown in Table 5.2-1.

Table 5.2-1 Median fracture force of 5-10 μm, 10-15 μm, and >15 μm calcium carbonate feed particles

Size fraction (μm)	Breakage force (mN)
5-10	0.8
10-15	1.1
>15	2.1

5.3 PARTICLE COMPRESSIVE STRENGTH

To break a calcium carbonate particle within a vertically stirred mill the compressive strength of the material must be exceeded at a collision (Kwade, 1999_A; Kwade, 1999_B). Compressive strength is a measure of a material's ability to withstand a compressive load prior to failure. Figure 5.3-1 shows a log-log plot of the compressive strength of calcium carbonate particles calculated using Equation 5.1-2 against particle size. The line of best fit shows how the average compressive strength of the particles tested varied with particle size.

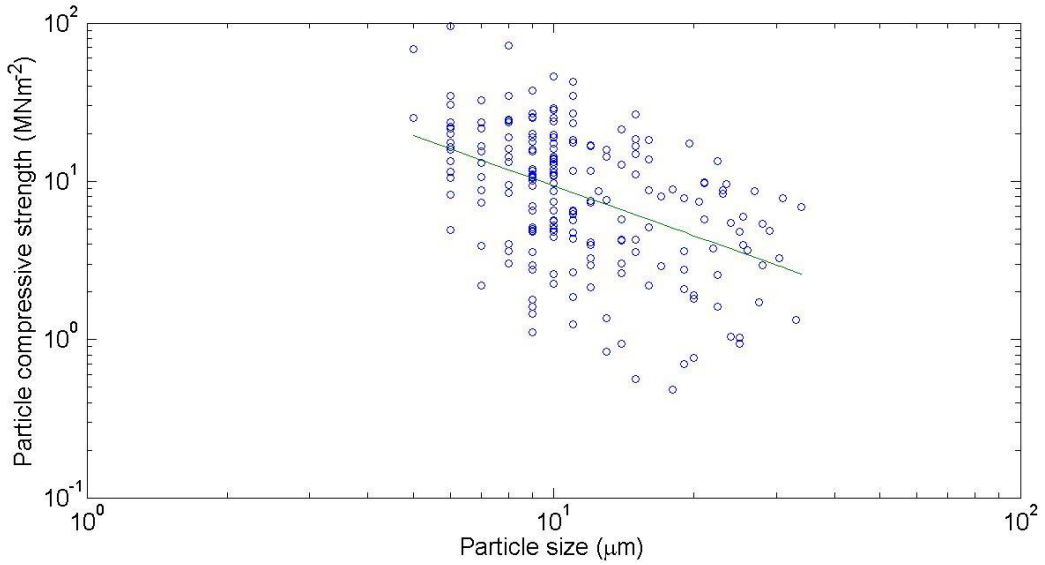

Figure 5.3-1 Compressive strength of calcium carbonate feed particles as a function of particle size

Figure 5.3-2 shows the probability of failure 5 to 10 μm, 10 to 15 μm and >15 μm calcium carbonate particles had when stressed. The median strength of each size range is shown in Table 5.3-1.

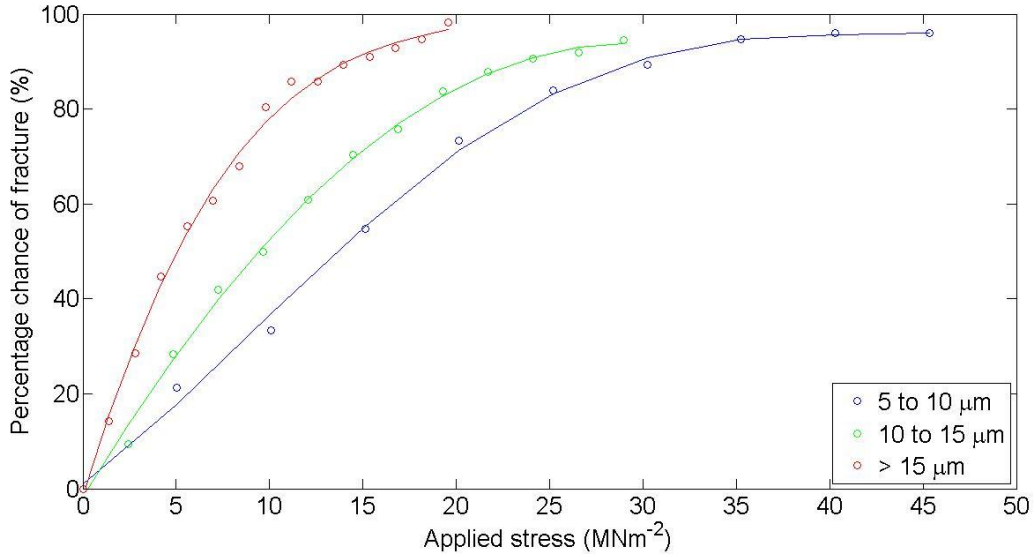

Figure 5.3-2 Breakage probability of calcium carbonate feed particles

Table 5.3-1 Median compressive strength of 5-10 μm, 10-15 μm and >15 μm calcium carbonate feed particles

Size range (μm)	Median compressive strength (MNm^{-2})
5-10	15.1
10-15	9.6
>15	8.4

From Figure 5.3-1 and Figure 5.3-2 it can be seen that particle strength increased as particle size decreased. This is to be expected as the strength of a material is not only dependent on the size of the material but also shape, orientation and number of surface flaws within each particle. As the particle size decreased so too do the number and size of flaws within the material which drastically alter the internal stress field of the particle increasing the amount of stress required to fracture a particle.

5.4 DISCUSSION

The data presented in this chapter show that as calcium carbonate particle size decreased so too did the force required to induce fracture. However the compressive strength of the particles increased as particle size decreased. It is theorised that the increased compressive strength of the particles arose due to the reduced size of any potential flaws within the material. This increased compressive strength with decreased particle size observation is consistent with the grinding data presented in Chapter 4 which show that as particle size decreased the rate of grinding decreased. The compressive strength data of calcium carbonate particles measured using the micromanipulator will be compared with the stress exerted at a media-media collision within a vertically stirred mill measured using PEPT in Chapter 6.

6 The use of Positron Emission Particle Tracking (PEPT) to measure regions of the mill suitable for fracture

6.1 INTRODUCTION

Positron Emission Particle Tracking allows non-invasive study of particulate systems. By irradiating a tracer particle, in this case a single grinding media particle, it is possible to determine where in the mill grinding media are located and the velocity, acceleration and force of the tracer within the mill. Combining this, Kwade's stress intensity and stress number models (Kwade, 1999_A; Kwade 1999_B; Kwade, et al., 1996), and particle fracture data it is possible to approximate when the grinding media can cause particle breakage, and how often fracture events can occur.

The objectives of the work presented here were:

1. To determine the regions within a vertically stirred media mill where calcium carbonate feed particles can be fractured by measuring the number of media-media collisions and the stress at the media-media collisions
2. To compare the different operating parameters discussed in Chapter 4 to determine how varying the conditions affect milling performance

As discussed in Section 3.2.6, using PEPT it is possible to locate the position of a tracer particle in time as it moves through a system. This allows the following parameters to be measured:

1. Occupancy – The percentage time the tracer spends within a given block volume
2. Velocity – The average velocity of the tracer as it moves through a block volume
3. Force – The force acting on the tracer particle as it moves through a block volume
4. Stress – The stress exerted by a grinding media particle as it collides with other particles. This is the total stress available for fracture at a collision. It is assumed that there is only one calcium carbonate feed particle stressed between grinding media particles at a collision
5. Collisions – The number of collisions grinding media undergo within a block volume. This is calculated using collision frequency equations based on the relative velocity of the grinding media and the number density of grinding media within a block volume

6.2 RESULTS FOR BENCHMARK SYSTEM

In this section an analysis is presented for a grind that was performed under the same conditions as used in the PEPT methodology Section 3.2.6.3.

6.2.1 Occupancy

Within a vertically stirred mill the mill contents are fluidised and the grinding media are accelerated away from the impeller resulting in two regions: (i) an impeller region below the upper edge of the top impeller and (ii) a recirculation region above the impellers. Figure 6.2-1 shows how the occupancy of the tracer varied throughout the cross-section of the mill. To better represent the data the position of the impeller and pot have been superimposed onto the plot. Regions of high occupancy are coloured red, low occupancy in blue and regions where no grinding media was present are shown as white. It can be seen that a central vortex was formed where no grinding media was present.

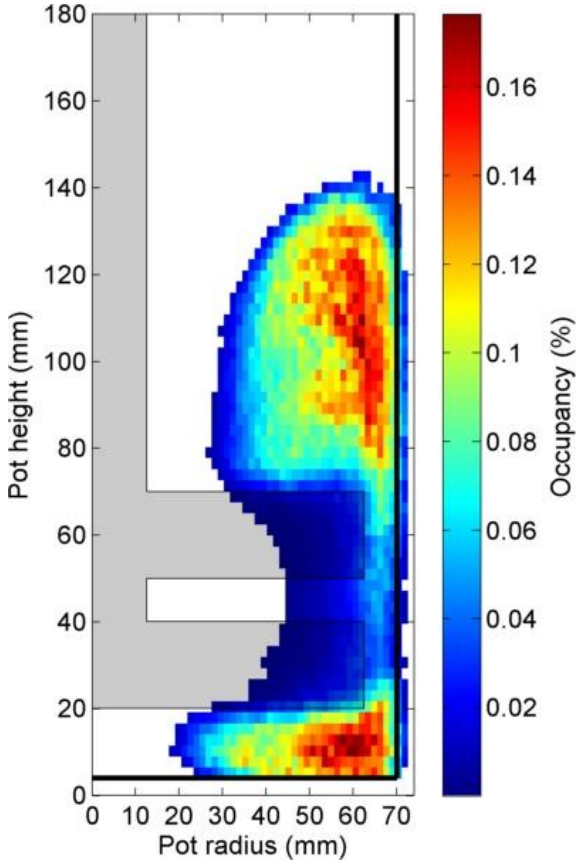

Figure 6.2-1 Occupancy plot of grinding media within a vertically stirred media mill

Figure 6.2-1 and Figure 6.2-2 show how the percentage of time the tracer spends at different heights in the mill varied with pot height. It can be seen that the tracer spent less time between the impellers than below or above them. Because the system is considered well mixed, it can be assumed that the percentage time spent in a block volume is proportional to the volume of grinding media within each block volume / height.

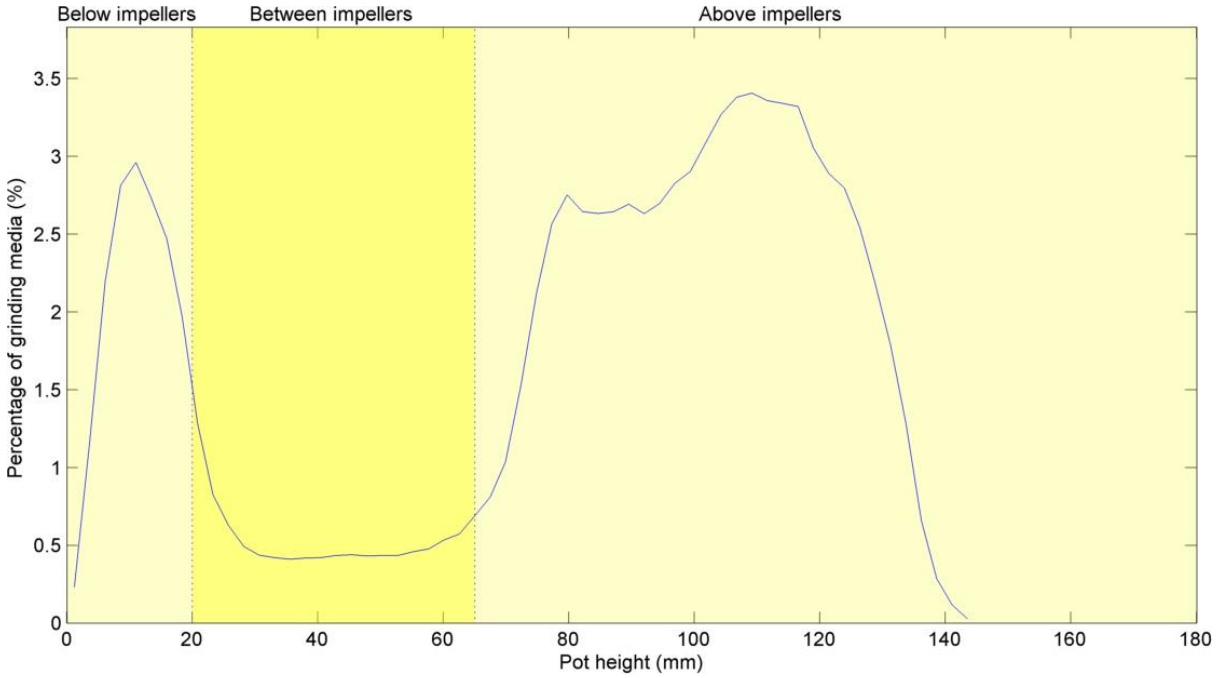

Figure 6.2-2 Percentage of grinding media against pot height

Previous studies have suggested that comminution occurs around the impeller (Blecher, et al., 1996; Kwade, 1999_A; Kwade, 1999_B). Figure 6.2-3 shows the cumulative distributions of how the percentage of grinding media varied throughout the mill as a function of height. The vertical dashed lines indicate the maximum and minimum position of the impellers, and the blue shaded regions show where the cumulative percentage of the grinding media reaches 25, 50, 75 and 100 %. Again these plots suggest there were less grinding media particles between the impellers compared to below or above them and that only 28 % of the grinding media were found in the impeller zone as displayed in Figure 6.2-4.

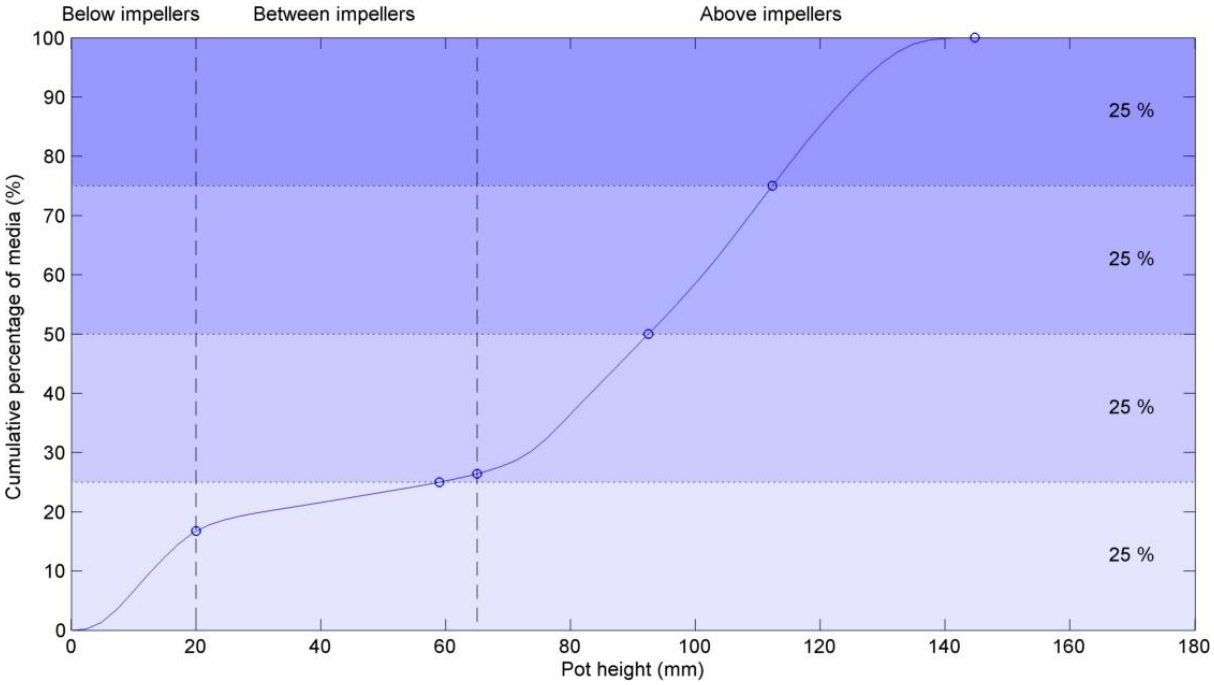

Figure 6.2-3 Cumulative percentage of grinding media as a function of height showing the percentage of media below, between and above the impellers and the median, upper and lower quartile height of the grinding media particles

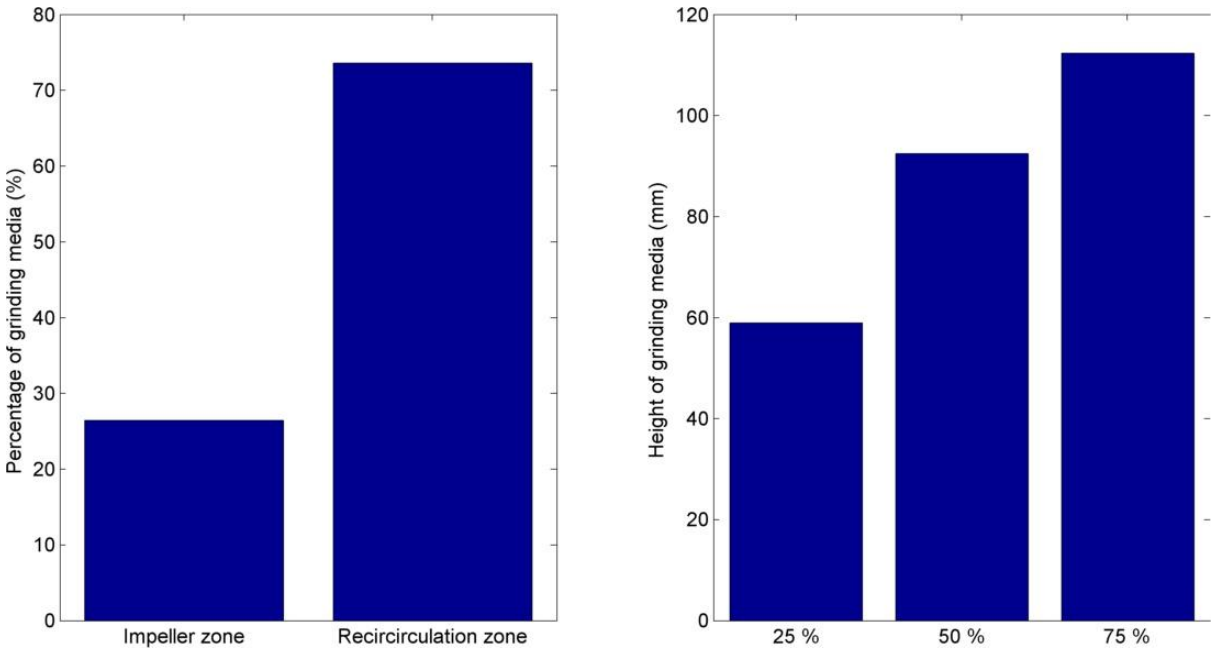

(a) (b)

Figure 6.2-4 (a) Percentage of grinding media in the impeller and recirculation zone (b) The height beneath which 25 %, 50 % and 75 % of the grinding media are located

6.2.2 Velocity

An impeller used in a cylindrical un-baffled vessel such as a stirred media mill produces a strong tangential flow with radial or axial components (Dong, et al., 1994) depending on the impeller configuration. Figure 6.2-5 (a) (b) and (c) show the flow regime which occurred within the mill. The size of the arrows indicated the magnitude of the velocity and the direction the grinding media was travelling. It can be seen that as the grinding media approached the impeller it was accelerated radially towards the pot wall. At this point the media was either lifted up into the recirculation zone, or forced downwards below the impellers producing a radial two loop flow pattern.

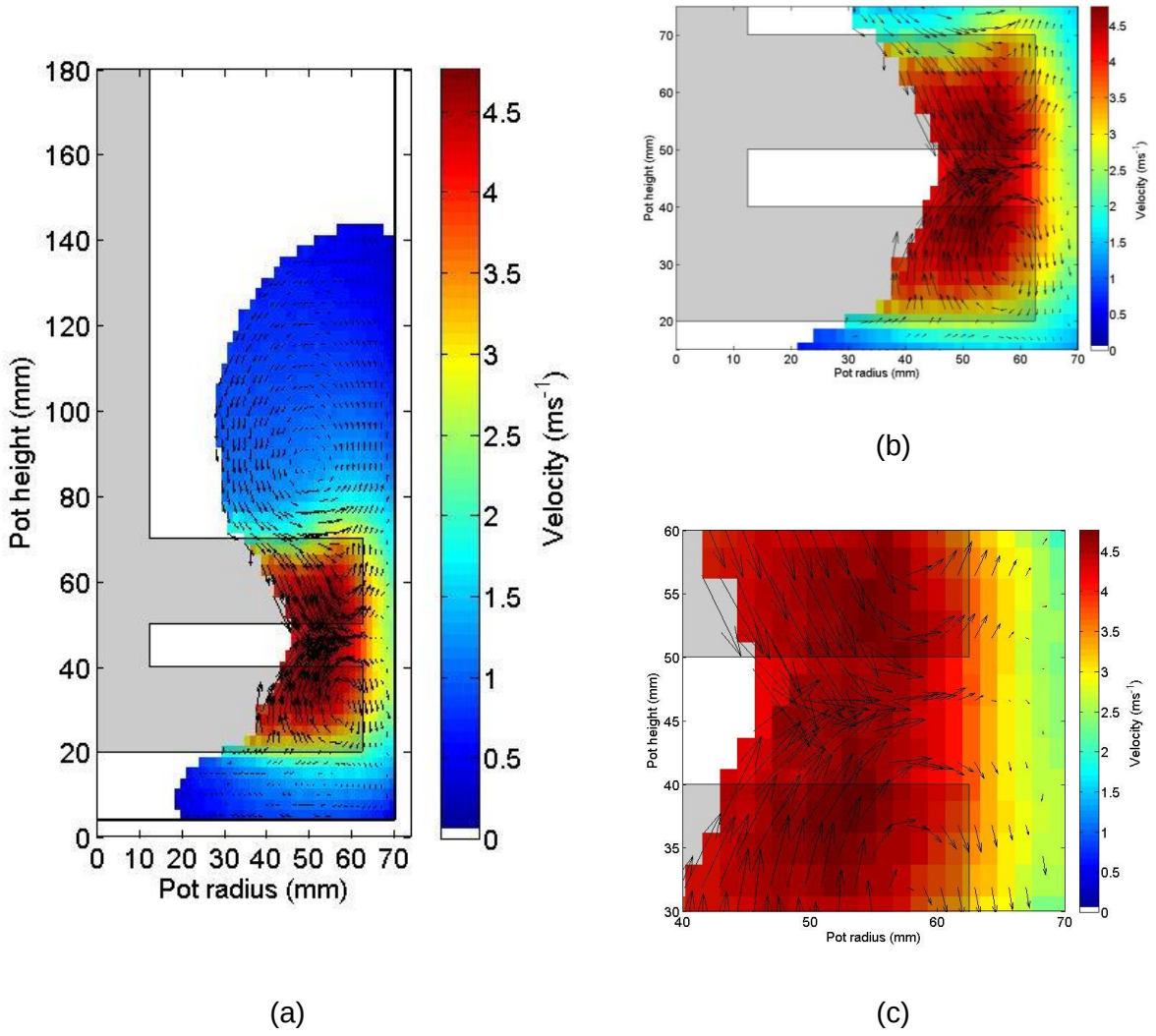

Figure 6.2-5 Velocity flow field within a vertically stirred mill (a) throughout the entire pot (b) the regions around the impeller and (c) between the impellers

The stress intensity model assumes that the tangential velocity of the grinding media is proportional to the tip speed of the disk (impeller) (Kwade, 1999_A). The stress intensity model only considers the tangential velocity because it is usually considerably higher than the axial and radial velocities and states: (i) that the velocity of the grinding media is proportional to the velocity of the fluid and (ii) that the velocity gradient of the grinding media is independent of the grinding media velocity. Therefore, the velocity of a grinding media particle is equal to the tip speed of the

impeller at the impeller and zero at the pot wall. The velocity of the grinding media can therefore be described by Equation 6.2.2-1 which predicts the velocity of a grinding media particle (v_{GM}) as a function of the distance (l) from the wall (l_0).

$$v_{GM} = (l_0 - l)\frac{v_{max}}{l_0}$$

Equation 6.2.2-1
(Kwade, 1999_A)

where v_{max} is the tip speed of the impeller.

Using PEPT it is possible to determine the velocity of the grinding media at different heights. Figure 6.2-6 shows how the grinding media velocity varied as a function of radius between and along both impellers. In the case presented the tip speed of the impeller was 7.6 ms^{-1} and it can be seen that velocity of the grinding media at the impeller tips was considerably lower than that of the tip speed, approximately 3 ms^{-1} at tip of the bottom impeller and 4 ms^{-1} at the tip of the top impeller. It can also be seen that the maximum velocity was not recorded at the impeller tip and that the velocity of the grinding media was not zero at the pot wall. This may suggest that the velocity of the grinding media and fluid are not proportional.

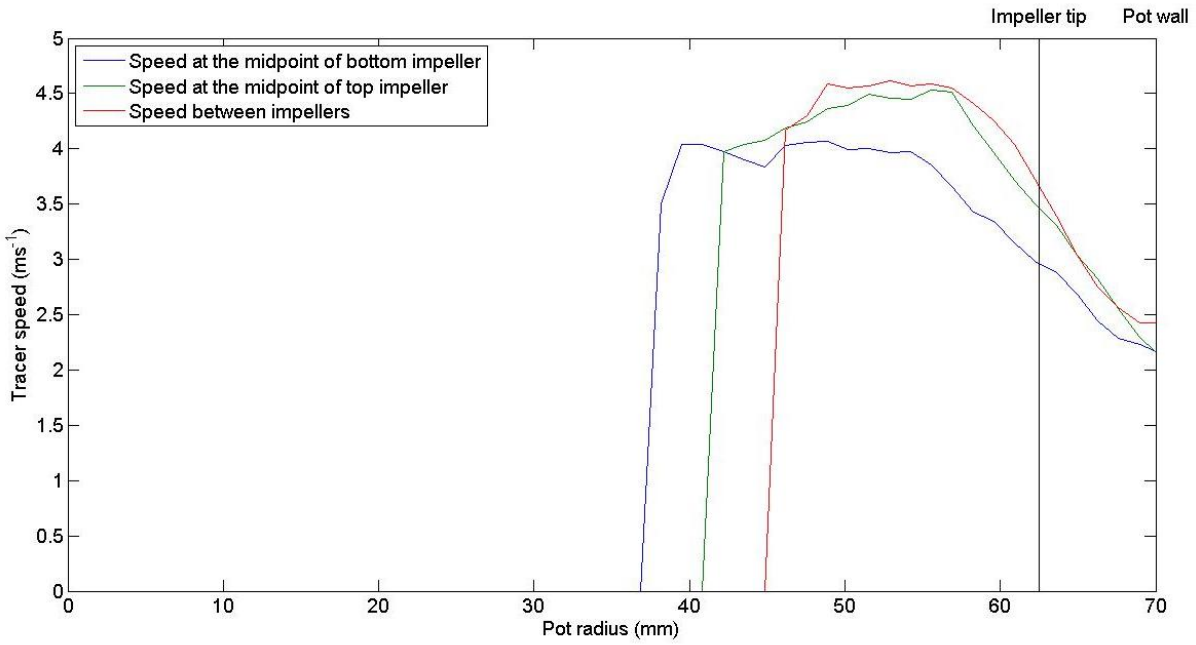

Figure 6.2-6 Average speed of the grinding media between the impellers and at the midpoint of both the top and bottom impeller

Figure 6.2-7 shows how (a) the velocity of the grinding media (b) the velocity of the grinding media relative to the impeller tip speed (dimensionless velocity) and (c) the mean relative velocity varied during a grind. From Figure 6.2-7 (a) it can be seen that the velocity of the grinding media particles was considerably higher in the region between the impellers and that the velocity of the grinding media within the recirculation zone and below the impellers was largely constant, approximately 0.5 ms^{-1}.

From Figure 6.2-7 (b) it can be seen that the maximum dimensionless velocity achieved was 60 % of the tip speed velocity (stirrer tip speed equals 7.6 ms^{-1} at 1200 rpm). Previously a Particle Image Velocimetry study had been carried out using transparent mill contents and chamber to measure the velocity profiles

between the impeller and wall (Theuerkauf & Schwedes, 1999). The study found that the highest velocities were measured at the impeller tip, and were approximately 40 % of the impeller tip speed. In the case presented here the relative velocity at the impeller tip is also approximately 40% of the impeller velocity, however the higher relative velocities were recorded between the impellers closer to the impeller shaft. Relative velocity is more closely examined in Section 6.3.4.

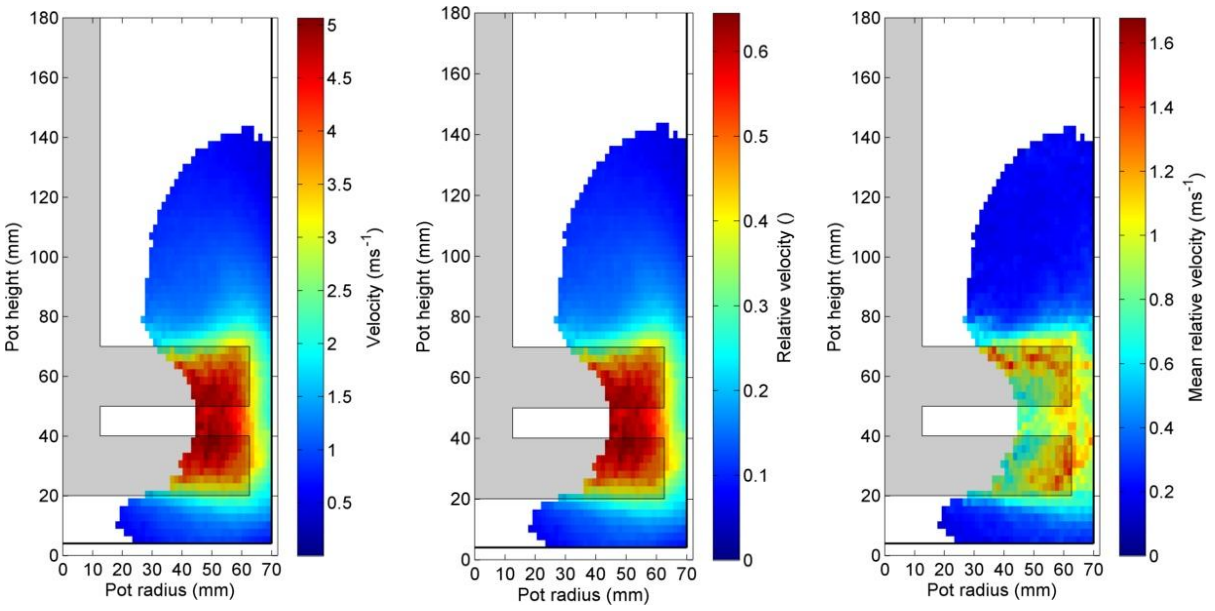

Figure 6.2-7 (a) Velocity distribution throughout the mill (b) Dimensionless velocity (velocity relative to impeller velocity) (c) Mean relative velocity (standard deviation of velocity).

The number of collisions between particles is dependent on the speed of the grinding media relative to other grinding media particles. If two particles are moving in the same direction with the same speed then the relative speed between the two is zero. If two grinding media particles with the same speed are moving in the opposite directions then the relative speed at the collision is the sum of their velocities as shown in Figure 6.2-8 (a) and (b) respectively. Kinetic theory of gases states that the mean relative speed for molecules travelling in a random motion is $\sqrt{2}v$, where *v* is the average speed of the molecules (particles). This is because the most common approach for two molecules is from the side, as shown in Figure 6.2-8 (c).

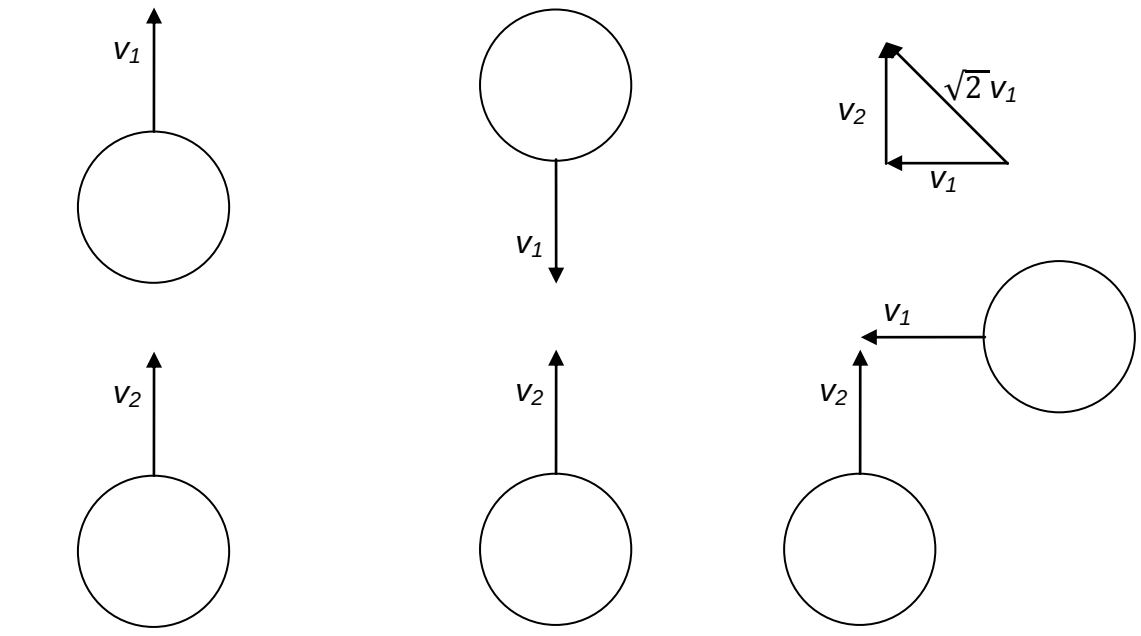

Figure 6.2-8 Relative velocity of particles depending on their approach (a) Two particles with the same speed travelling in the same direction (b) Two particles with the same speed travelling in opposite directions and (c) Two particles travelling at 90° to each other (the characteristic approach of gases).

Within a vertically stirred mill, grinding media does not experience random motion (Blecher, et al., 1996). Instead, as shown in Figure 6.2-5 the grinding media is accelerated by the impellers towards the pot wall where it is either lifted into the recirculation zone or pushed under the impellers. Collisions occur as the faster moving media close to the impeller catches up with the slower moving grinding media elsewhere in the mill, and therefore the mean relative velocity must reflect the difference in velocity grinding media has within a block volume. Figure 6.2-7 (c) shows the standard deviation of the grinding media particles as they pass through a block volume. It can be seen that the standard deviation of the grinding media velocity was higher at the impeller tips and lower elsewhere in the mill. This suggests that there were larger variations in velocity at the impeller tips than elsewhere in the mill and therefore larger values of relative velocity.

6.2.3 Force

Grinding media is accelerated by the impeller and decelerates as it collides with other grinding media within the mill. This results in stresses acting on the trapped feed particles between the colliding grinding media equivalent to the force the grinding media is experiencing over the area in contact with the feed material. Figure 6.2-9 shows how the force acting on the grinding media varied throughout the mill. It can be seen that the greatest forces were recorded at the impeller tips. To better illustrate the difference in force between the impellers and elsewhere in the mill the colour bar scale used has been made logarithmic. Figure 6.2-10 plots the average difference in force as a function of height. It can be seen that the force was an order of magnitude higher between the impellers than elsewhere in the mill.

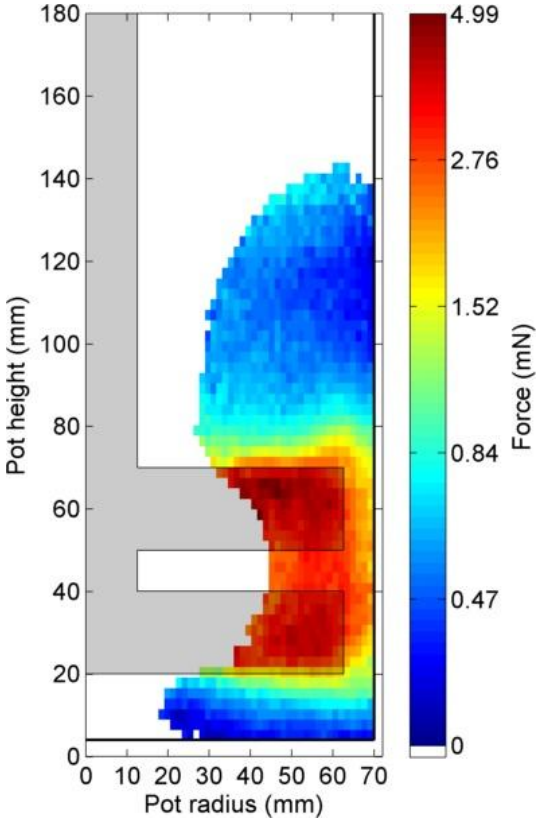

Figure 6.2-9 Force plot throughout the cross-section of a vertically stirred media mill

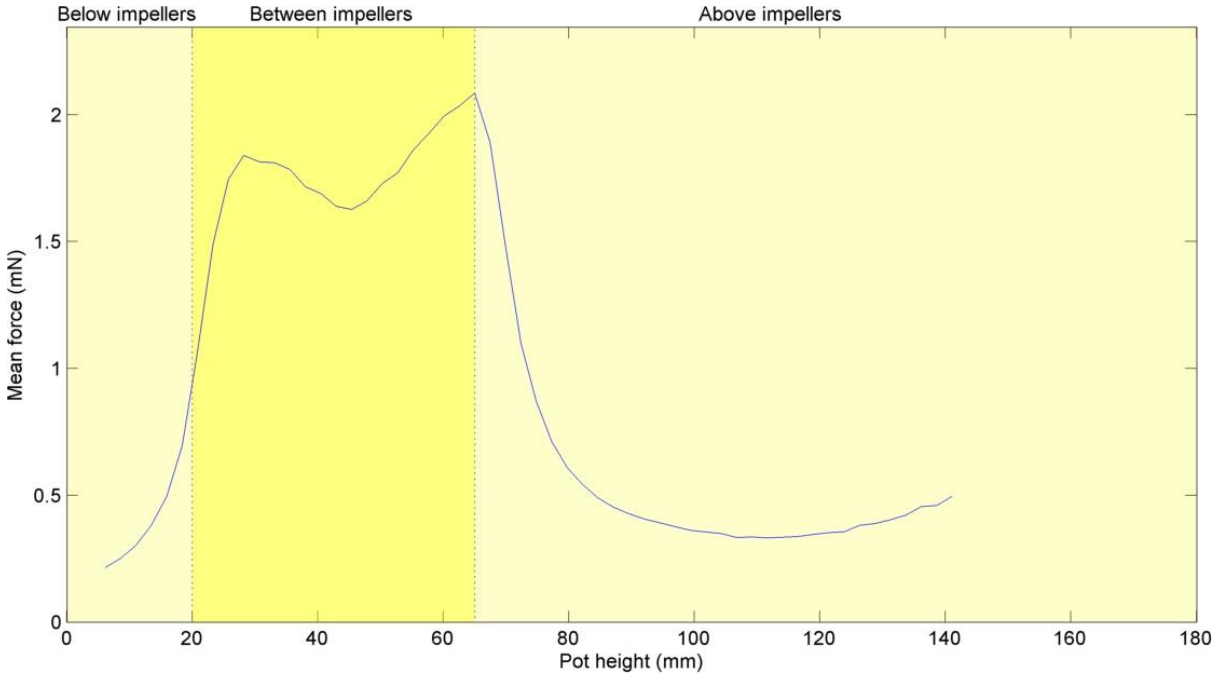

Figure 6.2-10 Average force of grinding media as a function of height in the mill

6.2.4 Stress

In order for successful collisions to occur the stress at a collision must be sufficient to break any trapped feed particles. An initial assumption based on Kwade's stress intensity model is that there is only one feed particle trapped at a collision and therefore the stress exerted at a collision is equal to the force acting on a feed particle divided by the cross-sectional area of the feed particle (Kwade, 1999_B). This approximation is used here to determine how the stress varied throughout the mill as a function of calcium carbonate particle size as shown in Figure 6.2-11. It can be seen that the stress was higher in the regions around the impeller and that the stress exerted increased as the particle size decreased. This is further illustrated in Figure 6.2-12.

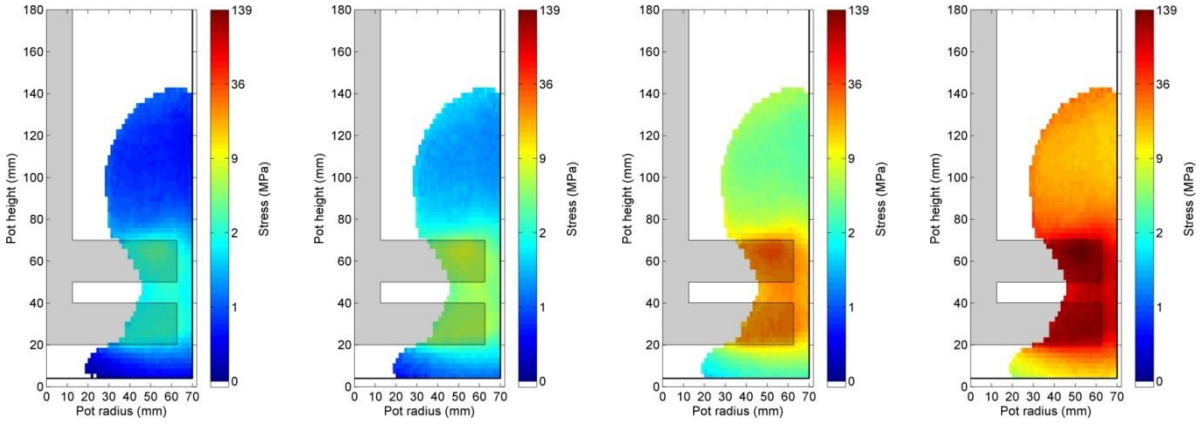

30 µm (a) | 20 µm (b) | 10 µm (c) | 5 µm (d)

Figure 6.2-11 Stress exerted at a collision for a (a) 30 µm (b) 20 µm (c) 10 µm and (d) 5 µm feed particle assuming single calcium carbonate particles are stressed per grinding media collision

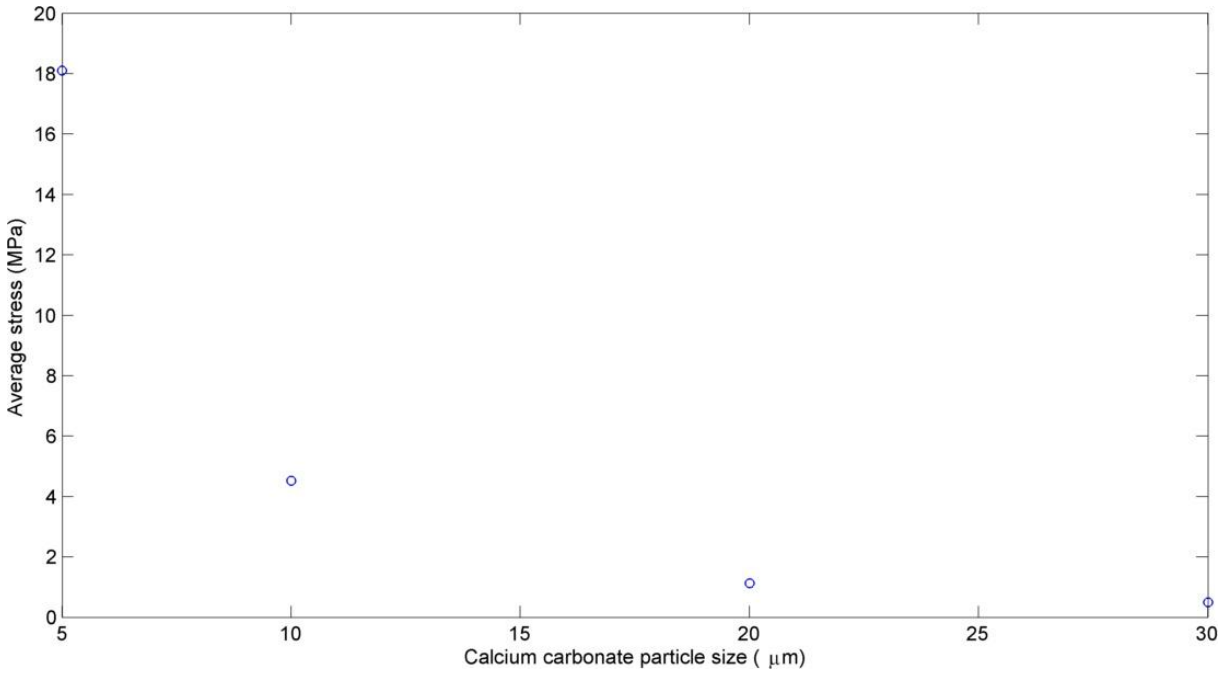

Figure 6.2-12 Average stress exerted by the grinding media as a function of calcium carbonate particle size

A material's ability to withstand a compressive stress prior to failure such as that experienced at a collision is its compressive strength. The compressive strength of calcium carbonate particles was measured using a micromanipulator (as reported in Section 5.3), it was found that the compressive strength of calcium carbonate increased as particle size decreased as shown in Figure 6.2-13.

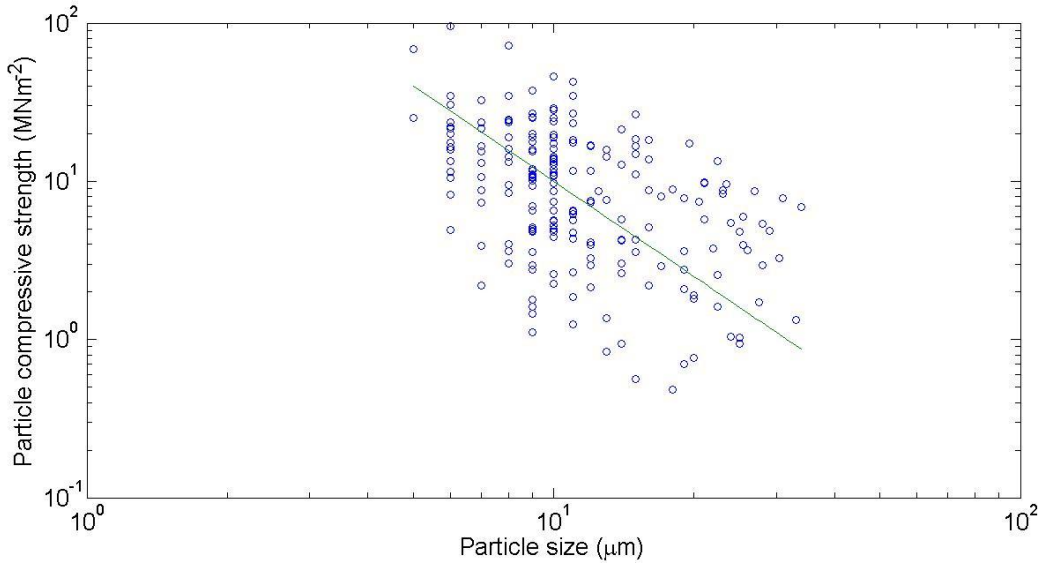

Figure 6.2-13 Particle compressive strength of calcium carbonate particles as a function of particle size

Figure 6.2-14 (a) (b) (c) and (d) show the stress at a collision acting on the calcium carbonate particles at calcium carbonate particle sizes of 30, 20, 10 and 5 μm respectively. The compressive strength required to fracture calcium carbonate particles at each particle size (as determined by the micromanipulator experiments) is marked on each graph. It can be seen that as calcium carbonate particle size decreased the percentage of the grinding media capable of exerting sufficient stress to induce breakage increased as shown in Figure 6.2-15.

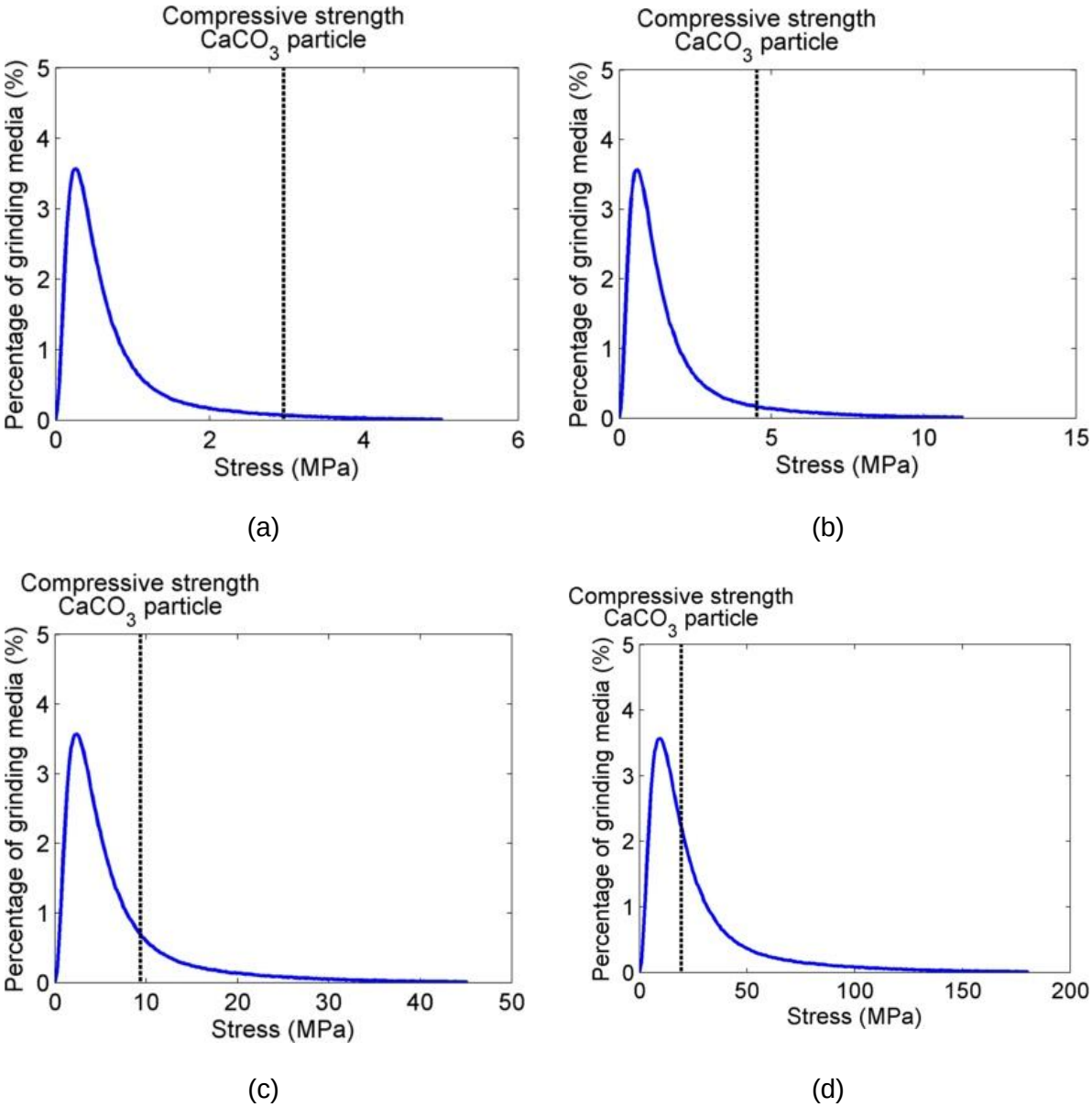

Figure 6.2-14 Distribution of stress exerted by grinding media when calcium carbonate particle size is (a) 30 (b) 20 (c) 10 and (d) 5 μm

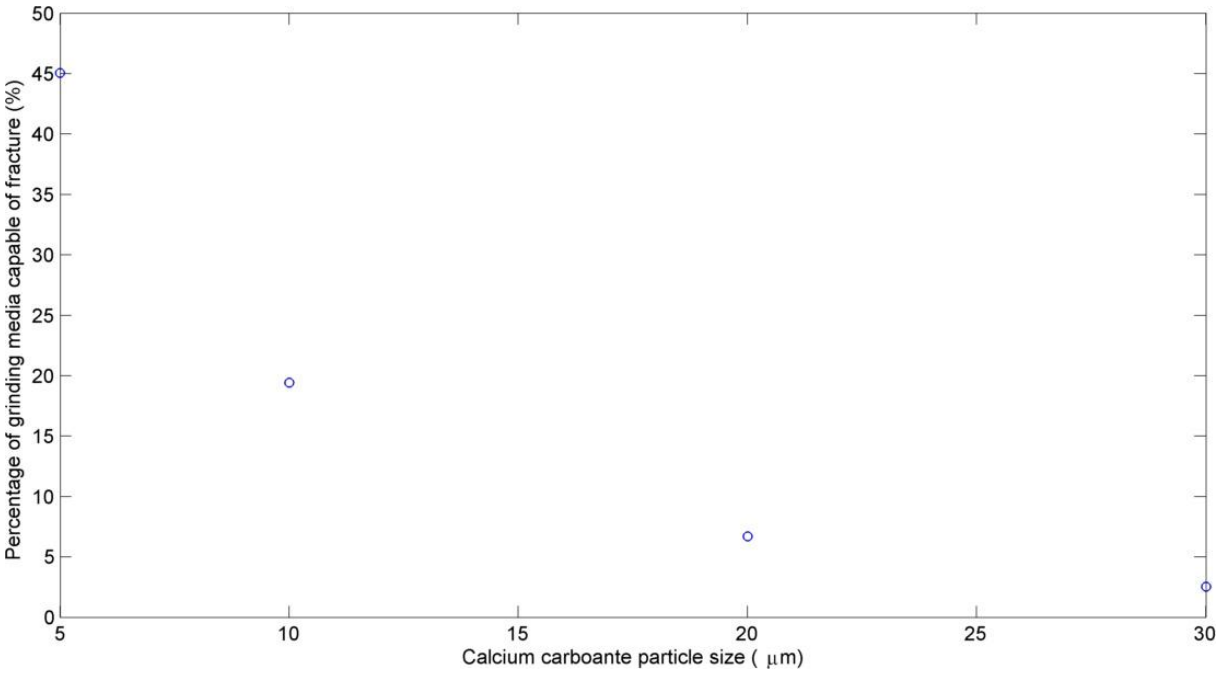

Figure 6.2-15 Percentage of grinding media suitable to fracture calcium carbonate particles as a function of calcium carbonate feed size (based on average strength of calcium carbonate particles at a given size)

Figure 6.2-16 (a) (b) (c) and (d) show how the regions in the mill where the grinding media have sufficient stress to fracture the calcium carbonate particles varied with calcium carbonate particle size.

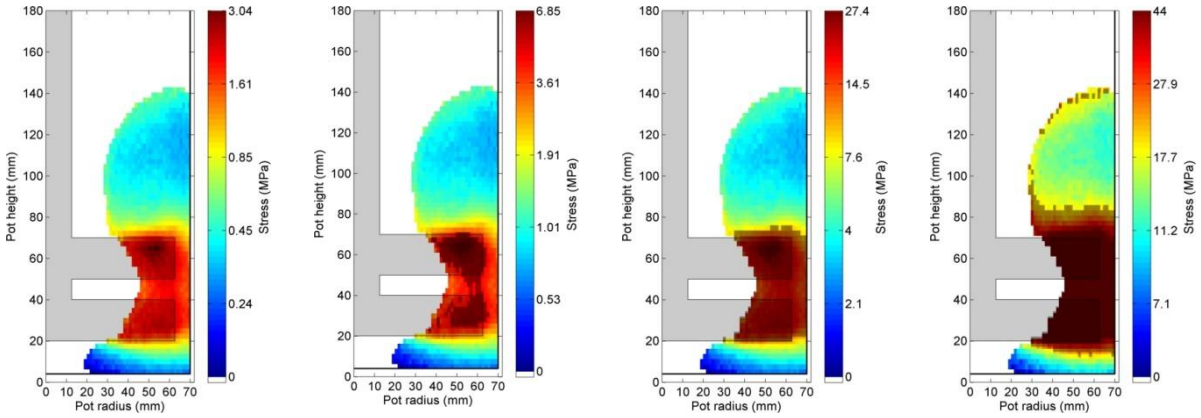

30 µm (a) | 20 µm (b) | 10 µm (c) | 5 µm (d)

Figure 6.2-16 Regions of the mill capable of fracturing calcium carbonate feed particles when calcium carbonate particle size is (a) 30 (b) 20 (c) 10 and (d) 5 µm.

These findings suggest that the regions within the mill suitable for fracture to occur increased as particle size decreased. However, as energy input is increased (and the particle size of the calcium carbonate decreases) the grinding rate decreases and increasingly large amounts of energy are required for any further reduction in particle size.

6.2.5 Collisions

Figure 6.2-17 (a) and (b) show the media-media collision rate (collisions s^{-1}) and number of collisions within the mill calculated using the collision theory outlined in Section 3.2.5. It can be seen that the collision rate and number of collisions were highest above and below the impellers. This occurred because these regions have both large numbers of grinding media present and high mean relative velocities. The collision rate and the number of collisions were low in the impeller zones since there was less grinding media present. This is further illustrated by Figure 6.2-18 and Figure 6.2-19.

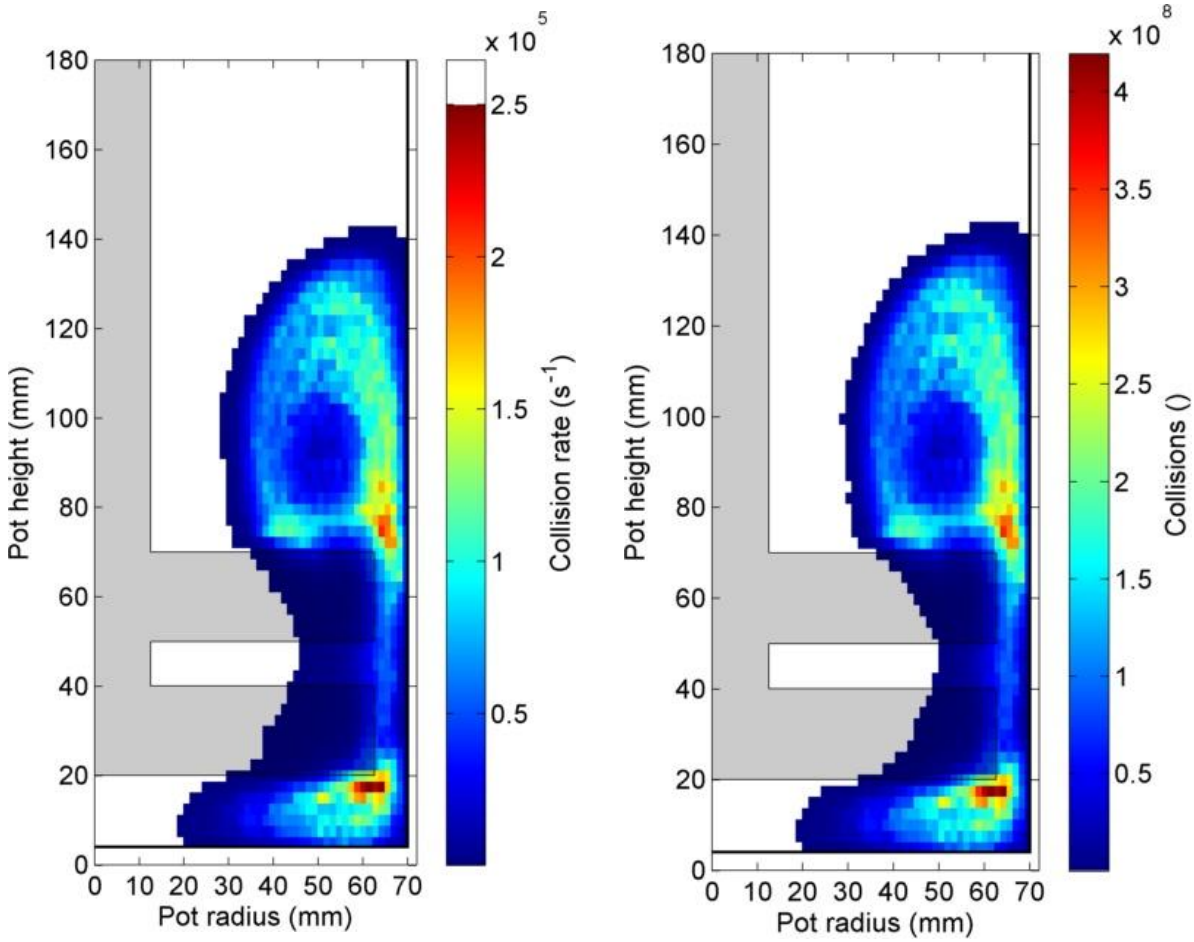

(a) (b)

Figure 6.2-17 (a) Collision rate within a vertically stirred mill (b) Number of collisions during a 50 Wh grind

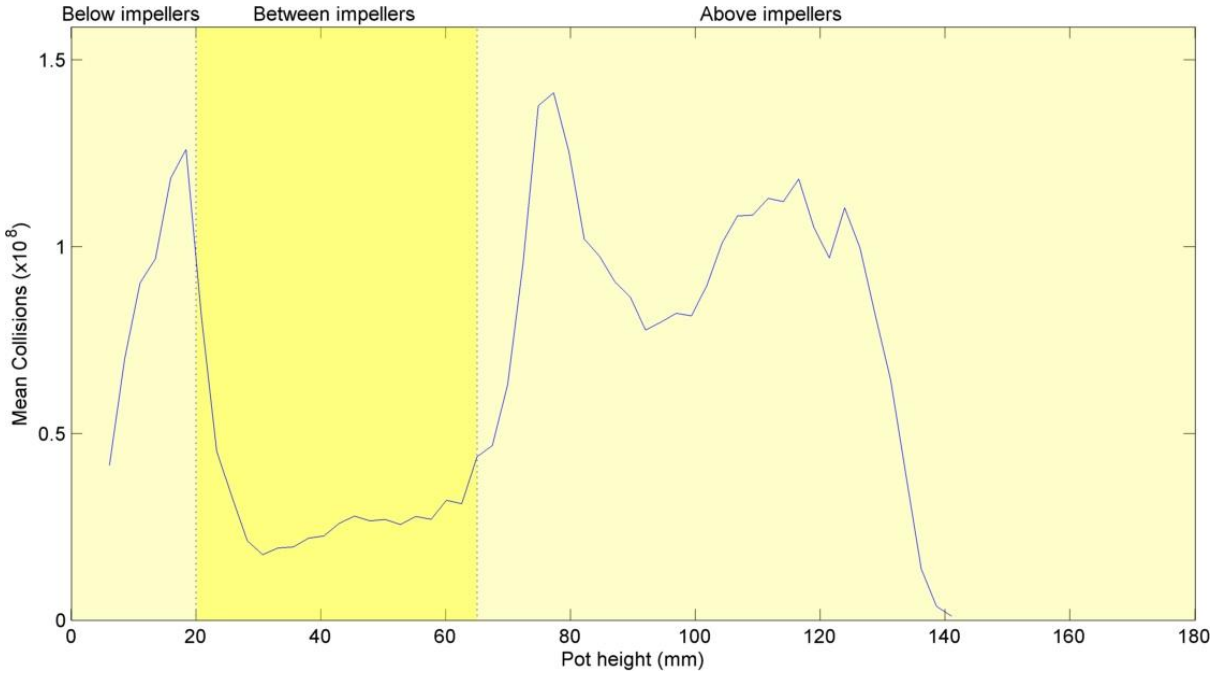

Figure 6.2-18 Collisions as a function of height in the mill

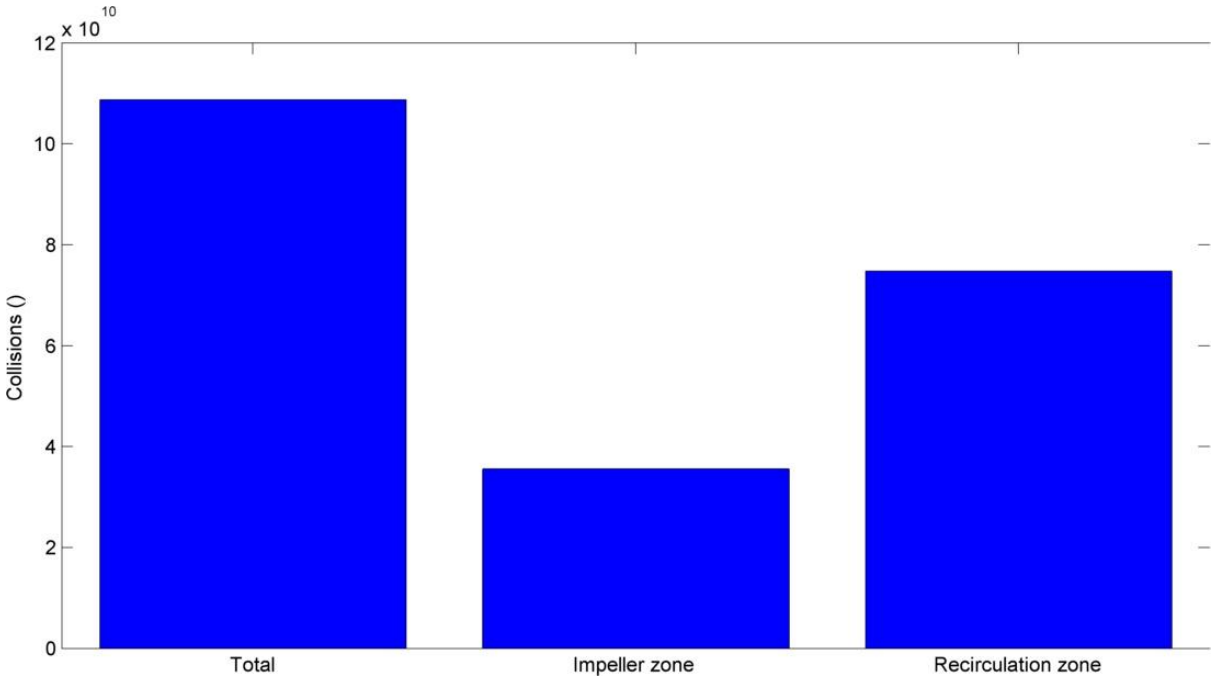

Figure 6.2-19 Number of collisions in different regions of the mill

So far, the work reported in this section has built towards the measurement of the percentage of the media-media collisions which lead to particle breakage and has concluded that the percentage of grinding media particles capable of breaking calcium carbonate particles increases with decreasing calcium carbonate size. However, the grinding work reported in Chapter 4 indicated that the grinding rate decreased with decreased calcium carbonate particle size. This observation is inconsistent with the above findings. The explanation most likely concerns the number of collisions and the number of particles stressed at each collision.

In the Kwade model, and approach used here, it is assumed that a single calcium carbonate particle is stressed at each collision (Kwade, 1999_B). If this assumption is valid then the decreased grinding rate at finer calcium carbonate size can be explained in terms of particle numbers. Whilst the proportion of the grinding media suitable to break calcium carbonate increases with decreasing calcium carbonate particle size, the number of carbonate particles increased at a greater rate.

In the case presented above, it is estimated that over the course of the 67 kWh/tonne grind there were 4.9×10^{11} media collisions. Because the percentage of grinding media capable of exerting sufficient stress to overcome the average strength of the calcium carbonate particles increased from 2.4 % to 46.0 % as calcium carbonate particle size decreased from 30 to 5 μm, the total number of successful collisions increased from 0.3×10^{8} to 7.1×10^{8} as shown in Figure 6.2-20. However, since 0.75 kg of calcium carbonate feed was ground and assuming cubic particles, the total number of particles within the system increased from 1×10^{9} to 2.2×10^{12} as the particle size decreased from 30 μm to 5 μm as shown in Figure 6.2-21. Therefore

calcium carbonate particles are being generated at a greater rate than the increase in the proportion of the media capable of fracturing them. This resulted in a decrease in the percentage of the calcium carbonate particles fractured as particle size decreased as shown in Figure 6.2-22. Therefore additional collisions (and grinding energy) would be required to break the same mass of calcium carbonate particles.

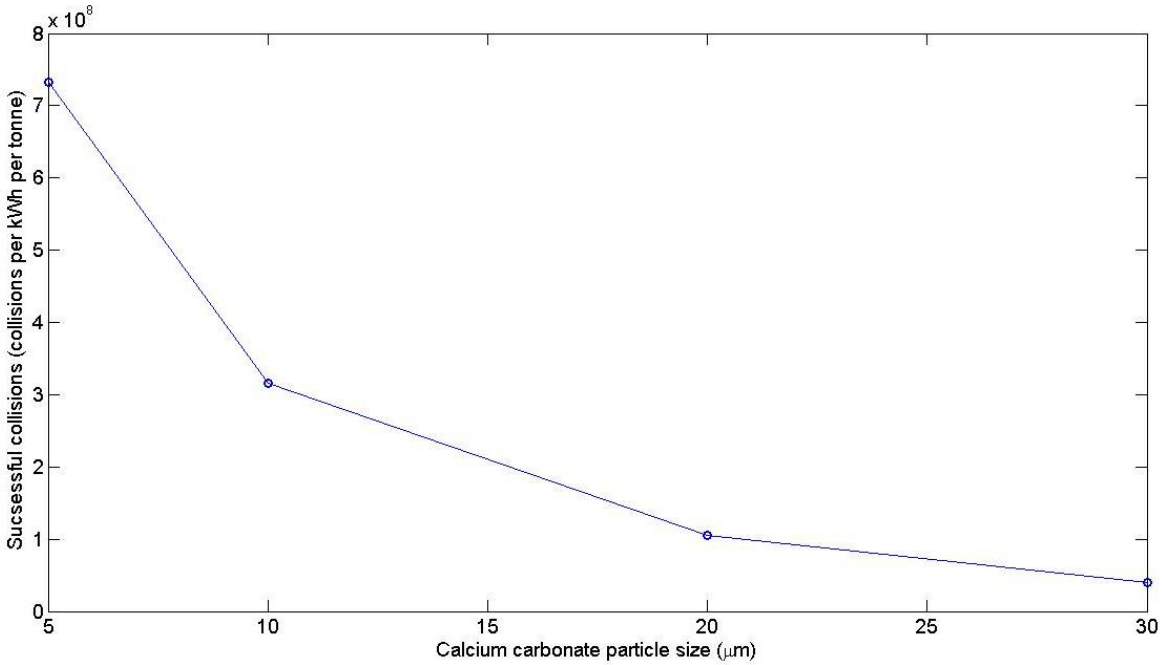

Figure 6.2-20 Number of successful collisions (collisions per kWh per tonne) as a function of particle size

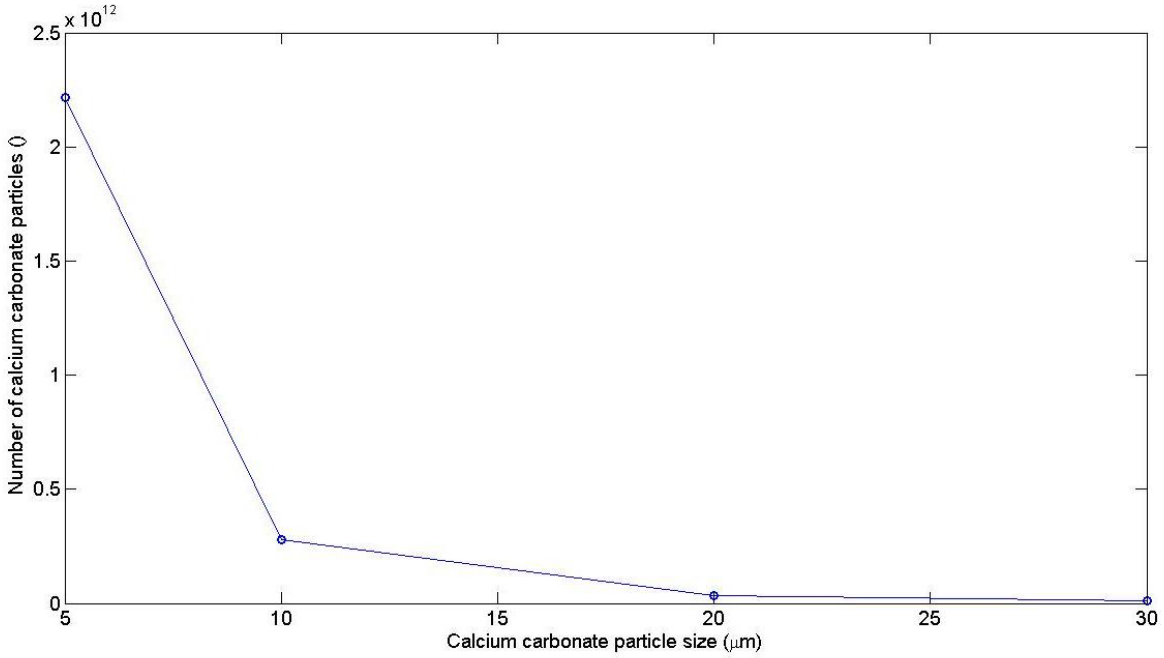

Figure 6.2-21 Number of calcium carbonate particles in the mill as a function of particle size

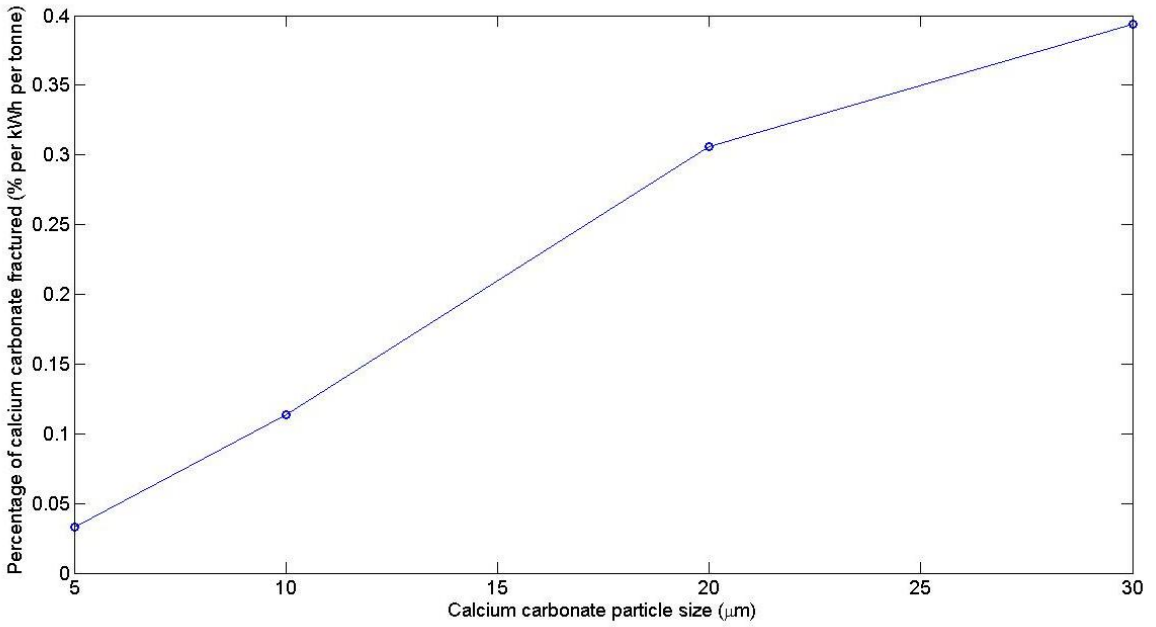

Figure 6.2-22 Percentage of the calcium carbonate particles stressed at a given particle size per kWh per tonne

6.2.6 Summary of results for benchmark system

The data presented in this section for the benchmark system indicate:

1. A large vortex was present in the mill. Three zones can be defined; (1) below the impellers (2) between the impellers and (3) above the impellers.
2. The tracer spent less time in the impeller zone (regions 1 and 2) than in the recirculation zone (region 3), 28 % and 72 % respectively.
3. The mean media height was 90 mm from the bottom of the pot which is 27.5 mm above top of the impeller zone.
4. The impellers created a radial flow regime within the mill resulting in a two loop flow pattern where the grinding media was accelerated by the impellers towards the pot wall then either upwards or downwards before returning to the impeller.
5. In the impeller zone the grinding media velocity varied as a function of radial position. The maximum velocity was not recorded at the impeller tip (62.5 mm from the mill centreline) but between 45 to 60 mm from the centreline. The maximum velocity recorded was approximately 4.5 ms^{-1} whilst the velocity at the tip was between 3 to 4 ms^{-1} for a tip speed of 7.6 ms^{-1}. The velocity of the grinding media at the pot wall was between 2 to 2.5 ms^{-1}. These observations are not consistent with earlier theories that suggest the velocity of the grinding media would be at a maximum at the impeller tip and the velocity at the wall is zero. Possible explanations for these behaviours are that radial velocity at the tip was reduced because of decelerations caused by impacting other media closer to the pot wall and the velocity at the wall was not zero because the velocity of the grinding media is not proportional to velocity of the fluid.

6. The grinding media velocity in the recirculation zone was much lower than the velocity between the impellers. The velocity in the recirculation zone was approximately constant at 0.5 ms^{-1}.
7. The highest forces occurred between the impellers at the impeller tips. The highest force was about 5 mN and the force throughout the recirculation zone was around 0.5 mN, approximately an order of magnitude lower.
8. The highest stresses were exerted between the impellers (the stress was calculated assuming only one particle is stressed at a collision).
9. Stress increased as calcium carbonate size decreased (maximum stress at: 30 μm was 3 MPa, 20 μm was 7 MPa, 10 μm was 27 MPa, and 5 μm was 44 MPa). These stresses measured by PEPT in some areas of the mill were higher than the average compressive strength of calcium carbonate particles measured by a micromanipulation technique.
10. As calcium carbonate particle size decreased the percentage of the grinding media capable of supplying sufficient stress to overcome the average strength of calcium carbonate particles in that size range increased and therefore the regions within the mill suitable for breakage to occur increased.
11. Media-media collisions were higher in the regions above and below the impellers. This was because the mean relative velocity and numbers of grinding media particles were both high in these regions.
12. Despite a larger percentage of the grinding media having sufficient stress to break finer calcium carbonate particles, the proportion of the calcium carbonate fractured decreased as the calcium carbonate size decreases. This was because the number of new particles created increased at a faster rate.

6.3 IMPACT OF OPERATING PARAMETERS ON PERFORMANCE

The analytical approach used in Section 6.2 were applied to the operating parameter study and a series of graphs was prepared for each parameter. Each series comprised the following graphs:

Occupancy

- Occupancy contour plots
- Percentage of grinding media present as a function of height in the grinding pot
- Cumulative percentage of grinding media below, between and above the impellers
- Lower quartile, median, upper quartile and maximum height of grinding media.
- Bar chart comparing findings from cumulative plots

Velocity

- Velocity contour plots
- Mean velocity of grinding media present as a function of height in the grinding pot
- Bar chart comparing mean, impeller zone and recirculation zone velocities.
- Mean relative velocity contour plot
- Average mean relative velocity grinding media present as a function of height in the grinding pot

Force

- Force contour plot
- Mean force of grinding media present as a function of height in the grinding pot
- Bar chart comparing mean, impeller zone and recirculation zone forces

Stress

- Stress contour plots as a function of calcium carbonate particle size
- Mean stress as a function of calcium carbonate particle size
- Stress distribution profiles as a function of calcium carbonate particle size
- Percentage of grinding media with sufficient stress to fracture calcium carbonate particles as a function of calcium carbonate particle size
- Stress contour plots showing regions in the mill capable of fracturing calcium carbonate particles as a function of calcium carbonate particle size
- Percentage of mill capable of fracturing calcium carbonate particles as a function of calcium carbonate particle size

Collisions

- Collision rate and total collisions contour plots
- Total number of collisions between grinding media as a function of height in the grinding pot
- Bar chart comparing mean, impeller zone and recirculation zone collisions
- Breakage rate (successful collisions per kWh/tonne) against calcium carbonate particle size
- Percentage of the calcium carbonate fractured per kWh per tonne against calcium carbonate particle size

The code used to create complete sets of all the plots outlined is given in Appendix B. Only key graphs are presented in this section.

6.3.1 Grinding media specific gravity

Lab grinding data with differing specific gravity media having approximately the same size are given in Section 4.3. These data show that increasing the grinding media specific gravity resulted in reduced energy requirements to achieve a specific grinding objective. It was suggested that since approximately equally sized grinding media were used for each experiment that grinding media specific gravity has little effect on the number of media-media collisions within the mill and therefore the improved performance with increased specific gravity resulted from increased specific energy (stress) at each collision.

6.3.1.1 PEPT data

6.3.1.1.1 Occupancy

Figure 6.3-1 (a) (b) and (c) show the occupancy plots for grinds performed using 4.2, 3.9 and 2.7 specific gravity grinding media (particle size approximately 1.6 mm) under the conditions described in Section 4.3. It can be seen that the maximum media height, general shape of the charge, vortex shape and occupancy distribution were approximately the same. The 4.2 specific gravity media grind had a higher percentage of the grinding media below the impellers than the other grinds, and consequently less grinding media above the impellers. This behaviour is also further shown in Figure 6.3-2.

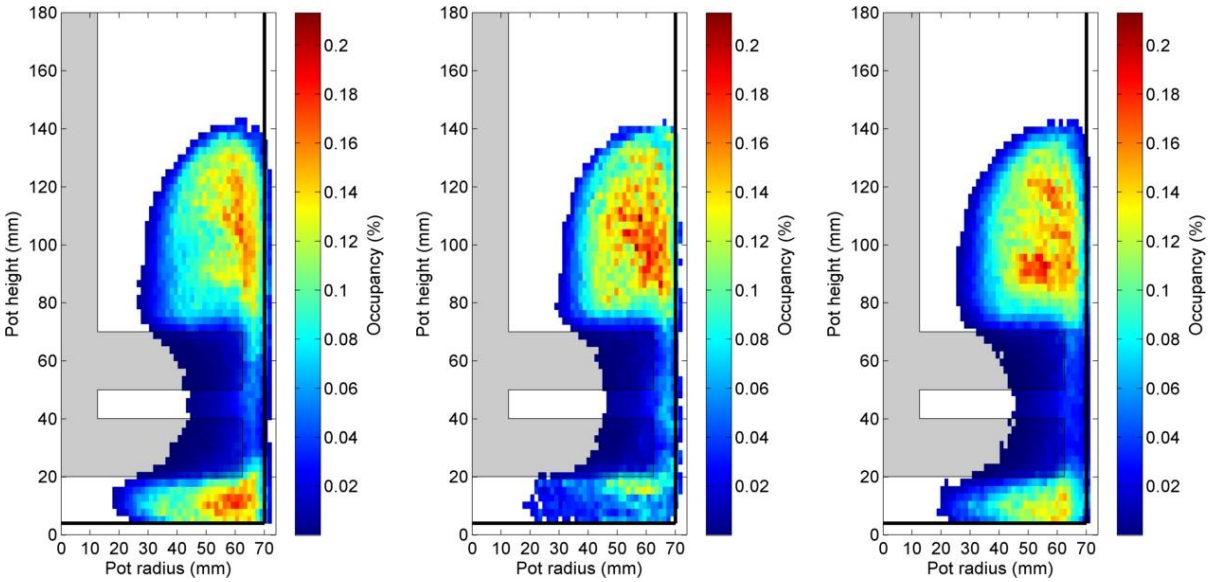

S.G. 4.2 (a) S. G. 3.9 (b) S. G. 2.7 (c)

Figure 6.3-1 Occupancy contour plots for (a) 4.2 (b) 3.9 and (c) 2.7 specific gravity grinding media

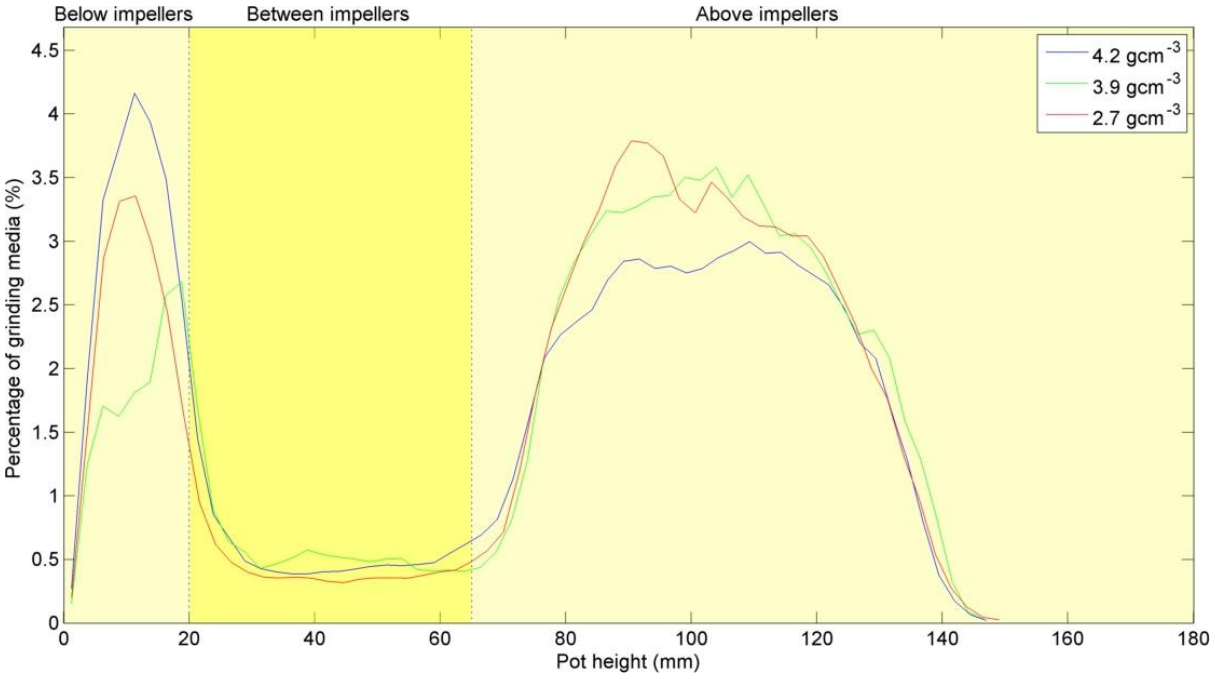

Figure 6.3-2 Percentage of grinding media as a function of height in the grinding pot

6.3.1.1.2 Velocity

Figure 6.3-3(a) (b) and (c) show the velocity contour plots for 4.2, 3.9 and 2.7 specific gravity grinding media systems respectively and Figure 6.3-4 shows the mean velocity of the grinding media as a function of pot height. These data indicate that there were no differences in grinding media velocity with changing media specific gravity. There were also no differences in the mean relative velocities with changing media specific gravity as shown in Figure 6.3-5.

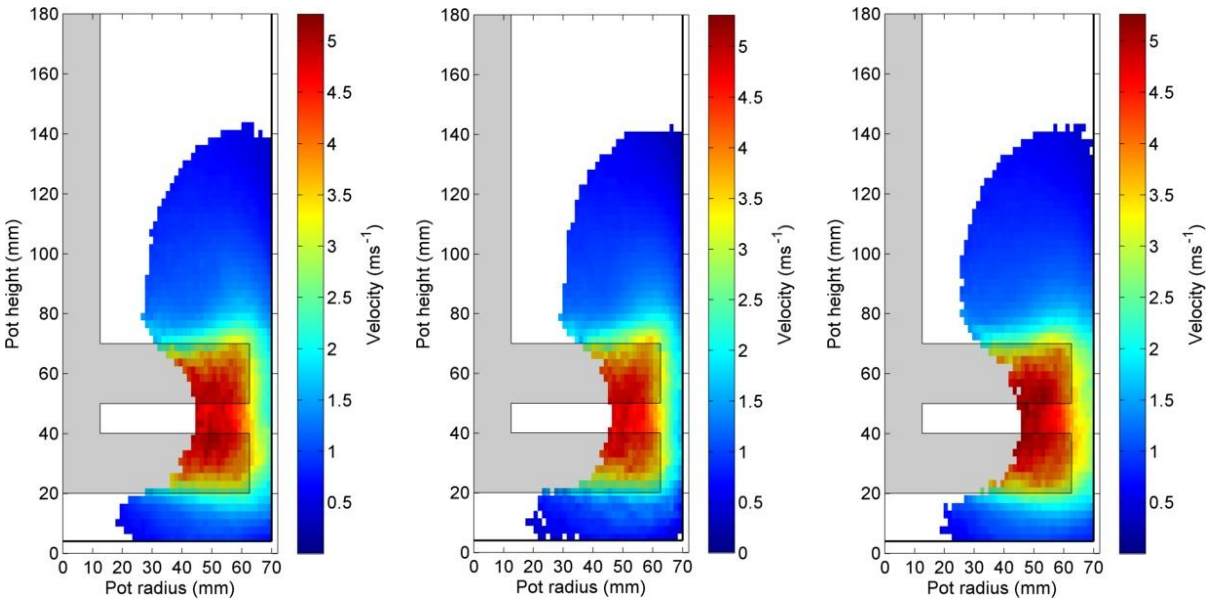

S.G. 4.2 (a) S.G. 3.9 (b) S.G. 2.7 (c)

Figure 6.3-3 Velocity contour plots for (a) 4.2 (b) 3.9 and (c) 2.7 specific gravity grinding media

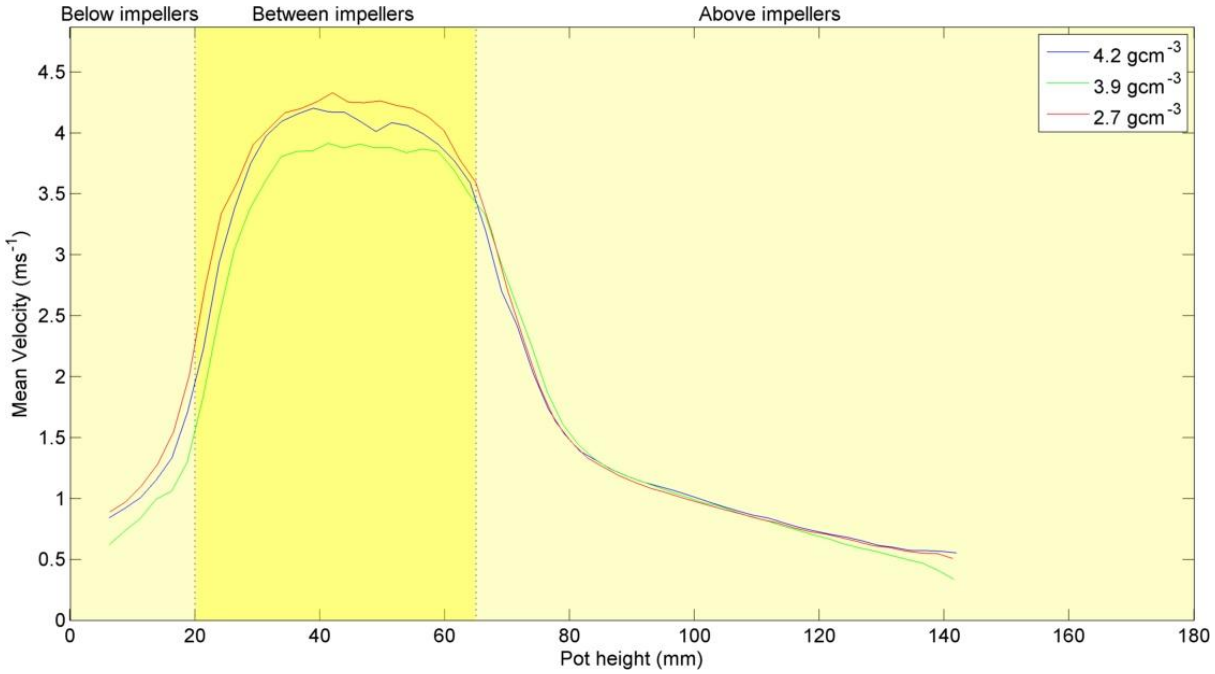

Figure 6.3-4 Mean velocity of grinding media as a function of height in the grinding pot

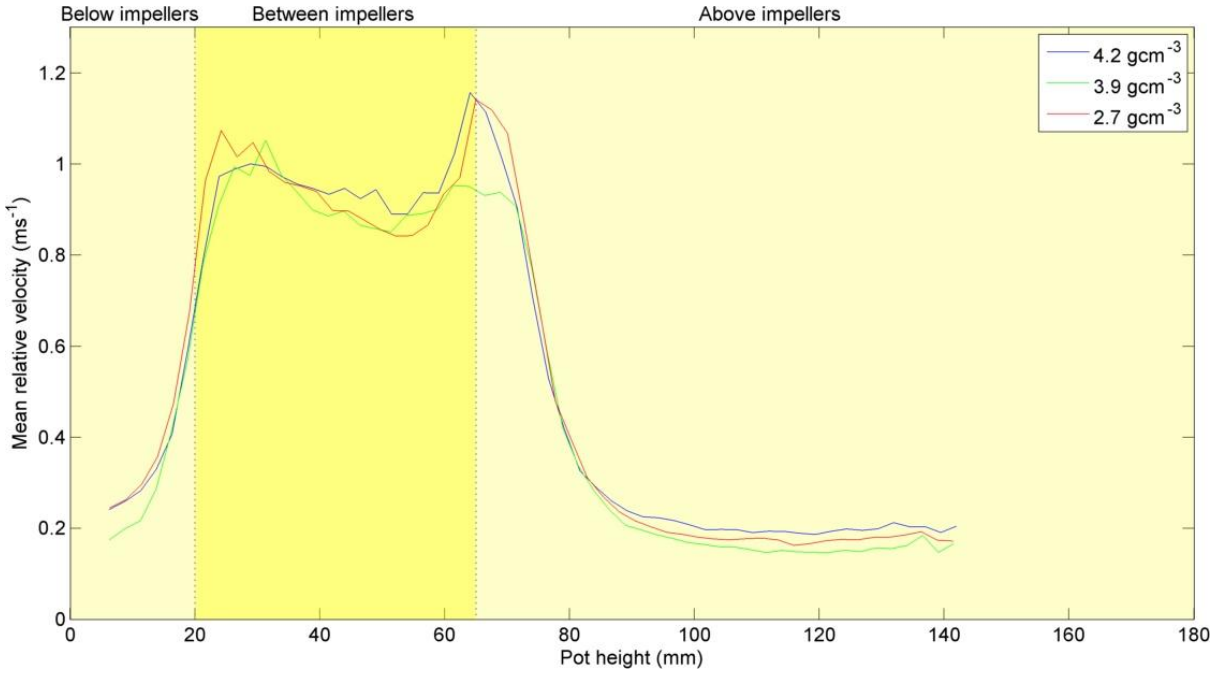

Figure 6.3-5 Mean relative velocity of grinding media as a function of height in the grinding pot

6.3.1.1.3 Force

Figure 6.3-6 (a), (b) and (c) show the force contour plots for the 4.2, 3.9 and 2.7 specific gravity grinding media systems respectively. It can be seen that the force experienced by the grinding media increased with increase in specific gravity. Most notably the higher specific gravity system showed higher force in the impeller zone. This is further illustrated in Figure 6.3-7 where the maximum force experienced by the 4.2 specific gravity grinding media was approximately 3.5 mN compared to a maximum of approximately 2.2 mN with the 2.7 specific gravity grinding media.

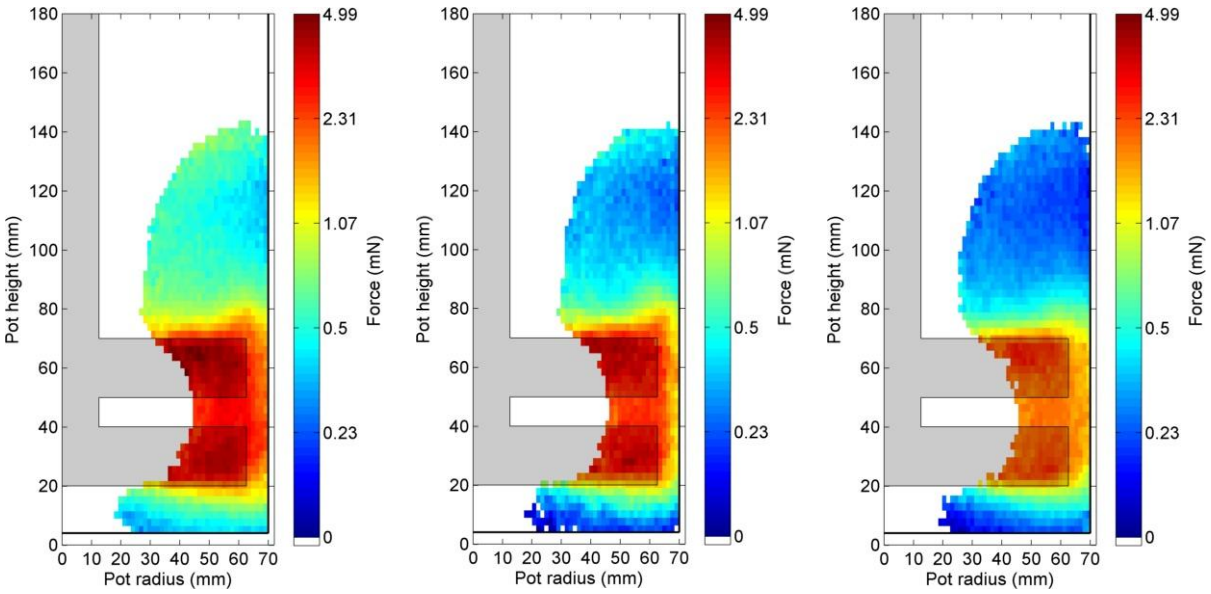

S.G. 4.2 (a) S.G. 3.9 (b) S.G. 2.7 (c)

Figure 6.3-6 Force contour plot for (a) 4.2 (b) 3.9 and (c) 2.7 specific gravity grinding media

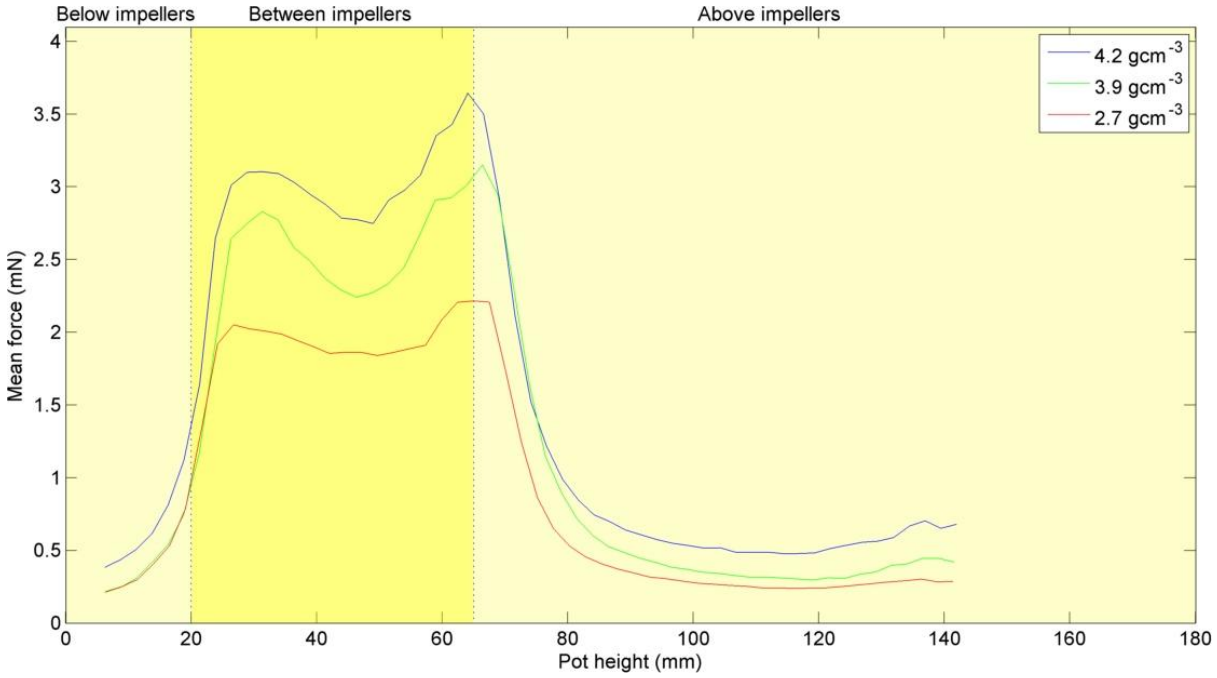

Figure 6.3-7 Mean force of grinding media as a function of height in the grinding pot

Figure 6.3-8 shows further emphasises these differences in force with media specific gravity.

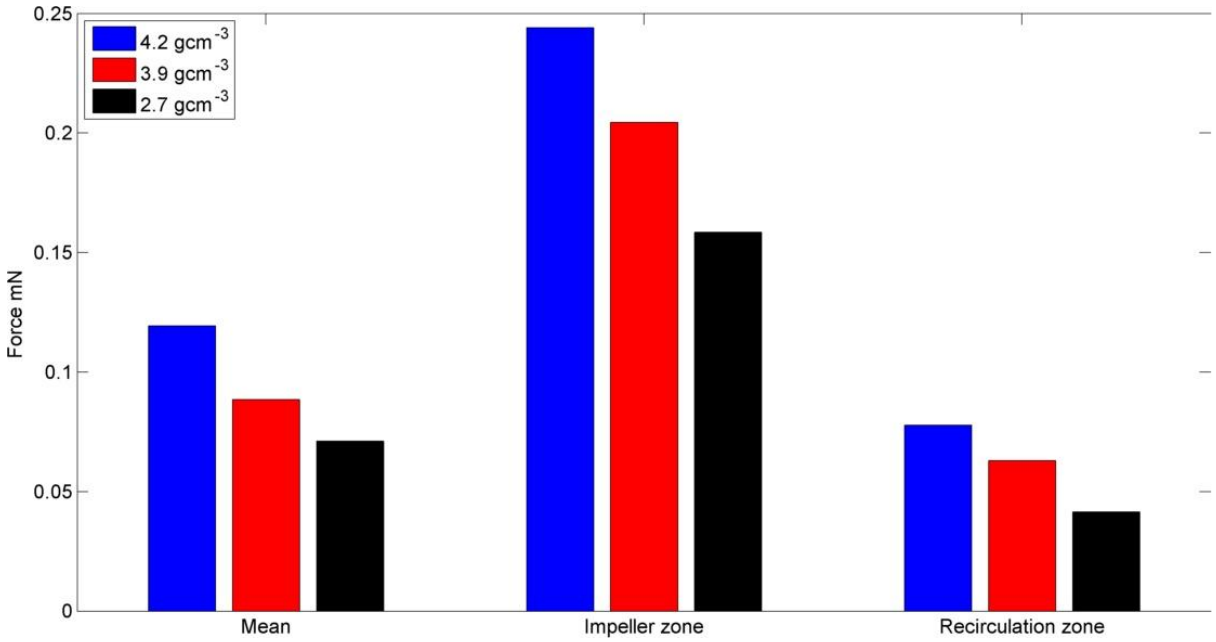

Figure 6.3-8 Bar chart comparing mean, impeller zone and recirculation zone forces

6.3.1.1.4 Stress

Figure 6.3-9 shows how the stress acting on calcium carbonate particles varied with calcium carbonate particle size and grinding media specific gravity. It can be seen that as the calcium carbonate size decreased the stress applied increased; and as media specific gravity increased the stress applied to calcium carbonate increased. This is further illustrated in Figure 6.3-10 which shows a comparison of the average stress applied to the calcium carbonate as a function of calcium carbonate particle size. As the calcium carbonate particle size decreased the difference in stress applied by the different specific gravity media increased. When 30 μm calcium carbonate was stressed the average difference in stress applied was very small (the applied stress was approximately 1 MPa for all three different specific gravity grinding media). However at finer calcium carbonate particle sizes differences in applied stress with differing specific gravity media were apparent. For example when stressing 5 μm calcium carbonate particles, grinding media with a specific gravity of 2.7 exerts approximately 18 MPa of stress, whilst the grinding media with a specific gravity of 4.2 exerts approximately 28 MPa of stress.

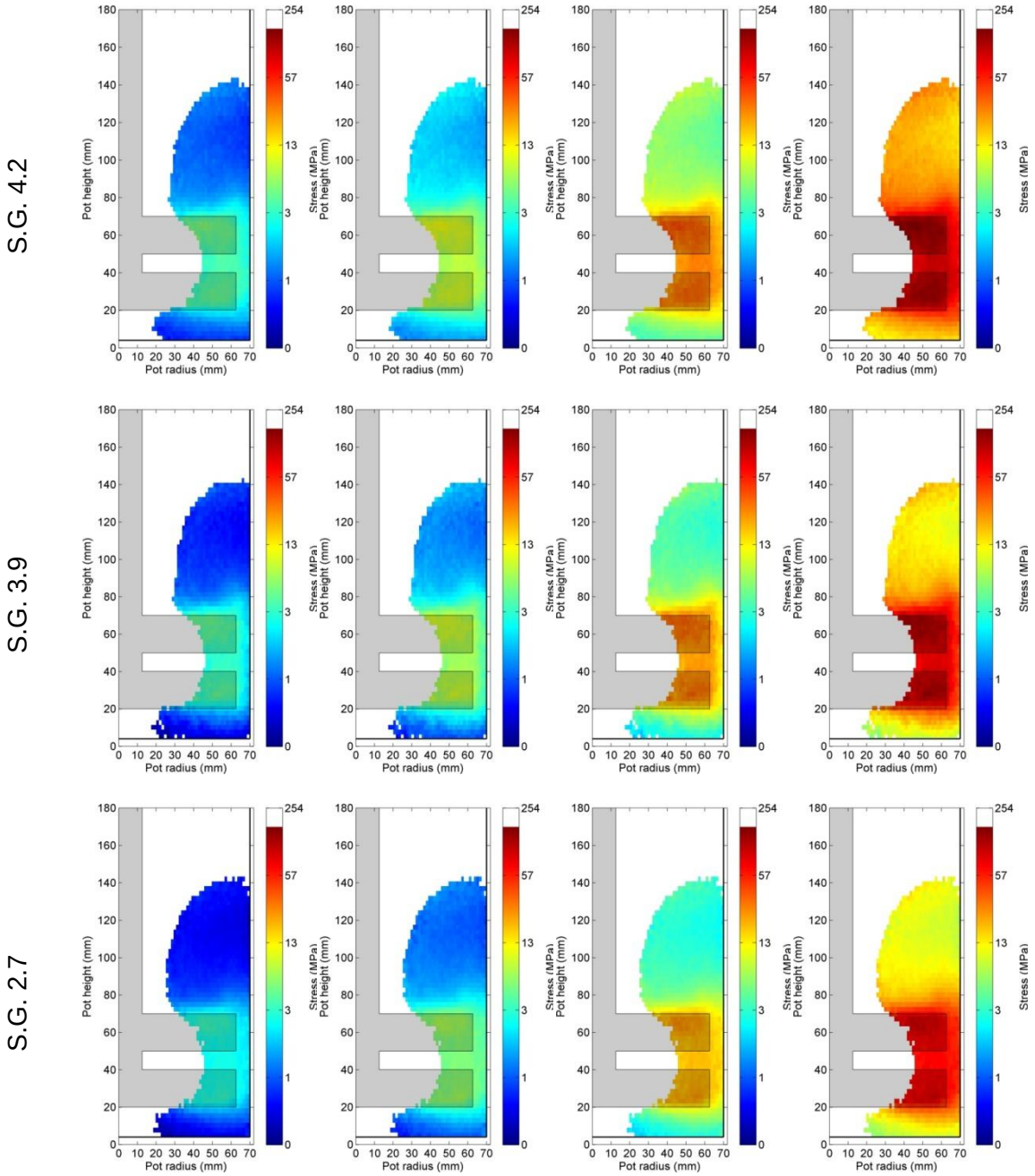

Figure 6.3-9 Stress contour plots comparing 4.2, 3.9 and 2.7 specific gravity grinding media when calcium carbonate particle size is (a) 30 (b) 20 (c) 10 and (d) 5 µm.

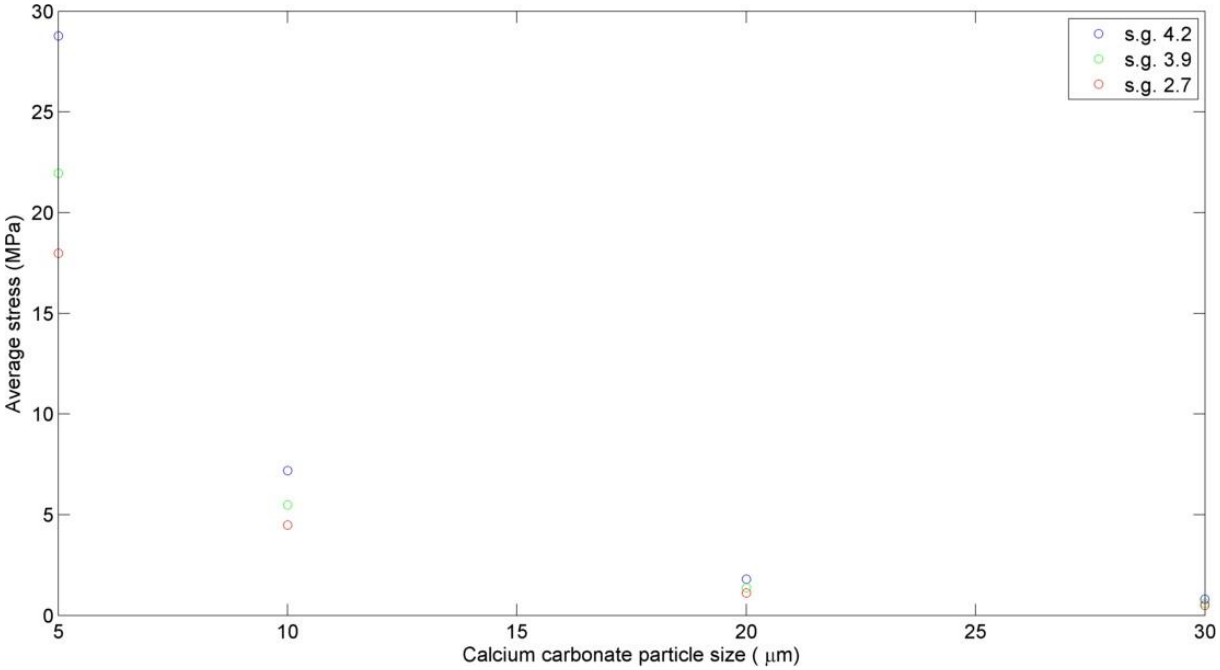

Figure 6.3-10 Mean stress within the mill as a function of calcium carbonate particle size

Figure 6.3-11 (a) (b) (c) and (d) show stress distribution profiles as a function of calcium carbonate particle size as determined using PEPT for each system and the mean strength of a calcium carbonate particle at that size as measured by micromanipulation. The data show that as calcium carbonate particle size decreased the proportion of the media capable of exerting sufficient stress to cause fracture increased, and that the proportion of the media capable of fracturing the calcium carbonate particles increased with media specific gravity. This is further illustrated in Figure 6.3-12 which shows the percentage of grinding media capable of fracturing calcium carbonate particles as a function of calcium carbonate particle size. Again, increased grinding media specific gravity gave an increased chance of calcium carbonate fracture.

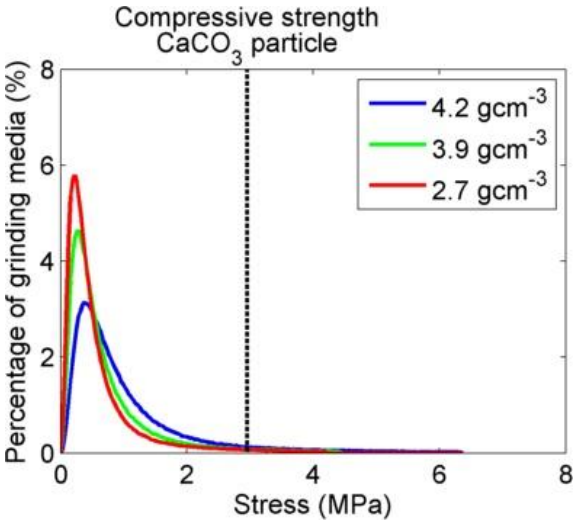

30 μm calcium carbonate particles

(a)

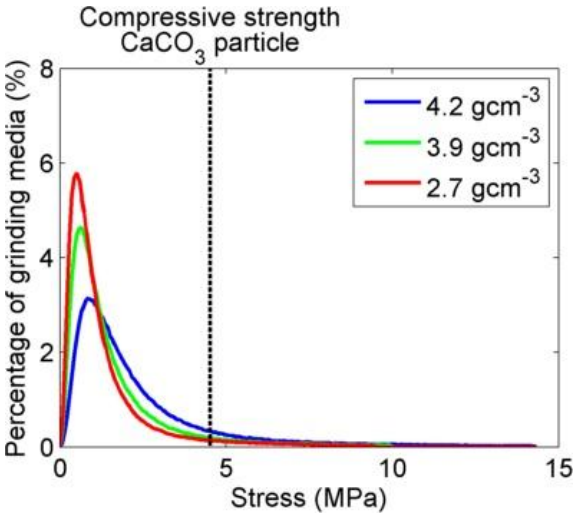

20 μm calcium carbonate particles

(b)

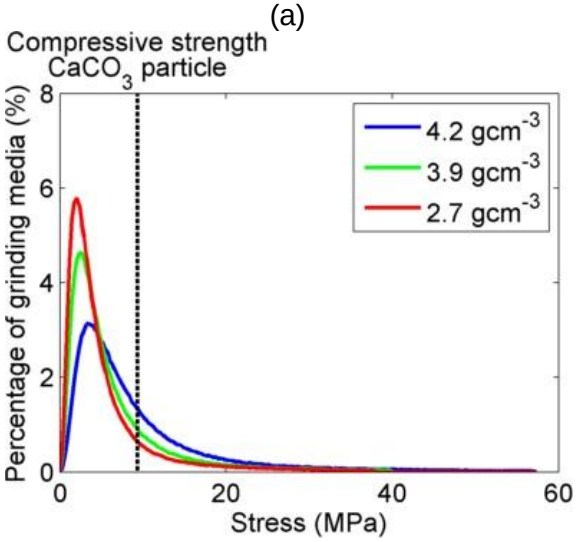

10 μm calcium carbonate particles

(c)

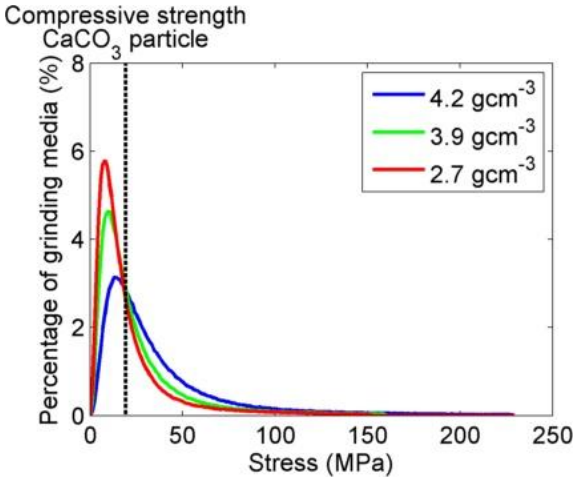

5 μm calcium carbonate particles

(d)

Figure 6.3-11 Distribution of stresses exerted by grinding media when calcium carbonate particle size is (a) 30 (b) 20 (c) 10 and (d) 5 μm (based on average strength of calcium carbonate particles at a given size)

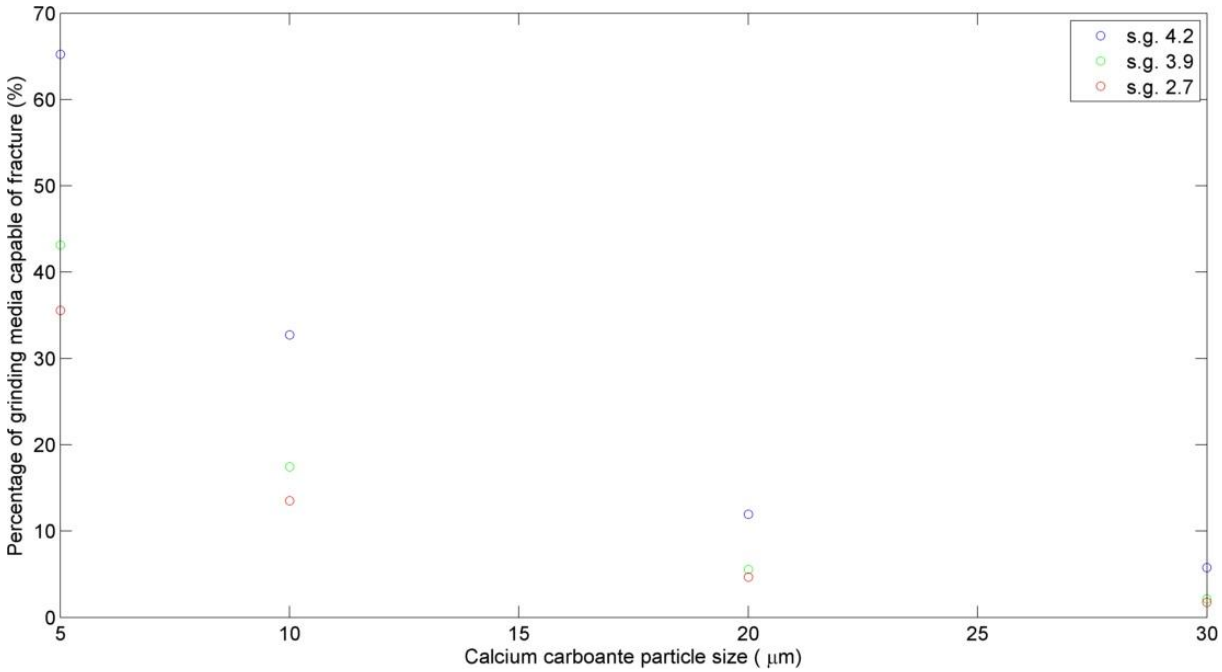

Figure 6.3-12 Percentage of grinding media suitable to fracture calcium carbonate particles as a function of calcium carbonate feed size (based on average strength of calcium carbonate particles at a given size)

Figure 6.3-13 (a) (b) (c) and (d) show the regions within the mill with sufficient stress to overcome the average compressive strength of the calcium carbonate particles. These data show that the regions within the mill where breakage could occur increased with increased grinding media specific gravity and decreased calcium carbonate size. These data are summarised in Figure 6.3-14.

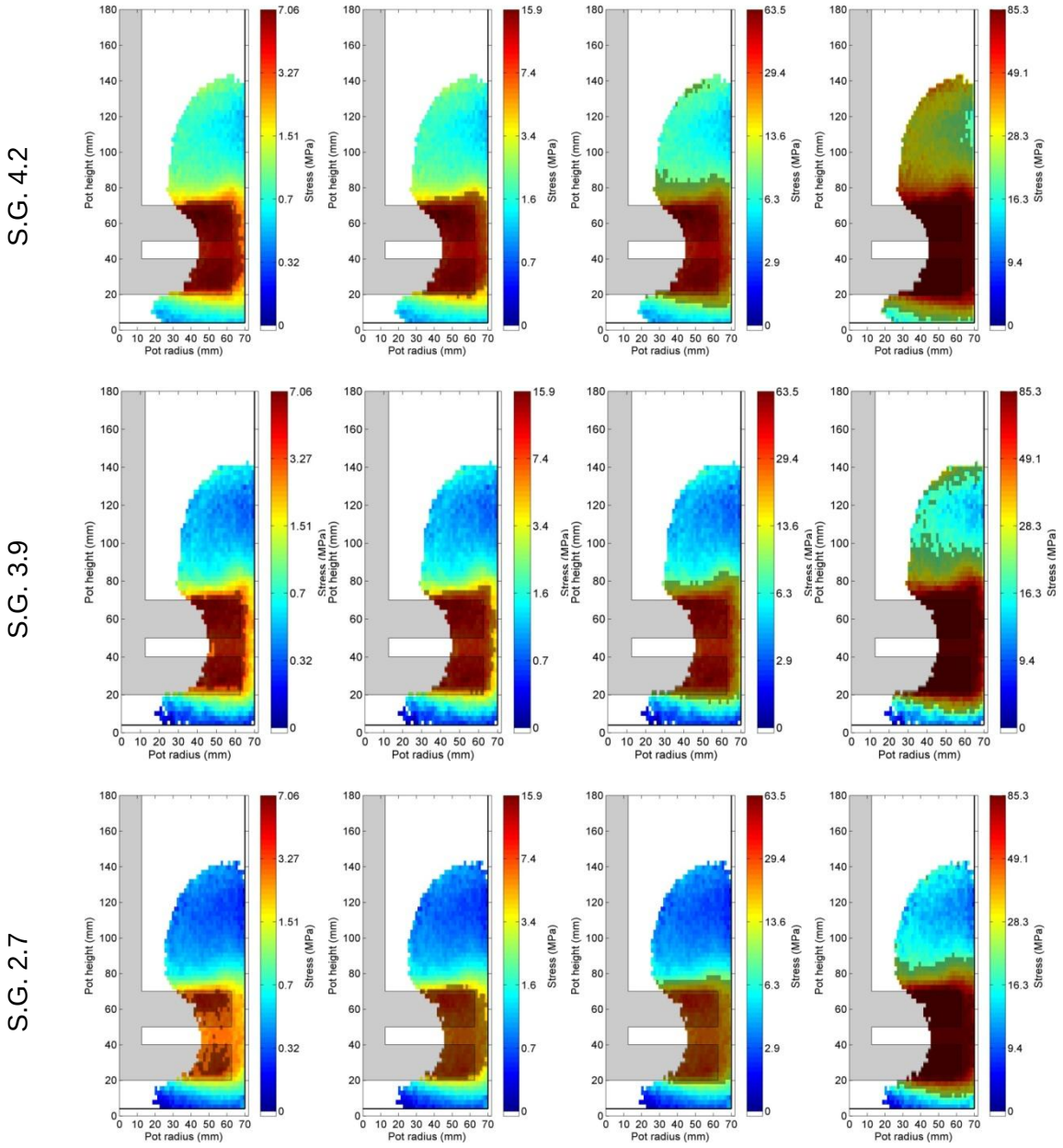

30 µm $CaCO_3$ particles (a)

20 µm $CaCO_3$ particles (b)

10 µm $CaCO_3$ particles (c)

5 µm $CaCO_3$ particles (d)

Figure 6.3-13 Regions of the mill capable of fracturing calcium carbonate feed particles comparing 4.2, 3.9 and 2.7 specific gravity grinding media when calcium carbonate particle size is (a) 30 (b) 20 (c) 10 and (d) 5 µm.

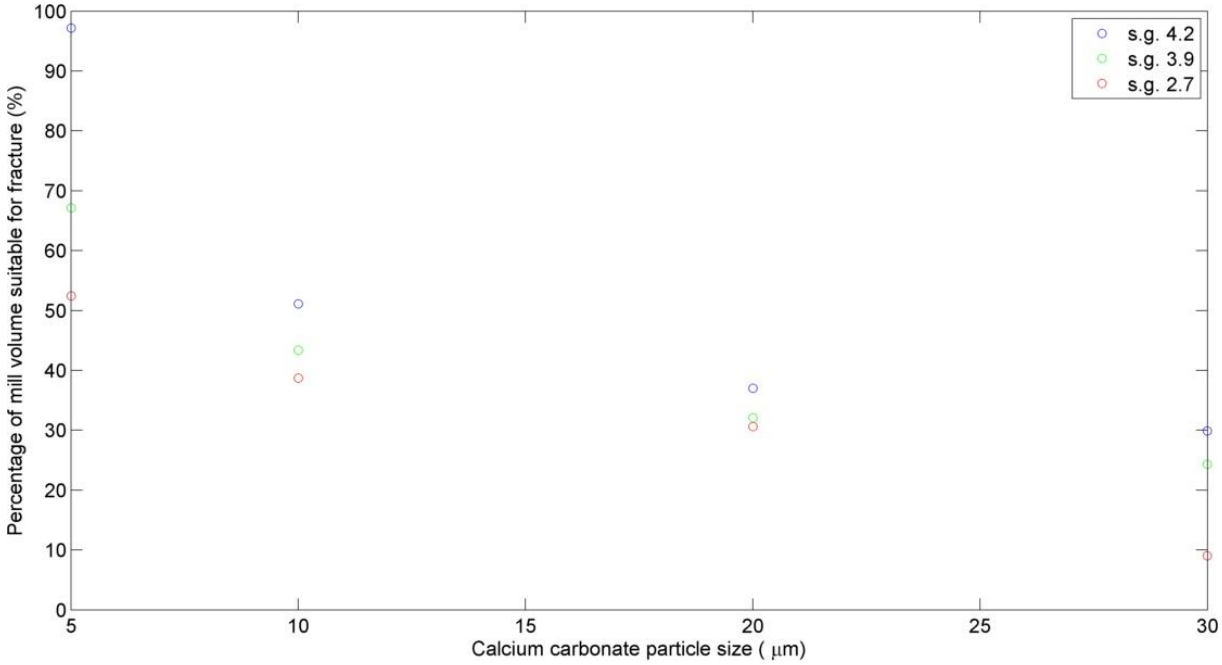

Figure 6.3-14 Percentage of the mill capable of fracturing calcium carbonate particles as a function of calcium carbonate feed size

6.3.1.1.5 Collisions

Figure 6.3-15 (a) (b) and (c) show the collision rate and total number of media-media collisions within the system and Figure 6.3-16 shows the total number of collisions as a function of pot height. No strong trends were observed. This was expected since the grinding media were all approximately the same size and the occupancy and velocity data showed little variation with change in specific gravity.

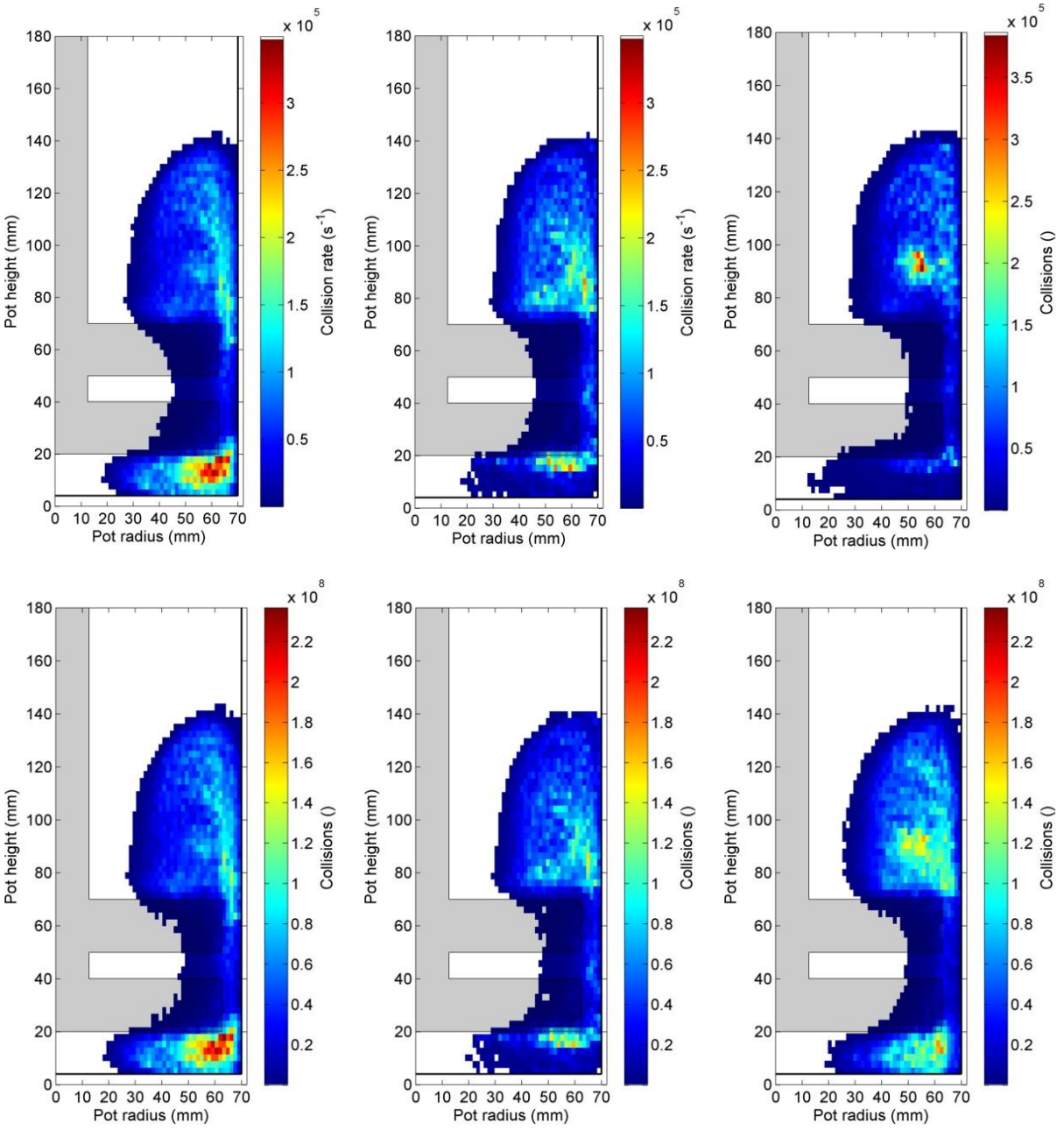

S.G. 4.2 (a) S.G 3.9 (b) S.G. 2.7 (c)

Figure 6.3-15 Collision rate and the number of collisions throughout the course of a grind contour plots for (a) 4.2 (b) 3.9 and (c) 2.7 specific gravity grinding media

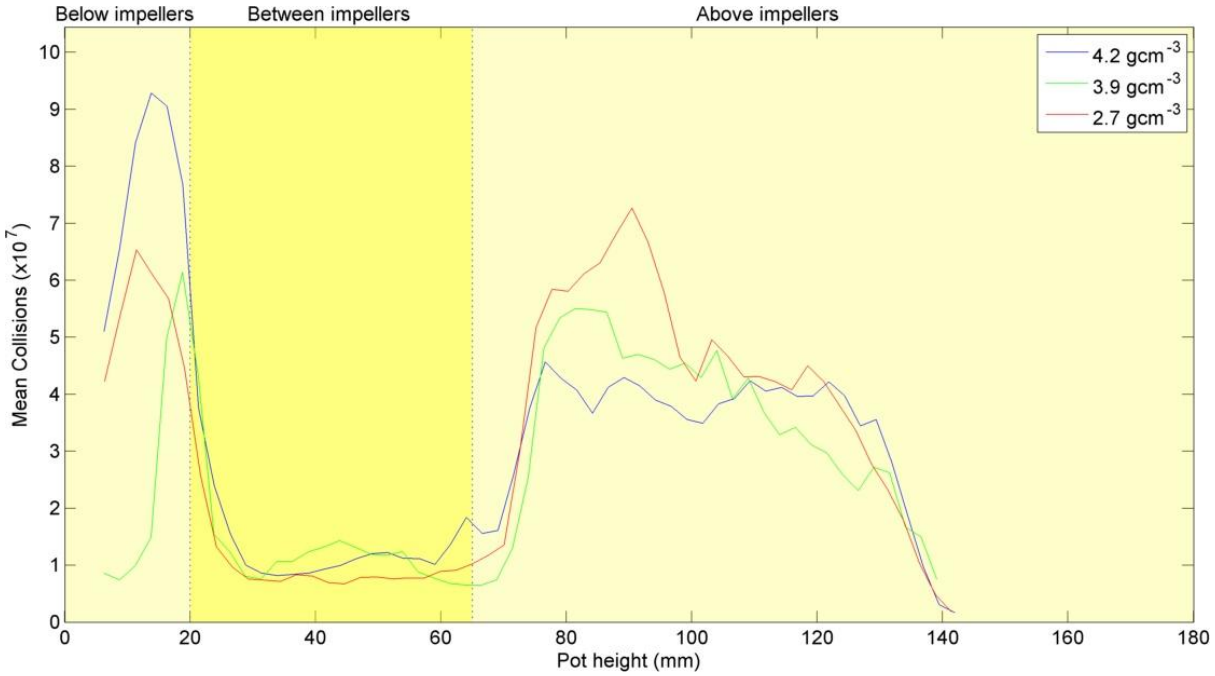

Figure 6.3-16 Total collisions between grinding media as a function of height in the mill

6.3.1.2 Comparison of PEPT data with laboratory grinding data

It was hypothesised in Section 4.3 that since the grinding media had approximately the same particle size then it was unlikely that the number of collisions would vary. Hence the observed improved grinding performance with increasing media specific gravity was likely because of increased stress intensity at media-media collisions. The PEPT data support this view. The data presented in Figure 6.3-15 and Figure 6.3-16 show no increase in collisions whilst the data presented in Figure 6.3-6 through Figure 6.3-14 indicate increased force and stress with increased specific gravity which resulted in the media within a greater volume of the mill being suitable to fracture calcium carbonate particles.

6.3.2 Grinding media particle size

Lab grinding data with differing grinding media particle size having approximately the same specific gravity are given in Section 4.4. These data show that decreasing the size of the grinding media resulted in reduced energy requirements to achieve a specific grinding objective. It was suggested that improved performance observed using finer media likely occurred because the effect of increasing the number of collisions outweighs the effect of reduced stress intensity. It is also suggested that the finest grinding media was the least effective during the coarse stage of the grind. This could be because the number of collisions is less important than stress intensity at this stage.

6.3.2.1 PEPT data

6.3.2.1.1 Occupancy

Figure 6.3-17 (a) (b) (c) and (d) show the occupancy contour plots for grinds performed using 0.80-1.00, 1.40-1.68, 1.68-2.00 and 2.00-2.40 mm zirconium silicate (specific gravity 3.9) grinding media under the conditions described in Section 4.4. It can be seen that total volume occupied by the media increased with grinding media particle size. Comparing Figure 6.3-17 (a) and (b) to (c) and (d) showed that the smaller diameter grinding media had higher occupancy in the recirculation zone. However, Figure 6.3-18 shows that there were no strong trends in the percentage of grinding media in the recirculation zone. This is likely because despite the higher occupancy with fine media, the total volume of the recirculation zone was higher with coarse grinding media. The reasons for this increased volume are unclear, but given the incompressible nature of fluids, the most likely explanation is air entrapment. It is

possible that the total charge viscosity with coarse grinding media is lower than fine grinding media leading to increased air entrapment.

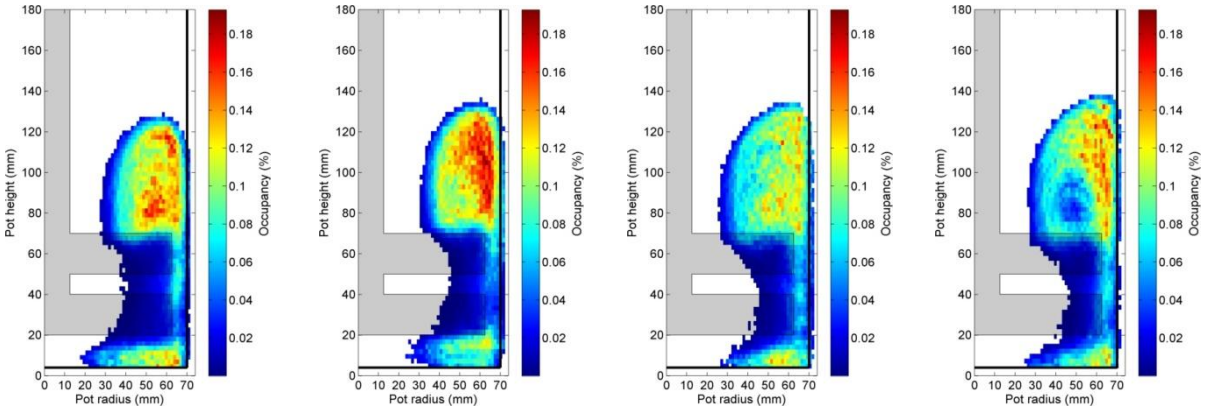

0.80-1.00 mm (a) | 1.40-1.68 mm (b) | 1.68-2.00 mm (c) | 2.00-2.40 mm (d)

Figure 6.3-17 Occupancy contour plots for (a) 0.80-1.00 (b) 1.40-1.68 (c) 1.68-2.00 and (d) 2.00-2.40 mm grinding media

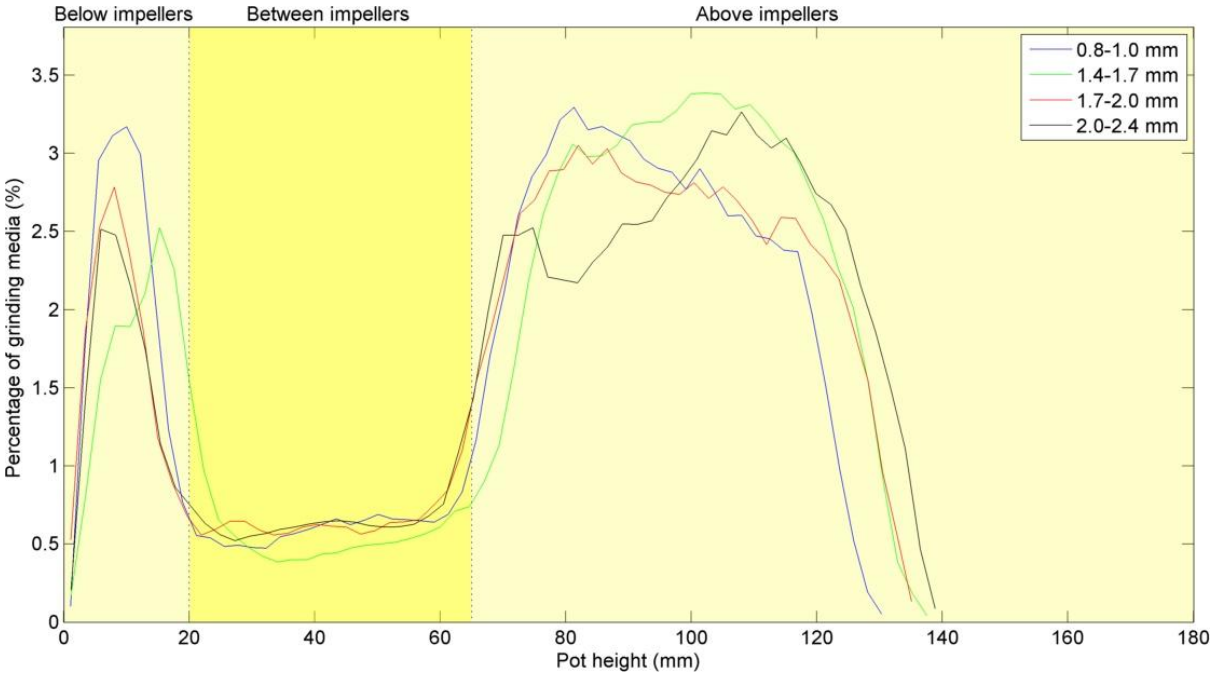

Figure 6.3-18 Percentage of grinding media as a function of height in the grinding pot

6.3.2.1.2 Velocity

Figure 6.3-19 (a) (b) (c) and (d) show the velocity contour plots for grinds performed using 0.80-1.00, 1.40-1.68, 1.68-2.00 and 2.00-2.40 mm grinding media and Figure 6.3-20 shows the mean velocity of the grinding media as a function of pot height. Whilst there are no strong trends these data indicate that the velocity in the impeller zone was lower with the 0.80-1.00 mm grinding media. A similar relationship was observed for the mean relative velocity as shown in Figure 6.3-21. The reduced velocity of the 0.80-1.00 mm grinding media system is likely due to the increased occupancy of the mill volume causing an increased number of media-media collisions, slowing the grinding media, or the reduced momentum of the grinding media due to the low mass of the media compared to larger grinding media.

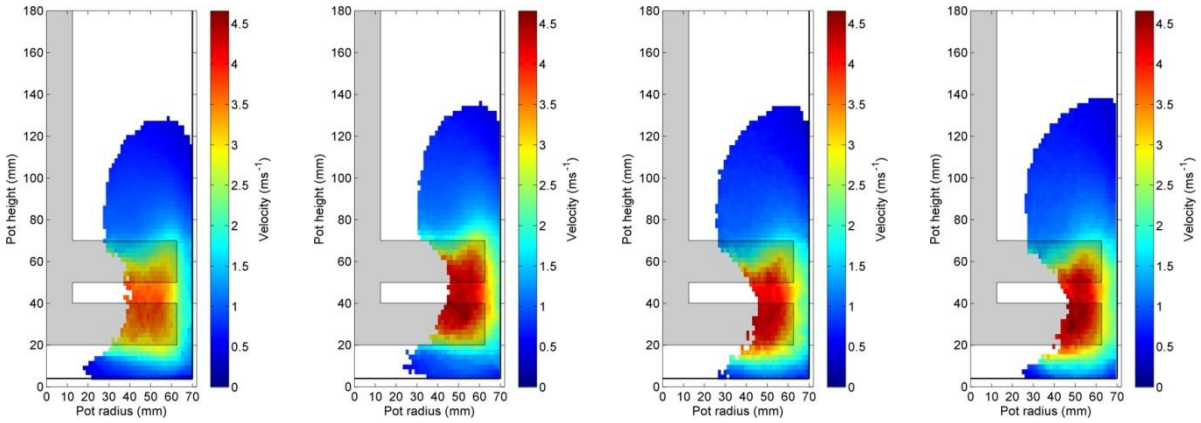

0.80-1.00 mm (a) | 1.40-1.68 mm (b) | 1.68-2.00 mm (c) | 2.00-2.40 mm (d)

Figure 6.3-19 Velocity contour plots for (a) 0.80-1.00 (b) 1.40-1.68, (c) 1.68-2.00 and (d) 2.00-2.40 mm grinding media

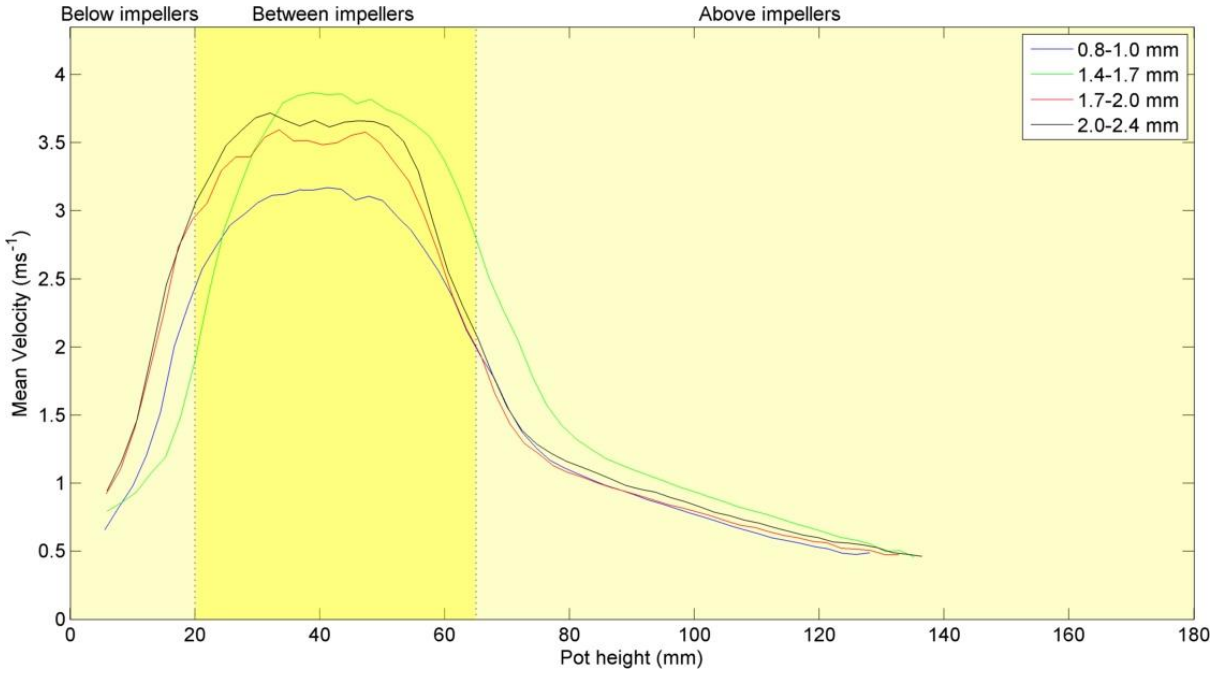

Figure 6.3-20 Mean velocity of grinding media as a function of height in the grinding pot

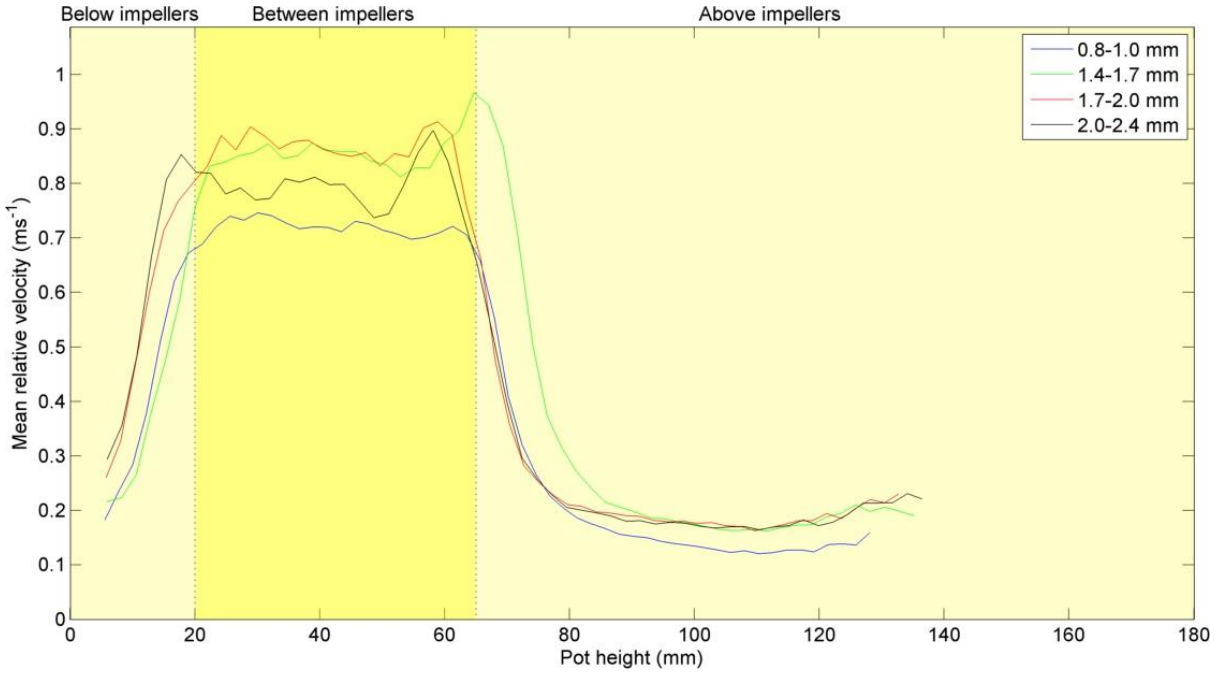

Figure 6.3-21 Mean relative velocity of grinding media as a function of height in the grinding pot

6.3.2.1.3 Force

Figure 6.3-22 (a) (b) (c) and (d) show the force contour plots for grinds performed using 0.80-1.00, 1.40-.68, 1.68-2.00 and 2.00-2.40 mm grinding media. It can be seen that the force experienced by the grinding media increased as grinding media diameter increased. This is further illustrated in Figure 6.3-23 where the maximum force experienced by the 2.00-2.40 mm grinding media was approximately 7 mN force as opposed to a force of 0.2 mN experienced by the 0.80-1.00 mm grinding media. Figure 6.3-24 compares the difference in force experienced by the different size grinding media. The increase in the force of the grinding media is a result of the increased mass of the media.

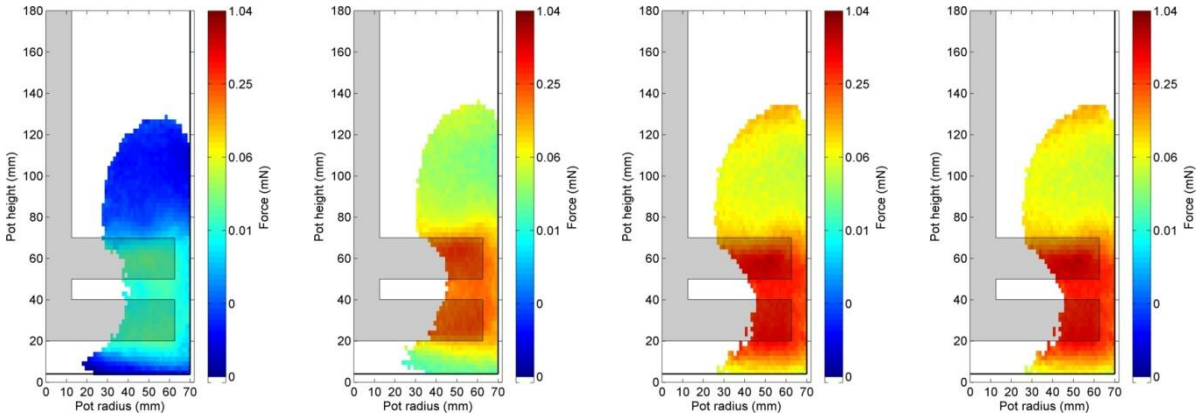

0.80-1.00 mm (a) | 1.40-1.68 mm (b) | 1.68-2.00 mm (c) | 2.00-2.40 mm (d)

Figure 6.3-22 Force contour plots for (a) 0.80-1.00 (b) 1.40-1.68 (c) 1.68- 2.00 and (d) 2.00- 2.40 mm grinding media

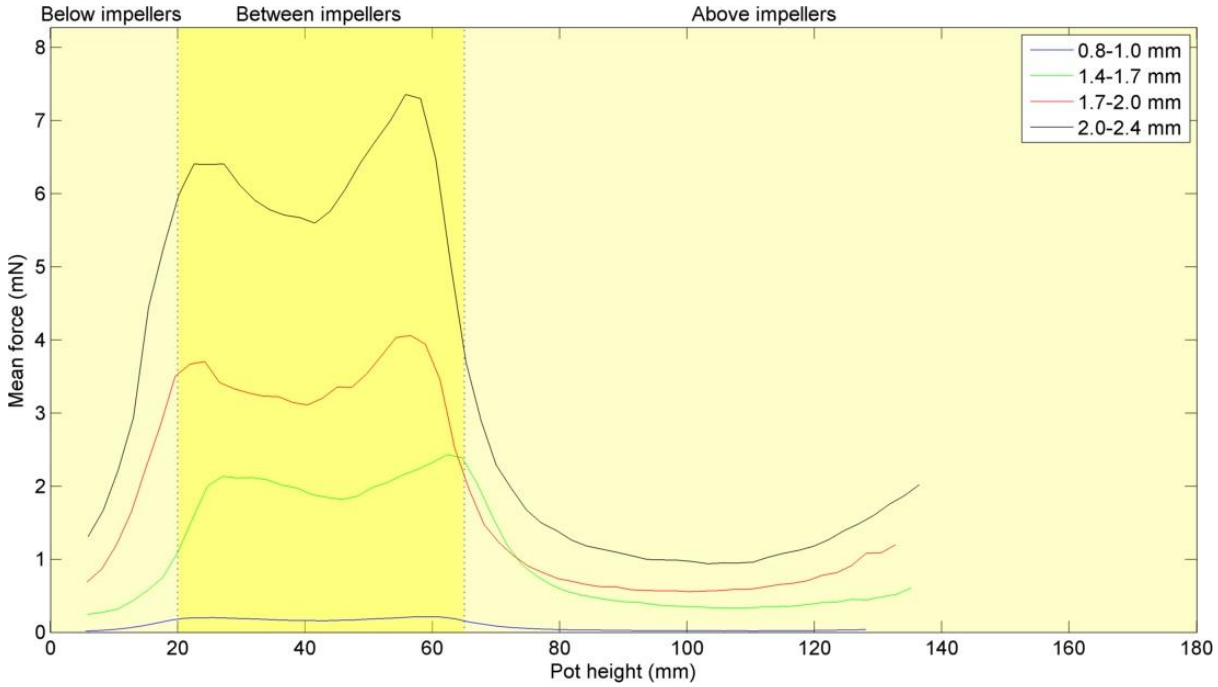

Figure 6.3-23 Mean force of grinding media as a function of height in the grinding pot

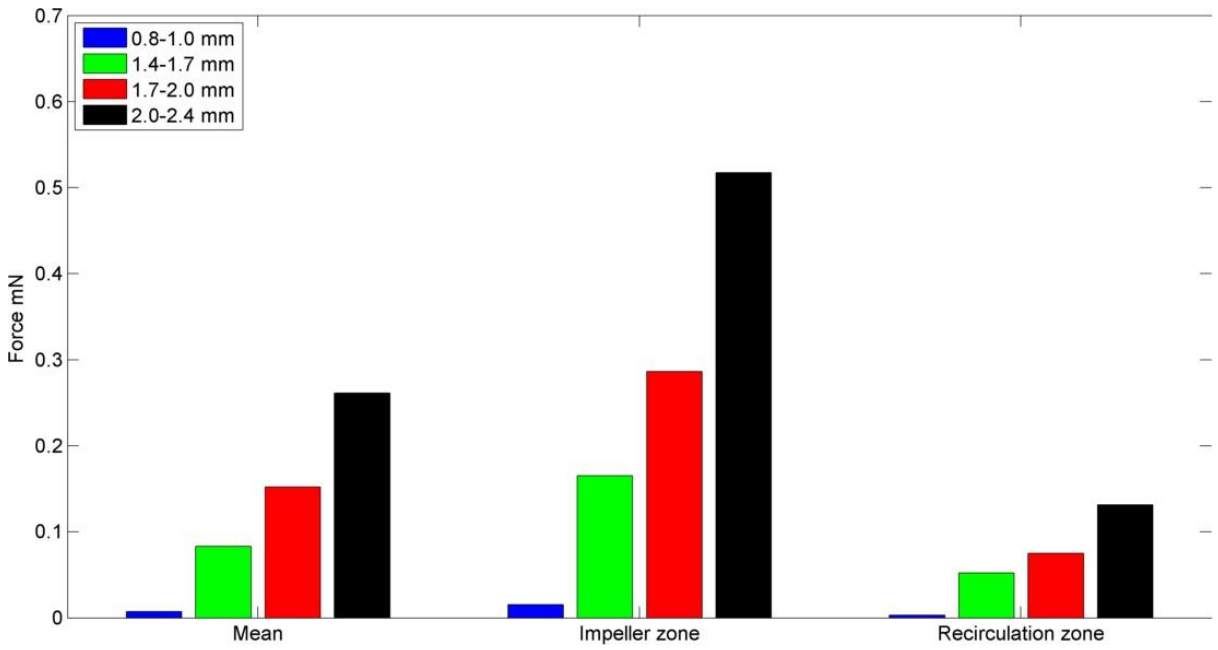

Figure 6.3-24 Bar chart comparing mean, impeller zone and recirculation zone forces

6.3.2.1.4 Stress

Figure 6.3-25 (a) (b) (c) and (d) show how the stress acting on calcium carbonate particles varied with calcium carbonate size and media size. It can be seen that for each case as the calcium carbonate particle size decreased the applied stress increased; and that the stress applied for a given size range increased as grinding media size increased. This is further illustrated in Figure 6.3-26 which shows a comparison of the average stress applied to the calcium carbonate as a function of calcium carbonate particle size. As the calcium carbonate particle size decreased the difference in stress applied by the different sized grinding media increased. When 30 μm calcium carbonate were stressed the difference in stress applied was small, approximately 0.1 to 1 MPa for all four sized grinding media. However at finer particle sizes differences in applied stress at differing sized media were apparent. For example, when stressing 5 μm calcium carbonate particles, 2.00-2.40 mm grinding media exerted 60 MPa stress whilst 0.8-1.00 exerted approximately 2 MPa stress.

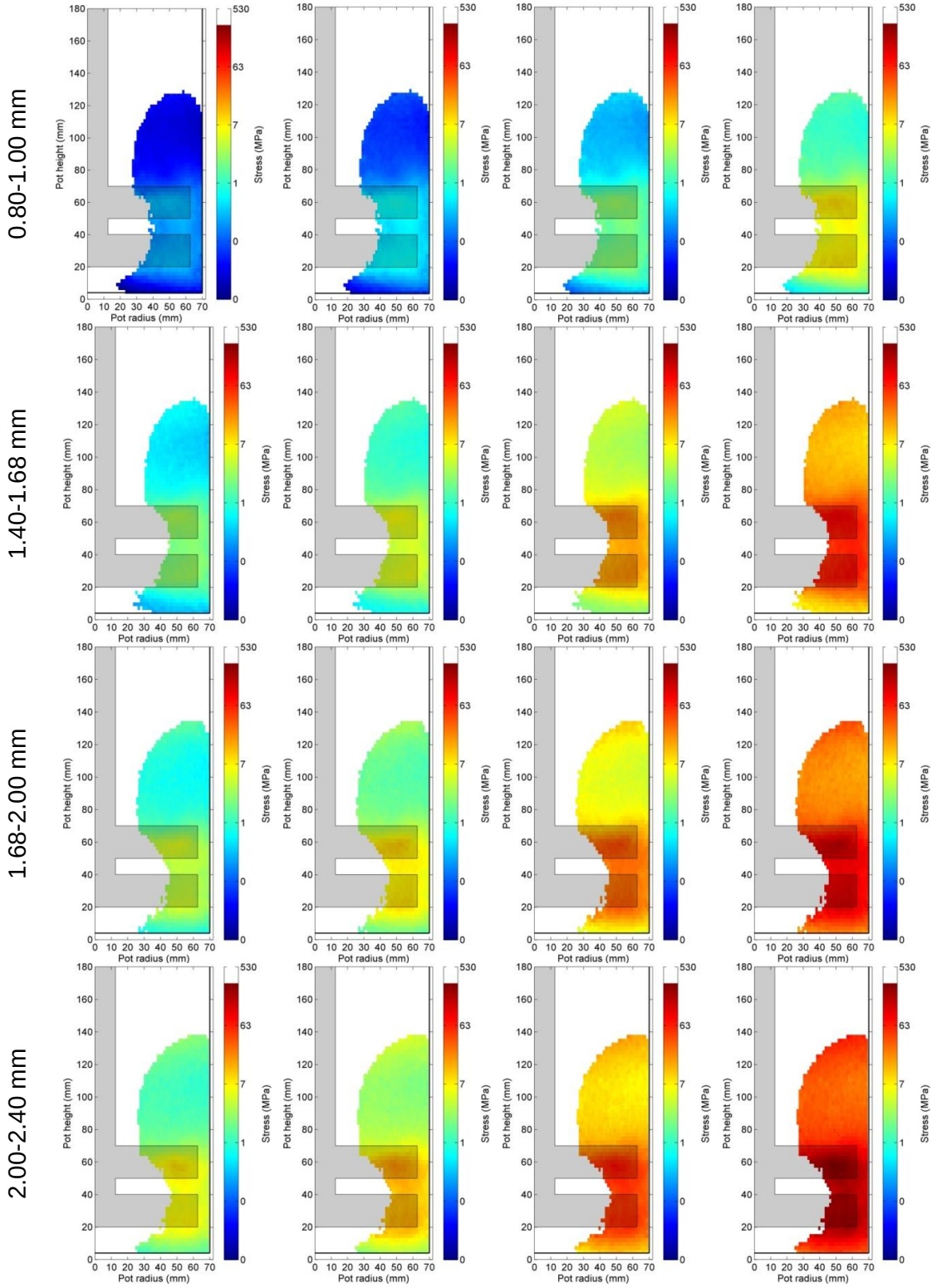

Figure 6.3-25 Stress contour plots comparing 0.80-1.00, 1.40-1.68, 1.68-2.00 and 2.00-2.40 mm grinding media when calcium carbonate particle size is (a) 30 (b) 20 (c) 10 and (d) 5 µm

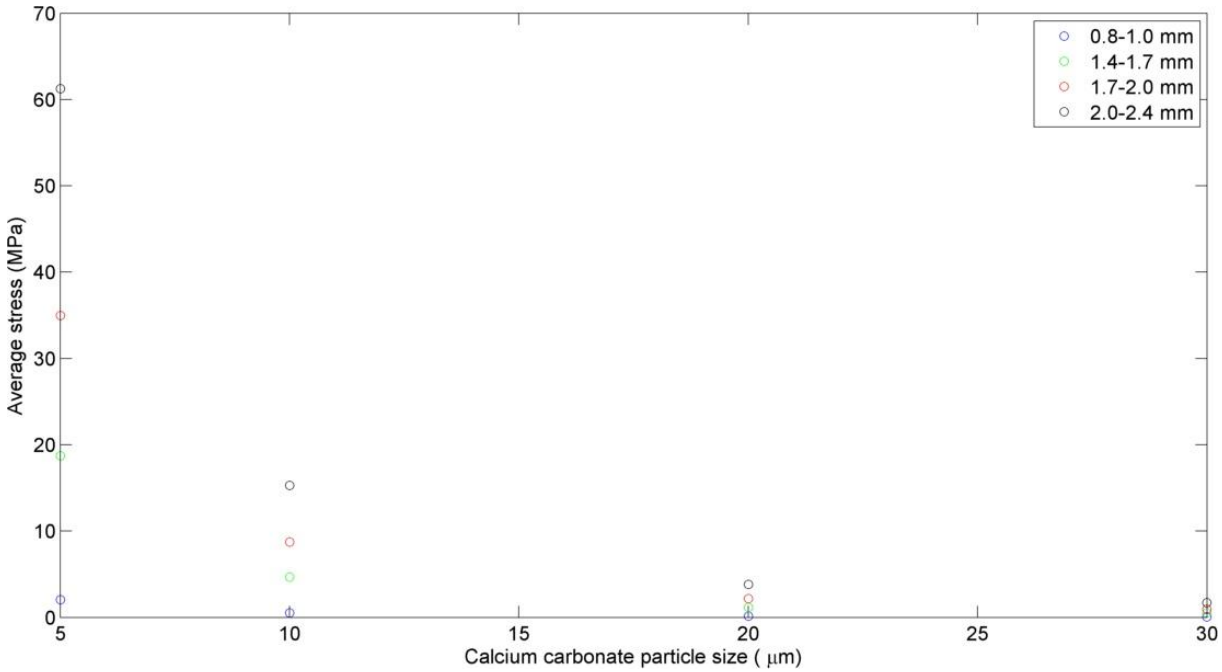

Figure 6.3-26 Mean stress within the mill as a function of calcium carbonate particle size

Figure 6.3-27 (a) (b) (c) and (d) show stress distribution profiles as a function of calcium carbonate particle size as determined using PEPT for each system and the mean strength of a calcium carbonate particle at that size as measured by a micromanipulation technique. The data show that as calcium carbonate particle size decreased the portion of the media capable of exerting sufficient stress to cause fracture increased, and that the proportion of the media capable of fracturing calcium carbonate particles increased with increased particle size. This is further illustrated in Figure 6.3-28 which shows the percentage of grinding media capable of fracturing calcium carbonate particles as a function of calcium carbonate particle size. Again, increased grinding media particle size gave an increased proportion of calcium carbonate fracture. It is apparent from Figure 6.3-27 and Figure 6.3-28 that the stress exerted by the finest grinding media was much lower than with the coarser

grinding media particles and was less than the average force required for the breakage of all the particle sizes of calcium carbonate considered in this work.

The grinding work shown in Section 4.4 indicated improved performance with fine media. This is likely explained by the increased number of collisions (see next section). However, for this explanation to be valid at least some of the collisions must be successful. Figure 6.3-29 (a) and (b) rather than showing only the mean compressive strength of calcium carbonate as a function of calcium carbonate particle size show instead the stress at which 5, 10, 20, 30 and 40 % of the calcium carbonate population were fractured by the 0.80-1.00 mm grinding media. It can be seen from Figure 6.3-29 (a) that 0.5 % of the grinding media had sufficient stress to fracture 30 μm calcium carbonate particles at 5 % of the collisions and from figure (b) that 36 % of grinding media had sufficient stress to fracture 5 % of 5 μm calcium carbonate particles.

Hence these data show that: (i) at least some of the fine particle size grinding media had sufficient stress to fracture calcium carbonate particles across all the calcium carbonate sizes investigated and (ii) the finest particle size grinding media were capable of breaking a much higher percentage of 5 μm calcium carbonate particles than 30 μm calcium carbonate particles.

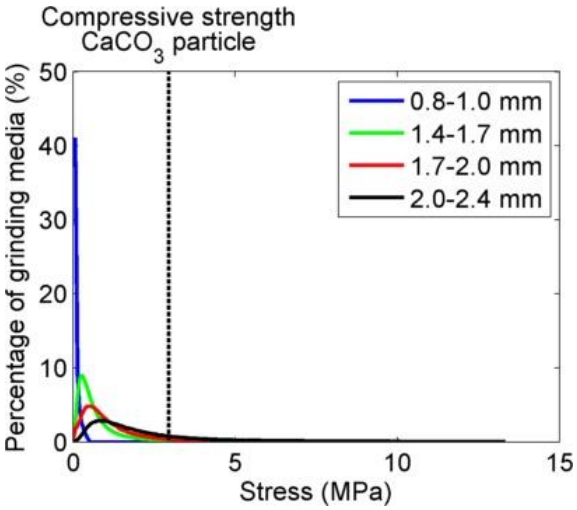

30 μm calcium carbonate particles

(a)

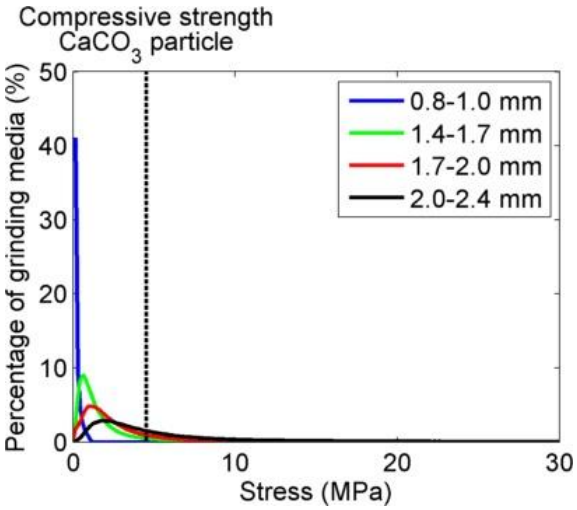

20 μm calcium carbonate particles

(b)

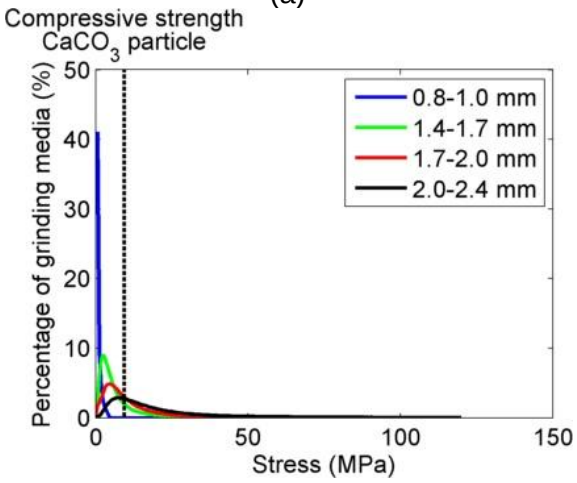

10 μm calcium carbonate particles

(c)

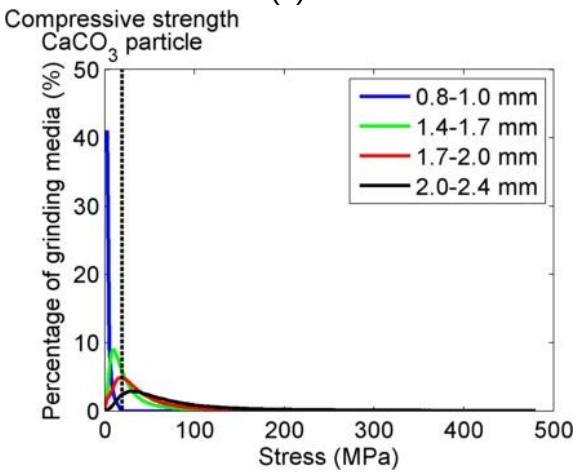

5 μm calcium carbonate particles

(d)

Figure 6.3-27 Distribution of stress exerted by grinding media when calcium carbonate particle size is (a) 30 (b) 20 (c) 10 and (d) 5 μm

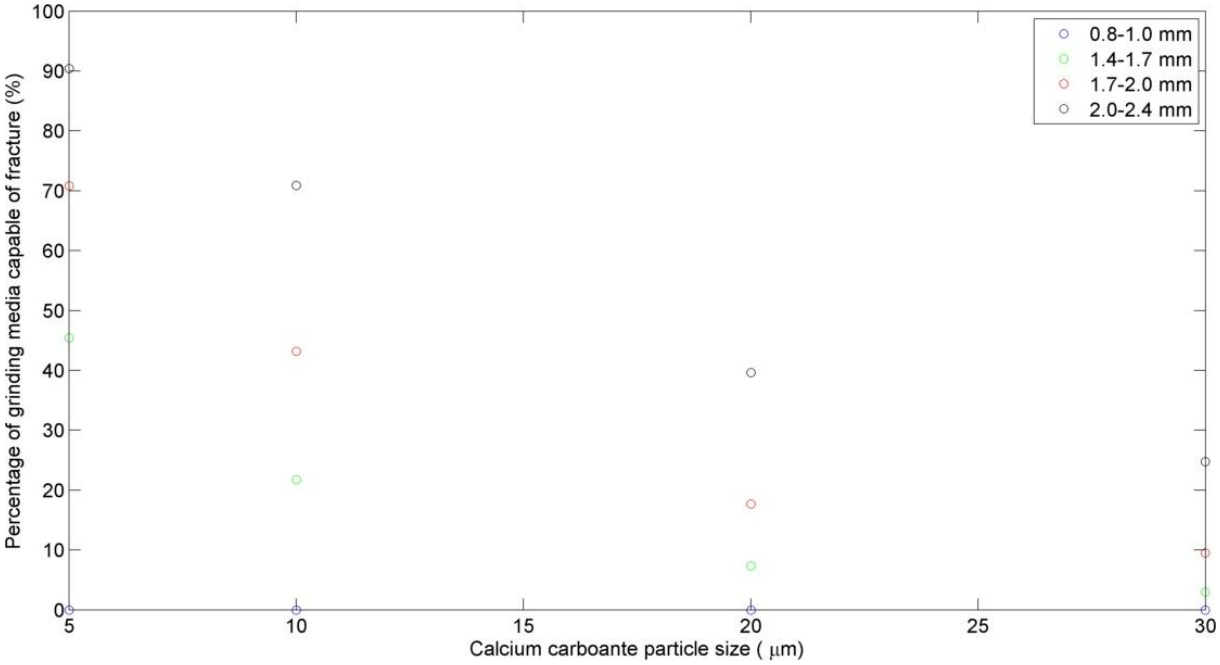

Figure 6.3-28 Percentage of grinding media suitable to fracture calcium carbonate particles as a function of calcium carbonate feed size (based on average strength of calcium carbonate feed particles at a given feed size)

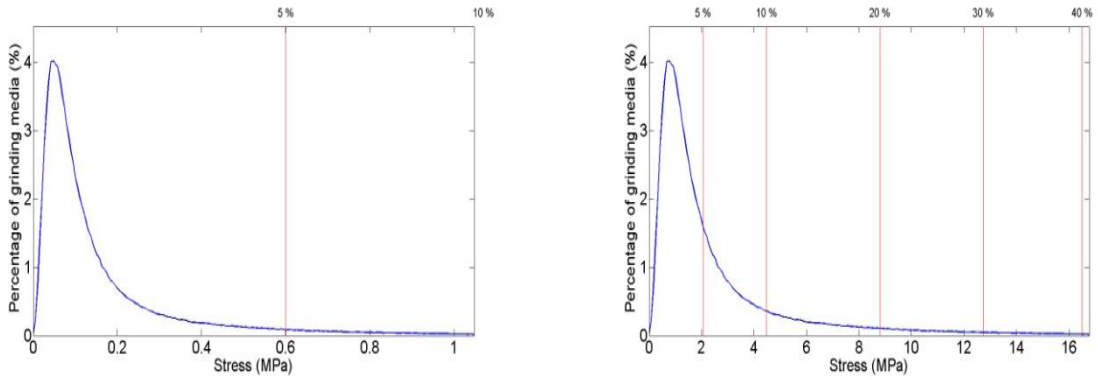

(a) (b)

Figure 6.3-29 Distribution of stresses exerted by 0.80-1.00 mm grinding media showing 5 %, 10 %, 20 %, 30 % and 40 % chance of fracturing calcium carbonate particles based on particle fracture distributions

Figure 6.3-30 (a) (b) (c) and (d) show the regions in the mill with sufficient stress to overcome the average compressive strength of the calcium carbonate particles. As discussed above, the finest sized grinding media did not have sufficient stress to overcome the average stress to fracture calcium carbonate at any of the size ranges shown. None-the-less Figure 6.3-30 clearly shows that the volumes of the mill with sufficient stress to cause particle breakage increased with increased particle size and decreased calcium carbonate size. These data are summarised in Figure 6.3-31.

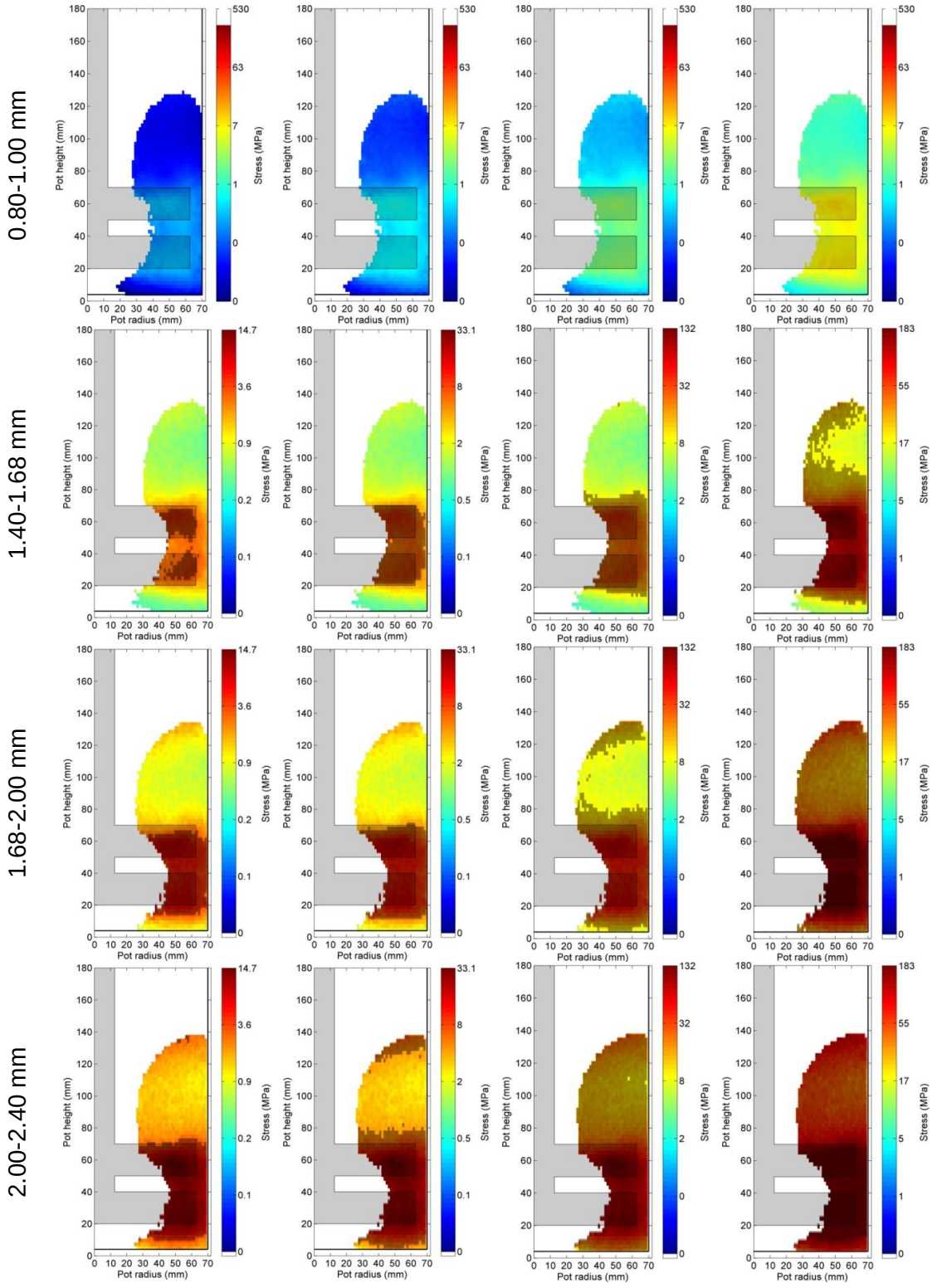

Figure 6.3-30 Regions of the mill capable of fracturing calcium carbonate feed particles comparing 0.80-1.00, 1.40-1.68, 1.68-2.00 and 2.00-2.40 mm grinding media when calcium carbonate particle size is (a) 30 (b) 20 (c) 10 and (d) 5 µm

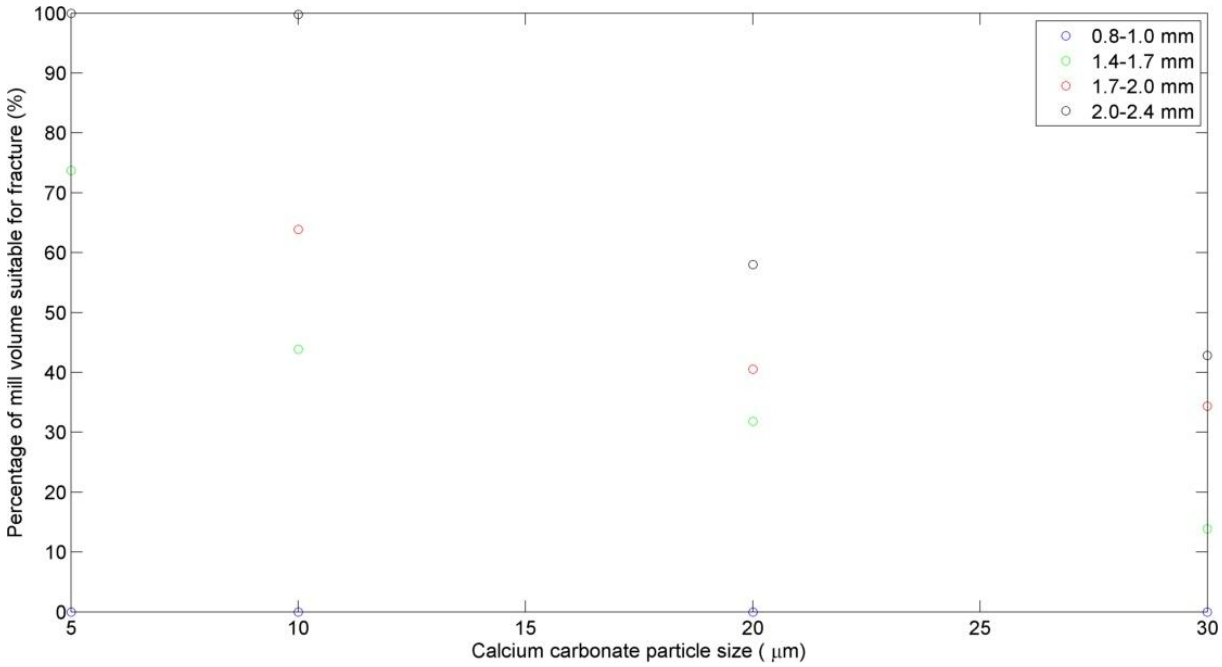

Figure 6.3-31 Percentage of the mill capable of fracturing calcium carbonate particles as a function of calcium carbonate feed size

6.3.2.1.5 Collisions

Figure 6.3-32 (a) (b) (c) and (d) show the collision rate and total number of media-media collisions within the system and Figure 6.3-33 shows the total number of collisions as a function of pot height. It can be seen that both the collision rate and the total number of collisions increased as grinding media size decreased. These data are summarised in Figure 6.3-34. It can be seen that the total collisions increased from $1x10^{10}$ when using 2.00-2.40 mm grinding media and to $4x10^{11}$ when using 0.80-1.00 mm grinding media.

Decreasing the grinding media size from 2.00-2.40 mm diameter to 0.8-1.00 mm diameter resulted in an increase of $1x10^5$ grinding media particles to $2x10^6$ grinding media particles in the mill. The increased number of media particles per unit volume resulted in higher collision frequencies between media particles and therefore more collisions.

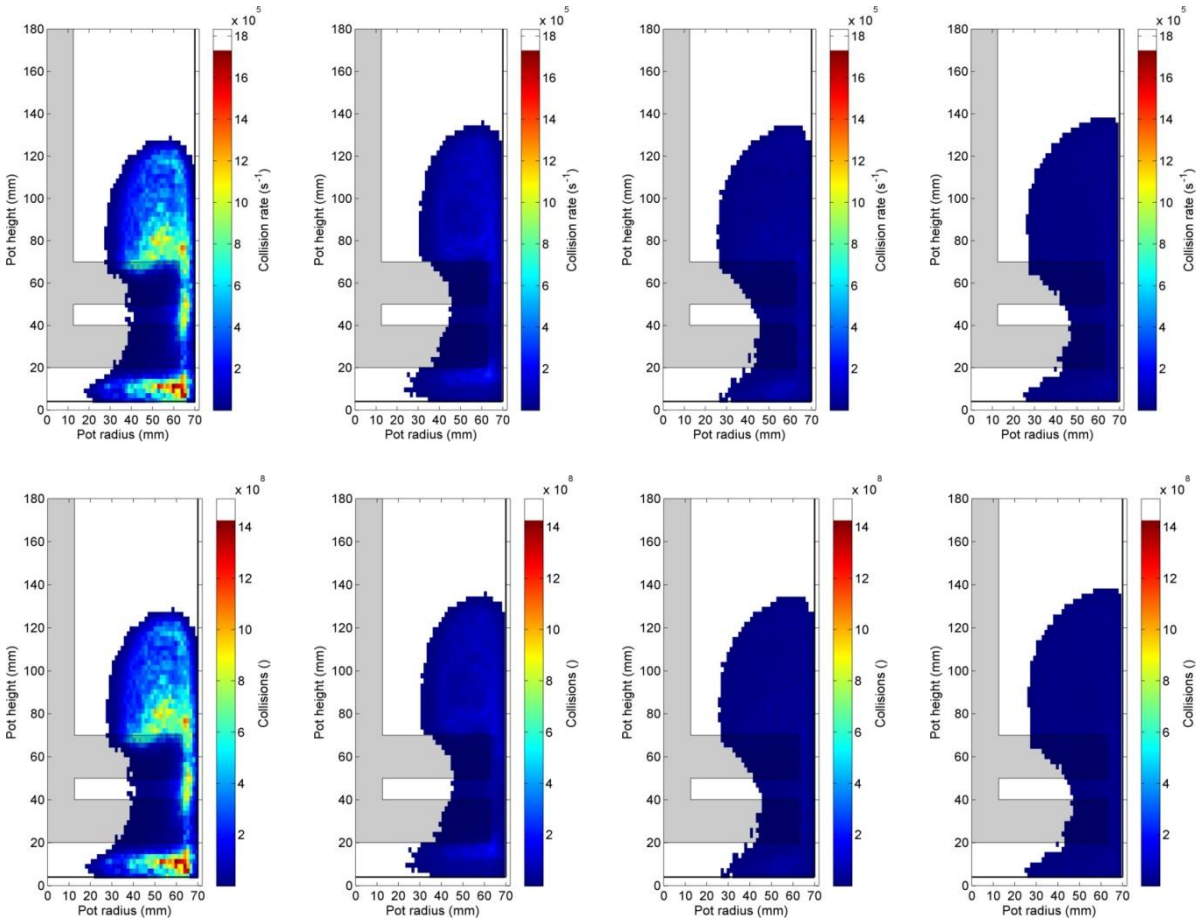

0.80-1.00 mm (a) | 1.40-1.68 mm (b) | 1.68-2.00 mm (c) | 2.00-2.40 mm (d)

Figure 6.3-32 Collision rate and the number of collisions throughout the course of a grind contour plots for (a) 0.80-1.00 (b) 1.40-1.68 (c) 1.68-2.00 and (d) 2.00-2.40 mm grinding media

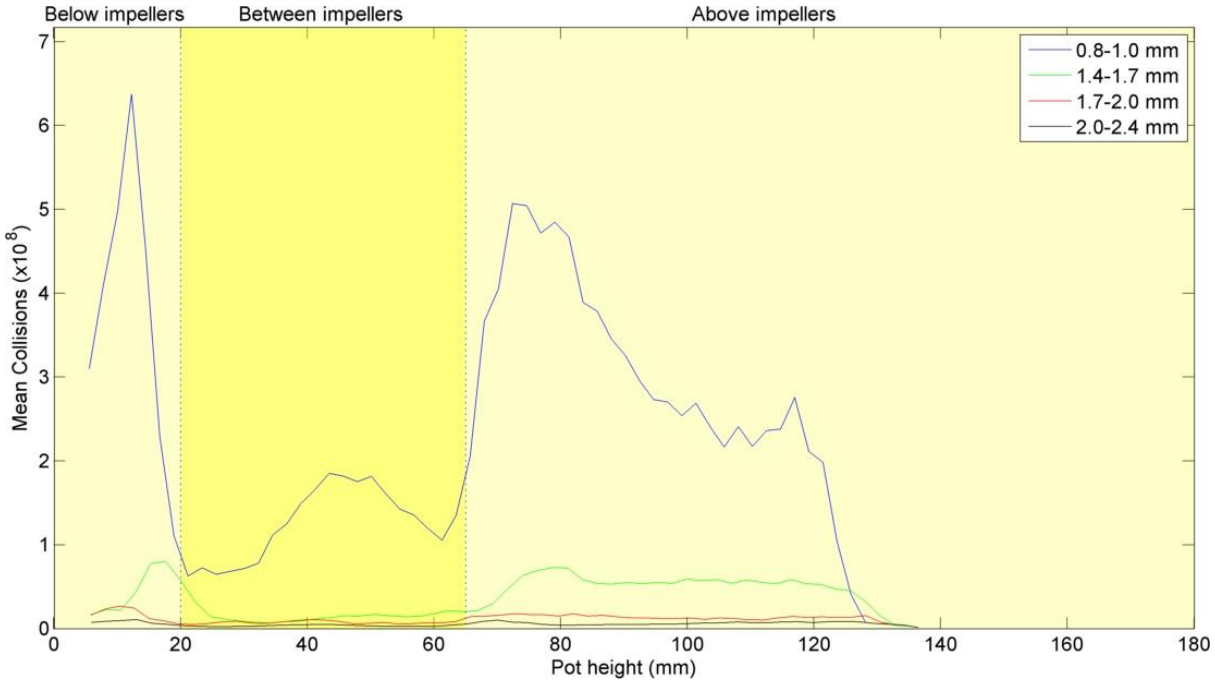

Figure 6.3-33 Mean collisions between grinding media as a function of height in the mill

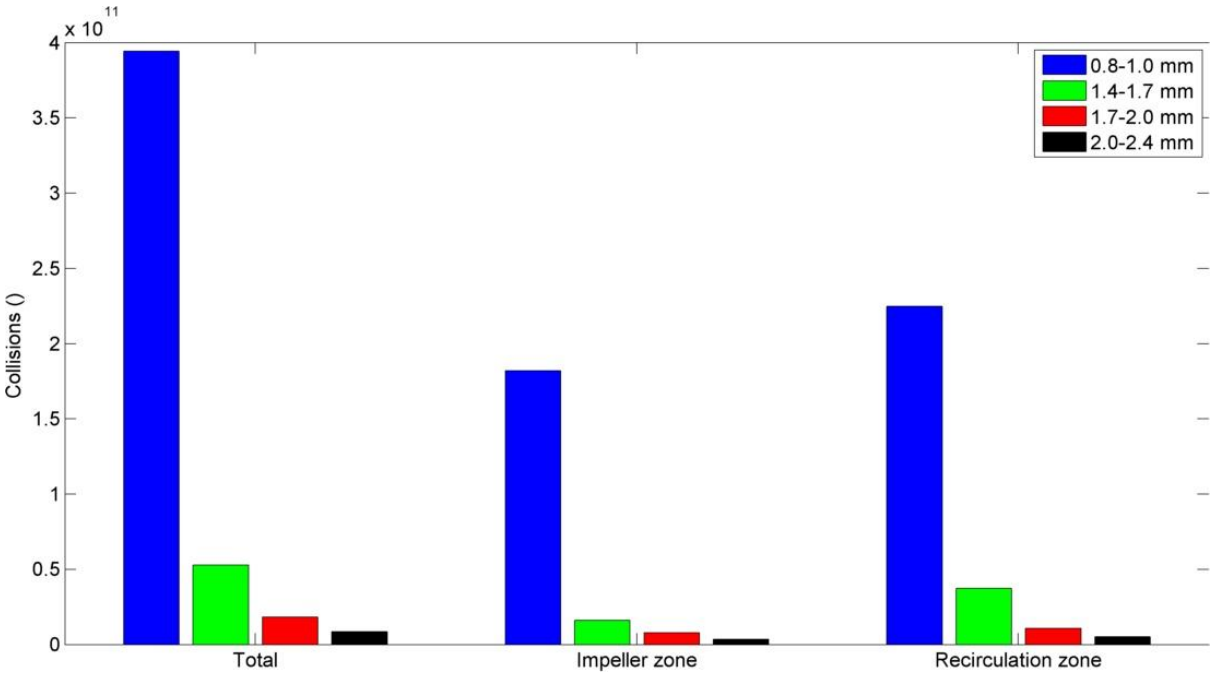

Figure 6.3-34 Bar chart comparing mean, impeller zone and recirculation zone media-media collisions

6.3.2.2 Comparison of PEPT data with laboratory grinding data

It was hypothesised in Section 4.4 that reducing the size of the grinding media reduced the stress at a collision but increased the number of collisions between grinding media particles. Therefore the observed improved grinding performance occurred despite the reduced stress because the total number of successful collisions increased. The PEPT data supports this view. The data presented in Figure 6.3-23 to Figure 6.3-31 show that the force and stresses acting on the grinding media decreased with grinding media diameter whilst the data shown in Figure 6.3-32 to Figure 6.3-34 indicates that the number of collisions increased with decreased grinding media particle size.

The data in Section 4.4 also suggested that the finest particle size grinding media was least effective during the coarse stage of the grind and that this could be because the number of collisions was less important than stress intensity during the coarse stages of grinding. The PEPT data also support this view as shown in Figure 6.3-29 (a) and (b) which suggest that the breakage rate of 30 μm calcium carbonate was much lower than that of 5 μm calcium carbonate when ground with the finest particle size grinding media.

6.3.3 Grinding media surface roughness

Lab grinding data with grinding media having differing surface roughness and approximately the same particle size and specific gravity were given in Section 4.5. These data indicated that changing the surface properties of the grinding media resulted in no improvement in energy requirements to achieve a specific grinding objective, however, it was noted that the power draw was considerably higher when using rough rather than smooth grinding media. The reason for this behaviour was unclear.

6.3.3.1 PEPT data

6.3.3.1.1 Occupancy

Figure 6.3-35 (a) and (b) show occupancy contour plots for grinds performed using rough and smooth grinding media (particle size approximately 3 mm and specific gravity approximately 5.5) under the conditions described in Section 4.5. It can be seen that the maximum media height of the recirculation zone was higher when using rough media although the general shape of the charge and vortex were approximately the same. It can also be seen that the occupancy of the rough media was higher close to the pot edge, whilst the occupancy of the smooth media was relatively constant throughout the recirculation zone. Figure 6.3-36 suggested that although a higher percentage of grinding media was found at a higher height in the mill when using rough media, elsewhere the percentage remained mostly constant.

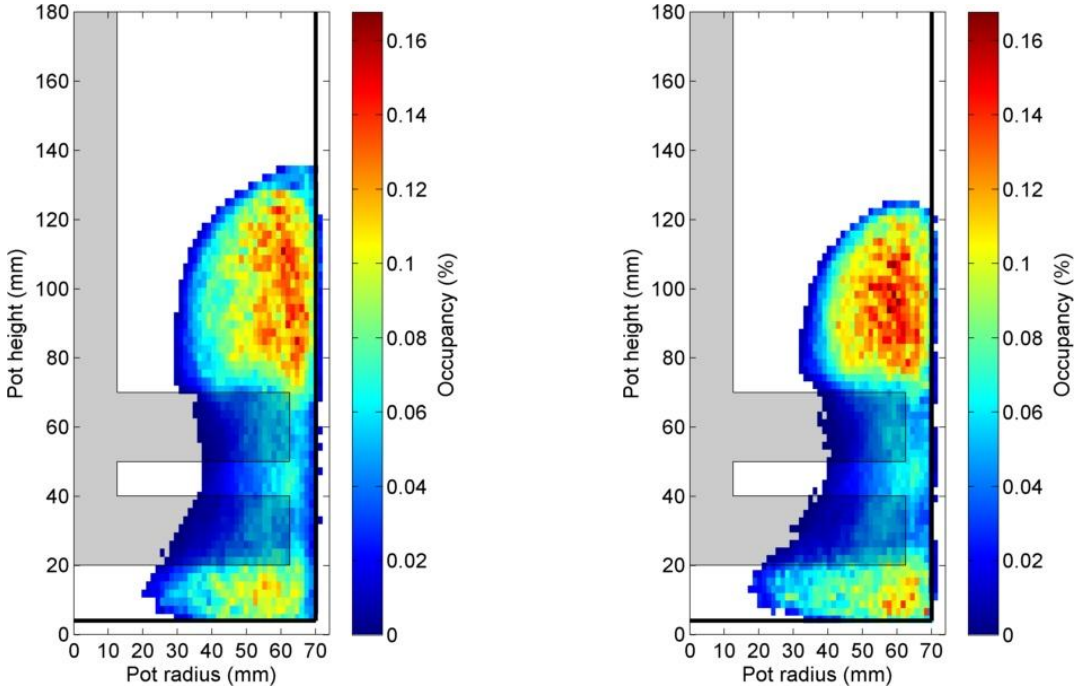

Rough grinding media
(a)

Smooth grinding media
(b)

Figure 6.3-35 Occupancy contour plots for (a) rough and (b) smooth grinding media

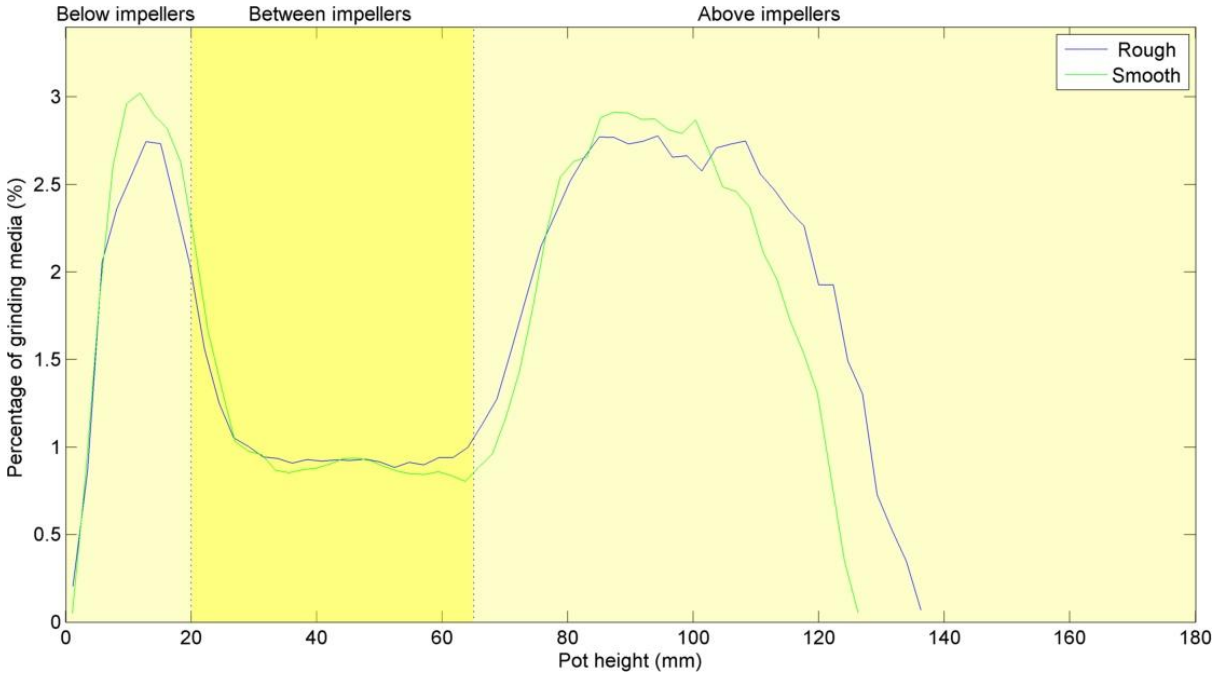

Figure 6.3-36 Percentage of grinding media as a function of height in the grinding pot

6.3.3.1.2 Velocity

Figure 6.3-37 (a) and (b) show the velocity contour plots for rough and smooth media systems. It can be seen that the velocity between the impellers was largely the same, however the velocities above and below the impellers were higher when using rough media. The velocity at the midpoint of the top and bottom impeller tips was approximately 2 ms^{-1} with rough and smooth grinding media. However the velocity of the media at the pot wall level with the impeller midpoints was approximately 1.5 ms^{-1} when using rough grinding media and 1ms^{-1} when using smooth grinding media. This was also confirmed by Figure 6.3-38, which showed similar velocities between rough and smooth grinding media around the top impeller, but lower velocities elsewhere in the mill when using smooth media. The same behaviour was noted when comparing mean relative velocity in Figure 6.3-39. The mechanism for the increased velocity of the rough grinding media away from the impeller is unclear, however it could be attributed to a boundary layer turbulence effect at the fluid-media interface resulting in less drag.

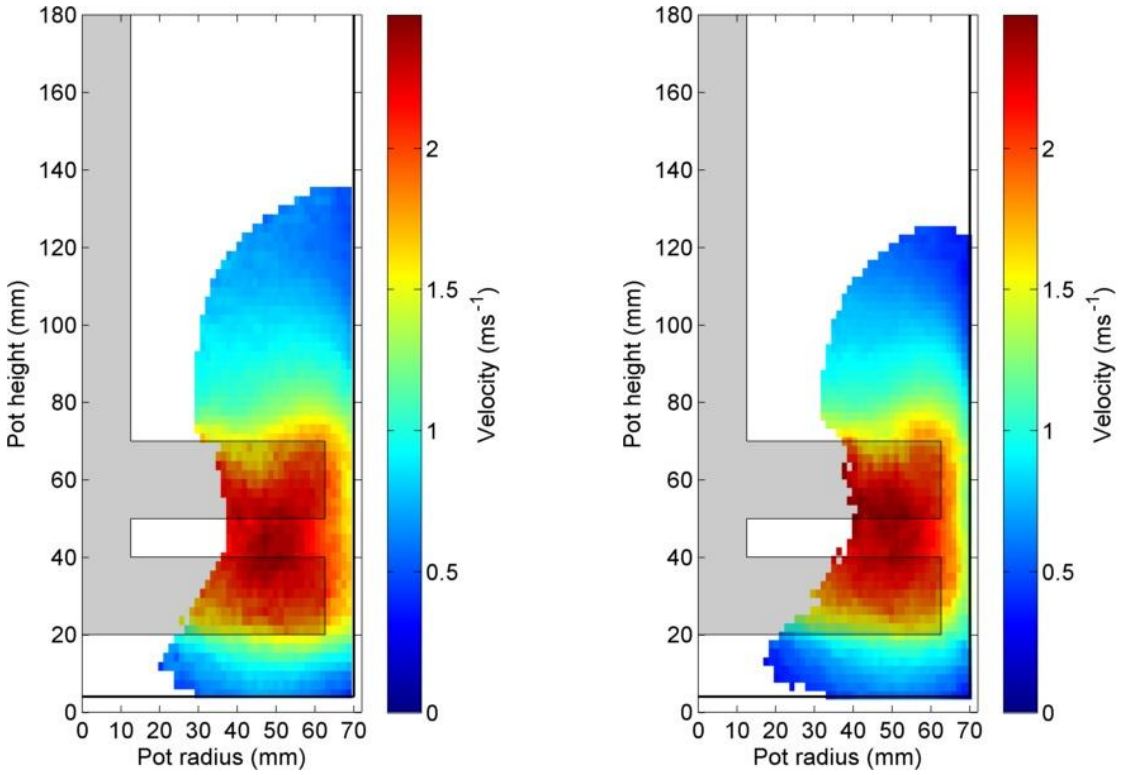

Rough grinding media
(a)

Smooth grinding media
(b)

Figure 6.3-37 Velocity contour plots for (a) rough and (b) smooth grinding media

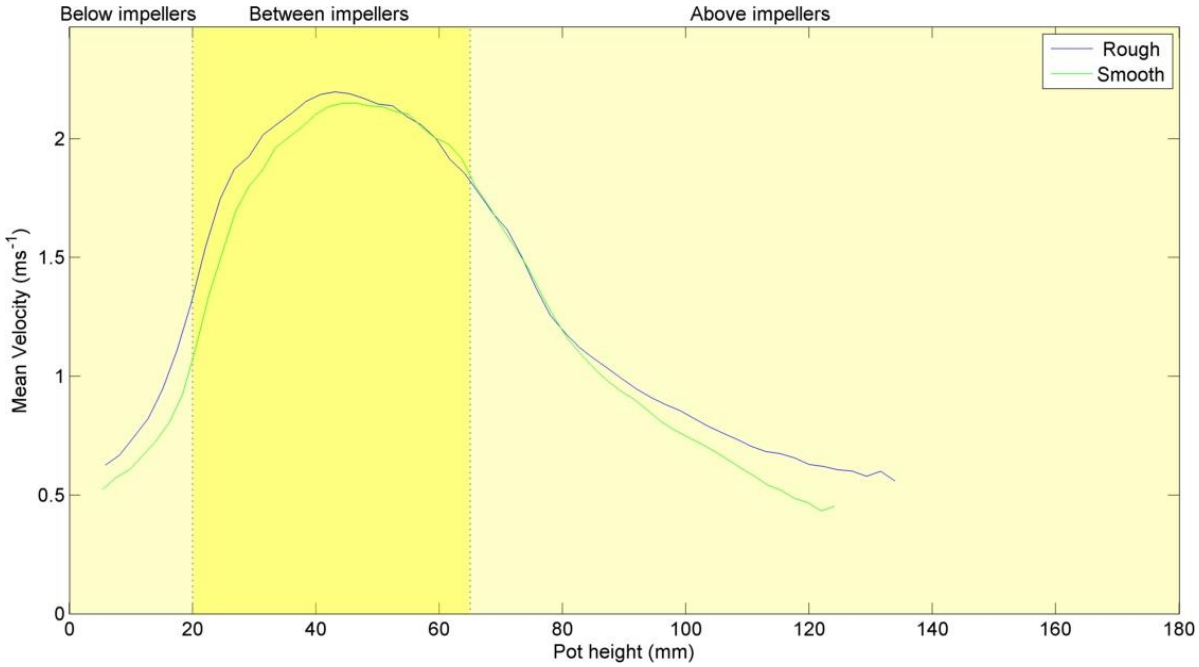

Figure 6.3-38 Mean velocity of grinding media as a function of height in the grinding pot

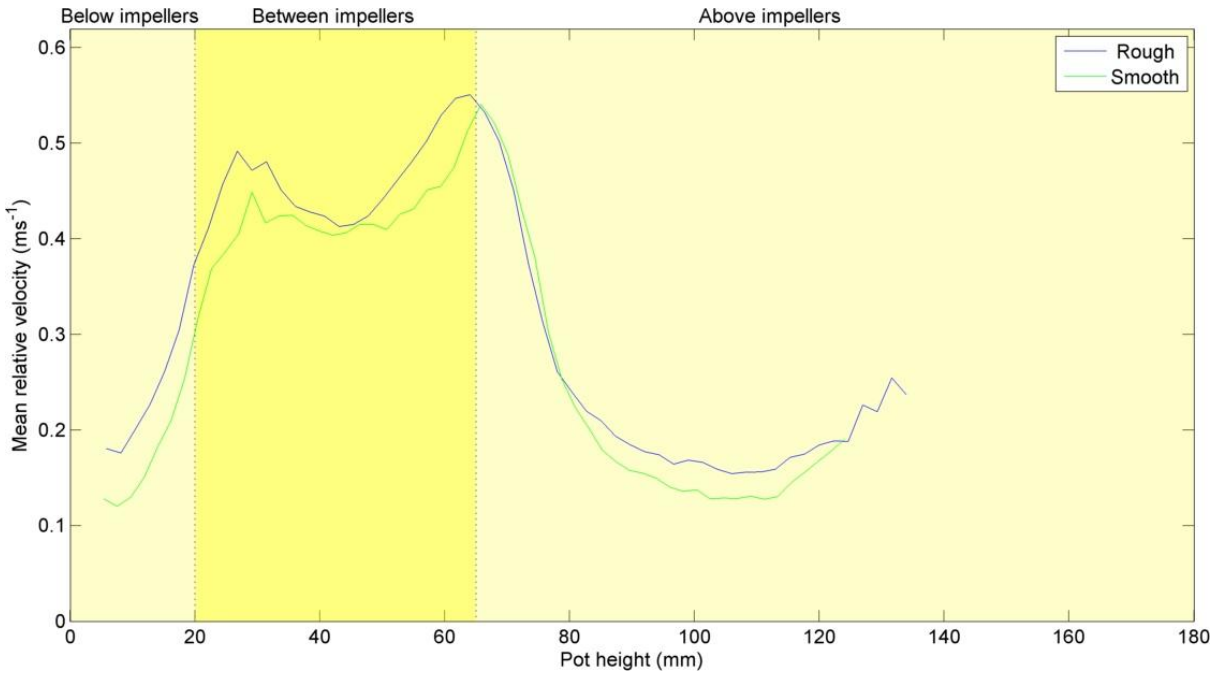

Figure 6.3-39 Mean relative velocity of grinding media as a function of height in the grinding pot

6.3.3.1.3 Force

Figure 6.3-40 (a) and (b) show the force contour plots for rough and smooth grinding media systems. It can be seen that the force experienced by the rough grinding media was higher than experienced by the smooth grinding media. The increased force observed when using rough grinding media was a result of increased acceleration experienced when the high velocity grinding media changes direction at the pot wall and was either pushed up into the recirculation zone or forced down beneath the impellers. Figure 6.3-40 (a) shows that with rough media there were regions of high force not only around the impeller but also at the interface between the grinding media and air at the top of the recirculation zone. This was not observed to the same extent with smooth grinding media in Figure 6.3-40 (b). This effect was due to the rough grinding media having increased velocity in the recirculation zone. These trends are further illustrated in Figure 6.3-41 and Figure 6.3-42.

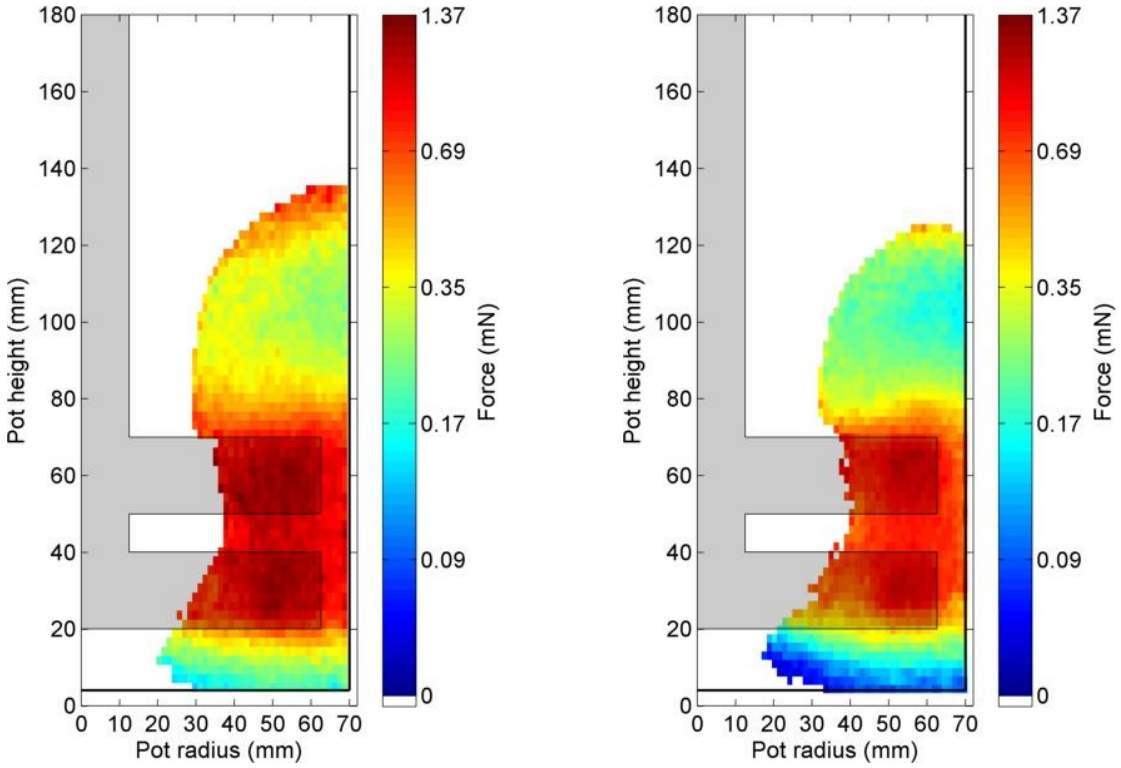

Rough grinding media
(a)

Smooth grinding media
(b)

Figure 6.3-40 Force contour plots for (a) rough and (b) smooth grinding media

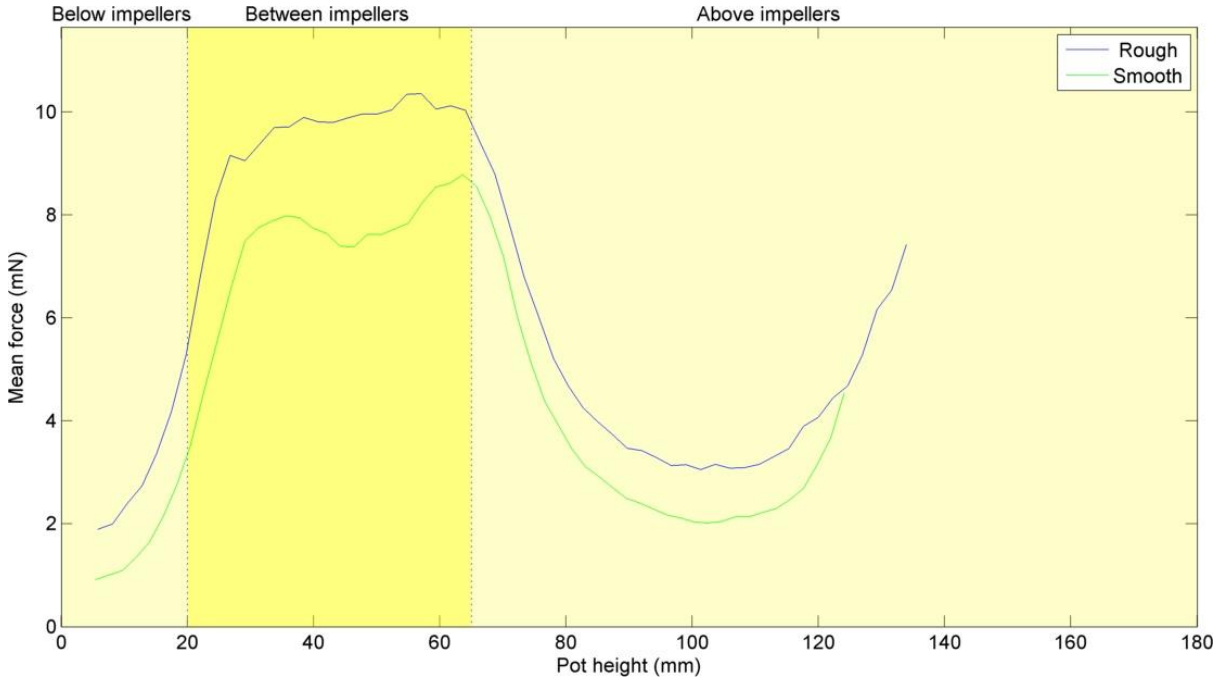

Figure 6.3-41 Mean force of grinding media as a function of height in the grinding pot

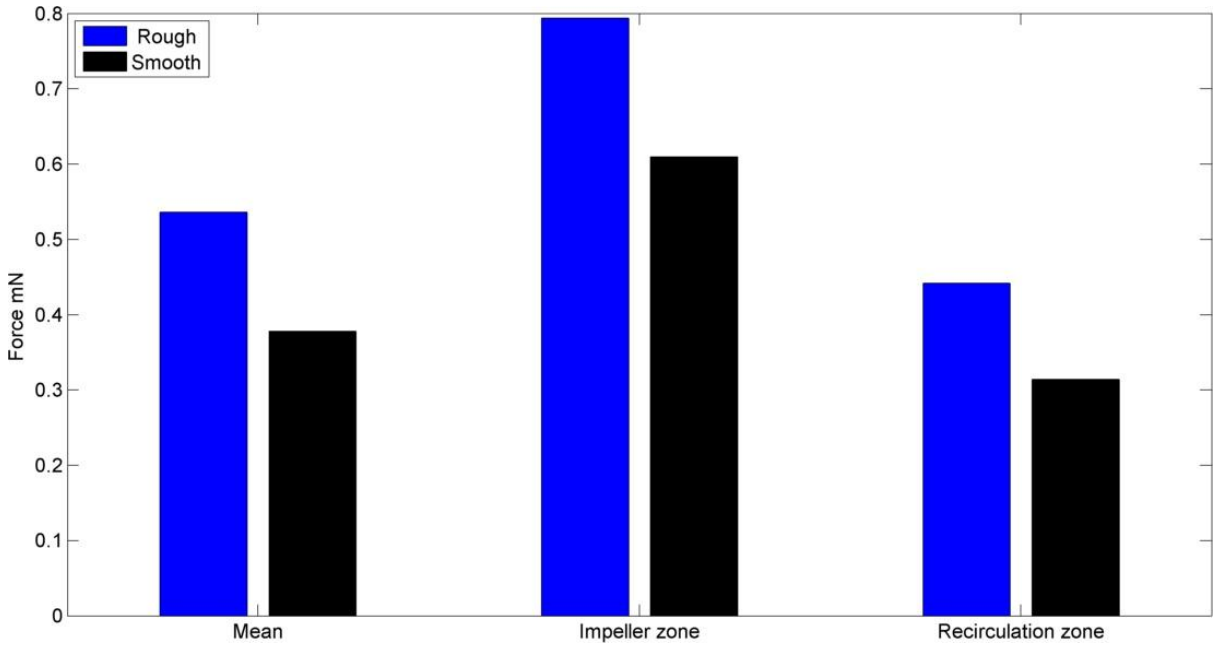

Figure 6.3-42 Bar chart comparing mean, impeller zone and recirculation zone forces

6.3.3.1.4 Stress

Figure 6.3-43 shows how the stress acting on calcium carbonate particles varied with calcium carbonate particle size and grinding media surface roughness. It can be seen that as calcium carbonate particle size decreased, the stress applied increased and that grinding media surface roughness increased the stress applied to the calcium carbonate particles. This is further illustrated in Figure 6.3-44 which shows a comparison of the average stress applied to the calcium carbonate as a function of calcium carbonate particle size. As the calcium carbonate particle size decreased the difference in stress applied by the different surface roughness grinding media increased. When 30 μm calcium carbonate was stressed the average difference in stress applied was very small (approximately 1 MPa). However at finer calcium carbonate particle sizes differences in applied stress with differing surface properties became more apparent. For example when stressing 5 μm calcium carbonate particles, rough grinding media exerted approximately 130 MPa of stress whilst smooth grinding media exerted approximately 100 MPa of stress.

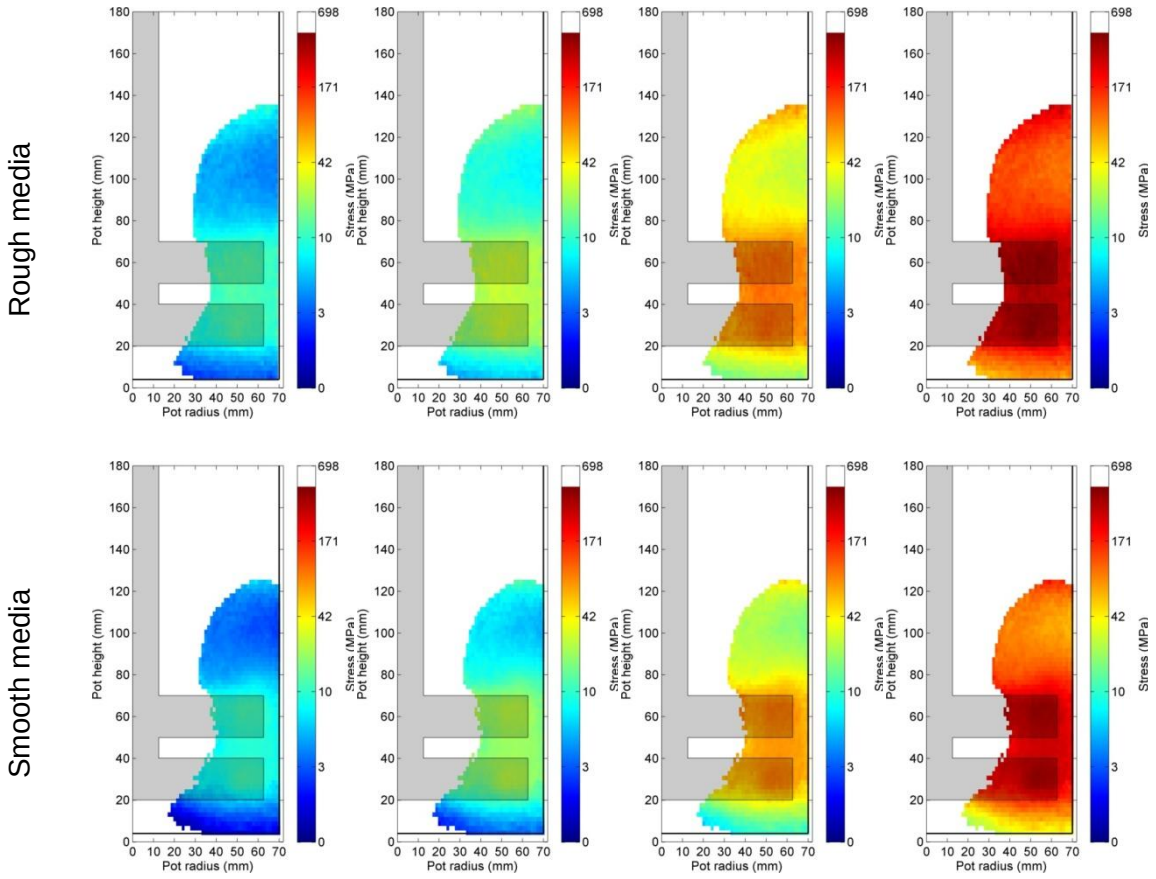

30 µm $CaCO_3$ particles (a)

20 µm $CaCO_3$ particles (b)

10 µm $CaCO_3$ particles (c)

5 µm $CaCO_3$particles (d)

Figure 6.3-43 Stress contour plots comparing rough and smooth grinding media when calcium carbonate particle size is (a) 30 (b) 20 (c) 10 and (d) 5 µm

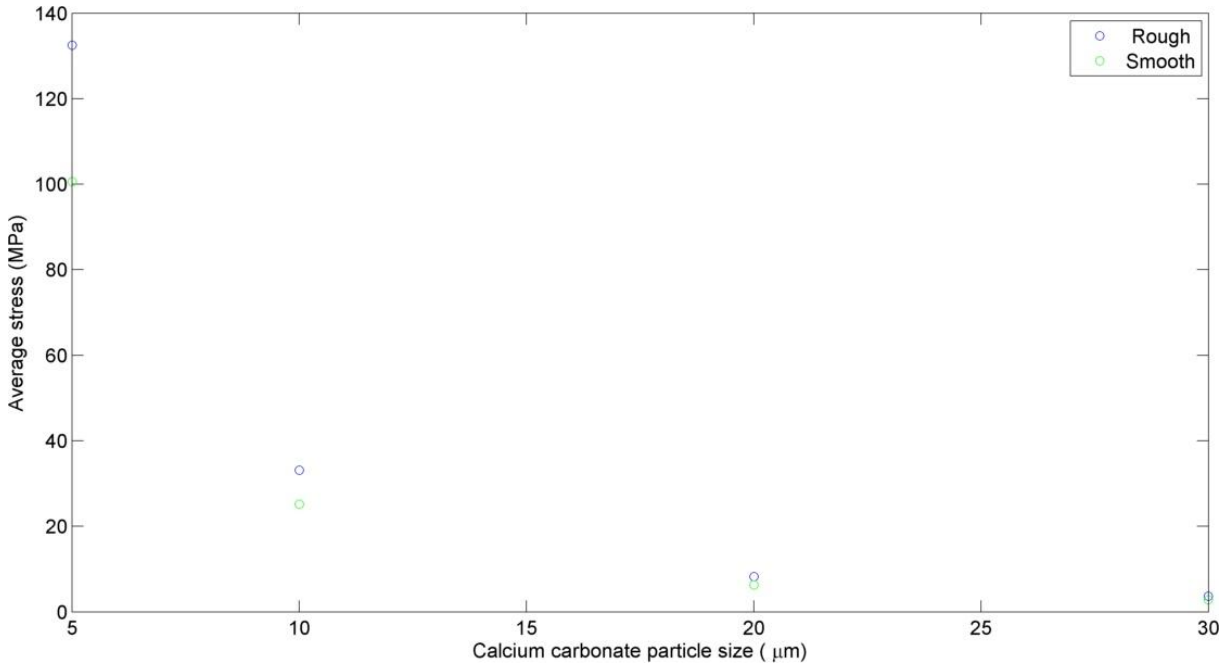

Figure 6.3-44 Mean stress within the mill as a function of calcium carbonate particle size

Figure 6.3-45 (a) (b) (c) and (d) show stress distribution profiles as a function of calcium carbonate particle size as determined using PEPT for each system and the mean strength of a calcium carbonate particle at that size as measured by a micromanipulation technique. The data show that as calcium carbonate particle size decreased the proportion of the media capable of exerting sufficient stress to cause fracture increased, and that the proportion of the media capable of fracturing the calcium carbonate particles increased when using rough media. This is further illustrated in Figure 6.3-46 which shows the percentage of grinding media capable of fracturing calcium carbonate particles as a function of calcium carbonate particle size. It can be seen that rough media had a higher percentage chance of causing fracture, but due to the large size of the media, both rough and smooth media had a high probability of fracture at a collision.

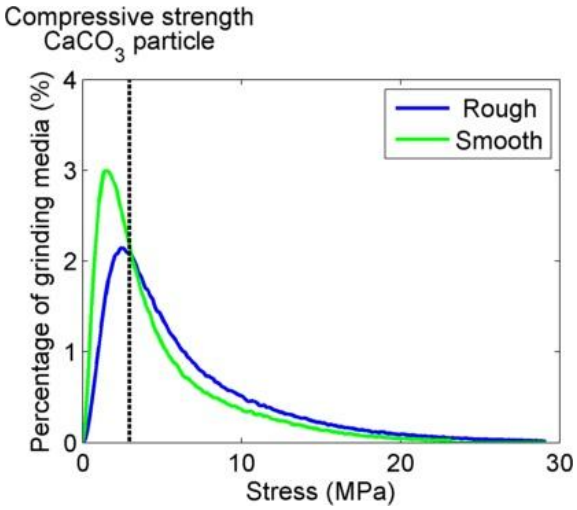

30 μm calcium carbonate particles

(a)

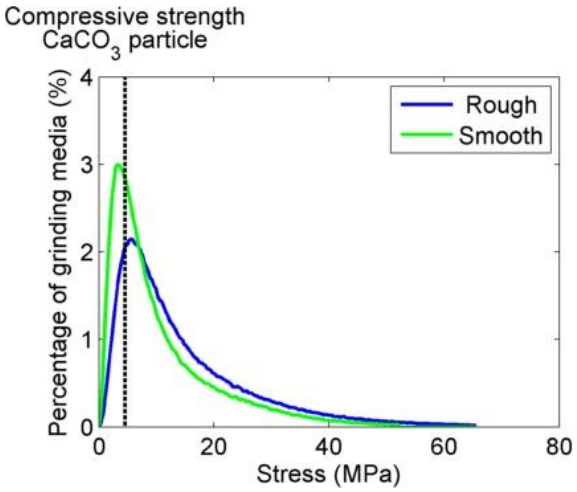

20 μm calcium carbonate particles

(b)

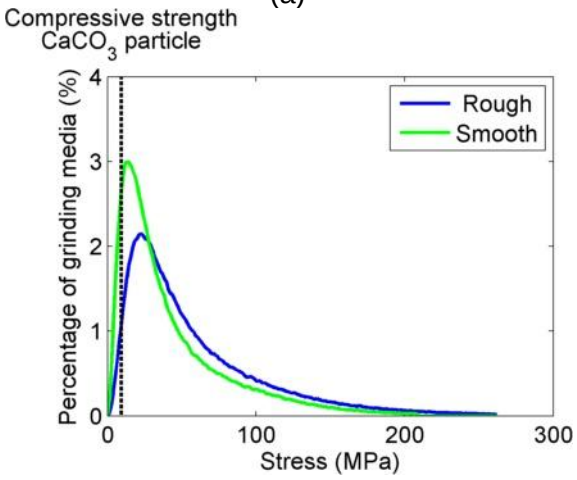

10 μm calcium carbonate particles

(c)

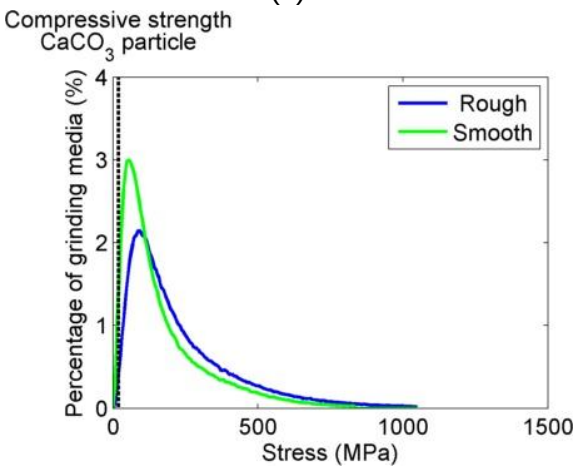

5 μm calcium carbonate particles

(d)

Figure 6.3-45 Distribution of stress exerted by grinding media when calcium carbonate particle size is (a) 30 (b) 20 (c) 10 and (d) 5 μm

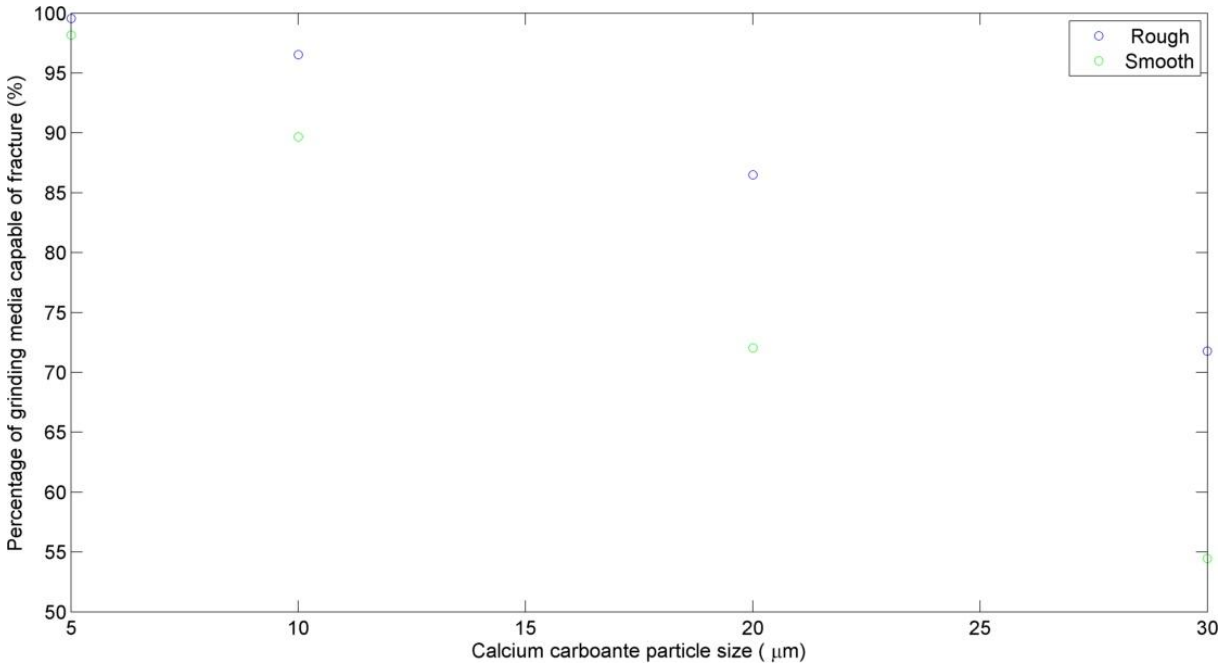

Figure 6.3-46 Percentage of grinding media suitable to fracture calcium carbonate particles as a function of calcium carbonate feed size (based on average strength of calcium carbonate feed particles at a given feed size)

Figure 6.3-47(a) (b) (c) and (d) show the regions within the mill with sufficient stress to overcome the average compressive strength of the calcium carbonate particles. These data show that the regions within the mill where breakage could occur increased when using rough grinding media rather than smooth. It can also be seen that when using rough media particle breakage was possible in almost all regions of the mill. These data are summarised in Figure 6.3-14.

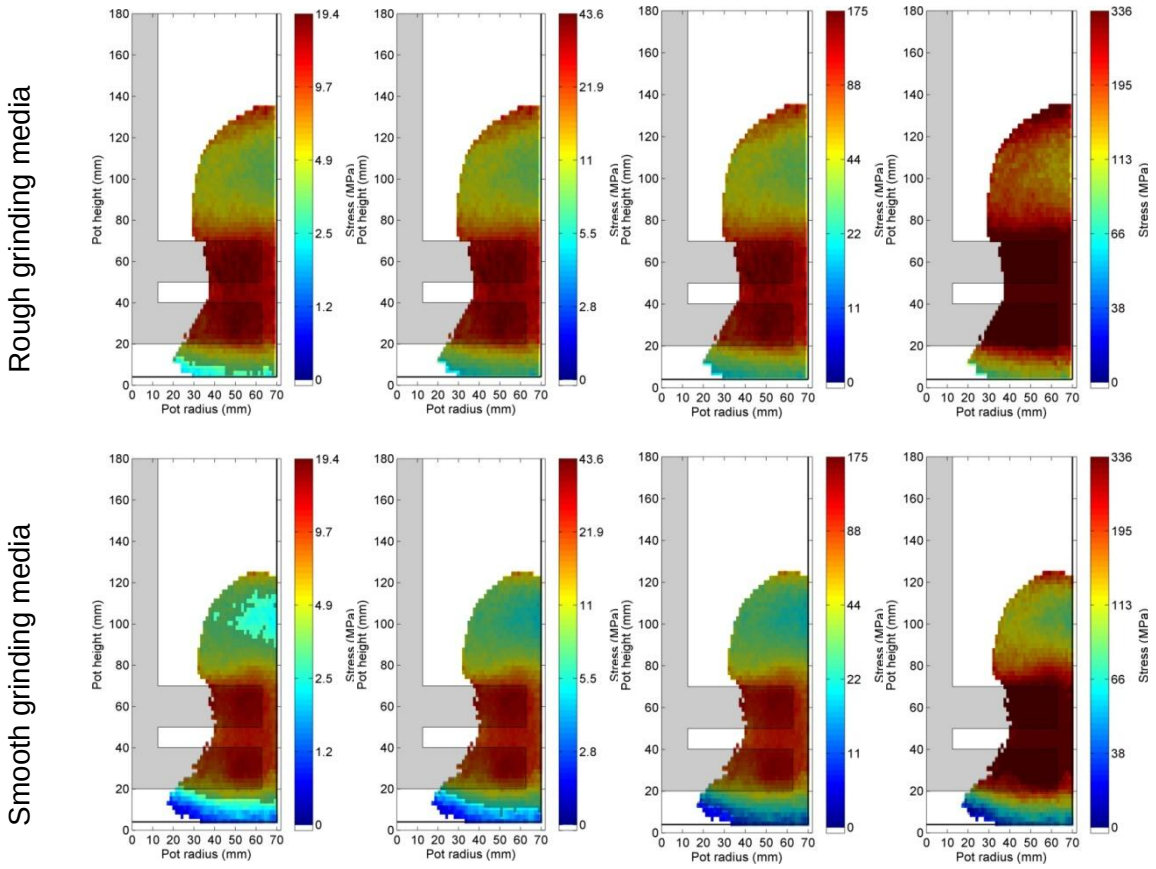

30 μm calcium carbonate particles

20 μm calcium carbonate particles

10 μm calcium carbonate particles

5 μm calcium carbonate particles

(a) (b) (c) (d)

Figure 6.3-47 Regions of the mill capable of fracturing calcium carbonate feed particles comparing rough and smooth grinding media when calcium carbonate particle size is (a) 30 (b) 20 (c) 10 and (d) 5 μm.

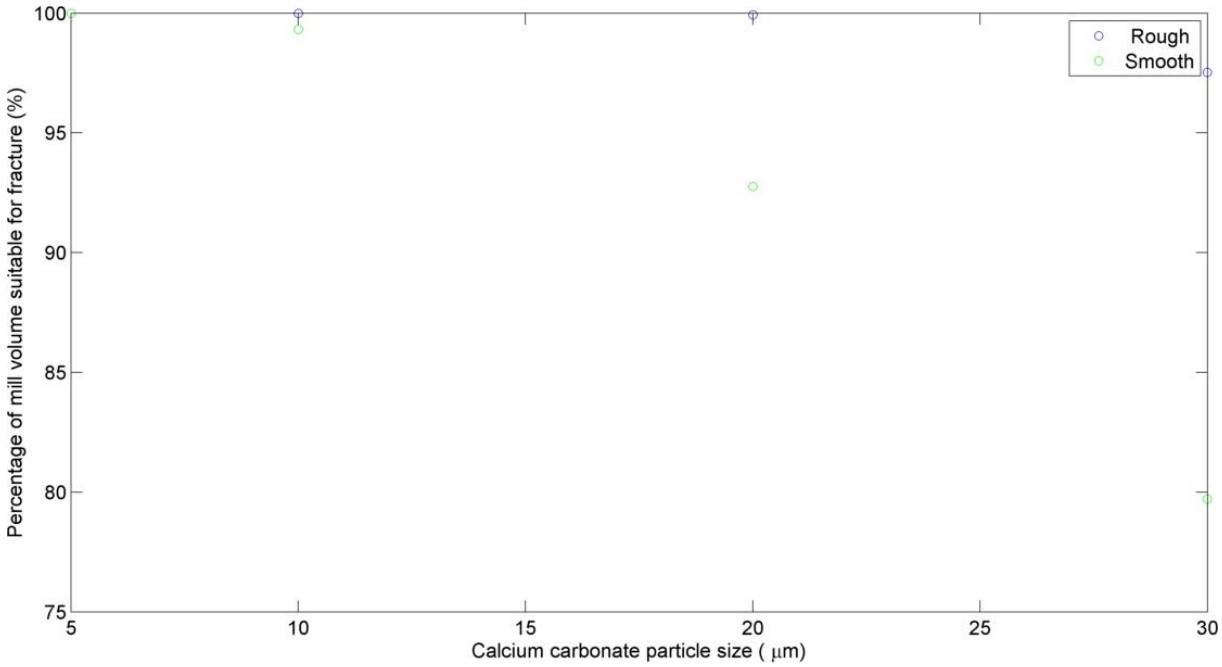

Figure 6.3-48 Percentage of the mill capable of fracturing calcium carbonate particles as a function of calcium carbonate feed size

6.3.3.1.5 Collisions

Figure 6.3-49 (a) and (b) show that the collision rate and the total number of collisions within the system and Figure 6.3-50 shows the total number of collisions as a function of pot height. No strong trends were observed. This was to be expected since the grinding media are all approximately the same size and the occupancy and velocity data showed little variation with change in surface roughness.

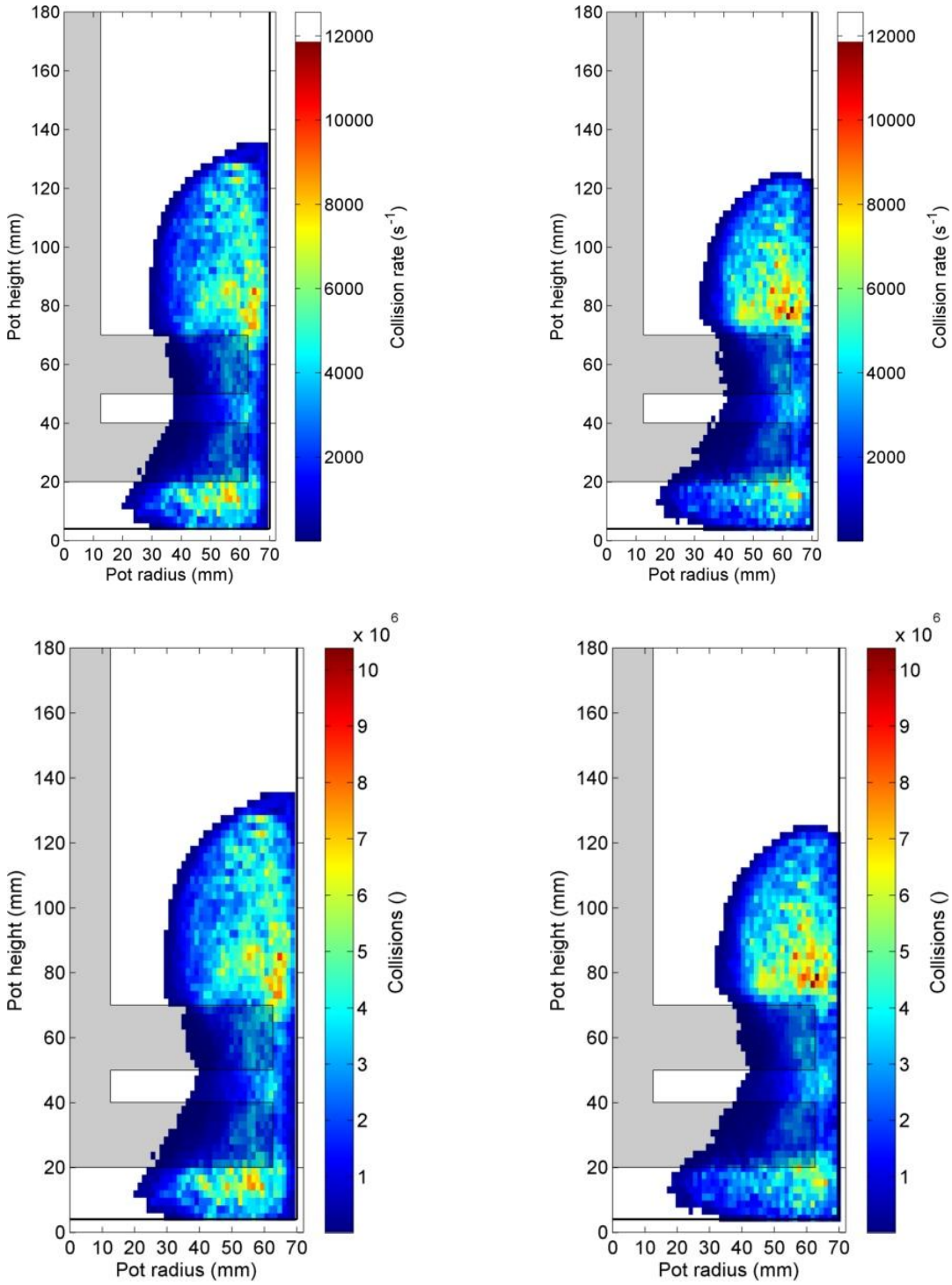

Rough grinding media (a)

Smooth grinding media (b)

Figure 6.3-49 Collision rate and the number of collisions throughout the course of a grind contour plots for (a) rough and (b) smooth grinding media

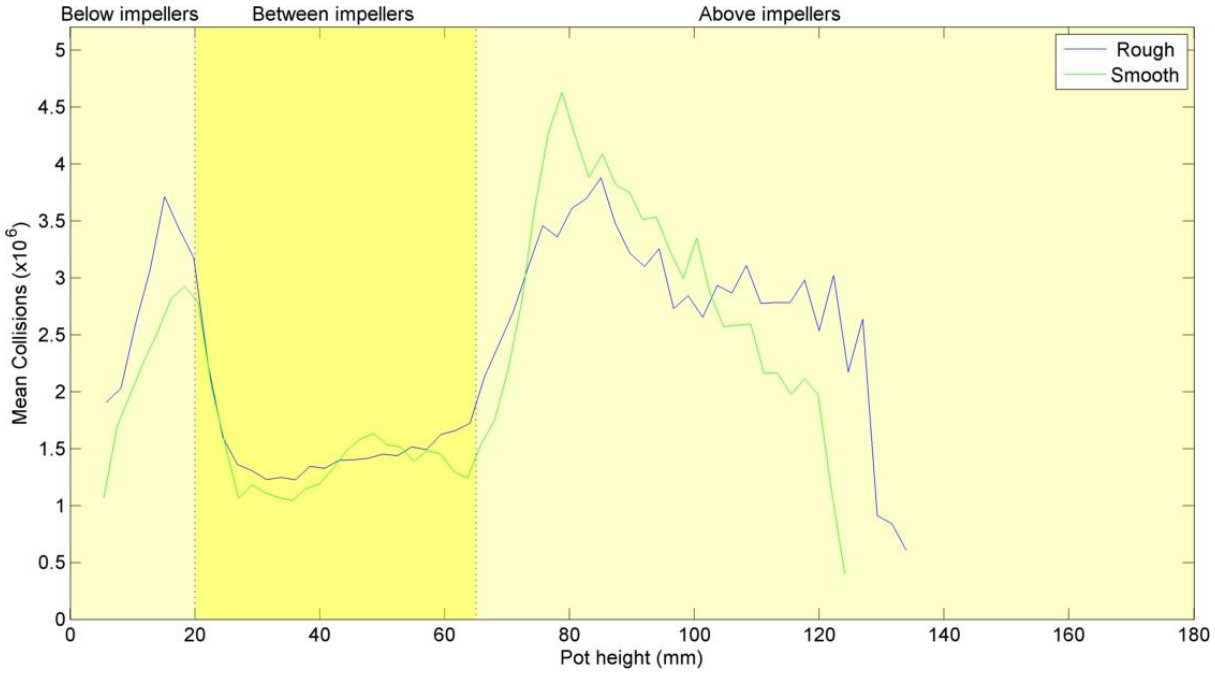

Figure 6.3-50 Total collisions between grinding media as a function of height in the mill

6.3.3.2 Comparison of PEPT data with laboratory grinding data

The laboratory grinding data shown in Section 4.5 suggested that surface roughness had no effect on the grinding energy required to achieve a target particle size distribution, but did result in the target distribution being achieved in less time.

The PEPT data showed similar occupancy and number of collisions but greater force and stresses exerted on calcium carbonate particles when grinding with rough media. This increased force with rough media along with a similar collision rate might have been expected to give a lower energy to achieve a target particle size distribution when using rough media. A possible explanation for the similar d90 achieved when grinding could be due to both media types having sufficient stress to achieve a very high percentage of successful collisions. Reasons for the reduced grind time when using rough grinding media remain unclear.

6.3.4 Impeller speed

Lab grinding data with differing impeller speeds are given in Section 4.6. The data indicated that the optimum impeller speed in terms of energy input to achieve a target d90 was 700 rpm (impeller tip speed 4.2 ms^{-1}). It was suggested that at impeller speeds lower than 700 rpm the stress energy supplied by the impeller to the grinding media was less than optimum to achieve calcium carbonate particle breakage at the size range required for this application. Whilst at impeller speeds greater than 700 rpm the stress energy supplied was in excess of the optimum required for particle breakage and therefore energy was wasted.

6.3.4.1 PEPT data

6.3.4.1.1 Occupancy

Figure 6.3-51 (a) (b) (c) and (d) show occupancy contour plots for grinds performed using 1200, 1000, 800 and 600 rpm under the conditions described in Section 4.6. It can be seen that the maximum bed height was lower at lower rpm and the vortex was smaller. Furthermore these data plus the data in Figure 6.3-52 suggest that a greater percentage of grinding media was located between the impellers at lower rpm. This effect could have occurred because at lower rpm the grinding media leaving the impeller zone had less momentum and therefore were not elevated as high in the mill.

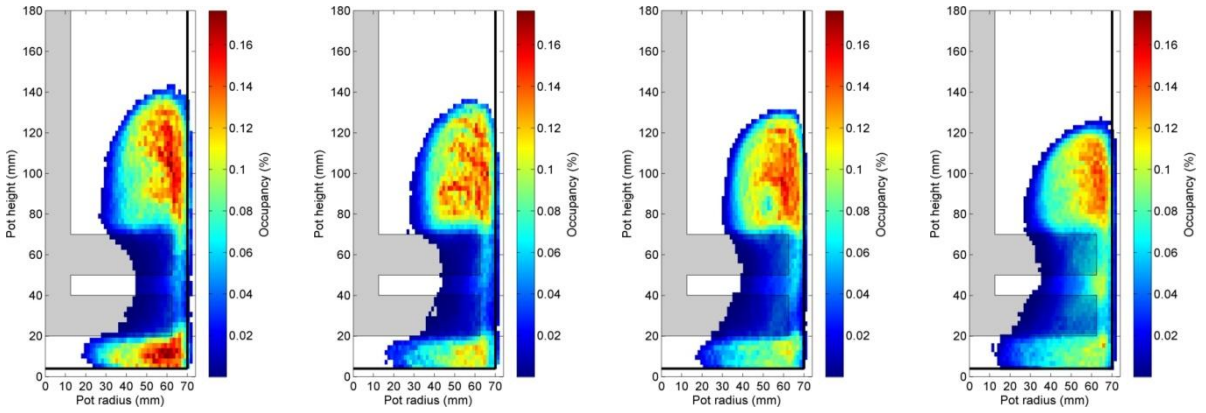

1200 rpm (a) | 1000 rpm (b) | 800 rpm (c) | 600 rpm (d)

Figure 6.3-51 Occupancy contour plots for (a) 1200 (b) 1000 (c) 800 and (d) 600 rpm stirrer speed

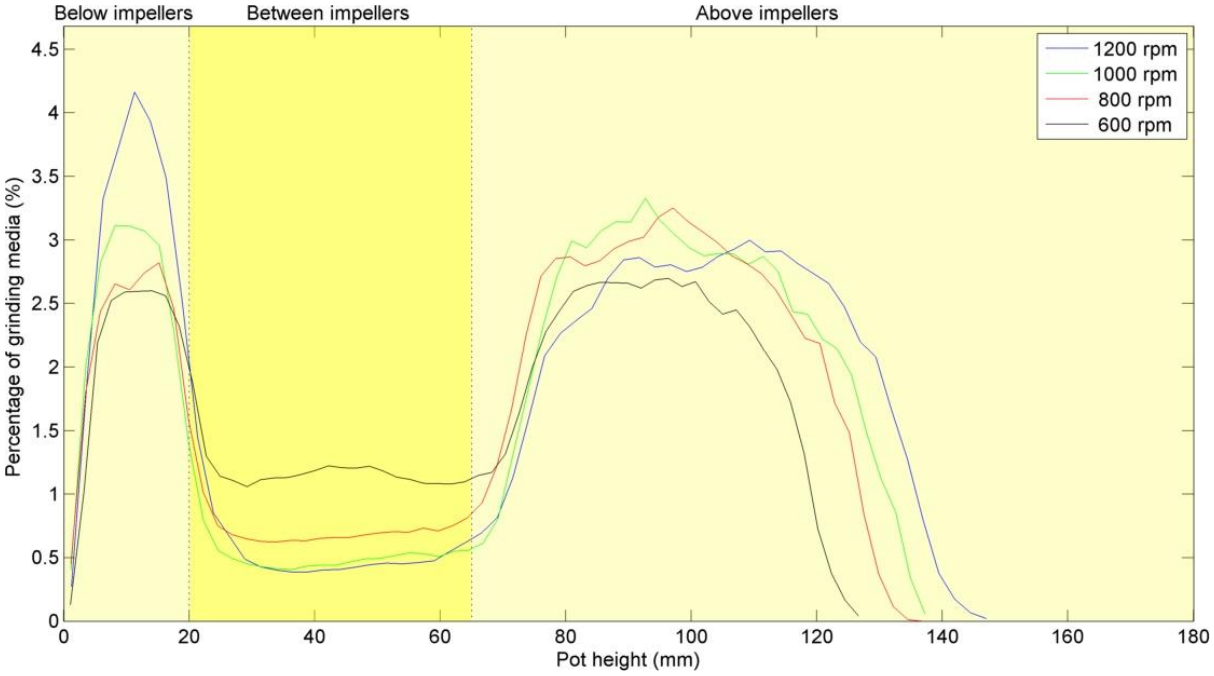

Figure 6.3-52 Percentage of grinding media as a function of height in the grinding pot

6.3.4.1.2 Velocity

Figure 6.3-53 (a) (b) (c) and (d) show velocity contour plots for grinds performed at 1200, 1000, 800 and 600 rpm. It can be seen that higher impeller speeds resulted in higher velocities in the impeller zone, but the velocities elsewhere in the mill remained relatively unchanged regardless of impeller speed. The velocity results are summarised in Figure 6.3-54 which showed the mean velocity in the impeller zone increased with increased rpm.

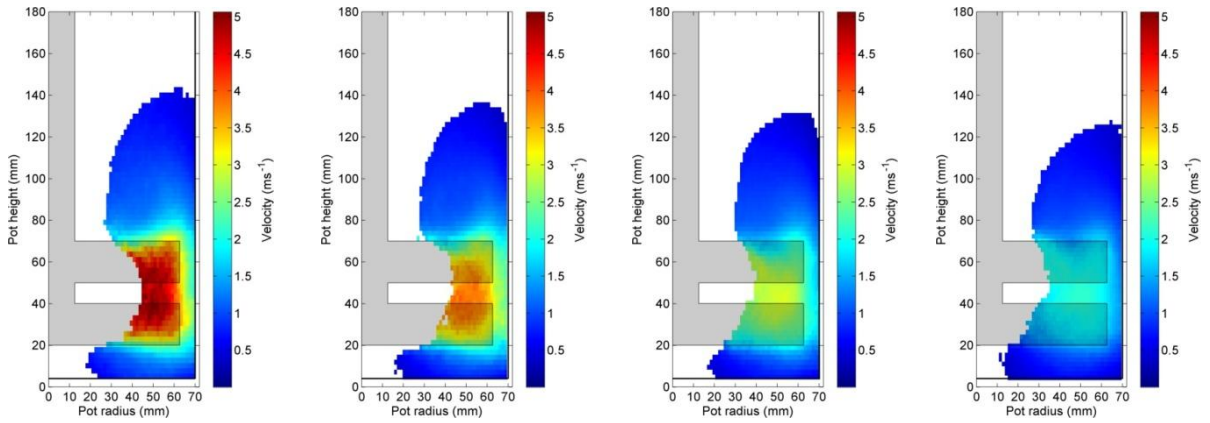

1200 rpm (a) | 1000 rpm (b) | 800 rpm (c) | 800 rpm (d)

Figure 6.3-53 Velocity contour plots for (a) 1200 (b) 1000 (c) 800 and (d) 600 rpm impeller speeds

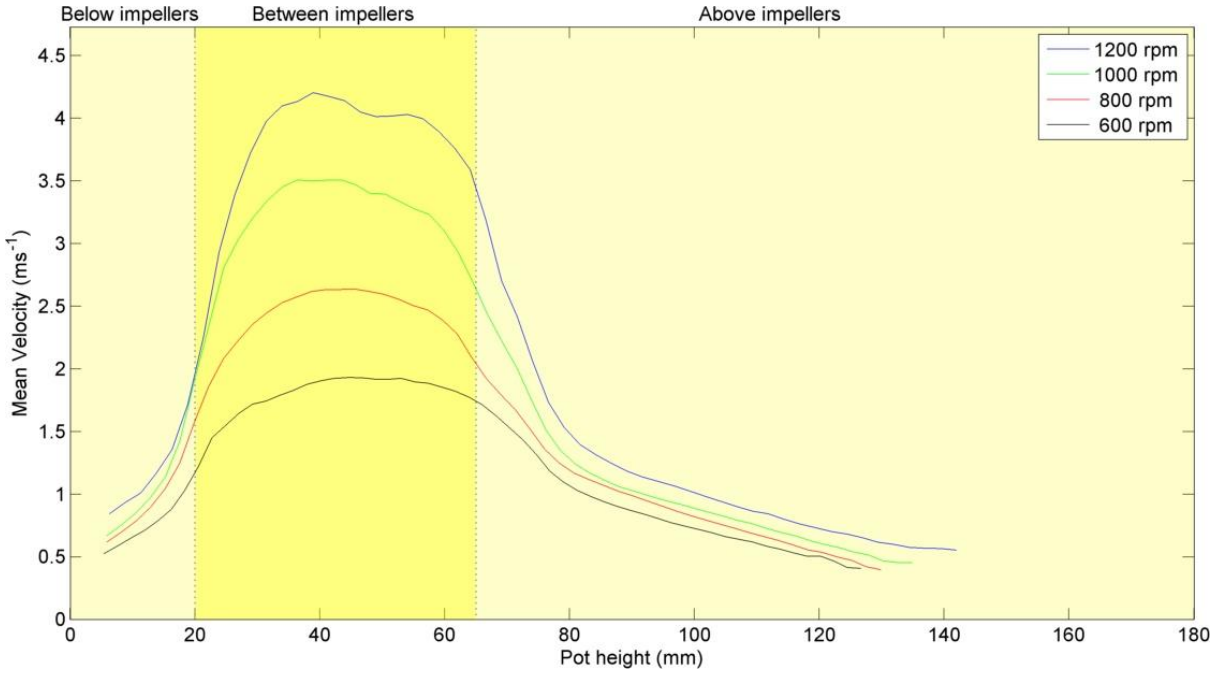

Figure 6.3-54 Mean velocity of grinding media as a function of height in the grinding pot

Figure 6.3-55 (a) (b) (c) and (d) show relative velocity contour plots (media velocity divided by tip speed) for grinds performed at 1200, 1000, 800 and 600 rpm. These data indicate that although high stirrer speeds resulted in increased relative velocity between the impellers the relative velocity of the grinding media elsewhere in the mill decreased. Figure 6.3-56 shows how the impeller tip speed and the average speed of the grinding media varied with stirrer speed. It can be seen that the difference between impeller speed and media speed increased as the impeller speed increased. Therefore, because the velocity of the grinding media relative to the impeller gives a measure of the efficiency of the impeller in transferring momentum to the media particles (Tamblyn, 2009) less energy supplied by the impeller was wasted fluidising the mill contents at lower stirrer speeds.

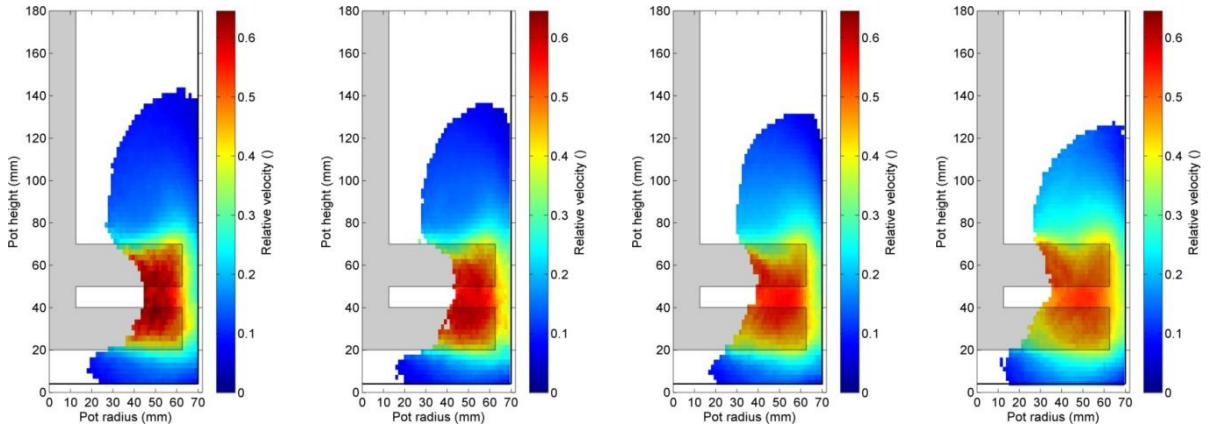

1200 rpm (a) | 1000 rpm (b) | 800 rpm (c) | 800 rpm (d)

Figure 6.3-55 Velocity and relative velocity contour plots for (a) 1200 (b) 1000 (c) 800 and (d) 600 rpm impeller speeds

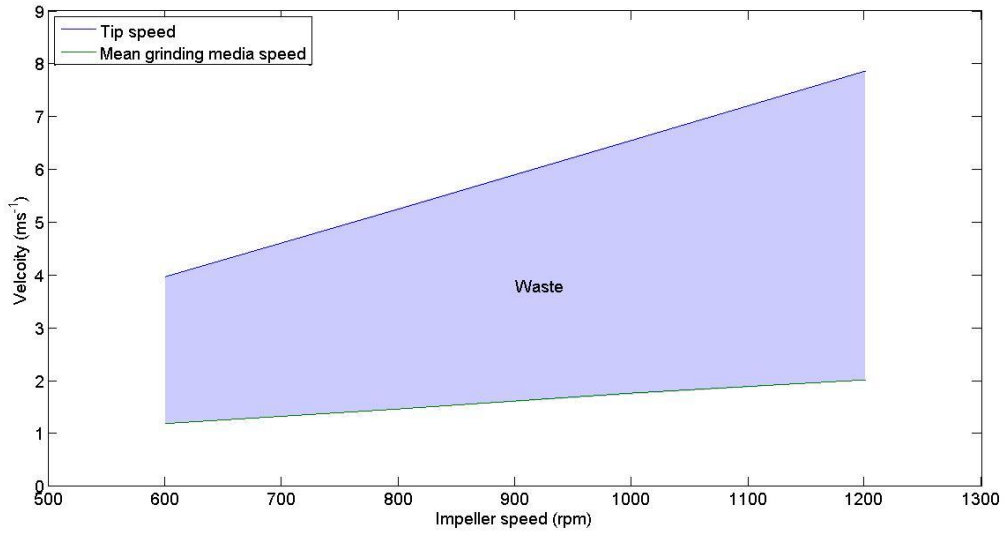

Figure 6.3-56 Tip speed and average media speed as a function of impeller speeds

Figure 6.3-57 (a) (b) (c) and (d) show mean relative velocity contour plots for grinds performed at 1200, 1000, 800 and 600 rpm. It can be seen that increased stirrer speed resulted in greater mean relative velocity in the impeller regions. This suggests that the media within this region underwent more collisions as larger deviations in velocity occurred. This is further illustrated in Figure 6.3-58.

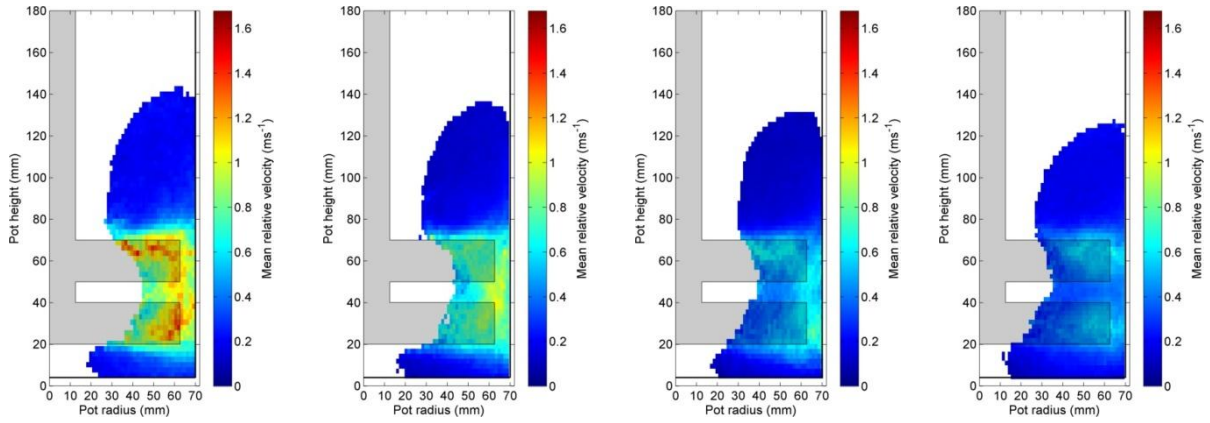

1200 rpm (a) | 1000 rpm (b) | 800 rpm (c) | 600 rpm (d)

Figure 6.3-57 Mean relative velocity contour plots for (a) 1200 (b) 1000 (c) 800 and (d) 600 rpm impeller speeds

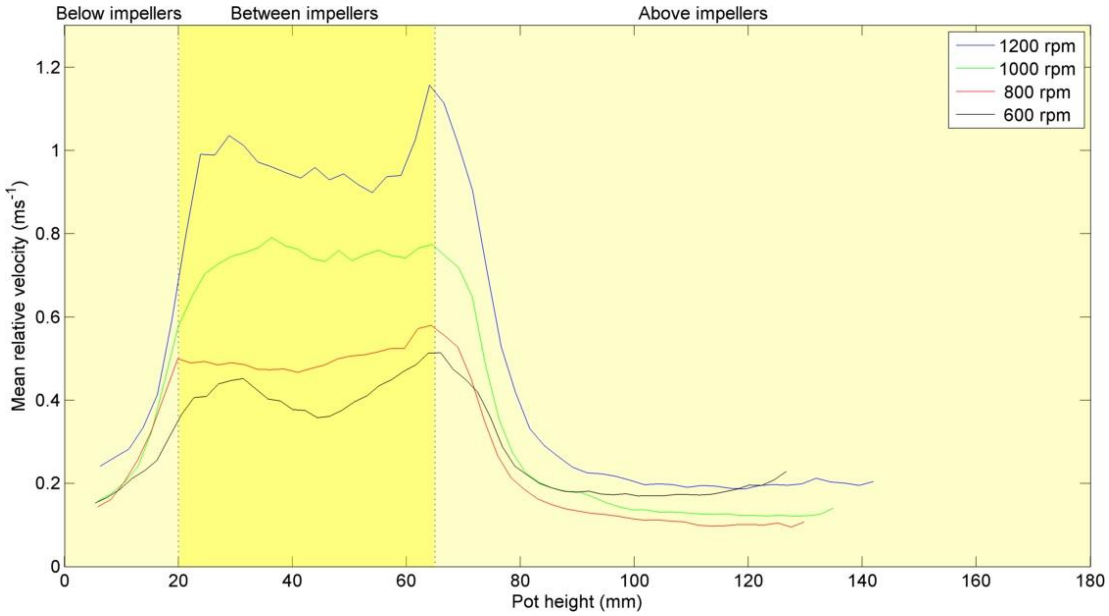

Figure 6.3-58 Mean relative velocity of grinding media as a function of height in the grinding pot

6.3.4.1.3 Force

Figure 6.3-59 (a) (b) (c) and (d) show the force contour plots for grinds performed at 1200, 1000, 800 and 600 rpm respectively. It can be seen that the force experienced by the grinding media increased with stirrer speed rpm. This is further illustrated in Figure 6.3-60 where the maximum force experienced as a function of height was approximately 3.5 mN at 1200 rpm impeller speed whereas the maximum force applied at 600 rpm was 0.5 mN. Figure 6.3-61 further emphasises these differences in force with changing stirrer speed.

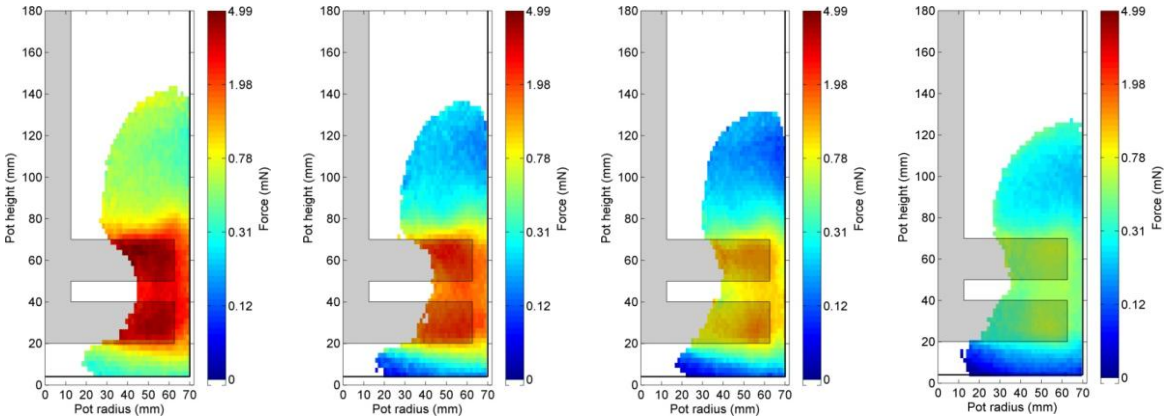

1200 rpm (a) | 1000 rpm (b) | 800 rpm (c) | 600 rpm (d)

Figure 6.3-59 Force contour plots for (a) 1200 (b) 1000 (c) 800 and (d) 600 rpm impeller speed

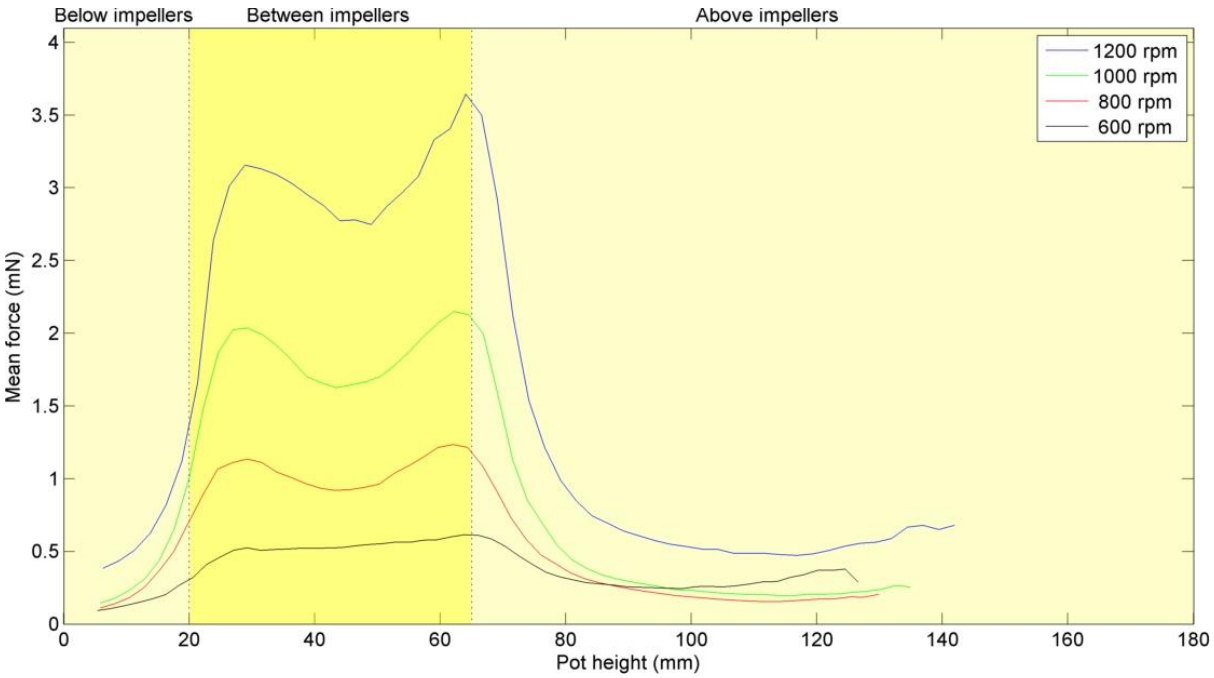

Figure 6.3-60 Mean force of grinding media as a function of height in the grinding pot

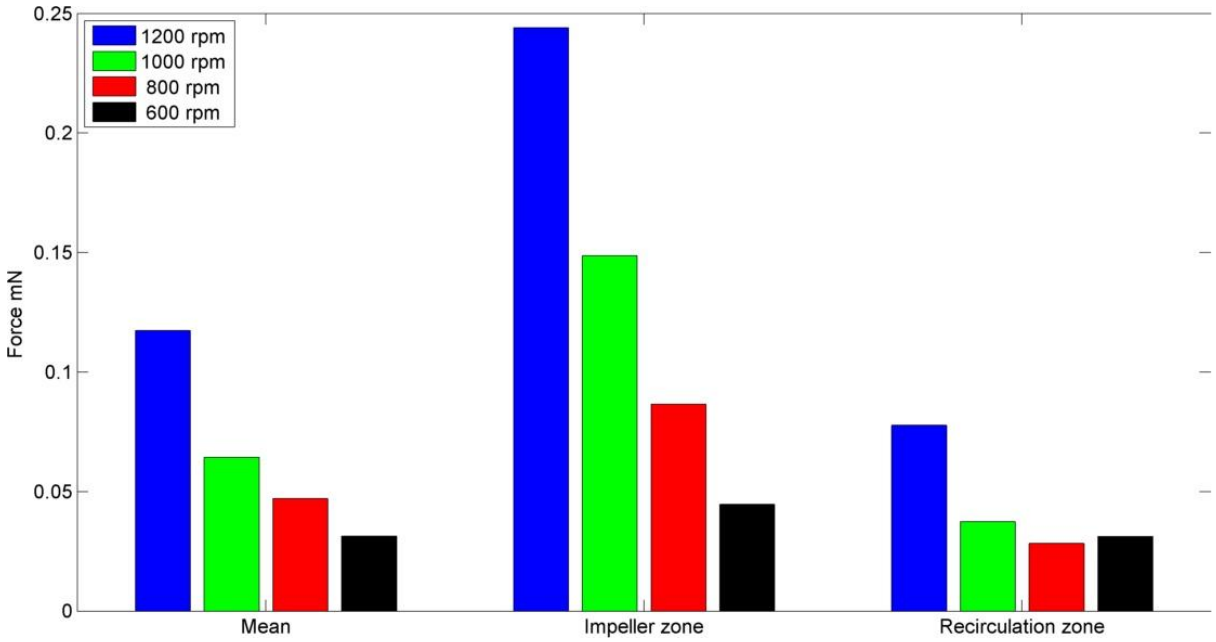

Figure 6.3-61 Bar chart comparing mean, impeller zone and recirculation zone forces

6.3.4.1.4 Stress

Figure 6.3-62 (a) (b) (c) and (d) show how the stress acting on calcium carbonate particles varied with calcium carbonate size and impeller speed. It can be seen that for each case as the calcium carbonate particle size decreased the applied stress increased, and that the stress applied for a given stirrer speed increased as stirrer speed increased. This is further illustrated in Figure 6.3-63 which shows a comparison of the average stress applied to the calcium carbonate as a function of calcium carbonate particle size. As the calcium carbonate particle size decreased the difference in stress applied by increasing the impeller speed increased. When 30 μm calcium carbonate particles were stressed the difference in stress applied was small, approximately 0.1 to 1 MPa at all four stirrer speeds. However at finer calcium carbonate particle sizes, differences in applied stress at differing stirrer speeds were apparent. For example, when stressing 5 μm calcium carbonate particles, a stirrer speed of 1200 rpm exerted 27 MPa of stress whilst a stirrer speed of 600 rpm only exerted approximately 8 MPa of stress.

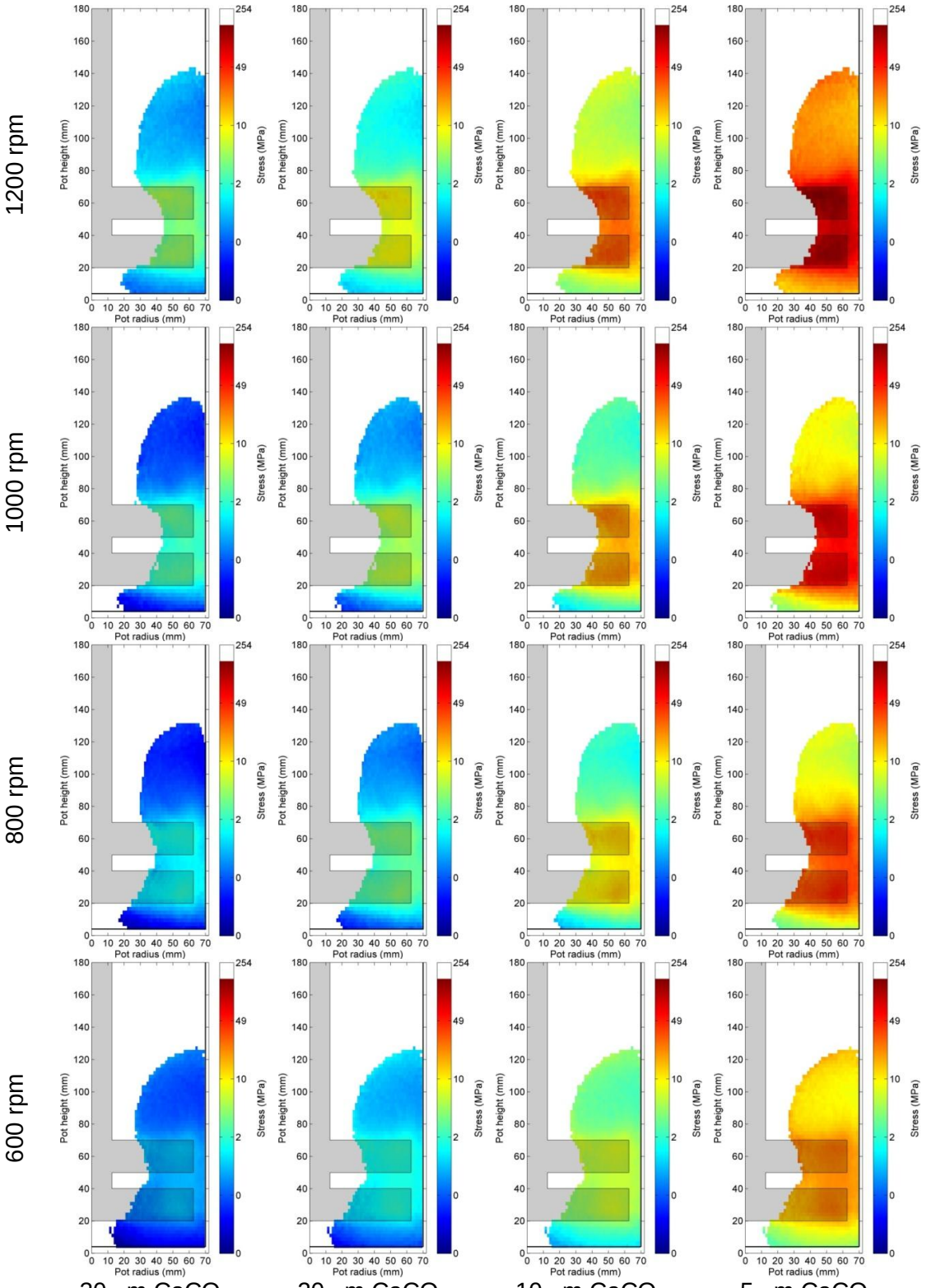

Figure 6.3-62 Stress contour plots comparing 1200, 1000, 800 and 600 rpm impeller speeds when calcium carbonate particle size is (a) 30 (b) 20 (c) 10 and (d) 5 µm

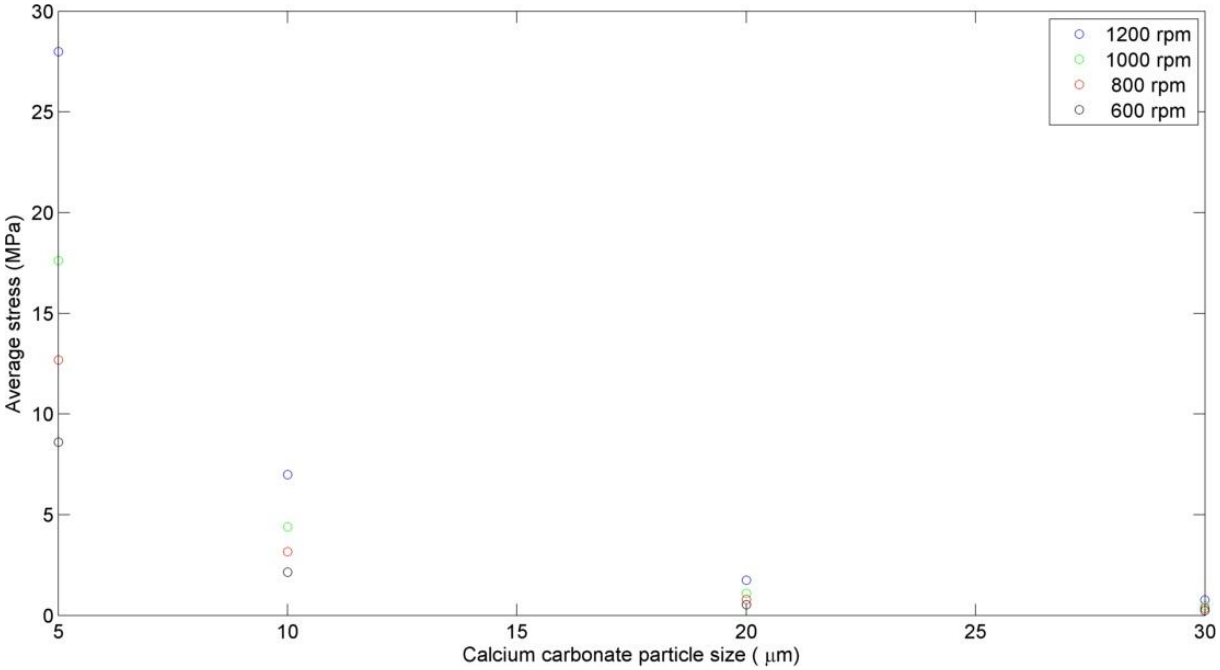

Figure 6.3-63 Mean stress within the mill as a function of calcium carbonate particle size

Figure 6.3-64 (a) (b) (c) and (d) show stress distribution profiles as a function of calcium carbonate particle size as determined using PEPT for each system and the mean strength of a calcium carbonate particle at that size as measured by a micromanipulation technique. The data show that as calcium carbonate particle size decreased the proportion of the media capable of exerting sufficient stress to cause fracture increased, and that the proportion of the media capable of fracturing the calcium carbonate particles increased with stirrer speed. This is further illustrated in Figure 6.3-65 which shows the percentage of grinding media capable of fracturing calcium carbonate particles as a function of calcium carbonate particle size. Again increased stirrer speed gave an increased percentage of calcium carbonate fracture.

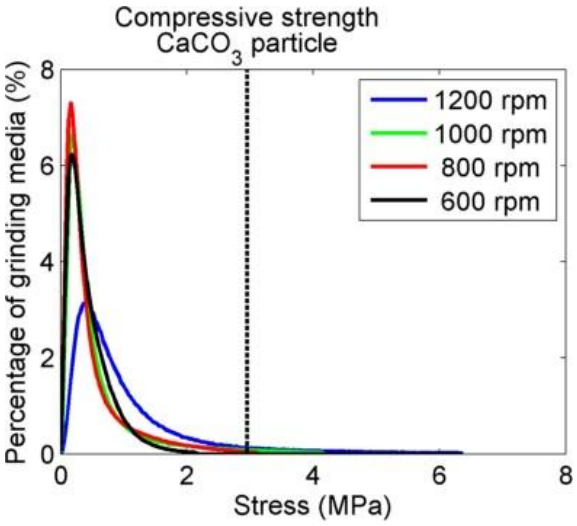

30 μm calcium carbonate particles

(a)

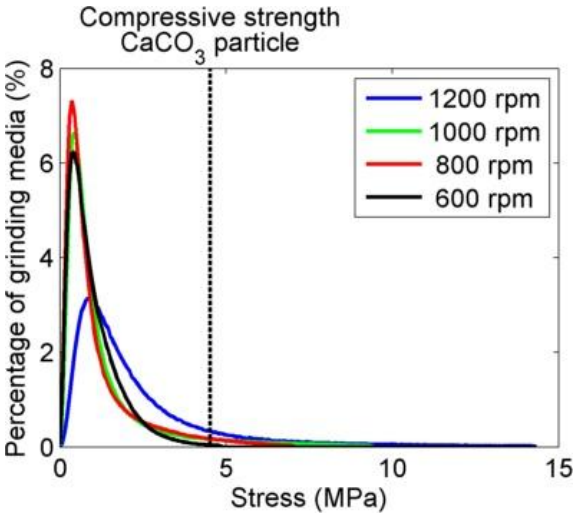

20 μm calcium carbonate particles

(b)

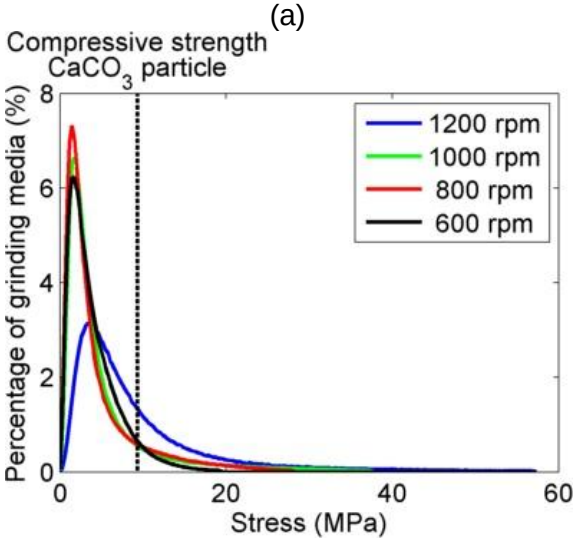

10 μm calcium carbonate particles

(c)

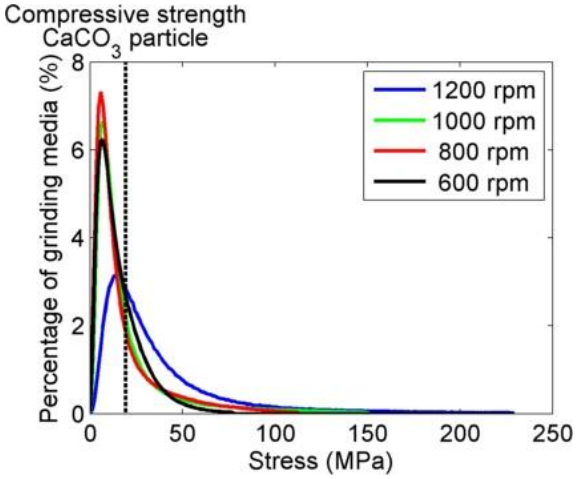

5 μm calcium carbonate particles

(d)

Figure 6.3-64 Distribution of stress exerted by grinding media when calcium carbonate particle size is (a) 30 (b) 20 (c) 10 and (d) 5 μm

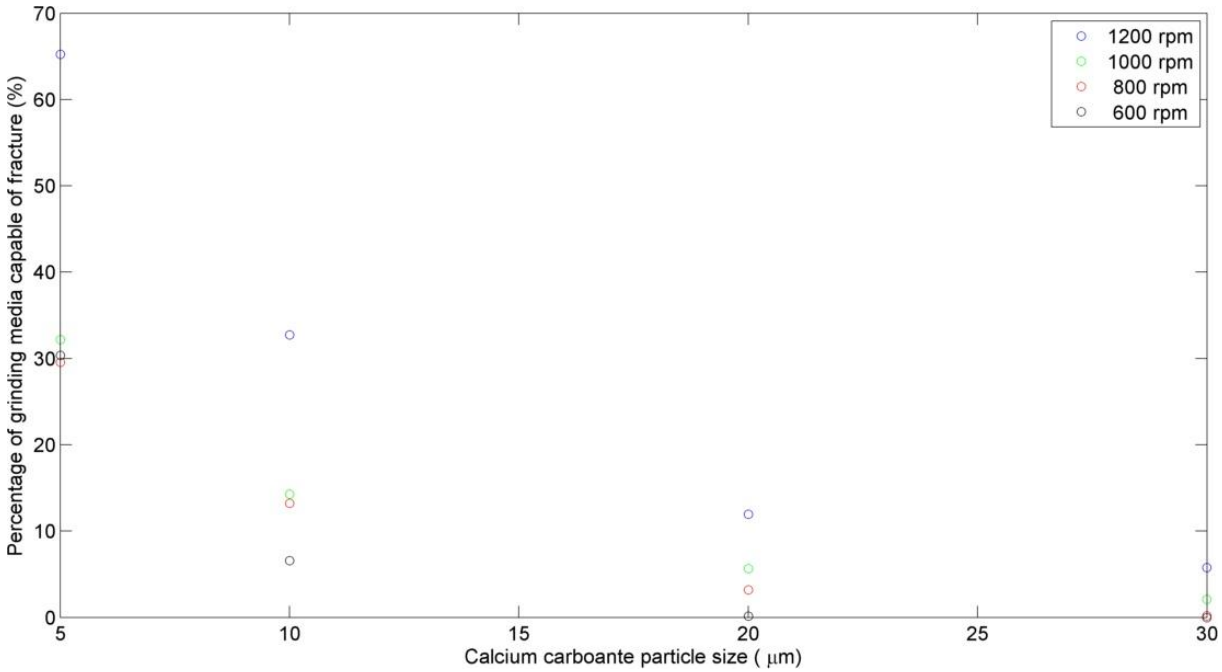

Figure 6.3-65 Percentage of grinding media suitable to fracture calcium carbonate particles as a function of calcium carbonate feed size (based on average strength of calcium carbonate feed particles at a given feed size)

Figure 6.3-66 (a) (b) (c) and (d) show the regions within the mill with sufficient stress to overcome the average compressive strength of the calcium carbonate particles. These data show that the regions within the mill where breakage occurred increased with increased stirrer rpm and decreased calcium carbonate particle size. These data are summarised in Figure 6.3-67.

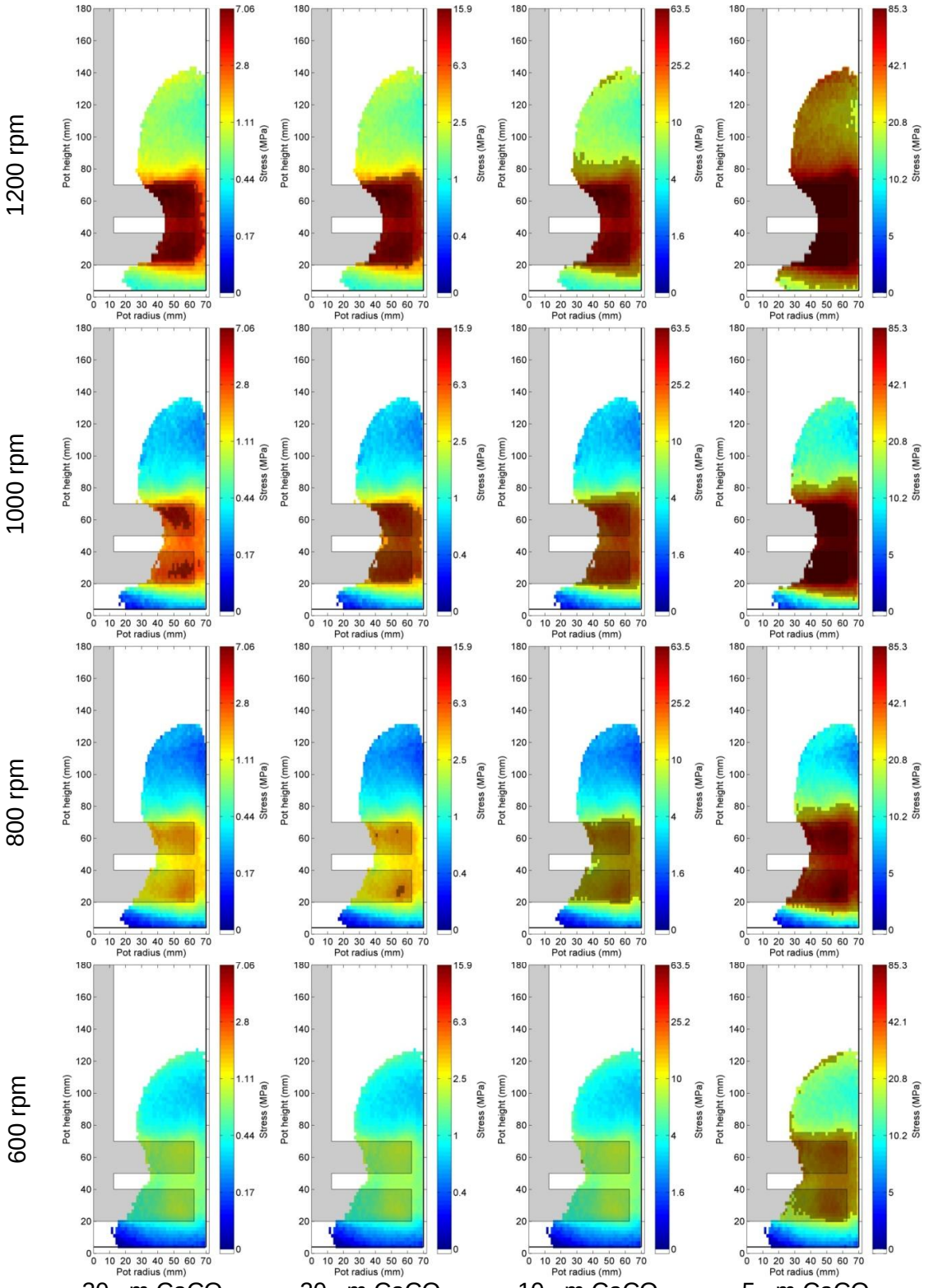

Figure 6.3-66 Regions of the mill capable of fracturing calcium carbonate feed particles comparing 1200, 1000, 800 and 600 rpm impeller speeds when calcium carbonate particle size is (a) 30 (b) 20 (c) 10 and (d) 5 µm

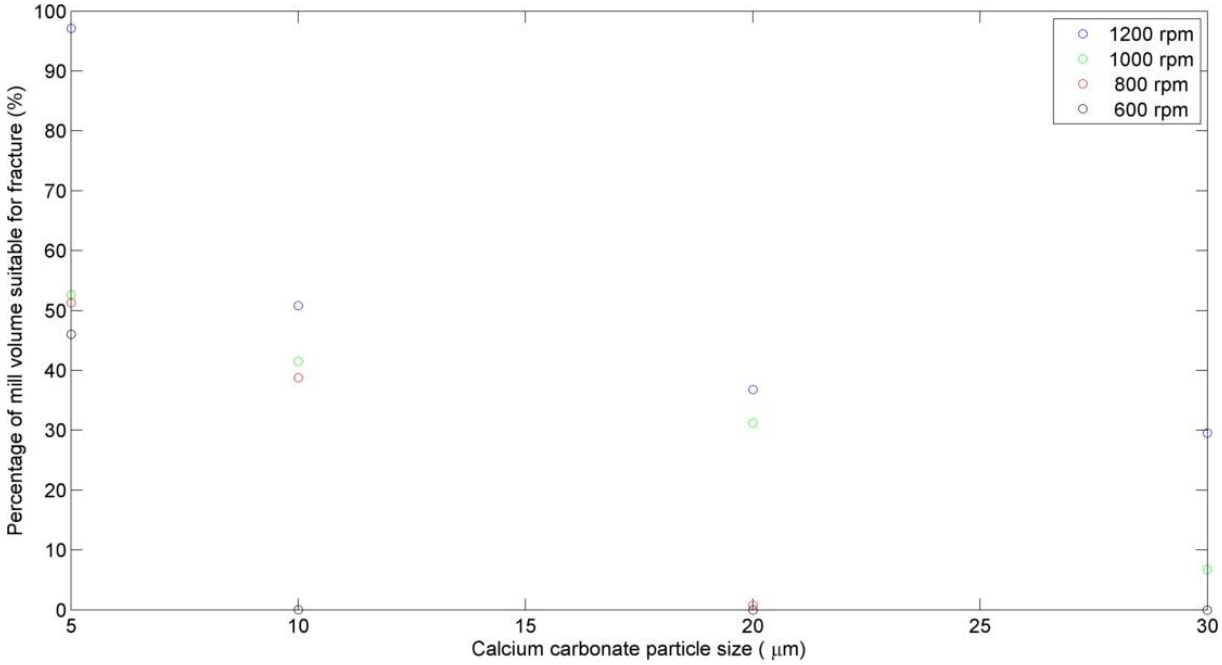

Figure 6.3-67 Percentage of the mill capable of fracturing calcium carbonate particles as a function of calcium carbonate feed size

6.3.4.1.5 Collisions

Figure 6.3-68 (a) (b) (c) and (d) show the collision rate and total number of collisions within the system. It can be seen that the collision rate increased with stirrer speed. It can also be seen that the collision rate below the impellers when the stirrer speed was 1200 rpm was higher than anywhere else in the mill. The increase in the collision rate was a result of the increased mean relative velocity at higher stirrer speeds and high occupancy of media below the impellers which occurred at 1200 rpm. It can also be seen that the number of collisions between media particles increased as stirrer speed decreased. This is because at lower rpm the grind took longer to run. These data are further summarised in Figure 6.3-69 and Figure 6.3-70.

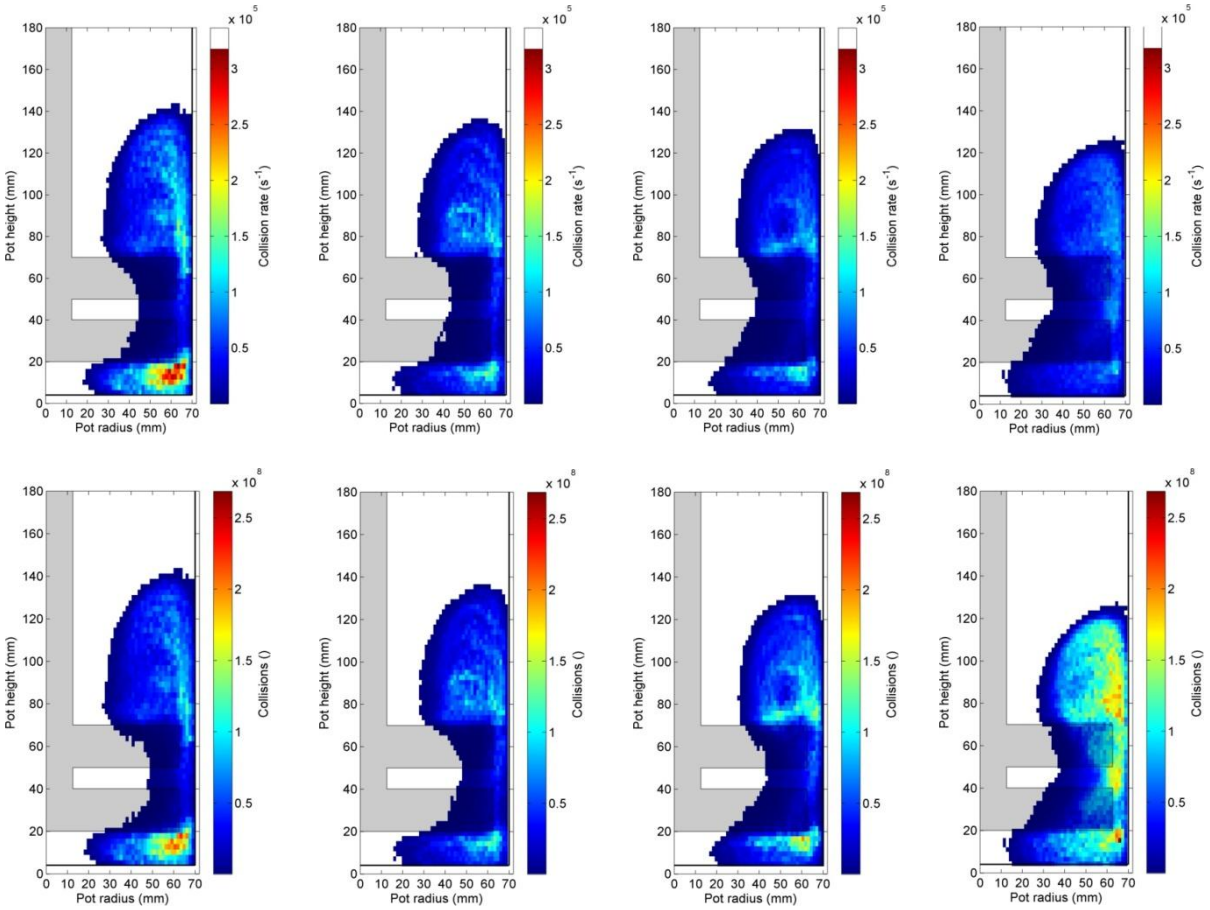

1200 rpm 1000 rpm 800 rpm 600 rpm

(a) (b) (c) (d)

Figure 6.3-68 Collision rate and the number of collisions throughout the course of a grind contour plots for (a) 1200 (b) 1000 (c) 800 and (d) 600 rpm stirrer speed

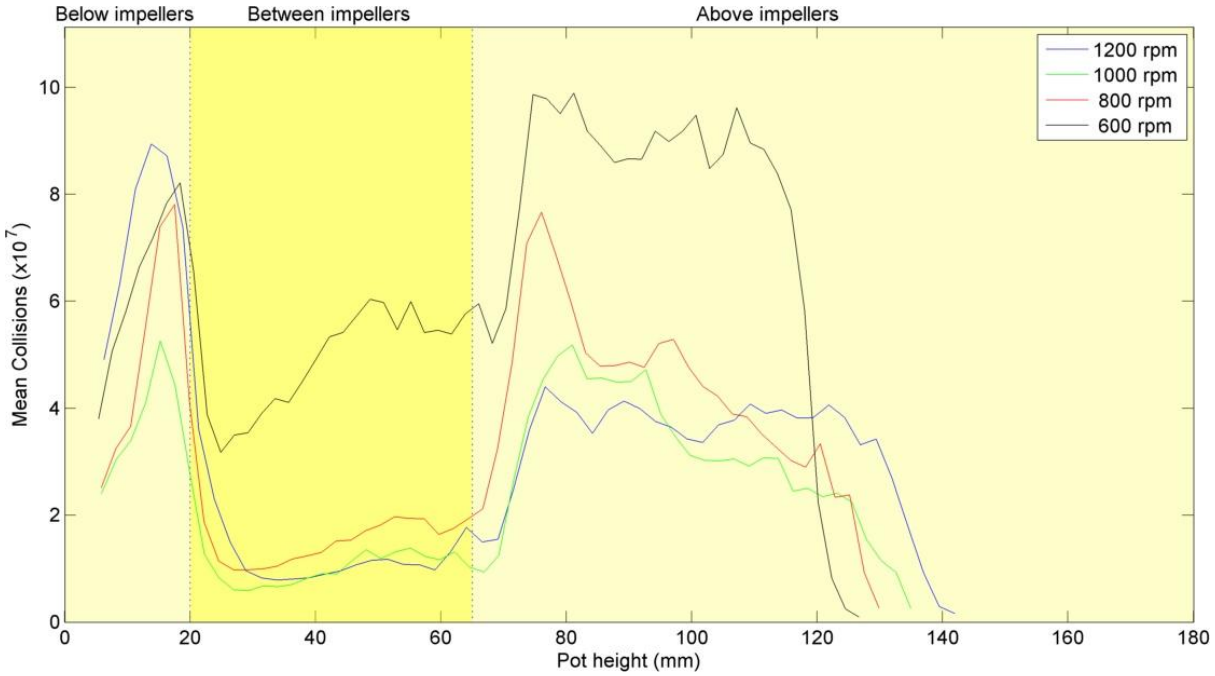

Figure 6.3-69 Mean number of collisions between grinding media as a function of height in the mill

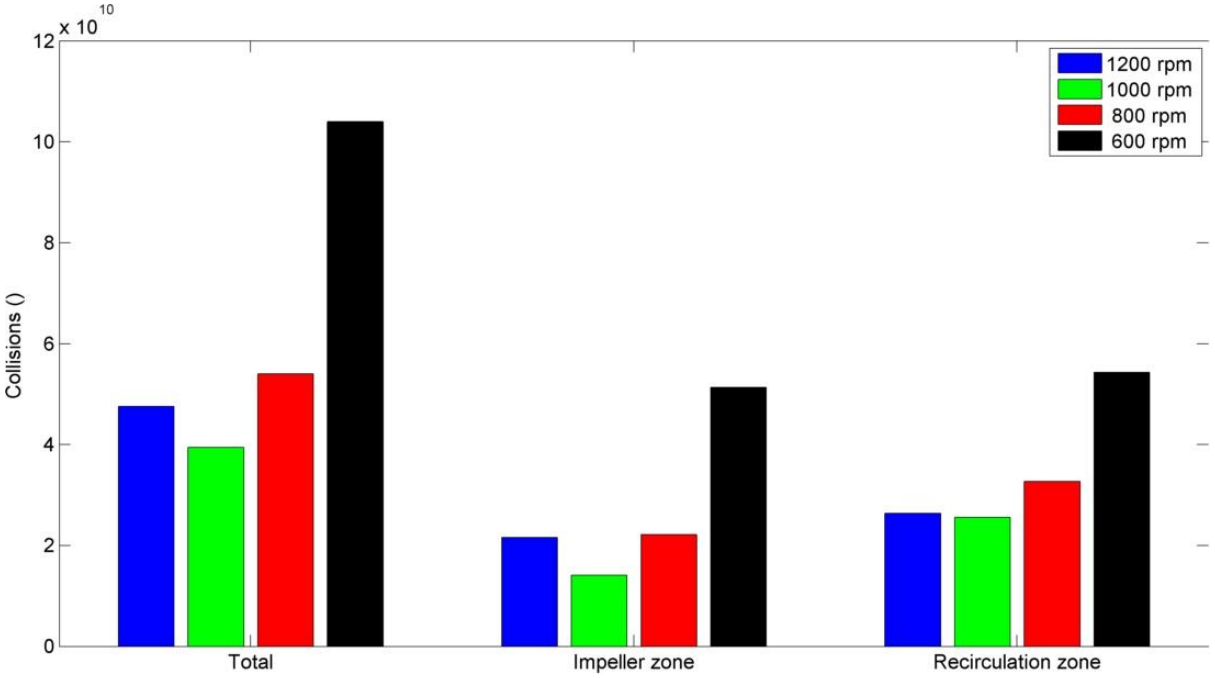

Figure 6.3-70 Bar chart comparing mean, impeller zone and recirculation zone media-media collisions

6.3.4.2 Comparison of PEPT data with laboratory grinding data

Lab grinding data with differing impeller speeds are given in Section 4.6. The data indicated that the optimum impeller speed in terms of energy input to achieve a target d90 was 700 rpm (impeller tip speed 4.2 ms^{-1}). It was suggested that at impeller speeds lower than 700 rpm the energy supplied by the impeller to the grinding media was less than optimum to achieve calcium carbonate particle breakage at the size range required for this application. However, at impeller speeds greater than 700 rpm the stress energy supplied was in excess of the optimum required for particle breakage and therefore energy was wasted.

The PEPT data support this view. The data presented in Figure 6.3-62 to Figure 6.3-67 indicate that increasing the speed of the impeller increased the stress exerted by the grinding media at collisions and Figure 6.3-67 to Figure 6.3-70 suggest that the collision rate increased as stirrer speed increased. However, it was also shown in Figure 6.3-56 that the differential between the tip speed and the grinding media speed increased with increasing rpm. Therefore the momentum was transferred from the impeller to the grinding media less effectively as impeller speed increased and more grinding energy was lost fluidising the grinding media. The additional wasted energy resulted in larger grinding energies required to achieve a target calcium carbonate particle size as stirrer speed increased despite the reduced stress exerted.

6.3.5 Grinding media solids volume concentration

Lab grinding data with differing solids volume concentration are reported in Section 4.7. The data indicate that the highest energy efficiency occurred at the lowest volume solids concentration investigated. This was explained in terms of reduced calcium carbonate particle numbers.

6.3.5.1 PEPT data

6.3.5.1.1 Occupancy

Figure 6.3-71 (a) (b) and (c) show the occupancy contour plots for grinds performed at 75, 70 and 65 % volume solids concentration, respectively. It can be seen that the maximum media height of the media increased as solids volume concentration decreased and the width of the recirculation zone decreased as solids volume concentration decreased. This behaviour is also further shown in Figure 6.3-72 which also suggests the amount of media beneath the impeller increased as solids volume concentration decreased. These differences likely occurred because calcium carbonate slurry viscosity decreased with decreased solids volume concentration (Fortier, et al., 2004).

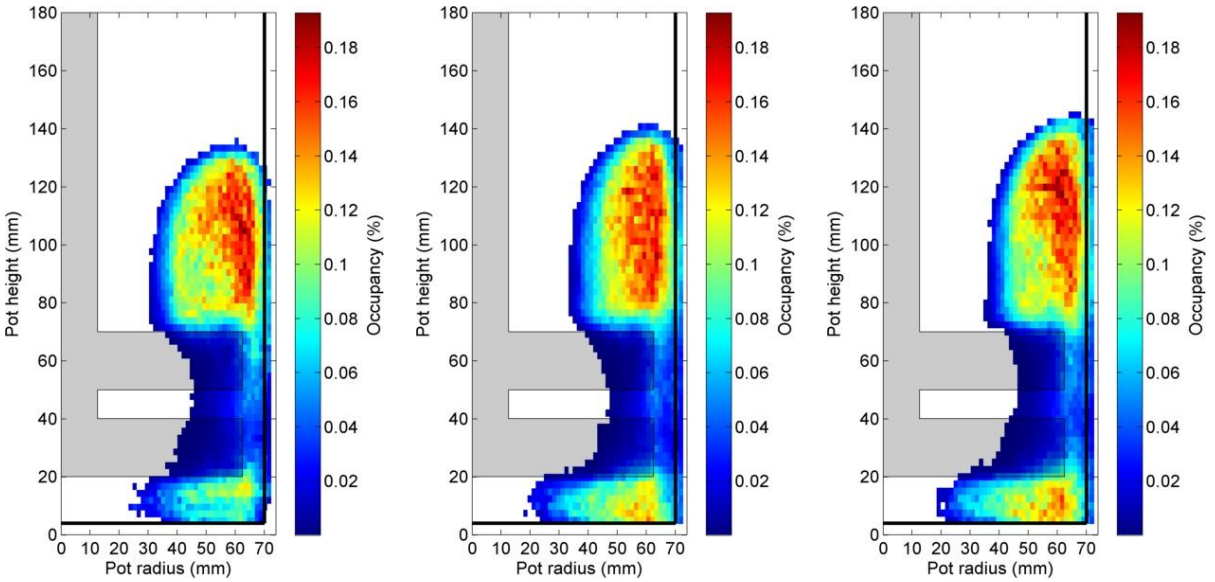

75 % Solids volume conc. (a) | 70 % Solids volume conc. (b) | 65 % Solids volume conc. (c)

Figure 6.3-71 Occupancy contour plots for (a) 75 (b) 70 and (c) 65 % solids volume concentration

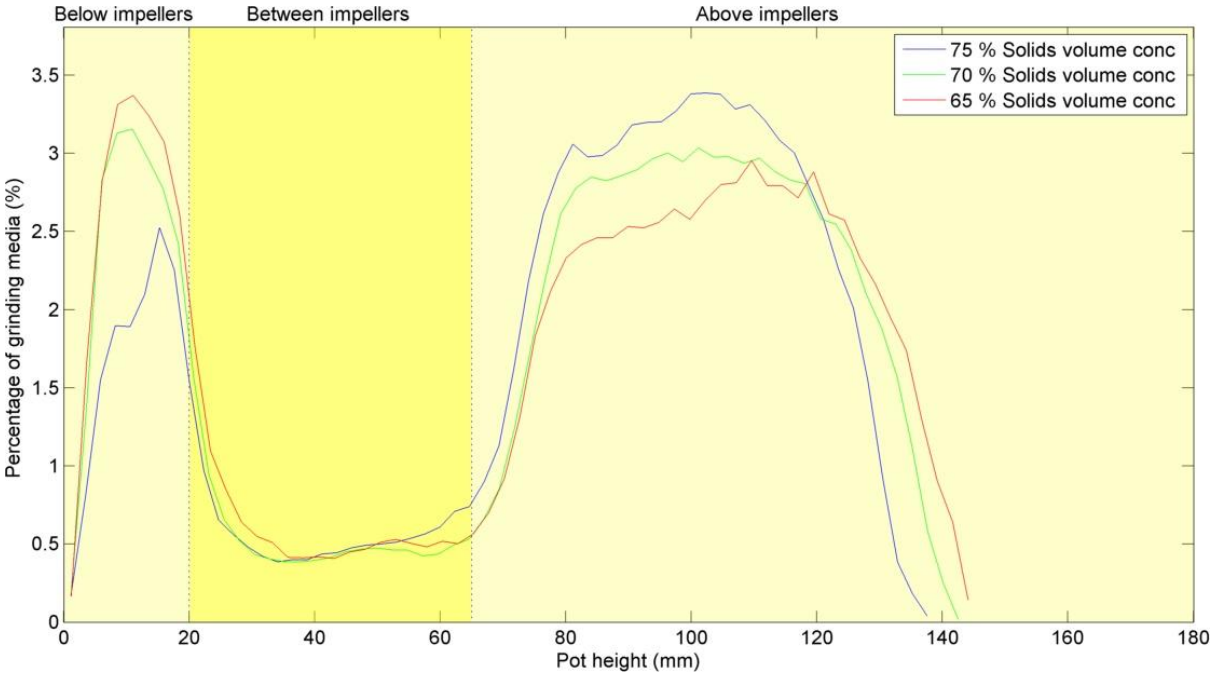

Figure 6.3-72 Percentage of grinding media as a function of height in the grinding pot

6.3.5.1.2 Velocity

Figure 6.3-73 (a) (b), and (c) show velocity contour plots for grinds performed at 75, 65 and 60 % solids volume concentration, respectively. These data are summarised in Figure 6.3-74. No strong trends were observed. Likewise no strong trends in solids volume concentration were observed in Figure 6.3-75 which shows mean relative velocity as a function of pot height.

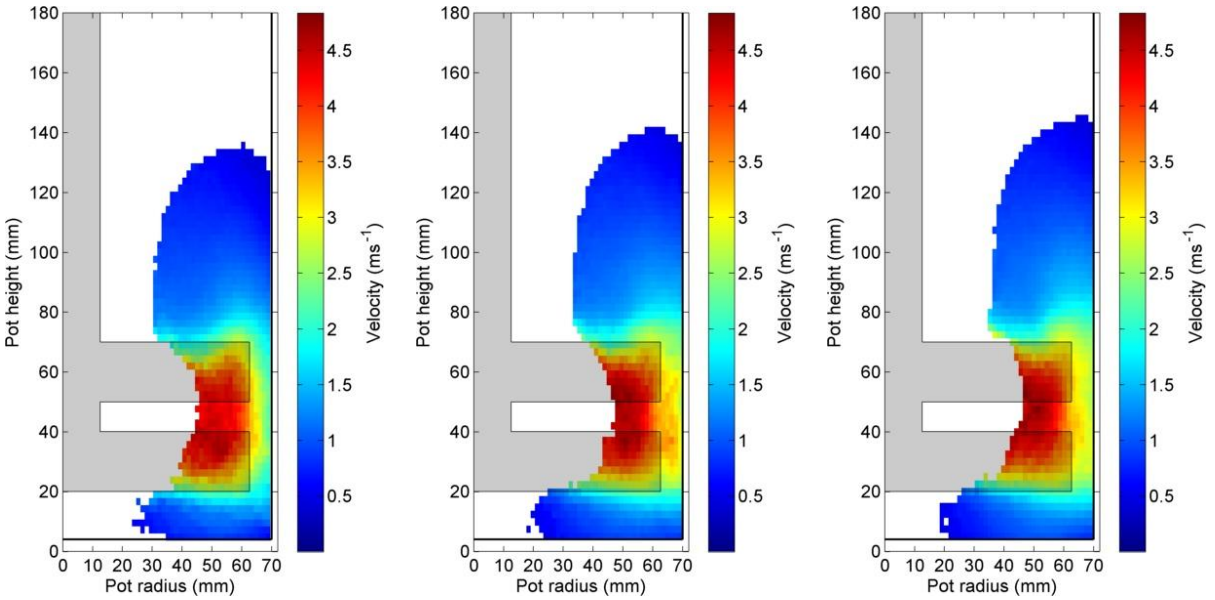

75 % Solids volume conc. (a) | 70 % Solids volume conc. (b) | 65 % Solids volume conc. (c)

Figure 6.3-73 Velocity contour plots for (a) 75 (b) 70 and (c) 65 % solids volume concentration

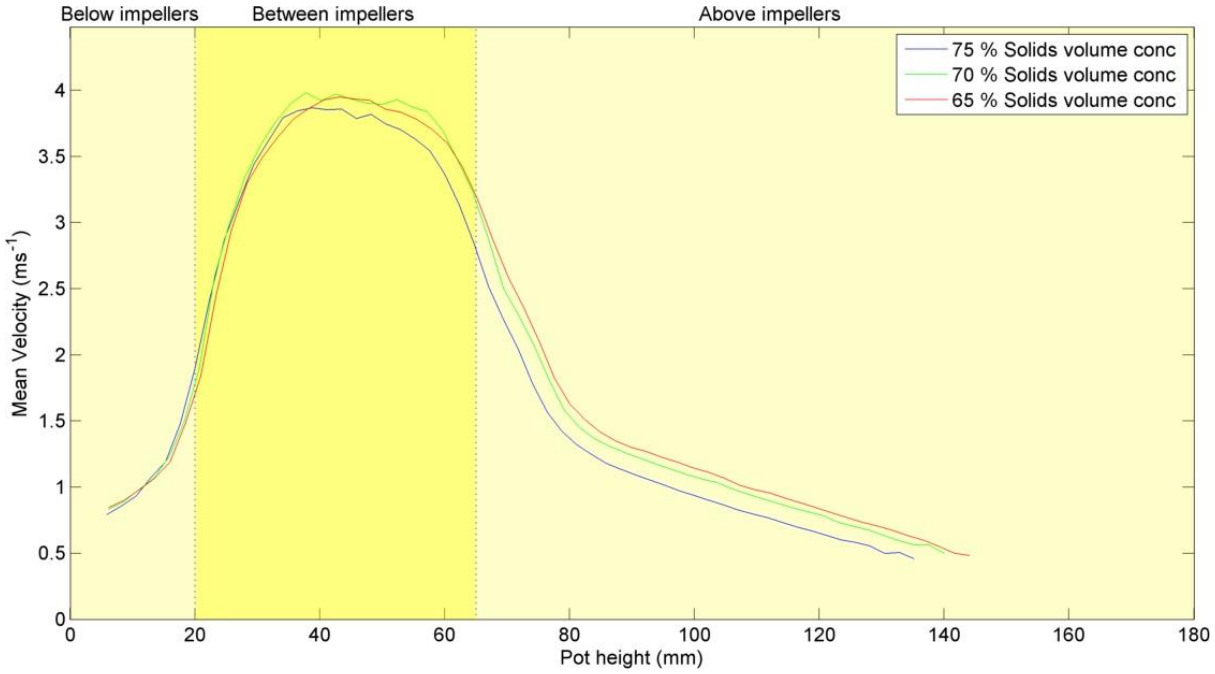

Figure 6.3-74 Mean velocity of grinding media as a function of height in the grinding pot

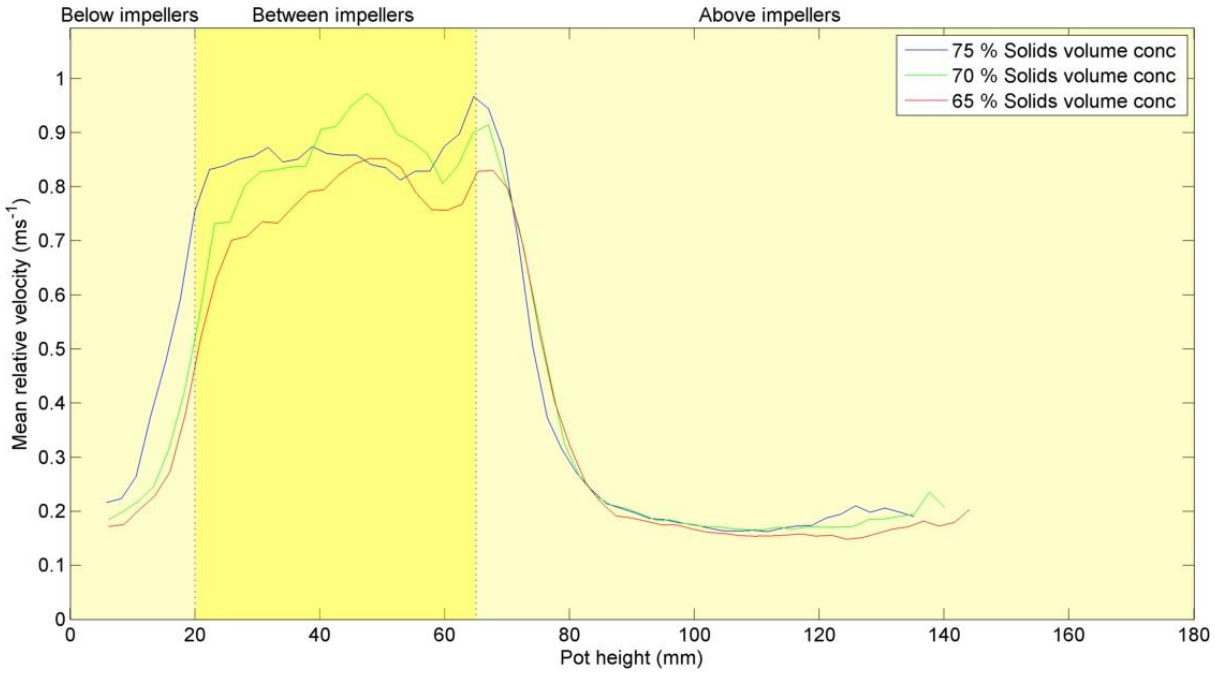

Figure 6.3-75 Mean relative velocity of grinding media as a function of height in the grinding pot

6.3.5.1.3 Force

Figure 6.3-76 (a) (b), and (c) show force contour plots for grinds performed at 75, 65 and 60 % solids volume concentration and Figure 6.3-77 shows the force acting on the media as a function of pot height. It can be seen that the distributions of force and force as a function of pot height varied only slightly within the mill at heights greater than 100 mm from the pot floor and beneath the impellers. These data are summarised in Figure 6.3-78 which show a small increase in the mean grinding media force, force of the grinding media within the impeller zone and in the recirculation zone at higher solids volume concentrations.

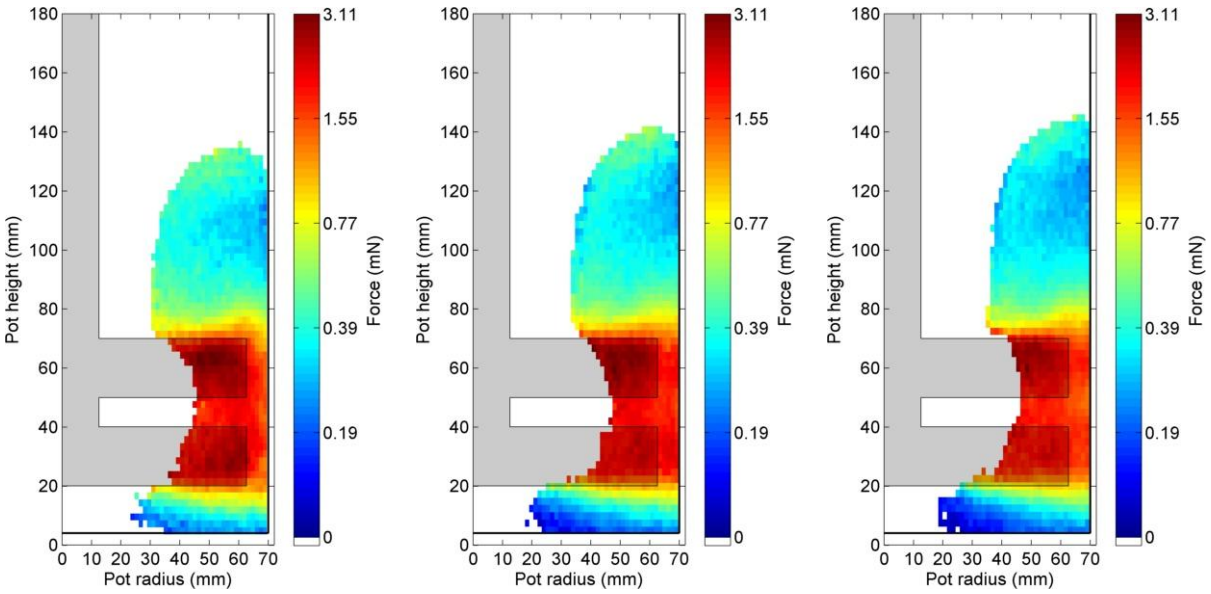

75 % Solids volume conc. (a) | 70 % Solids volume conc. (b) | 65 % Solids volume conc. (c)

Figure 6.3-76 Force contour plots for (a) 75 (b) 70 and (c) 65 % solids volume concentration

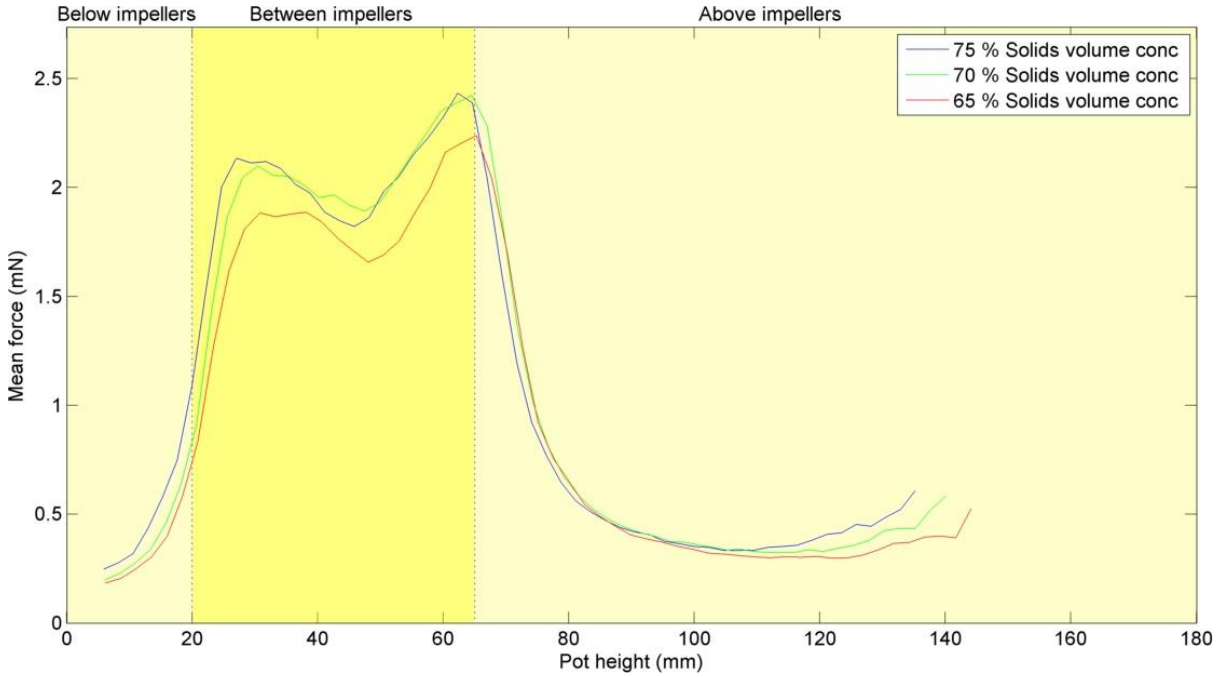

Figure 6.3-77 Mean force of grinding media as a function of height in the grinding pot

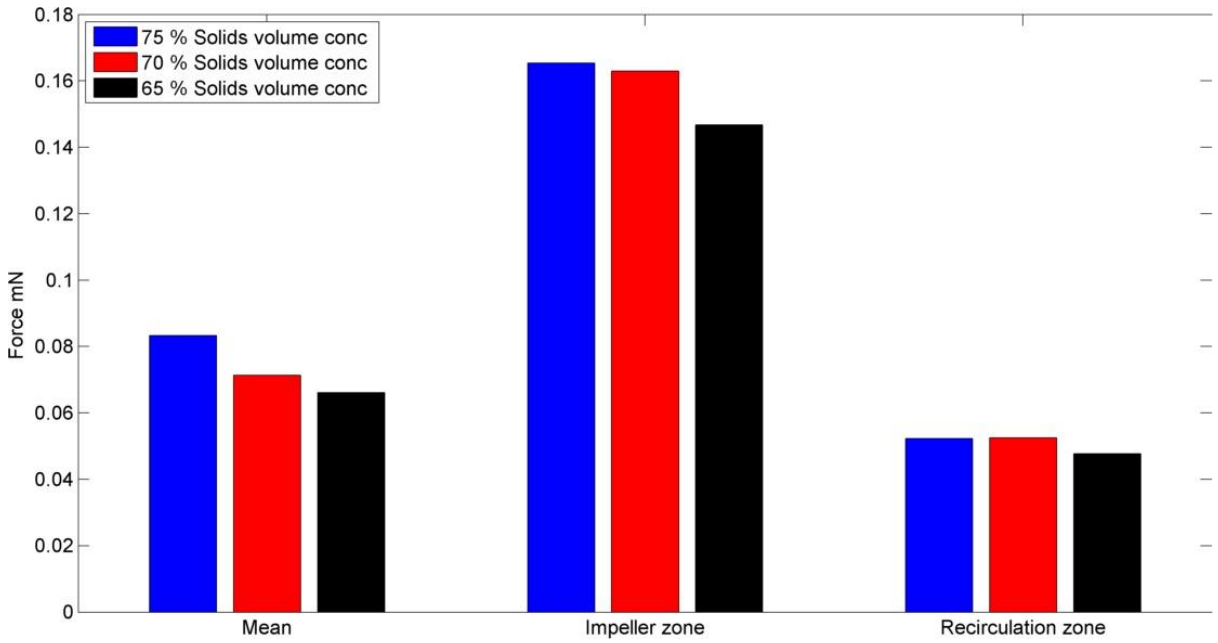

Figure 6.3-78 Bar chart comparing mean, impeller zone and recirculation zone forces

6.3.5.1.4 Stress

Figure 6.3-79 (a) (b), (c) and (d) show how the stress acting on calcium carbonate particles varied with calcium carbonate size and solids volume concentration. It can be seen that in each case as the calcium carbonate particle size decreased the applied stress increased and the stresses applied increased slightly with increased solids volume concentration. This is further illustrated in Figure 6.3-80 which shows a comparison of the average stress applied to the calcium carbonate as a function of calcium carbonate particle size. As the calcium carbonate particle size decreased the difference in stress applied by varying solids volume concentration increased. However the difference in stress applied remains less than 5 MPa when stressing 5 μm calcium carbonate particles.

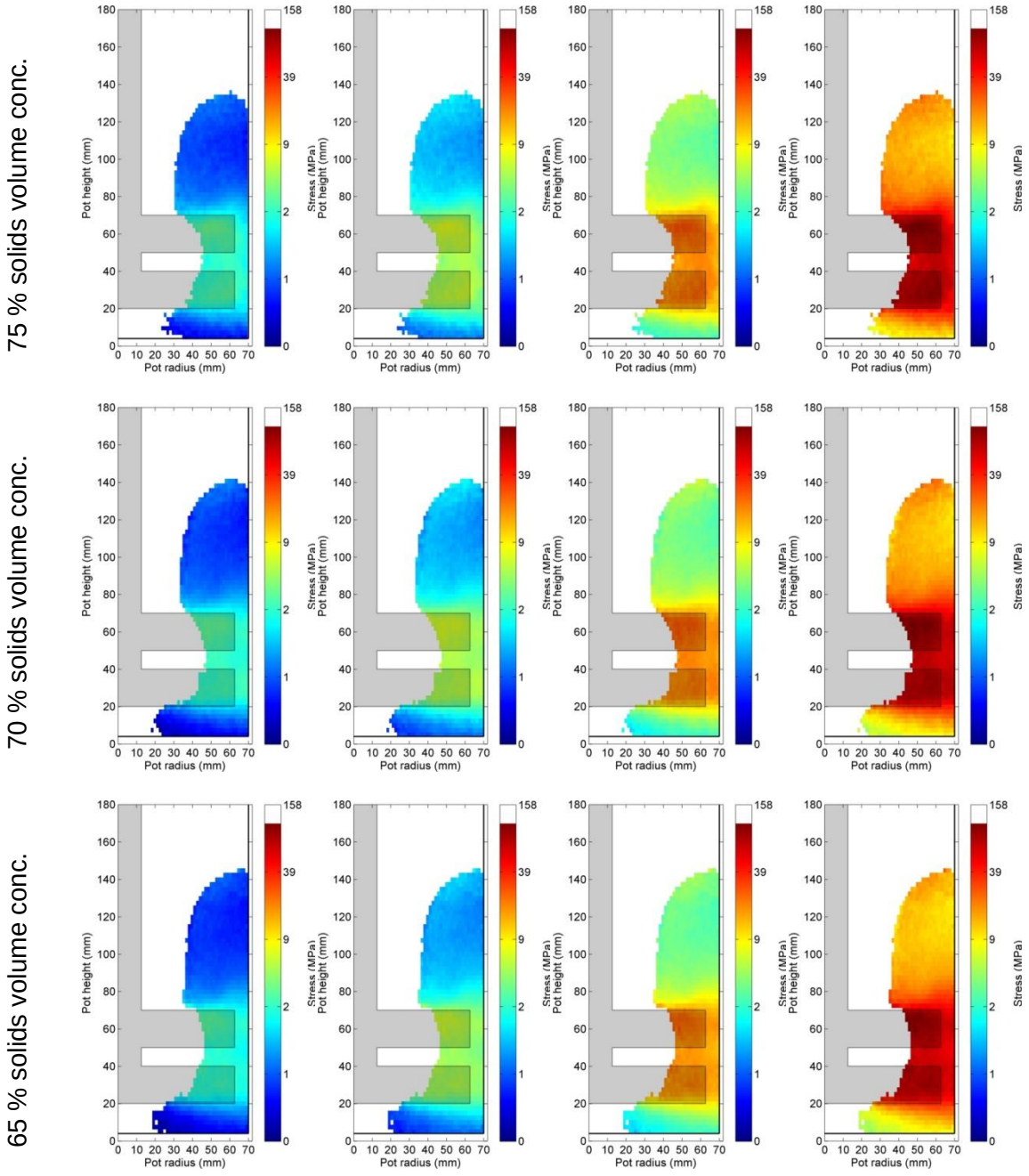

Figure 6.3-79 Stress contour plots comparing 75, 70 and 65 % solids volume concentration when calcium carbonate particle size is (a) 30 (b) 20 (c) 10 and (d) 5 µm

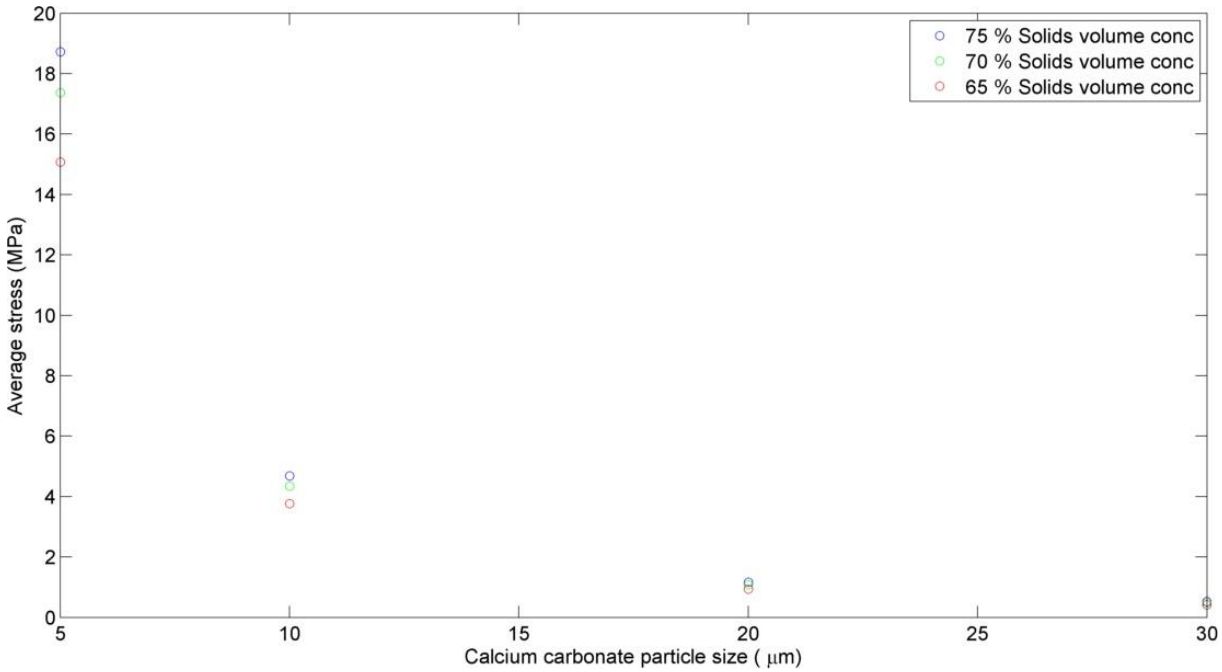

Figure 6.3-80 Mean stress within the mill as a function of calcium carbonate particle size

Figure 6.3-81 (a) (b) (c) and (d) show stress distribution profiles as a function of calcium carbonate particle size as determined using PEPT for each system and the mean strength of a calcium carbonate particle at that size as measured by a micromanipulation technique. The data show that as calcium carbonate particle size decreased the proportion of the media capable of exerting sufficient stress to cause fracture increased, and that the proportion of the media capable of fracturing the calcium carbonate particles increased slightly with solids volume concentration. This is further illustrated in Figure 6.3-82 which shows the percentage of grinding media capable of fracturing calcium carbonate particles as a function of calcium carbonate particle size. Again increased solids volume concentration gave a slight increase in the percentage of calcium carbonate fracture.

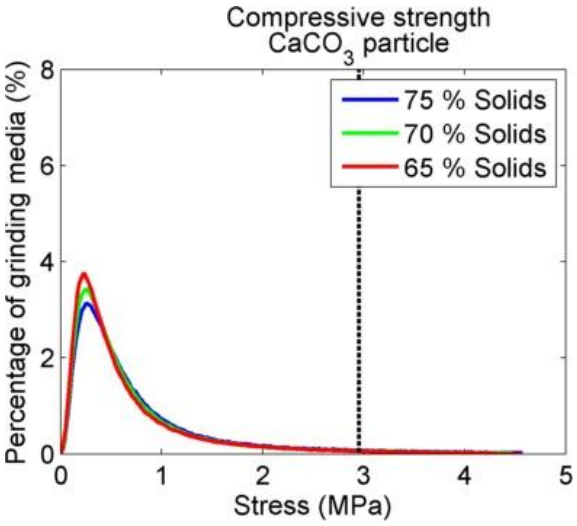

30 μm calcium carbonate particles

(a)

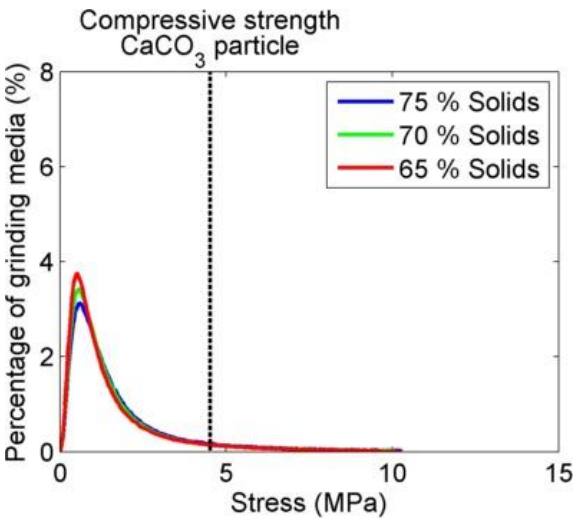

20 μm calcium carbonate particles

(b)

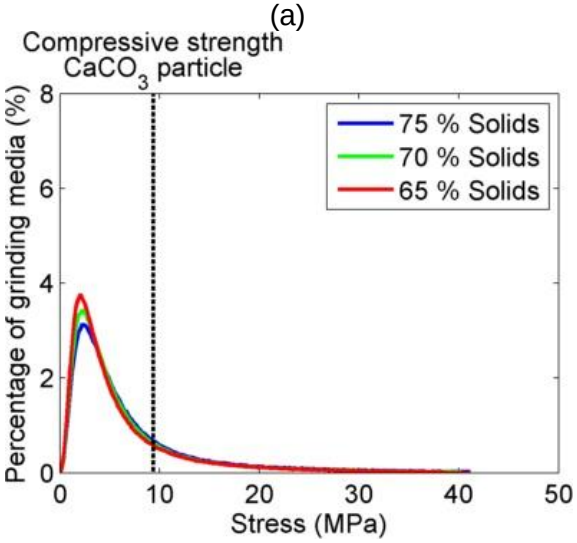

10 μm calcium carbonate particles

(c)

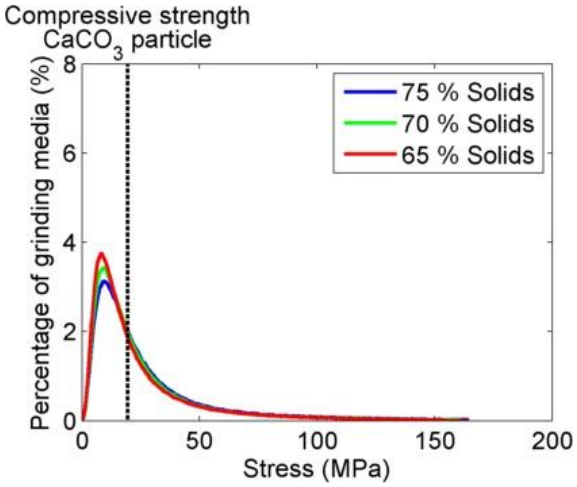

5 μm calcium carbonate particles

(d)

Figure 6.3-81 Distribution of stress exerted by grinding media when calcium carbonate particle size is (a) 30 (b) 20 (c) 10 and (d) 5 μm

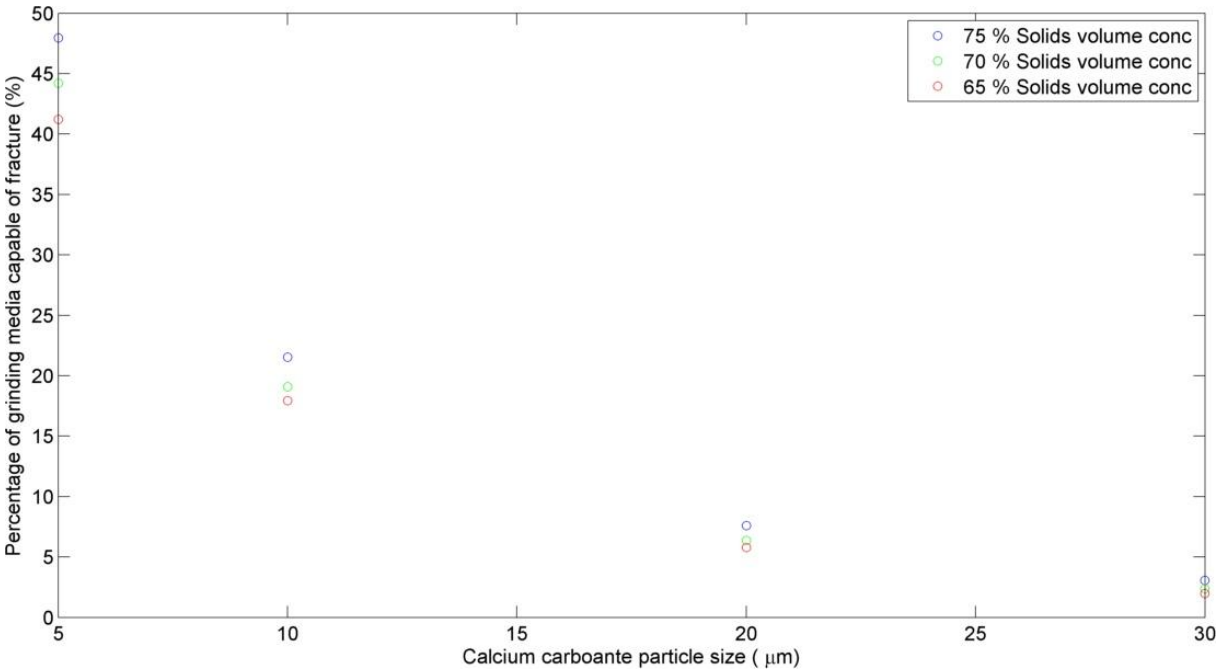

Figure 6.3-82 Percentage of grinding media suitable to fracture calcium carbonate particles as a function of calcium carbonate feed size (based on average strength of calcium carbonate feed particles at a given feed size)

Figure 6.3-83 (a) (b) (c) and (d) show the regions within the mill with sufficient stress to overcome the average compressive strength of the calcium carbonate particles. These data show that the regions within the mill where breakage could occur increased when using high solids volume concentrations. These data are summarised in Figure 6.3-84.

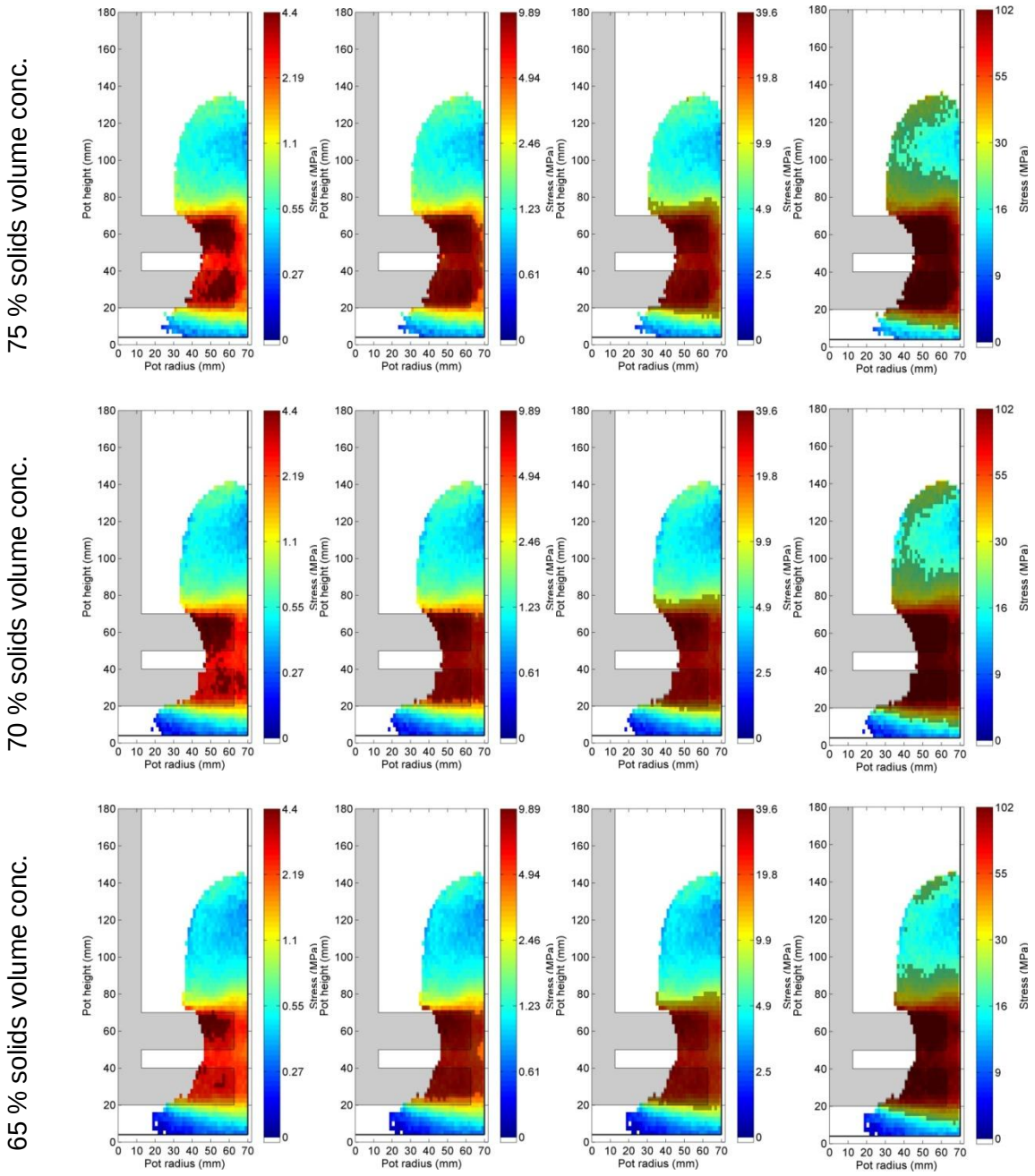

Figure 6.3-83 Regions of the mill capable of fracturing calcium carbonate feed particles comparing 75, 70 and 65 % solids volume concentration when calcium carbonate particle size is (a) 30 (b) 20 (c) 10 and (d) 5 µm

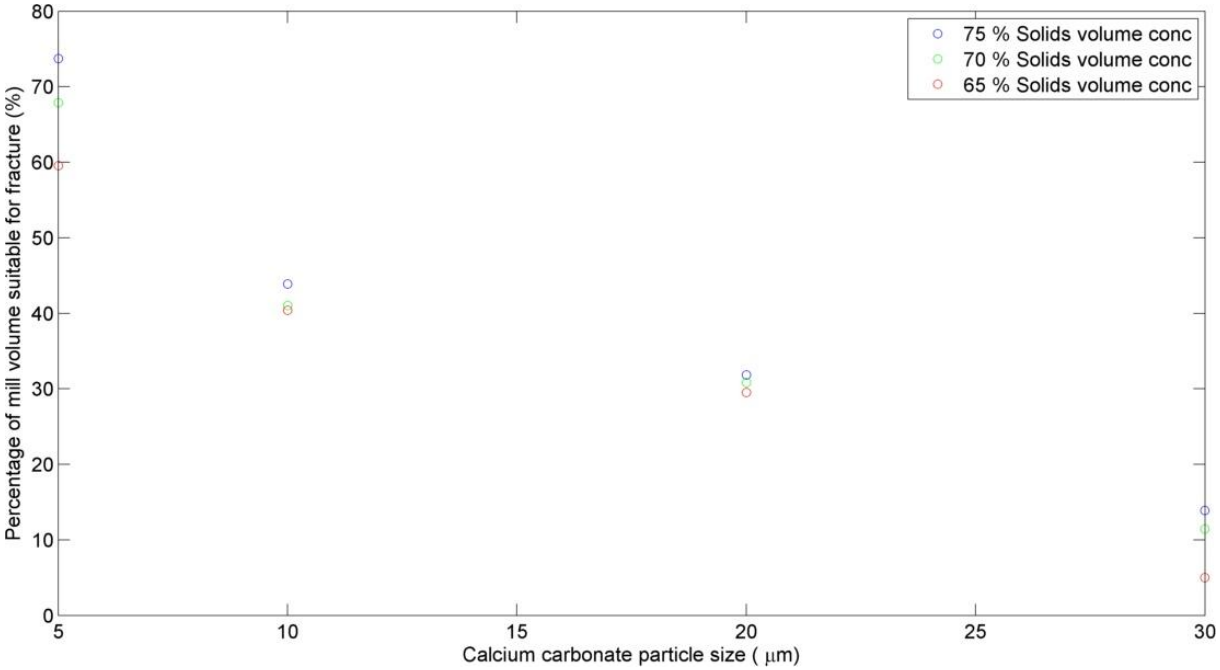

Figure 6.3-84 Percentage of the mill capable of fracturing calcium carbonate particles as a function of calcium carbonate feed size

6.3.5.1.5 Collisions

Figure 6.3-85 (a) (b) and (c) show the collision rate and total number of collisions within the system. No strong trends can be observed. These data are further summarised in Figure 6.3-85, Figure 6.3-86 and Figure 6.3-87.

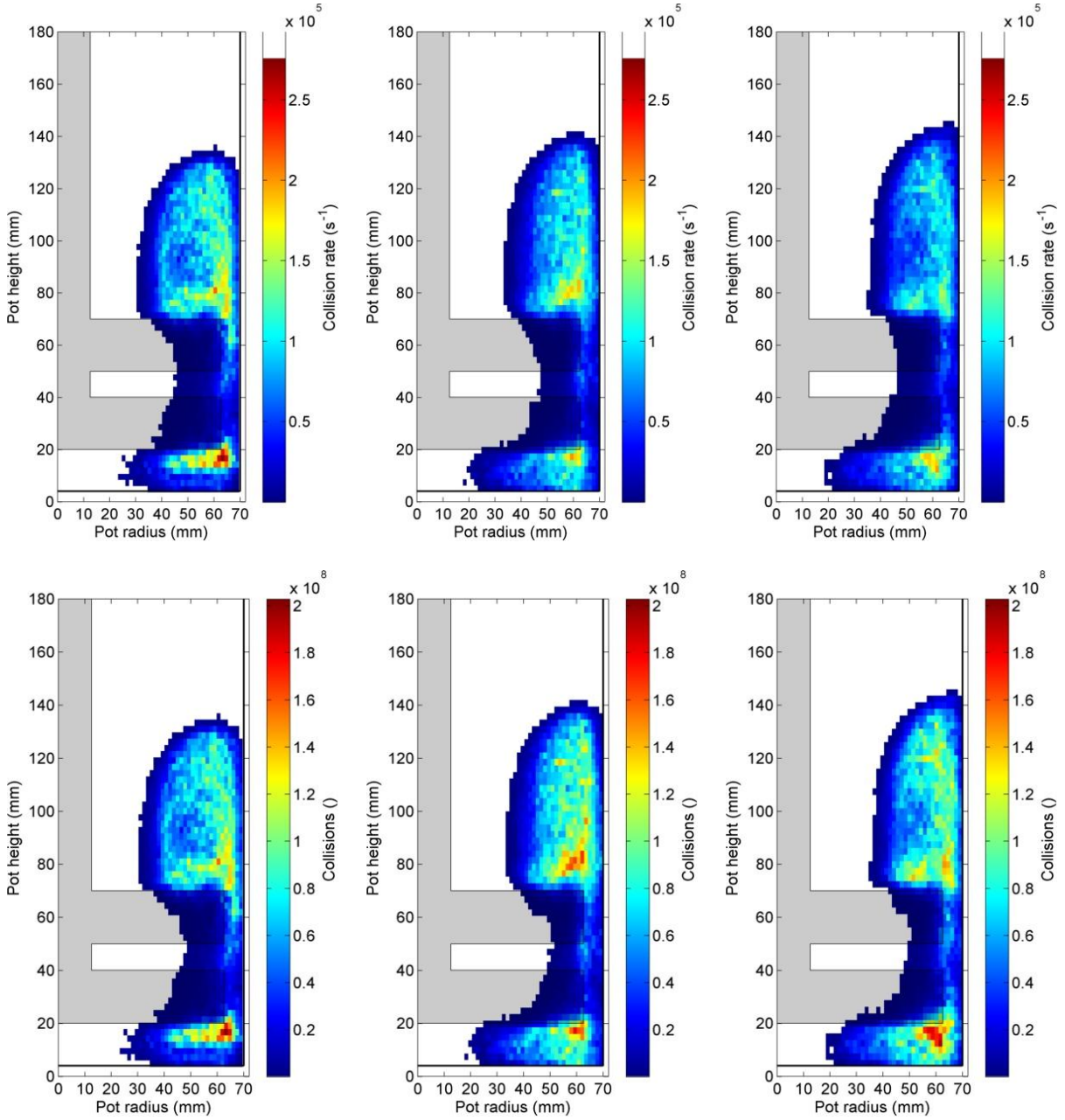

75 % Solids volume conc. (a)

70 % Solids volume conc. (b)

65 % Solids volume conc. (c)

Figure 6.3-85 Collision rate and the number of collisions throughout the course of a grind contour plots for (a) 75 (b) 70 and (c) 65 % solids volume concentration

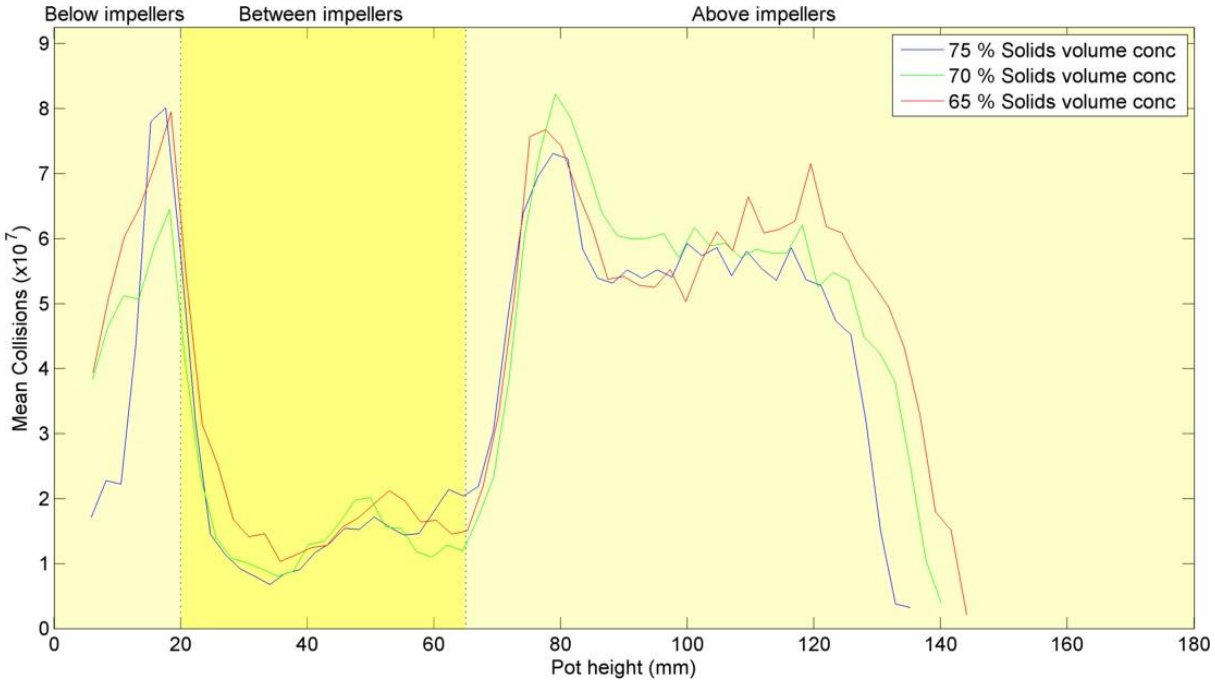

Figure 6.3-86 Total collisions between grinding media as a function of height in the mill

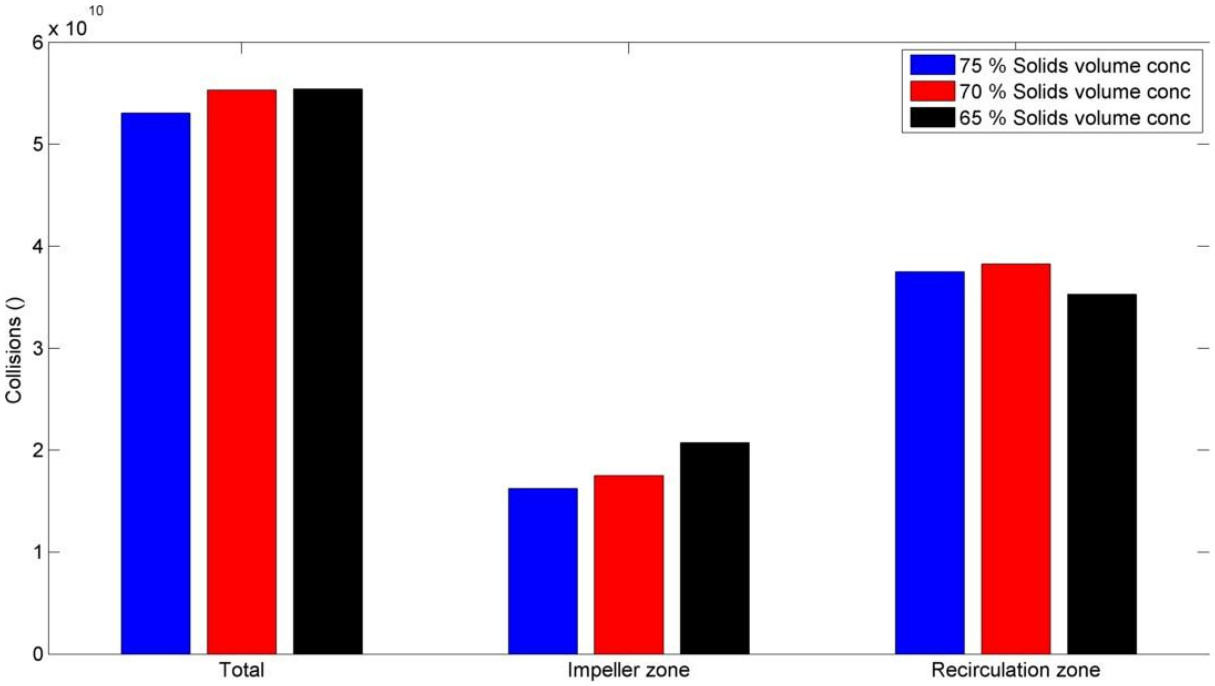

Figure 6.3-87 Bar chart comparing mean, impeller zone and recirculation zone media-media collisions

6.3.5.2 Comparison of PEPT data with laboratory grinding data

Lab grinding data with differing solids volume concentration are reported in Section 4.7. The data indicated that the highest energy efficiency occurred at the lowest volume solids concentration investigated. This was explained in terms of reduced calcium carbonate particle numbers.

The PEPT data do not support this above view. The PEPT data suggest that high solids volume concentration slightly favoured grinding efficiency as show in Figure 6.3-76 to Figure 6.3-84 by increasing the stress and success rate at media-media collisions. However, the PEPT data does not give any information about the number of calcium carbonate particles in the system or their collision behaviour. Reducing the calcium carbonate solids volume concentration led to reduced numbers of calcium carbonate feed particles being added to the system and with less calcium carbonate particles in the system it is reasonable to assume that a greater percentage of the added calcium carbonate particles was stressed at each media-media collision resulting in an increased grinding rate at lower calcium carbonate slurry concentrations.

6.4 DISCUSSION OF OPERATING PARAMETERS STUDY

The objectives of the work presented in this chapter were:

1. To determine the regions within a vertically stirred media mill where calcium carbonate feed particles can be fractured by measuring the number of media-media collisions and the stress at the media-media collisions.
2. To compare the different operating parameters discussed in Chapter 4 to determine how varying the conditions affect milling performance.

The initial analysis was performed on a benchmark system and the results of this analysis have been presented and summarised in Section 6.2.6 Subsequently the same analytical approach was used to study the effect of varying the following operating parameters:

(i) Media specific gravity

(ii) Media particle size

(iii) Media surface roughness

(iv) Impeller speed

(v) Solids volume concentration

Each system displayed similar general behaviour to that reported for the benchmark system. However, several different behaviours were observed as the mill operating parameters were varied. These are summarised below:

(i) Media specific gravity

Increased media specific gravity led to higher force and stress and an increased percentage of the mill being suitable for fracture. Occupancy, velocity and collisions were approximately the same regardless of specific gravity. The improved grinding performance with increased media specific gravity reported in Section 4.3 was therefore, most likely, a result of the increased force and increased stress at collisions which resulted in a higher percentage of media with sufficient stress for breakage.

(ii) Media particle size

Reduced grinding media particle size led to lower forces and stresses at collisions and a lower percentage of the media capable of fracturing calcium carbonate particles. However, reduced media particle size gave an increased number of media-media collisions. Therefore the improved grinding performance with reduced media particle size reported in Section 4.4 was likely a result of the increased number of media-media collisions.

The data in Section 4.4 also suggested that the finest particle size grinding media was least effective during the coarse stage of the grind and that this could be because the number of collisions was less important than stress intensity during the coarse stages of grinding. The PEPT data also support this view as shown in Figure 6.3-29 (a) and (b) which show that the breakage rate of 30 μm calcium carbonate was much lower than that of 5 μm calcium carbonate when ground with the finest particle size grinding media.

(iii) Media surface roughness

Use of rough media led to higher force and stress and an increased percentage of the mill being suitable for fracture. Occupancy, velocity and collisions were approximately the same regardless of surface roughness. The grinding performance reported in Section 4.5 showed that use of rough media offered no benefit in terms of the amount of energy required to achieve a target calcium carbonate particle size. However, the grind was completed in a much shorter time when rough media was used. The reason for this behaviour is likely due to a turbulent boundary layer.

(iv) Impeller speed

The grinding data reported in Section 4.6 showed that optimum performance occurred at 700 rpm. Increasing impeller rpm led to higher velocity, force, stress and collision rate. However, the differential between the tip speed and the grinding media speed increased with increasing rpm. This suggests that the momentum was transferred from the impeller to the grinding media less effectively as impeller speed increased. Therefore, the most efficient stirrer speed occurred at a compromise point where the stress exerted by the grinding media was sufficient to fracture calcium carbonate particles and the momentum transferred was at a maximum. This observation is consistent with the grinding data which show an optimum performance at 700 rpm and that more grinding energy was required at higher rpm to achieve a target particle size. The grinding data also indicated that grinds at higher impeller speeds were completed faster than at lower stirrer speeds.

(v) Solids volume concentration

Increasing solids volume concentration increased the force and stress and increased the percentage of the mill suitable for fracture, although these increases were small. The grinding data, however, suggest that reducing the solids volume concentration resulted in reduced energy to achieve a target d90, again this was a small effect. Reducing the calcium carbonate solids volume concentration led to reduced numbers of calcium carbonate feed particles being added to the system and with less calcium carbonate particles in the system it is reasonable to assume that a greater percentage of the added calcium carbonate particles would be stressed, resulting in an increased grinding rate at lower calcium carbonate slurry concentrations.

7 CONCLUSIONS AND FURTHER WORK

7.1 CONCLUSIONS

The aim of the work presented here was to determine the regions within a vertically stirred media mill where breakage occurs and to determine how variations in operating conditions affect milling performance.

There were three components to this work: (i) mill performance was characterised using laboratory grinding experiments, (ii) single calcium carbonate particle breakage behaviour was determined using direct stress measurements with a micromanipulator based technique and (iii) PEPT was used to measure grinding media occupancy, velocity, force, stress and the number of media- media collisions that occurred during grinding.

In the laboratory grinding experiments increased media specific gravity, decreased media particle size, an optimum impeller speed of 700 rpm and decreased calcium carbonate solids volume concentration all resulted in reduced grinding energy required to achieve a target d90. The use of rough grinding media had no effect on energy requirements but led to reduced grinding time due to higher power draw.

In the micromanipulator work it was found that finer particle size calcium carbonate required less force but more stress for breakage than coarse calcium carbonate particles.

A PEPT methodology was developed that allowed the measurement of media occupancy, velocity, force, stress, and media-media collisions at different positions within the mill. Stress measurements were calculated by assuming that there was only one feed particle trapped at a collision and that the stress exerted at the collision was equal to the force acting on a feed particle divided by the cross-sectional area of the feed particle. The collision frequency and total number of collisions were estimated using a modified Arrhenius equation approach and by measuring the mean relative velocity of the grinding media (estimated to be the standard deviation of velocity measurements made in a block volume) and the number of media particles in a unit volume.

This approach was used to characterise the behaviour of a benchmark grinding experiment performed under standard conditions and to understand the effect different operating conditions had on the number of collisions and stress exerted at these collisions.

A number of characteristics were common to all conditions examined. Namely that: (i) a large vortex was formed and three zones could be defined: below, between and above the impellers, (ii) the tracer spent less time in the impeller zone than the recirculation zone, (iii) the average media height was above the impeller zone, (iv) there were radial flow regimes resulting in a two loop recirculating flow pattern, (v) the grinding media velocity varied as a function of radial position, (vi) grinding media velocity was much lower in the recirculation zone than between the impellers, (vii) the highest forces occurred at the impeller tips, (viii) the highest stresses were exerted between the impellers, (ix) stress increased as calcium carbonate particle size decreased, (x) as calcium carbonate particle size decreased the percentage of the

grinding media capable of supplying sufficient stress for breakage increased and the areas within the mill capable of fracturing calcium carbonate particles also increased, (xi) media-media collisions were higher in the regions above and below the impellers and (xii) despite a larger percentage of the grinding media having sufficient stress to break finer calcium carbonate particles, the proportion of the calcium carbonate fractured decreased as calcium carbonate size decreased. This was because the number of calcium carbonate particles created increased at a faster rate.

The same analytical approach was used on the operating parameters investigated:

1. Increased media specific gravity led to higher force and stress and an increased percentage of media being suitable for fracture, but no variation in the numbers of media-media collisions. Therefore the improved grinding behaviour observed with high specific gravity media was attributed to additional stress exerted at the media-media collisions.
2. Reduced grinding media particle size led to lower forces and stresses at collisions and a lower percentage of the media capable of fracturing the calcium carbonate particles. However reduced media particle size gave an increased number of media-media collisions. Therefore the improved grinding performance with reduced media particle size was likely a result of the increased number of media-media collisions.
3. Use of rough media led to higher force and stress and an increased percentage of the media suitable for fracture. However, the use of rough media offered no benefit in terms of the amount of energy required to achieve a target calcium carbonate particle size. The lack of improved performance was attributed to

both media types, large size resulting in low numbers of collisions most of which having sufficient stress to achieve breakage.

4. Increasing impeller rpm led to higher velocity, force, stress and collision rate. However, the differential between the tip speed and the grinding media speed increased with increasing rpm. This suggests that the momentum was transferred from the impeller to the grinding media less effectively as impeller speed increased. Therefore the most efficient stirrer speed occurred at a compromise point where the stress exerted by the grinding media was sufficient to fracture calcium carbonate particles and the momentum transferred at a maximum. This observation is consistent with the grinding data which showed an optimum performance at 700 rpm and that more grinding energy was required at higher rpm to achieve a target particle size. The grinding data also indicated that grinds at higher impeller speeds were completed faster than lower stirrer speeds.

5. Increasing solids volume concentration increased the force and stress and increased the percentage of the mill suitable for fracture, although these increases were small. The grinding data however suggest that reducing the solids volume concentration resulted in reduced energy to achieve a target d90, again this was a small effect. Reducing the calcium carbonate solids volume concentration led to reduced numbers of calcium carbonate feed particles being added to the system and with less calcium carbonate particles in the system it is reasonable to assume that a greater percentage of the added calcium carbonate particles will be stressed resulting in an increased grinding rate at lower calcium carbonate slurry concentrations.

7.2 SUGGESTIONS FOR FURTHER WORK

7.2.1 Stressing multiple calcium carbonate particles at a collision

Stress exerted at a collision has thus far been assumed to be exerted over the cross-section of a single calcium carbonate particle. However, at high solids volume concentrations and fine particle size it is possible to stress a bed of particles which would reduce the stress of a collision. Work to determine the number of calcium carbonate particles in an active volume, and how the calcium carbonate particles are carried with the fluid as the media approach would lead to a better understanding of the breakage mechanism at a collision. This could be achieved using a combination of DEM and CFD.

7.2.2 Performance optimisation

The analysis suggests that optimum grinding conditions occur where the force acting on the grinding media is highest. These conditions occur in the regions around the impeller tips. Therefore to improve efficiency:

- It could be possible to increase the number of impellers in the mill and therefore increase the number of high force grinding zones.
- It could be possible to increase the force by increasing the length of the impellers.
- It could be possible to increase the force by reducing the slip at the impeller, for example using a textured impeller surface or shaped impeller.

Alternatively it could be possible to increase the relative areas in the mill having high force by reducing the areas with low force. This could be achieved by:

- compressing the upper recirculation zone by use of a lid
- reducing the volume of the recirculation loops by additional impellers
- the use of baffles to redirect the media into the impeller zone

Conversely in situations where delamination rather than particle fracture is desirable an opposite approach might be utilized for example single impellers, short impellers, and a large recirculation zone.

Currently industrial processes run at high rpm despite reduced energy efficiency to improve process throughput despite higher efficiency at lower stirrer speeds. To ensure the minimum costs per unit volume of material, an objective function to cost time, waste and energy should be conducted.

The work presented here suggests that grinding performance at fine particle size is dominated by the number of media-media collisions and that the number of media-media collisions is principally dependent on grinding media particle size. The limitation on fineness of grinding media used is media removal. Therefore a possible approach to improved ultrafine grinding could be to develop improved methods to remove ultrafine media from grinding systems.

7.2.3 Condition sensing

The PEPT contour plots suggest that it may be possible to develop grinding control techniques based on the shape of the grinding charge and the vortex. For example, it may be possible to control the grinding process by controlling parameters such as the maximum height of the charge, the distance of the vortex from the impeller at a given height, or the shape of the recirculation zone.

Figure 7.2-1 (a) (b) (c) and (d) show the volume grinding media occupies and the interface between the grinding media and air above the impeller highlighted in blue for grinds performed at 1200, 1000, 800 and 600 rpm under the conditions described in Section 4.6. It is possible to compare the height of the grinding media and the shape of the recirculation zone with respect to stirrer speed as shown in Figure 7.2-2 and Figure 7.2-3 respectively.

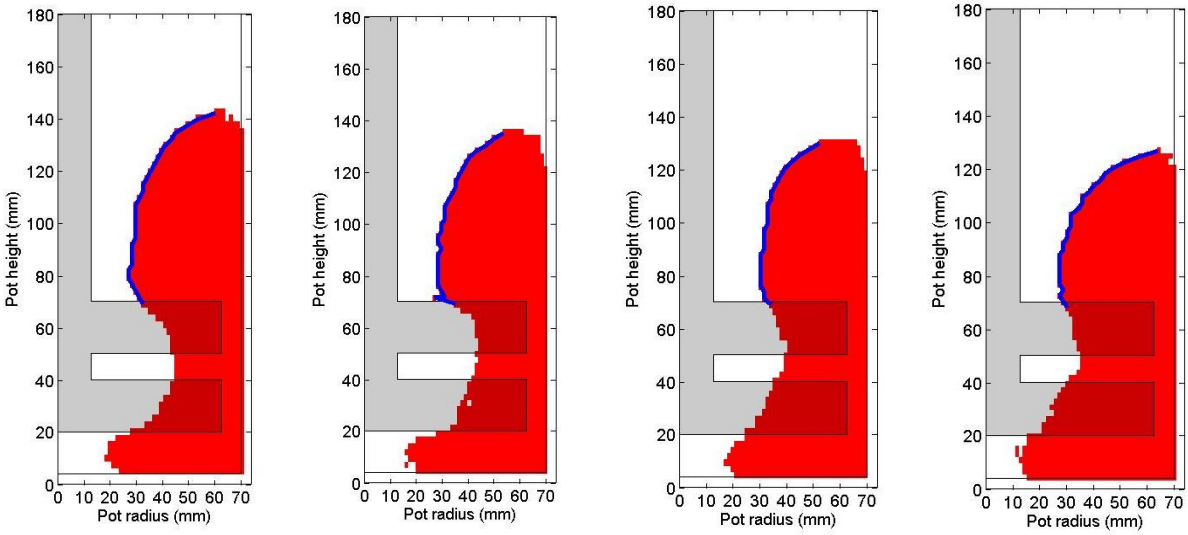

1200 rpm (a) | 1000 rpm (b) | 800 rpm (c) | 600 rpm (d)

Figure 7.2-1 Volume media occupies showing interface between media and air

Figure 7.2-1 and Figure 7.2-2 show that increasing stirrer speed increases the height of the mill contents. A first order trend line was fit to the data, from which it can be seen that a reduction in stirrer speed of 100 rpm results in a 3 mm difference in height.

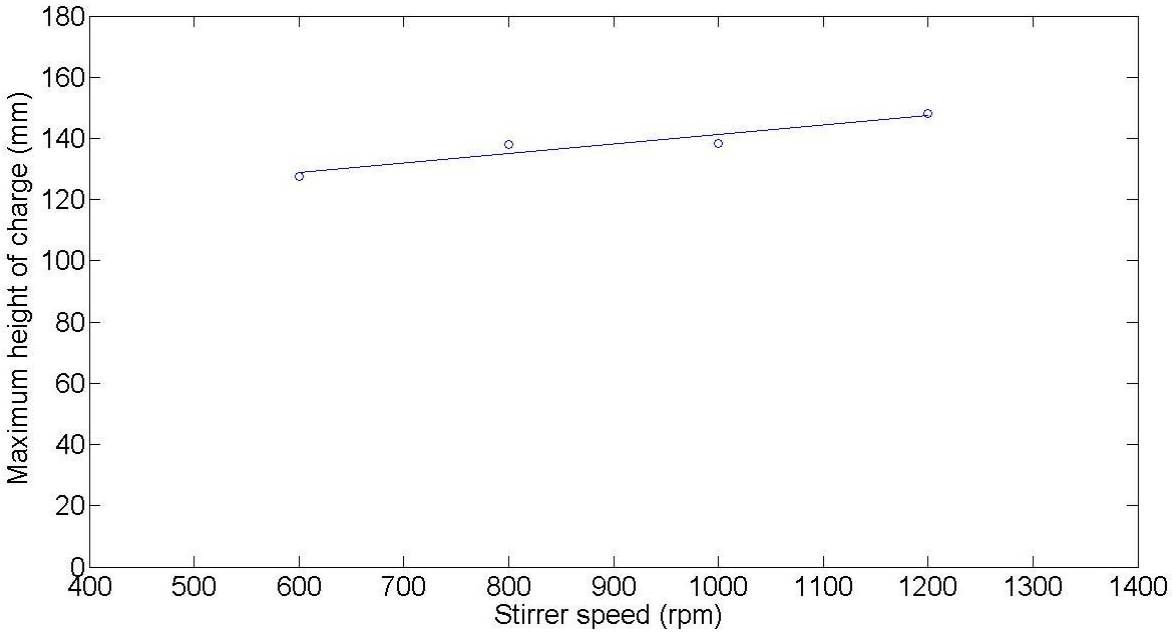

Figure 7.2-2 Maximum height of grinding media as a function of stirrer speed

Figure 7.2-3 shows how the position of the interface between the grinding media varies as a function of height. It can be seen that there are only small differences below a pot height of 100 mm, but clear trends observed thereafter. Positioning a bank of digital laser measures could allow the maximum height of the media and or the shape of the recirculation zone interface to be determined. This could be used to allow non-invasive instantaneous feedback when a mill is no longer running at optimum conditions.

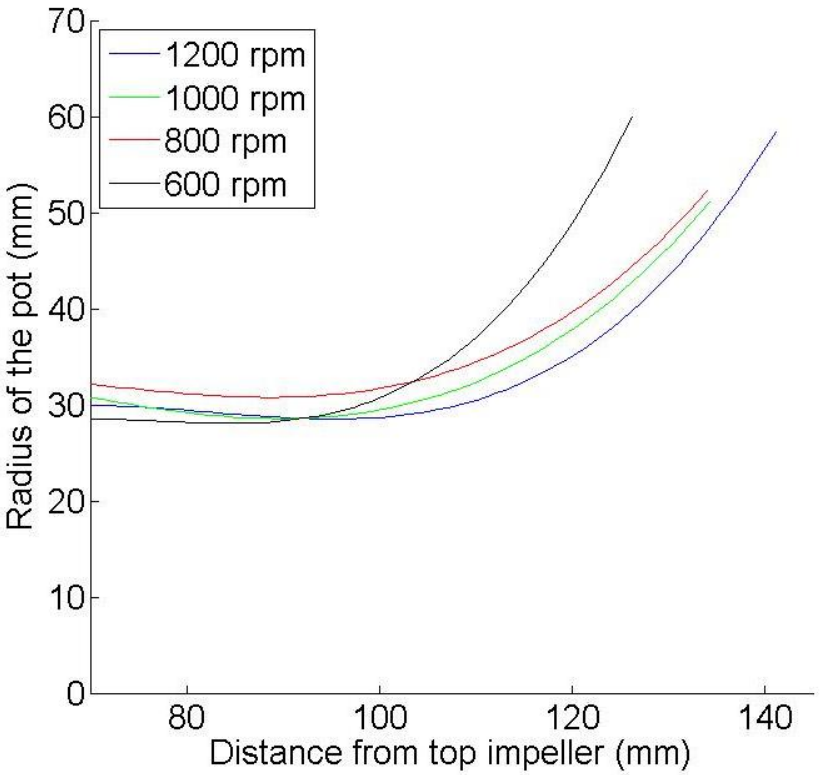

Figure 7.2-3 Shape of media-air interface at 1200, 1000, 800 and 600 rpm

8 REFERENCES

Askeland, D. R., Fulay, P. P. & Wright, W. J., 2006. *The science of engineering materials.* 6 ed. Stamford: Cengage Learning.

Atkins, P. & De Paula, J., 2010. *Physical chemistry.* 9 ed. Oxford: Oxford University Press.

Bakalis, S. & Fryer, P. J., 2004. Measuring velocity distributions of viscous fluids using Positron Emission Particle Tracking (PEPT). *AIChE Journal,* 50(7), pp. 1606-1613.

Blecher, L., Kwade, A. & Schwedes, J., 1996. Motion and stress intensity of grinding media in a stirred media mill. Part 1: Energy density distribution and motion of single grinding beads. *Powder technology,* Volume 86, pp. 59-68.

Bourgeois, F., 1993. *Microscale modeling of comminution proesses.* University of Utah: PhD thesis.

Callister, J. W. D., 2001. *Fundamentals of materials sciences and engineering.* 5 ed. New York: John Wiley & sons.

Conway-Baker, J., Barley, R. A., Clarke, A. J., Kostuch, J., Parker, D. J., 1999. Investigation and Model Validation of Media Motion in a Vertical Stirred Mill Using Positron Emission Particle Tracking. *1st World Congress on Industrial Process Tomography,* pp. 244-248.

Conway-Baker, J. Barley, R. W., Williams, R. A., Jia, X.,Kostuch, J., McLoughlin, B., Parker, D. J., 2002. Measurement of the motion of grinding media in a vertically

stirred mill using positron emission particle tracking (PEPT). *Minerals Engineering,* pp. 53-59.

Dong, L., Johansen, S. T. & Engh, T. A., 1994. Flow induced by an impeller in an unbaffled tank -I. Experimental. *Chemical Engineering Science,* 49(4), pp. 549-560.

Fan, X., Parker, D. J. & Smith, M. D., 2006. Enhancing 18F uptake in a single particle for positron emission particle tracking through modification of solid surface chemistry. *Nuclear instruments & methods in physical research,* Volume 558, pp. 542-546.

Fortier, S. M., Kostuch, J. A. & Skuse, D. R., 2004. Processing of calcium carbonate. *36th Annual meeting of the Canadian mineral Processors,* pp. 167-175.

Gope, P. C., 2012. *Machine Design-Fundamentals and applications.* New Delhi: PHI learning .

Griffith, A. A., 1921. The phenomena of rupture and flow in solids. *Philisophical Transactions of the royal society of London. Series A, containing papers of a mathmatical or physical character,* Volume 221, pp. 163-198.

He, M., Wang, Y. & Forssberg, E., 2006. Parameter effects on wet ultrafine grinding of limestone through slurry rheology in a stirred media mill. *Powder technology,* Volume 161, pp. 10-21.

Holdich, R. G., 2002. *Fundamentals of particle technology.* Shepshed: Midland Information Technology and Publishing.

Imerys, 2014. *Annual report 2014.* [Online]
Available at: http://www.imerys.com/scopi/group/imeryscom/imeryscom.nsf
[Accessed 18 September 2015].

Jankovic, A., 2003. Variables affecting fine grinding of minerals using stirred mills. *Minerals engineering,* Volume 16, pp. 337-345.

Kendall, K., 1978. The impossibility of comminuting small particles by compression. *Nature,* Volume 272, pp. 710-711.

King, R. P., 2001. *Modeling and simulation of mineral processing systems.* Oxford: Reed educational and processional publishing LtD.

Klimpel, R., 1997. *Introduction to the Principles of Size Reduction of Particles by Mechanical Means,* Florida: NSF Engineering Research Center for Particle Science & Technology.

Kogel, J. E., Trivedi, N. C., Barker, J. M. & Krukowsk, S. T., 2006. *Industrial Minerals & Rocks.* 7 ed. Colorado: SME.

Kwade, A., 1999_A. Determination of the most important grinding mechanism in stirred media mills by calculating stress intensity and stress number. *Powder technology,* Volume 105, pp. 382-388.

Kwade, A., 1999_B. 1. Wet comminution in stirred media mills — research and its practical application. *Powder Technology,* pp. 14-20.

Kwade, A., 2006. Specific energy consumption, stress energy, and power draw of stirred media mills and their effect on the production rate. In: S. k. Kawatra, ed.

Advances in comminution. Colorado: Society for mining, metallurgy, and exploration, pp. 99-114.

Kwade, A. & Bernotat, S., 2002. Present and future trends in dry fine grinding. *Industrial minerals,* pp. 69-71.

Kwade, A., Blecher, L. & Schwedes, J., 1996. Motion and stress intensity of grinding beads in a stirred media mill. Part 2: Stress intensity and its effect on comminution. *Powder Technology,* Issue 86, pp. 69-76.

Leadbeater, T. W., Parker, D. J. & Gargiuli, J., 2012. Positron imaging systems for studying particulate, granular multiphase flows. *Particuology,* 10(2), pp. 146-153.

Lichter, J. K. H. & Davey, G., 2006. Selection and sizing of ultrafine and stirred grinding mills. In: S. K. Kawatra, ed. *Advances in comminution.* littleton: Society for Mining, Metallurgy and Exploration, Inc, pp. 69-87.

Lofthouse, C. H. & Johns, F. E., 1999. The Svedala (ECC international) detritor and the metals industry. *Minerals engineering,* 12(2), pp. 205-217.

Malvern Instruments, 2012. *A basic guide to particle characterization,* Malvern: Malvern instruments limited.

Merkus, H., 2009. *Particle size fundamentals, practice, quality.* s.l.:Springer.

Mingzhao, H., Wang, Y. & Forssberg, E., 2004. Slurry rheology in wet ultrafine grinding of industrial minerals: a review. *Powder Technology,* Issue 147, pp. 94-112.

Parker, D. J., Broadbent, C. J., Fowles, P., Hawkesworth, M. R., McNeil, P., 1993. Positron emission particle tracking - a technique for studying flow within engineering

equiptment. *Nuclear instruments & methods in physics research,* Volume A326, pp. 592-607.

Parker, D. J., Leadbeater, T. W., Fan, X., Hausard, M. N., Ingram, A., Yang, A., 2008. Positron imaging techniques for process engineering: recent developments at Birmingham. *Measurement science and technology,* 19(9).

Prasher, C. L., 1987. *Crushing and grinding process handbook.* s.l.:John & Sons.

Rogan, K. R., Bentham, A. C., Beard, G. W. A., George, I. A., Skuse, D. R., 1994_A. Sodium polyacrylate mediated dispersion of calcite. *Colloid Polymer Science,* pp. 97-102.

Rogan, K. R., Bentham, A. C., George, I. A. & Skuse, D. R., 1994_B. Colloid stability of calcite dispersion treated with sodium polyacrylate. *Colloid and Polymer Science,* pp. 1175-1189.

Salman, A. D., Ghadiri, M. & Hounslow, M. J., 2007. *Handbook of powder technology.* Volume 12 (Handbook of Powder Technology) ed. Amsterdam: Elsevier.

Schonert, K., 1991. *Aufbereit-Tech,* Volume 32, p. 487.

Sikong, L., Hashimoto, H. & Yashima, S., 1990. Breakage Behavior of Fine Particles of Brittle Minerals and Coals. *Powder technology,* Issue 61, pp. 51-57.

Stender, H. H., Kwade, A. & Schwedes, J., 2004. Stress energy distribution in different stirred media mill geometries. *International journal of mineral processing ,* Volume 74S, pp. S103-S117.

Sun, C. T. & Jin, Z. H., 2012. *Fracture Mechanics.* Waltham: Elsevier.

Tamblyn, R. J., 2009. *Analysis of Energy Requirements in Stirred Media Mills.* The University of Birmingham: PhD thesis.

Tavares, L. M., 2007. Breakage of Single Particles: Quasi-Static. In: A. D. Salman, M. Ghadiri & M. J. Hounslow, eds. *Particle Breakage Handbook of Powder Technology Volume 12.* s.l.:Particle Breakage, pp. 3-6.

Tavares, L. M. & King, R. P., 1998. Single-particle fracture under impact loading. *International journal of mineral processing,* Volume 54, pp. 1-28.

Tegethoff, F. W., Rohleder, J. & Kroker, E., 2001. *Calcium carbonate: From the Cretaceous period into the 21st century.* English ed. Basel: Bertelsmannspringer.

Theuerkauf, J. & Schwedes, J., 1999. Theoretical and experimental investigation on particle and fluid motion un stirred media mills. *Powder technology,* 105(1-3), pp. 406-412.

Tromans, D., 2008. Mineral comminution: Energy efficiency considerations. *Minerals engineering,* Volume 21, pp. 613-620.

Wang, Y. & Forssberg, E., 2007. Enhancement of energy efficiency for mechanical production of fine and ultra-fine particles in comminution. *China Particuology,* 5(1), pp. 193-201.

Whitehouse, D., 2002. *Surfaces and their measurement.* Oxford: Kogan page science.

Wills, B. A. & Finch, J. A., 2015. *Chapter 4 - Particle size analysis.* 8 ed. Boston: Butterworth-Heinemann.

Yap, S. F., 2006. *Micromechanics and powder compaction.* The University of Birmingham: PhD thesis.

Yap, S. F., Adams, M., Seville, J. & Zhang, Z., 2006. Understanding the Mechanical Properties of Single Micro-Particles and their Compaction Behaviour. *China Particuology,* pp. 35-40.

Yashima, S. & Kanda, Y., 1987. Relationship between particle size and fracture energy of impact velocity required to fracture as estimated from single particle crushing. *Powder technology,* Issue 51, pp. 277-282.

Zhang, Z. & Stenson, J. D., 2009. Micromipulation in Mechanical Characterisation of single particles. *Advances in chemical engineering: Characterisation of flow, particles, and interfaces,* Volume 37.

9 APPENDIX

9.1 APPENDIX A

The section below discusses how the homemade code PEPTsove.m works to determine tracer, occupancy, velocity, acceleration, force, and media-media collisions from PEPT input data (time of location, position in x, position in y and position in z). The full code is located in the attached CD.

Inputs:

1. Tracer coordinates in time (x, y, z, t)
2. Number of points to be measured (h)
3. Number of pixels to an image (nb)
4. Mass of tracer (m)
5. Mean mass of grinding media (Mm)
6. Mean diameter of media (Dm)
7. Total mass of media (M)
8. Total volume of media (V)
9. Time milestone (tE)

Outputs:

1. nb-1, nb-1 matrix of media occupancy throughout a cross-section of the mill (meanocc)
2. nb-1, nb-1 matrix of media velocity throughout a cross-section of the mill (meanvel)
3. nb-1, nb-1 matrix of media mean relative velocity throughout a cross-section of the mill (meanstd)
4. nb-1, nb-1 matrix of media acceleration throughout a cross-section of the mill (meanacc)
5. nb-1, nb-1 matrix of media force throughout a cross-section of the mill (meanfor)
6. The instantaneous force of the tracer at 20 ms time interval (fc)
7. nb-1, nb-1 matrix of media collisions throughout a cross-section of the mill (meancol)

Homemade functions called:

1. Mediatype.m
2. cellno.m
3. delrepeat.m
4. fcubevel.m
5. findroots2.m
6. fvelspline.m

Breakdown of code

1. Loop 1

Batch processing of multiple datasets: Input data from PEPT (x, y, z, t) must be saved in .mat file called datan.mat. Where n corresponds to an integer representing the data set to be investigated. The physical properties of the tracer and bulk grinding media (m, Mm, Dm, M, V, tE) are saved within called function mediatype2.m.

2. Loop 2

Spline fitting: Fitting splies is computationally expensive. Therefore loop 2 divides the data set into sections length j and fits cubic splines to data points in both Cylindrical (to determine the correct bin) and Cartesian coordinates (to differentiate to determine velocity and acceleration).

3. Loop 3

Function 1: Determines the time at which the spline enters and exits each block volume and calculates the midpoint for each pass through a block volume.

Function 2: Calculates the desired flow parameter at each midpoint.

4. Loop 4

Bins data: Determines the average parameter within a block volume

All desired outputs are saved to a datanresultage.mat

9.2 APPENDIX B

The section below discusses how the homemade code, PEPTprocess.m, works to generate plots to compare different parameters from PEPTsolve.m output data (meanocc). The full code is located in the attached CD.

Inputs (from PEPTprocess.m) saved as in datanresultage.mat file:

1. nb-1, nb-1 matrix of media occupancy throughout a cross-section of the mill (meanocc)
2. nb-1, nb-1 matrix of media velocity throughout a cross-section of the mill (meanvel)
3. nb-1, nb-1 matrix of media mean relative velocity throughout a cross-section of the mill (meanstd)
4. nb-1, nb-1 matrix of media acceleration throughout a cross-section of the mill (meanacc)
5. nb-1, nb-1 matrix of media force throughout a cross-section of the mill (meanfor)
6. The instantaneous force of the tracer at 20 ms time interval (fc)
7. nb-1, nb-1 matrix of media collisions throughout a cross-section of the mill (meancol)

Inputs (User input, added to a matrix for each parameter investigated):

8. dataset investigated (b)
9. Diameter of grinding media (dm)
10. Average volume of a grinding media particle (mvol)
11. Total volume of a grinding media particle (tvol)
12. Tip speed of the impeller (impt)
13. Name of output folder (User input)
14. Parameter to be investigated (‘User input)
15. X label for plots (‘User input)
16. Plot legend text (User input)

Outputs

1. Occupancy
    a. Occupancy contour plots
    b. Occupancy as a function of height in the mill
    c. Bar chart comparing percentage of grinding media in impeller zone and recirculation zone and the median upper and lower quartile height of the grinding media particles.

2. Velocity
    a. Velocity contour plot
    b. Velocity as a function of height
    c. Dimensionless velocity
    d. Mean relative velocity
    e. Mean relative velocity as a function of height
    f. Bar chart comparing mean velocity, velocity in the impeller zone and velocity in the recirculation zone
3. Acceleration
    a. Acceleration contour plot
    b. Acceleration as a function of height
    c. Bar chart comparing mean acceleration, acceleration in the impeller zone and acceleration in the recirculation zone
4. Force
    a. Force contour plot
    b. Force as a function of height
    c. Bar chart comparing mean force, force in the impeller zone and force in the recirculation zone

5. Stress
    a. Stress contour plot when particle size equals 30, 20, 10 and 5 μm
    b. Mean stress as a function of calcium carbonate particle size
    c. Distributions of stresses as a function of particle size
    d. Percentage of media capable of fracturing calcium carbonate when particle size equals 30, 20, 10 and 5 μm
    e. Regions in the mill capable of fracturing calcium carbonate when particle size equals 30, 20, 10 and 5 μm
6. Collisions
    a. Collision rate contour plot
    b. Total collisions contour plot
    c. Collisions as a function of height
    d. Bar chart comparing total number of collisions, collisions in the impeller zone and collisions in the recirculation zone.